AN INVESTIGATION OF METHODS TO ENHANCE STRATIFICATION IN SOLAR DOMESTIC HOT WATER TANKS

by

Fozi Saleh Alsagheer

Submitted in partial fulfillment of the requirements
for the degree of Doctor of Philosophy

at

Dalhousie University
Halifax, Nova Scotia
March 2011

DALHOUSIE UNIVERSITY

DEPARTMENT OF MECHANICAL ENGINEERING

The undersigned hereby certify that they have read and recommend to the Faculty of Graduate Studies for acceptance a thesis entitled "An Investigation of Methods to Enhance Stratification in Solar Domestic Hot Water Tanks" by Fozi Saleh Alsagheer in partial fulfillment of the requirements for the degree of Doctor of Philosophy.

Dated: March 10th, 2011

External Examiner: _____

Research Supervisor: _____

Examining Committee: _____

_____

Departmental Representative: _____

DALHOUSIE UNIVERSITY

DATE: March 10th, 2011

AUTHOR: Fozi Saleh Alsagheer

TITLE: An Investigation of Methods to Enhance Stratification in Solar Domestic Hot Water Tanks.

DEPARTMENT OR SCHOOL: Department of Mechanical Engineering

DEGREE: PhD CONVOCATION: May YEAR: 2011

_____

Signature of Author

To

Allah,

My home land...Libya,

My unforgettable father…Saleh,

My merciful mother… Fatma,

My beloved wife… Amal and my children Marwan and Mayar,

My dear sisters… Mrs. Omm al-alwo, Mrs. Fatma, and Mrs. Khadija,

My dear brothers...Mr. Alsagheer, Dr. Mohmed, Dr. Milad, and Dr. Ayad,

My nephews and nieces,

My father, mother, brothers, and sisters in law,

To all of you I dedicate this work.

TABLE OF CONTENTS

LIST OF TABLES

LIST OF FIGURES

ABSTRACT

Solar domestic hot water (SDHW) systems collect energy with a solar collector, transfer the energy to the water through a heat exchanger, and store it in a storage tank. The water in the tank should be thermally stratified to the highest possible degree to maximize system efficiency because a stratified tank has higher availability than a mixed tank temperature. The objective of this research is to develop a manifold that will enhance thermal stratification in the SDHW tank.

In this work a new immersion shell-and-coil heat exchanger with a perforated manifold that extends from the heat exchanger to the top of the tank was used to enhance the thermal stratification. The purpose of the perforated manifold is to deliver the water heated by the heat exchanger to the tank at the level where the temperature of the water in the tank matches the temperature of the heated water, thereby enhancing stratification.

The effectiveness of the perforated manifold was determined experimentally. An experimental set-up was designed and constructed. The experimental results were analyzed for each manifold design then compared to determine the most effective manifold. The experimental work included testing and comparing different manifold designs. To simulate an actual system, experiments were conducted on three initial tank conditions, namely cold, hot, and mixed tank conditions.

The thermal performance of the system in terms of tank availability and entropy, maximum tank temperature, and thermal stratification were studied. A method to determine and design a perforated manifold that works with the standard Canadian SDHW system was established and evaluated experimentally. An availability analysis approach was developed to evaluate the thermal performance of manifolds, which have been operated at different times of the year.

Theoretically, gradually increasing the diameter of the holes in the manifold from the bottom into the top should reduce the unwanted flow of cold water from the bottom of the tank to the manifold and enhance the thermal performance of the manifold. However, the experimental did not confirm this.

LIST OF ABBREVIATIONS AND SYMBOLS USED

A	.....	Cross-sectional area of the manifold.
CFD	.....	Computational Fluid Dynamics.
$C_{p,g}$	.....	Glycol specific heat, kJ/kg · K.
$C_{p,w}$	.....	Water specific heat, kJ/kg · K.
F	.....	Friction force per unit length of manifold.
FCTR	.....	Fixed collector temperature rise.
g	.....	Gravitational acceleration, m/s^2.
h	.....	Fluid enthalpy, kJ/kg.
I_{max}	.....	Maximum current.
ISCHX	.....	Immersion shell-and-coil heat exchanger.
I_{sc}	.....	Short-circuit current.
k	.....	Thermal conductivity, W/m · K.
L	.....	Vertical distance between inlet and outlet, m.
L^*	.....	Mixing region height, m.
L/D	.....	Height to diameter aspect ratio.
L/min	.....	Liter per minute, L/min.
LFP	.....	Liquid flat plate.
$\dot{m}_w$	.....	Mass flow rate through manifold, kg/s.
$\dot{m}_g$	.....	Glycol flow rate, kg/s.
m_w	.....	Mass of water in the storage tank, kg.
p	.....	Pressure, kPa.
Pe	.....	Peclet number.
P_{max}	.....	Maximum power, kW.
Pr	.....	Prandtl number.
q_{coll}	.....	Solar collector heat transfer rate, kW.
Q_{end}	.....	Heat stored at a particular time during the day, MJ.
Q_{start}	.....	Heat stored at the beginning of the day, MJ.
Q_T	.....	Accumulated heat addition to the tank, MJ.
Q_{t1}	.....	Energy stored in the tank at time (t_1), kWh.
Q_{t2}	.....	Energy stored in the tank at time (t_2), kWh.
q_{tank}	.....	Rate of heat loss from the storage tank, kW.
Re	.....	Reynolds number.
Ri	.....	Richardson number.
SCHX	.....	Shell and coil heat exchanger.
SCOT	.....	Specified collector outlet temperature.
SDHW	.....	Solar domestic hot water.
T_{air}	.....	Ambient air temperature, °C.
$T_{avr,T}$	.....	Storage tank average temperature, K.
$T_{c,w}$	.....	Cold water temperature, K.
$T_{g,i}$	.....	Glycol inlet temperature to the solar collector, K.
$T_{g,o}$	.....	Glycol outlet temperature from the solar collector, K.
$T_{i,\ tank}$	.....	Initial temperature of the storage tank, K.
UA	.....	Overall heat transfer coefficient-area product, W/K.
V	.....	Voltage.
V_{max}	.....	Maximum voltage, m/s.
z	.....	Vertical coordinate distance.
Ω	.....	Ohm.
ΔT_g	.....	Temperature difference between inlet and outlet of glycol in

		the heat exchanger, K.
ΔT_{lm}	.....	Log-mean temperature difference, K.
ΔT_{tank}	.....	Temperature difference between the top and the bottom of the tank, K.
β_{th}	.....	Coefficient of volumetric thermal expansion, K^{-1}.
α	.....	Thermal diffusivity, m^2/s.
v	.....	Kinematic viscosity.

ACKNOWLEDGEMENTS

I wish to express my great appreciation and thanks to my friend and supervisor Dr. Peter Allen for his guidance, patience, and academic support during this work.

I am grateful to my friend and supervisor Dr. Ismet Ugursal for his motivation, support, and extensive guidance in my study and life in general.

Thanks are extended to Dr. J. Militzer, Dr. G. Jarjoura, and Dr. A. Mohamed for participating on the examining committee and their effort in reading my thesis and providing me with valuable comments.

I would like to acknowledge the moral support and assistance of many friends from the Mechanical Engineering Department in Dalhousie University.

I would like to thank my Libyan friends who have supported me throughout this work especially Mr. A. Darafon.

I would like to thank the Libyan Ministry of Education for my scholarship and the financial support.

I am indebted to my mother and the spirit of my father as much as to my wife and children and all of my family members.

Above all, I would like to express my gratitude to Allah who has given me the power to carry out this work.

CHAPTER 1: INTRODUCTION

1.1 SOLAR ENERGY

Due to concerns about the size of petroleum and natural gas reserves and also about the environmental impact of the combustion of fossil fuels, the search for more sustainable resources to provide alternate sources of energy is intensifying. Solar energy is one of the most important sources of renewable energy and can be used to produce electricity and heat.

1.2 SOLAR DOMESTIC HOT WATER (SDHW) SYSTEMS

Using solar energy to provide domestic hot water is not a new idea. In certain countries black painted water tanks have been used as simple solar water heaters for centuries. Today, millions of modern solar water heaters are in use.

Solar water heating technology has improved greatly in recent years. For example, modern solar water heaters work even when the outside temperature is well below freezing and they are protected from overheating on hot, sunny days. Many models also have their own built-in, back-up heaters, which can meet all of a user's hot water needs, even when there is no sunshine.

Solar water heating can reduce the demand for conventional fuels. This, in turn, can reduce damage to the environment and reduce the amount of money spent on oil imports, exploration, and new electrical generating capacity. Therefore, research is required in solar technology and it is supported by the federal government of Canada.

1.2.1 OPERATION OF THE SOLAR WATER HEATER

Solar water heaters perform three basic operations:

Collection: solar radiation is collected and converted to heat energy by a solar collector.

Transfer: circulating fluids transfer the heat to a storage tank using a heat exchanger.

Storage: hot water is stored until needed for domestic use.

Figure 1 shows a schematic diagram of the system containing these components.

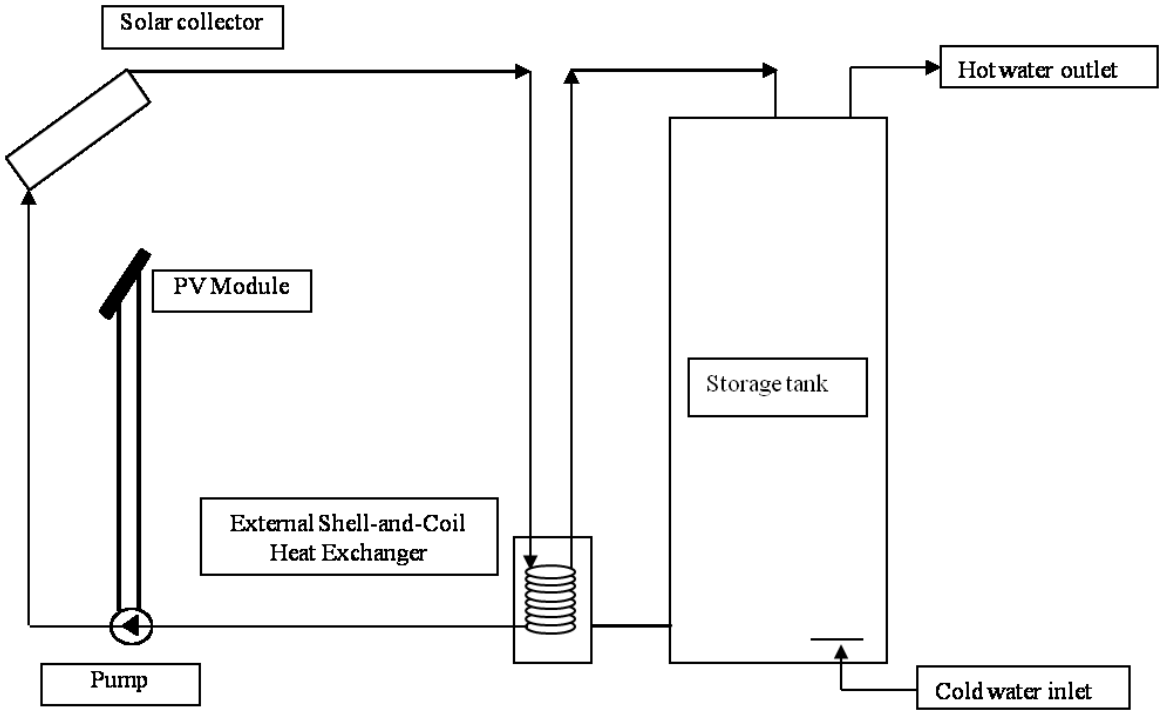

Figure 1 Schematic of SDHW system with external SCHX.

1.2.1.1 COLLECTION

The first operation is based on the "greenhouse effect". The solar collector is mounted on or near the building, facing south. Sunlight passing through glass or plastic glazing strikes an absorber plate coated with a radiation-absorbing material. The absorber plate converts the sunlight into heat, which is prevented from escaping by the glazing.

The most common solar collectors used in solar water heaters are "liquid flat plate" and "evacuated tube" collectors. A flat plate collector consists of a shallow rectangular box with a transparent glass or plastic "window" covering a flat black painted plate. The black plate acts as the absorber of solar energy and the solar collector coolant passes through pipes attached to the plate.

An evacuated tube collector consists of glass tubes, each containing a black painted metal pipe through which the solar collector coolant passes. The space between the pipe and the glass tube is evacuated. This results in the collector trapping more of the sun's

heat and producing hotter water than in a flat plate collector. This means that a smaller collector is required to produce a given amount of hot water.

Neither of these collector types is necessarily better than the other. Each has its advantages, and each can perform well if matched with a well-designed, storage unit.

1.2.1.2 TRANSFER

The second operation involves the transfer of heat from the collector to the water storage. In some solar water heaters, the solar collector coolant is pumped from the collector to the storage unit. In others, the sun heats the storage tank directly, or the fluid in the collector is heated and rises naturally to a storage tank above the collector. This latter type of solar water heater is referred to as a thermosiphon system.

Two kinds of heat exchangers can be used to transfer the heat from the solar collector coolant to the cold water in the case of a closed loop system. The first kind is an internal or immersion heat exchanger, where the heat transfer between the hot solar collector coolant and the cold water occurs inside the storage tank. The second kind is an external heat exchanger, where the heat transfer between the solar collector coolant and the water occurs outside the storage tank.

1.2.1.3 STORAGE

The third operation involves the storage of the solar heated water in an insulated tank. Hot water is drawn from the tank when tap water is used and cold make-up water enters at the bottom of the tank.

Solar water heaters have a larger hot water storage capacity than electric, gas, or other water heaters. This is because solar heat is available only during the day and sufficient hot water must be collected to meet evening and early morning needs, and possibly the needs for the following days in the event of inclement weather and low solar energy availability.

Increased utilization of solar energy depends on cost reduction and/or improvements in the performance of solar systems. Use of a properly designed stratified storage tank is one factor in reducing overall solar system costs. On the market today there are several tanks and stratifier designs is used to enhance the SDHW system efficiency by improving the

thermal stratification in the storage tank. In a thermally stratified tank the utilization of energy is higher than in a non-stratified tank. In other words, a stratified tank has higher availability than a mixed tank temperature. Also, the solar collector efficiency is higher with a stratified tank, because, the heat rate from the solar collector increases with an increasing temperature difference between the cold water at the bottom of the tank and the solar collector coolant. Stratification improves collector efficiency by lowering the collector inlet temperature.

Thermal stratification of water in storage tank is a process that takes place naturally due to the lower density of the water at higher temperature. This natural process is a challenging subject and very important in a number of engineering applications. This fact is reflected by the size of the research effort dedicated to this topic in recent years (as discussed in Section 3.1). However, the proper design of a manifold to enhance the stratification inside the storage tank is not determined yet.

According to the laws of thermodynamics, the water in the storage tank should be thermally stratified to the highest possible degree to maximise system efficiency. It is more efficient to have a tank stratified linearly from a lower temperature, e.g., 20ºC at the bottom of the tank to a higher temperature, e.g., 60ºC at the top compared with a tank that is at a uniform 40ºC. In both cases the energy stored in the tank is the same, however, with the stratified tank, the potential for the utilization of the energy is higher than in the non-stratified tank. The stratified tank is a lower entropy system than the non-stratified tank, and lower entropy systems naturally have higher availability.

The degree of stratification in a tank depends on the design of the tank, the size, the location and design of the inlets and outlets, and the velocities of the entering and exiting streams. Gari and Loehrke (1982) have shown that, it is possible to design tanks with low inlet and outlet velocities that will be highly stratified.

CHEAPER 2: AREA OF RESEARCH AND OBJECTIVE

2.1 AREA OF RESEARCH

Operating a SDHW system under the meteorological conditions found in Canada requires a closed loop arrangement in which a heat exchanger must be installed between the solar collectors and the storage tank. This closed loop arrangement is utilized to avoid freezing of the solar collector coolant, inside the collector piping. The closed loop also isolates the glycol from the domestic water. The heat exchanger can be installed outside or inside the storage tank. Each of these installation methods of the heat exchanger has advantages and disadvantages.

The objective of this work is to study the thermal and economic performance of a SDHW storage tank, heated with an immersion shell and coil heat exchanger (ISCHX*)* with a longitudinally perforated manifold that extends from the top of the heat exchanger to the top of the tank, and is used to enhance thermal stratification as shown in Figure 2.

To achieve this objective this work focused on and solved a number of issues and problems which were identified and discussed in a previous work by Alsagheer (2003). In this work a measure of stratification was observed with an ISCHX with a manifold supplying heated water only at the top of the tank.

Figure 3 shows the temperature distribution in a SDHW system tank over 24 hours on a sunny day in Halifax. Figure 4 shows the solar flux on the same day. The system was operated with an ISCHX with a longitudinal manifold supplying heated water only at the top of the tank. Nine thermocouples were installed in a probe located in the centre of the tank to measure the temperature from the top to the bottom at nine levels as shown in Figure 2. To simulate domestic hot water load, 100 liters of hot water were drawn from the top of the tank at 7:30 AM and 5:30 PM.

As soon as heat addition started at 9:00 AM the lower zones started to increase in temperature, due to the downward flow of heated water from above. However, because the heated water was supplied only from the top, the temperature at the top of the tank dropped when the heated water temperature was lower than the temperature of the water at the top of the tank (7:30 AM until 10:15 AM). At 10:15 AM the water from the ISCHX

become hotter than the top tank temperature and the temperature at the top tank temperature began to increase.

The purpose of the longitudinally perforated manifold is to deliver the water heated by the immersion heat exchanger to the tank at the level where the temperature of the water in the tank matches the temperature of the heated water, thereby enhancing stratification. The effectiveness of the longitudinally perforated manifold was examined experimentally.

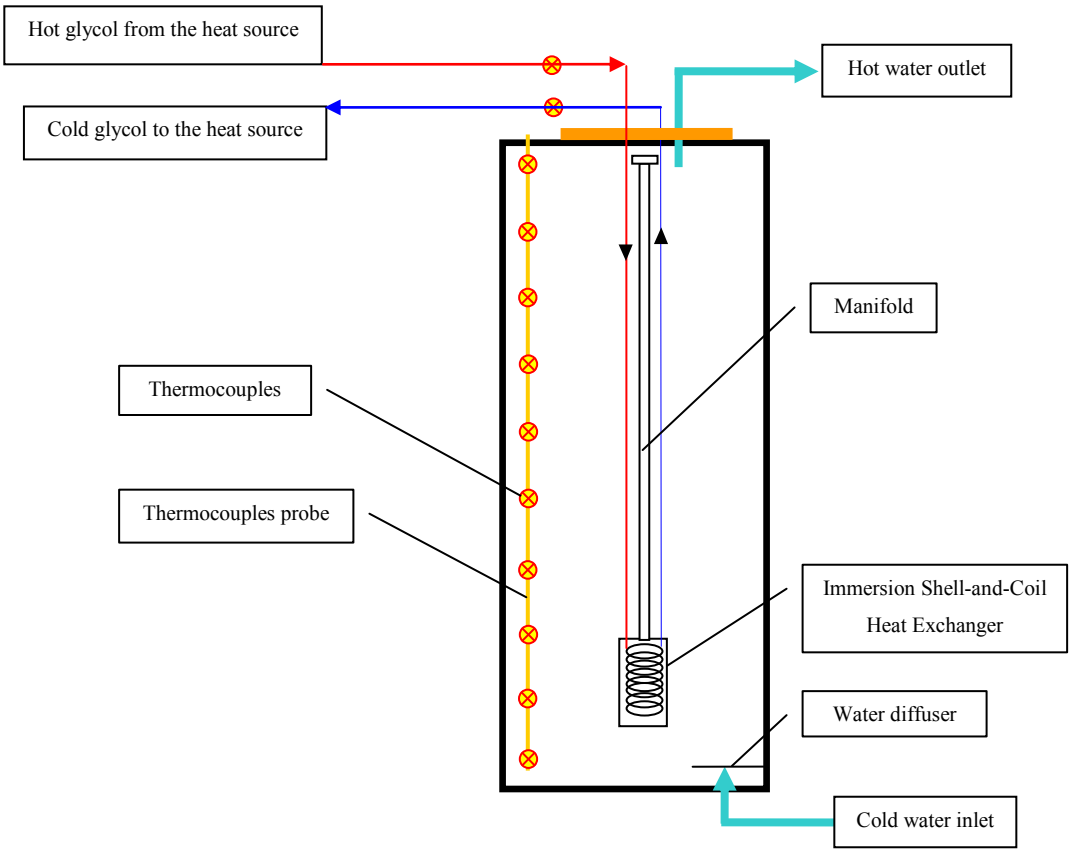

Figure 2 A schematic of the tank and ISCHX and thermocouples probe.

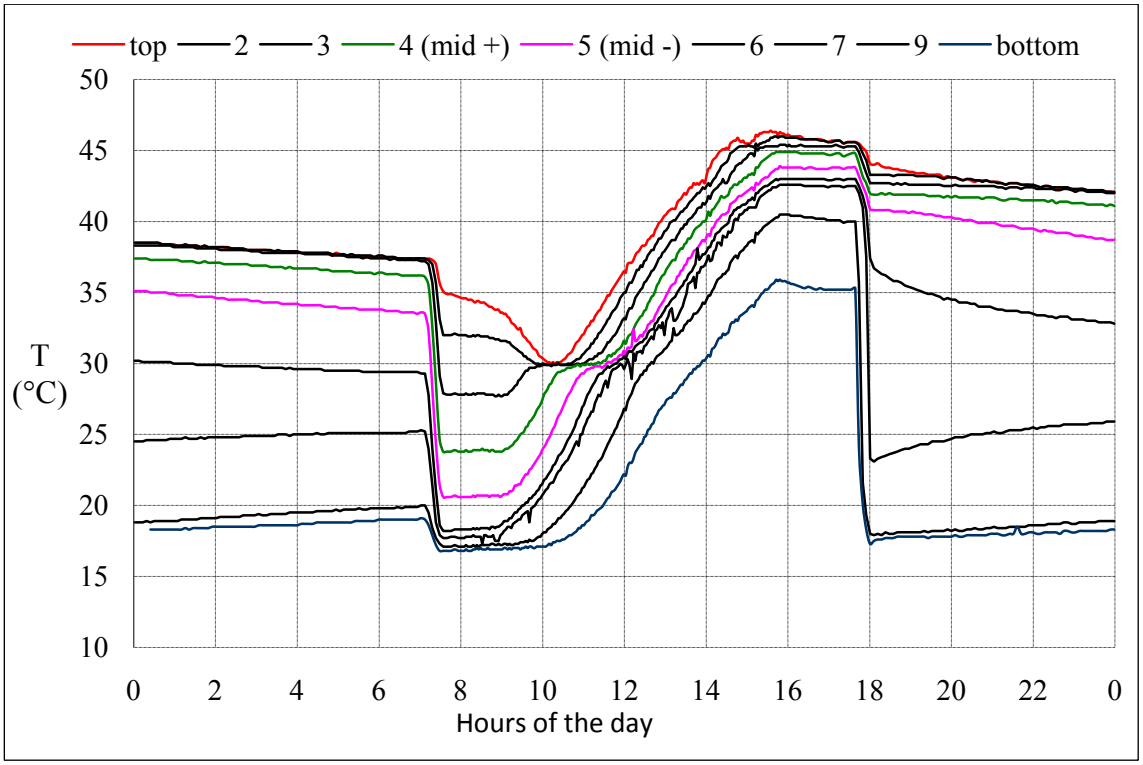

Figure 3 Temperature distributions in solar storage tank using an ISCHX and manifold.

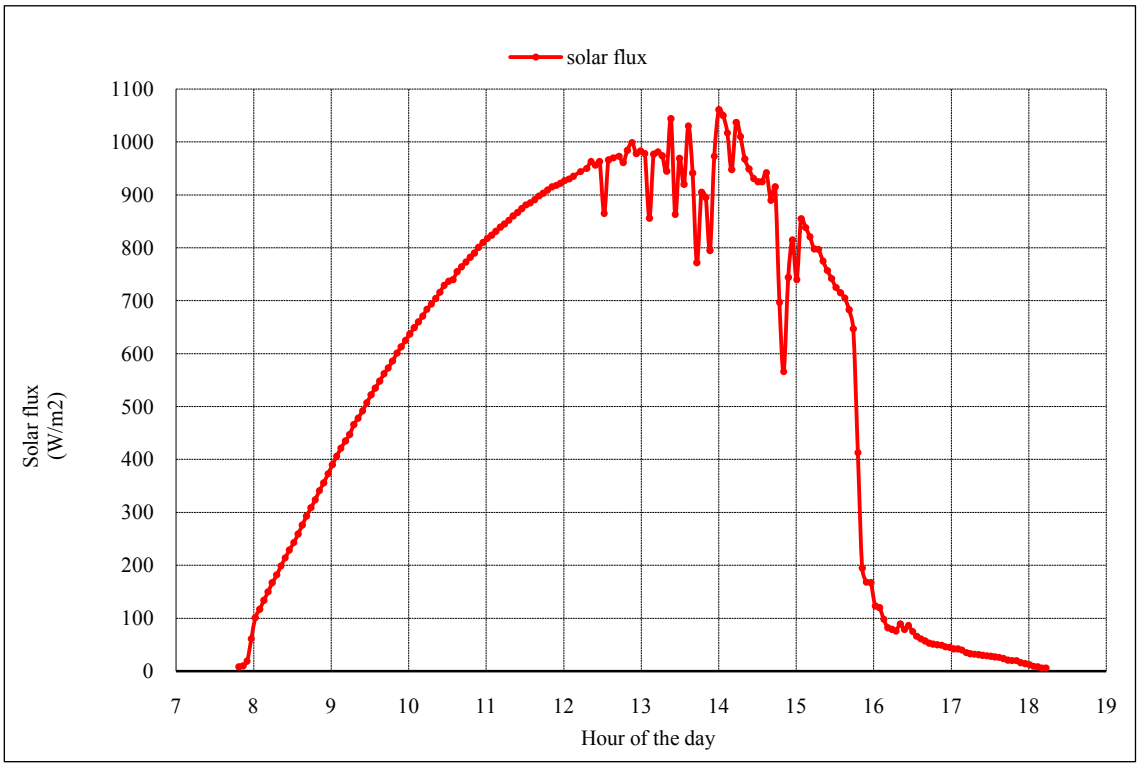

Figure 4 Solar flux on a sunny day

2.2 OBJECTIVE OF THIS RESEARCH

Solar tank designers attempt to solve destratification problems associated with heat transfer using several methods, such as placing insulation inside and/or outside the tank walls to reduce axial conduction heat transfer through the wall and heat losses from the storage tanks. Moreover, increasing the tank aspect ratio and inlet and outlet diameters will reduce the inlet jet mixing problems that cause destratification. However, more research is required to improve the process of delivering the hot water to the storage tank in order to improve the system efficiency as a result of enhanced storage tank stratification.

The objective of this research is to develop a heat exchanger/manifold design that enhances the thermal stratification in a solar domestic hot water system tank. Several designs of a longitudinally perforated manifold that extends from an immersion heat exchanger to the top of the tank were developed and used to enhance thermal stratification. The effectiveness of the longitudinally perforated manifold designs were

determined experimentally. The thermal performance of the system in terms of the maximum tank temperature, thermal stratification, tank entropy, tank availability, and overall system efficiency were studied.

To achieve this objective, the following tasks were performed:

1. Designed, built and tested different types and sizes of longitudinally perforated manifolds (a stratification enhancing device) whose purpose is to deliver the water heated by the immersion heat exchanger to the tank at the level where the temperature of the water in the tank matches the temperature of the heated water, in order to enhance stratification.
2. Tested and compared the thermal performance of the immersion shell-and-coil heat exchanger with a longitudinally perforated manifold, in terms of tank entropy and availability and the tank thermal stratification.
3. Developed an experimental model to study thermal stratification in the SDHW system tanks.
4. Used the developed model to extend the experimental study.
5. Developed a heat exchanger design for natural convection SDHW systems to maximize the system thermal performance.
6. Developed design guidelines for SDHW system designers.

CHEAPER 3: LITERATURE REVIEW

The phenomenon of stratification in water tanks heated by natural convection from immersion heat exchangers is not completely understood. Most of the factors that cause destratification inside the tank are known, but research is required to quantify the effects of the parameters that enhance the stratification. This fact is reflected by the size of the research effort during the past years dedicated to this topic. This section focuses on the studies of stratification phenomena.

The most important factors influencing the stratification and the destratification inside a storage tank are covered in this Section. These factors include the geometrical factors of the tank including tank size, the aspect ratio of the tank, inlet locations, and using baffles inside the storage tank, or using a manifold to enhance the thermal stratification in the storage tank. Also mixing caused by inlet jet and plume entrainment problems are discussed. Heat convection and conduction as well as envelope heat losses of the storage tank are also covered.

3.1 THERMAL STRATIFICATION IN THE STORAGE TANK

Lavan and Thompson (1977) experimentally studied thermally stratified hot water storage tanks. The objective of their study was to determine a method of removing hot water from the storage tank and adding cold water into it while maintaining a steep thermocline. The study was concentrated on the effects of inlet port location, inlet geometry and mass flow rate, aspect ratio of height to diameter of the tank, and inlet and outlet water temperature difference of the tank. The study had concluded that improving the stratification of the stored water in solar energy systems can significantly improve the collector and the system efficiency. The study had also shown that during discharge of the tank (drawing water from the tank), thermal stratification could be maintained in cylindrical water tanks. Stratification improved with an increase in the tank height to diameter aspect ratio (L/D), the temperature difference between the top and the bottom of the tank (ΔT), inlet and outlet port diameters. Stratification decreased with increasing flow rates. The best results were obtained when the inlet and outlet ports were near the end walls, and when the flow was directed towards those walls.

Sliwinski, et al. (1979) investigated the performance of stratified tanks during charging. They found that the size of the region affected by jet mixing was a function of the Richardson number (Ri)[1]. The Richardson number represents the importance of natural convection relative to the forced convection Sliwinski, et al. (1979), Hollands and Lightstone (1989). They concluded that stratification occurred at the storage inlet for Richardson numbers as low as 0.24 and the degree of stratification was sensitive to the variation of the Richardson number when the inverse of the Peclet number was low $\left(9.03\times10^{-4} \le \frac{1}{Pe} \le 9.99\times10^{-4}\right)$, however, at higher values of the inverse of the Peclet number $\left(2.13\times10^{-3} \le \frac{1}{Pe} \le 2.47\times10^{-3}\right)$ the degree of the stratification was insensitive to changes in the Richardson number.

It was suggested by Wildin and Truman (1985) that a Richardson number greater than or equal to one is sufficient for maintaining stratification.

Loehrke, et al. (1979) conducted studies for stratification enhancement in storage tanks by using different inlet manifold designs, which preserve stratification in a tank subjected to variable inlet temperature conditions. An ideal stratification model was also used to predict the temperature profiles during the tests. In his model, the collector return flow entered at the top of the tank. If the collector return temperature was as high as, or higher than the tank top temperature, no mixing occurred. However, If the collector return temperature was lower than the tank top temperature, the return flow and tank water mix downward until the mixed temperature was higher than the rest of the tank. Two types of vertical porous manifolds were constructed and tested, namely a rigid porous manifold and a flexible porous manifold, where the flexible one was attached to a rod to maintain it in a vertical orientation. The experiments indicated that an inlet that introduced fluid into the tank at a fixed location may be designed to provide a high degree of stratification during the charging portion of the experiment by minimizing the depth of the mixing

[1] $Ri = \frac{g\beta_{th}\Delta TL}{{V_i}^2} = \frac{Gr}{Re^2}$ and $\frac{1}{Pe} = \frac{1}{Re\,Pr}$ and $Pr = \frac{\nu}{\alpha}$

layer. This may be done by constraining the flow to enter the tank in a thin horizontal layer at low velocity. This approach may enhance mixing under variable inlet temperatures. The authors concluded that to achieve better stratification, an inlet distributor was required that would allow the incoming water to pass through the warm upper region of the tank during the recycle period without mixing.

One inlet design was tested. It had a vertical porous manifold, which minimizes shear-induced mixing between fluids of different temperature, yet allows for outflow into the tank at almost any level. The fluid entered the tank horizontally into a T-section of pipe. Perforated pipes were connected to the vertical arms of the T-section to form a continuous vertical manifold. If the incoming fluid density differed from the local tank density at the entry point, vertical momentum was imparted to this supply fluid. Under ideal conditions (fluid temperature and flow rate and tank temperature profile), the supply fluid (T-section of pipe) would rise or fall in the porous manifold maintaining a pressure balance with the tank fluid until it reached the level at which the manifold fluid density matches that of the surrounding tank fluid. The charging temperature profiles for both manifolds (rigid and flexible types) were very close to those predicted for an ideal stratification model. The performance of the flexible manifold was better than the rigid manifold.

Jaluria and Gupta (1982) conducted an experimental study of the temperature decay in thermally stratified water tank for solar energy storage. A tank was initially stratified by adding hot water to the top of the cold fluid. “It was found that the buoyancy-induced mixing that arose maintained the upper layers essentially isothermal and gaive rise to horizontal temperature homogeneity in the water body. The decrease in the surface temperature was initially accompanied by an increase in temperature in the bottom layers, followed by a decrease in temperature throughout the water body at the later stages. The cooling process was found to depend strongly on the initial temperature level and distribution”.

Eames and Norton (1998) performed a theoretical and experimental investigation into the thermal performance of stratified hot water tanks. A finite volume based model was validated by comparison with measured temperatures from a series of thirty-two experiments in which the inlet velocity and temperature ranged between 25 - 90 mm/s ,

and 11ºC - 52ºC, respectively, and various permutations of inlet and outlet port locations and initial storage stratification profiles were tested. A parametric analysis determined the effect of inlet and outlet port locations on storage performance for a range of operating conditions. The effects of finite volume size on predicted levels of entrainment and diffusion in the inlet region were reported. Simulations were conducted for storage tanks with aspect ratios (height to width) of 3:1 (tall) and 1:3 (short), with inlet ports either one ninth or half way down the storage side. The results indicated that storage tank charging was performed more efficiently for tall tanks with the inlet port near the top. Also, it was observed from the simulations that a single inlet port with variable inlet temperature jet lead to poor tank stratification. Enhanced performance could be achieved by having ports at different heights, with the inlet fluid entering the tank at the height at which the resident tank fluid temperature most closely matched the inlet fluid temperature.

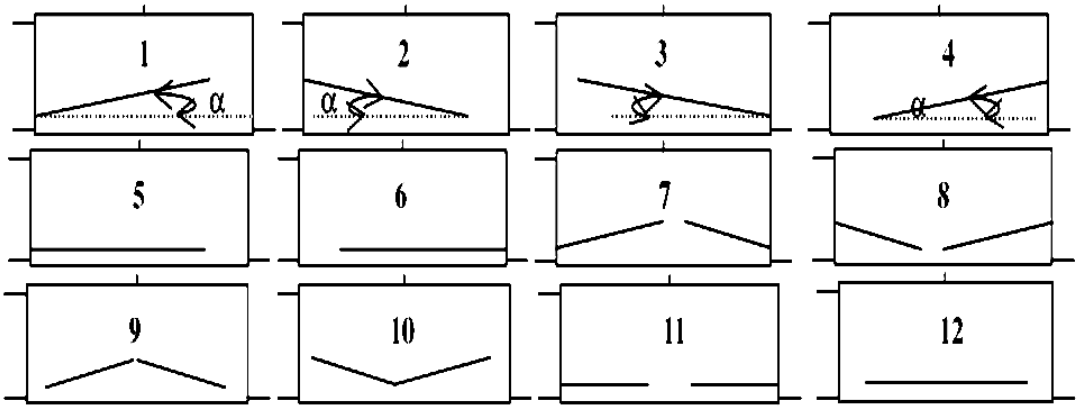

Figure 5 Baffle geometries and their assembly in the tank.

Altuntop, et al. (2005)

Altuntop, et al. (2005) studied the effect of using different baffles, shown in Figure 5, on thermal stratification in a cylindrical hot water tank using various mathematical models. Later the findings were validated by experimentation. Temperature distributions within the tank for 12 different baffles were obtained. The results indicated that placing baffles in the tank provides better thermal stratification compared to the no baffle case. The baffle types having a gap in the center appeared to have better thermal stratification than those having a gap near the tank wall. These baffles numbered 7 and 11 in Figure 5 represented better baffle shapes and configurations for thermal stratification among the

considered cases, and consequently tanks with these baffles can supply hot water at higher temperatures. Other baffle types had little effect on improving thermal stratification in the tank. Further comparisons of baffles 7 and 11 in terms of the temperatures of hot water supply indicated that baffle 11 provided the best thermal stratification in the tank among all the considered cases.

In the work done by Shah and Furbo (2003) the impact of the inlet design with different baffle plates on the flow patterns in the tank were investigated using numerical method and validated by experiments. A simple, straight pipe with no baffle, hemispherical baffle plate and a large flat baffle plate, as shown in Figure 6, were compared under different discharge times and flow rates (1 L/min or 10 L/min). The performance of the diffuser was characterized by the ability of the tank to maintain stratification, when cold fluid was added to the tank. Entropy and availability analyses were used to evaluate the level of stratification. The results showed that the entropy changes and availability changes in the storage during the draw-off were influenced by the Richardson number and initial temperature difference between top and bottom of the tank. Also, at lower flow rates, the cold water dropped to the bottom of the tank without creating any severe mixing.

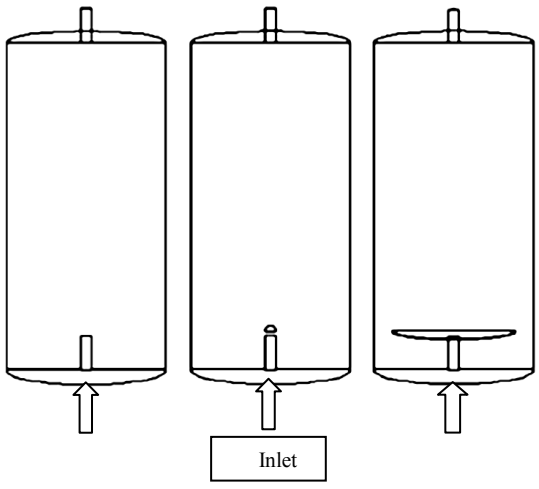

Figure 6 Tank with the three different inlets.

Shah and Furbo (2003)

Shah, et al. (2005) conducted theoretical and experimental investigations of inlet stratifiers for solar storage tanks. A rigid stratifier was investigated using Computational Fluid Dynamics (CFD) and tested experimentally. The stratifier consisted of a main tube with three circular openings as shown in Figure 7. The stratifier was mounted inside a 144 *L* water tank.

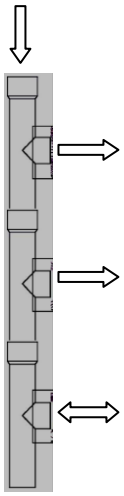

Figure 7 Illustration of the stratifier.

Shah, et al. (2005)

During a tank charge test, the investigations showed that cold water from the bottom of the tank was sucked into the stratifier through the lowest opening. The mixed fluid entered the tank through the top opening. As a result of the test, it was found that this type of stratifier actually works more as a ‘‘mixing device’’ than as a stratifying device. The researchers concluded that, flaps working as ‘‘check valves’’ at the stratifier openings, reduced the unwanted flows into the lowest openings.

In a study to enhance stratification in storage tanks, Cruickshank (2006) developed a numerical model and tested stratified multi-tank thermal storage tanks for solar heating systems. An experimental test rig was also constructed and instrumented to evaluate the characteristics of series and parallel connected multi-tank thermal storage units for solar applications. Test data were compared with results predicted by computer simulation. Both simulation and measured test results showed that high degrees of stratification can occur in both series and parallel storage tank arrangements, and both simulation and

modeling indicated that slightly higher storage rates were achieved with the parallel storage configuration relative to the series case. However, in light of the difficulty to achieve a balanced flow distribution in the parallel flow configuration, system designers may choose to utilize the series configuration. The results also indicated the feasibility of using side-arm, natural convection heat exchangers in a multi-tank storage system. This arrangement had the advantage of allowing the use of low cost, conventional hot water storage tanks.

3.2 INLET JET MIXING

The pattern of the inflow or outflow from the storage tank is affected by the geometry of the inlet and outlet ports, such as their diameters, positions and designs.

Lavan and Thompson (1977) carried out an experimental study to determine the effect of inlet geometry on thermal stratification in a water storage tank. It was found that the inlet location had a stronger influence on thermal stratification than the outlet.

Gari and Loehrke (1982) conducted an experimental study of an inlet manifold for introducing water of arbitrary temperature into a storage tank without destroying pre-existing stratification. A number of manifolds for enhancing stratification in solar thermal energy storage tanks were designed and tested. The authors concluded that the exit hole diameter of the manifold should be less than a quarter of the diameter of the manifold. Also, in order to prevent inflow or outflow from the manifold until the temperatures of the fluids inside and outside the manifold are matching, the pressure gradients of the two fluids must be matched. The one-dimensional differential momentum equation for the manifold is:

$$\frac{dP}{dz} = \rho g - \frac{F}{A} - \frac{1}{A}\frac{d}{dz}\left(\frac{\dot{m}^2}{\rho A}\right) \qquad 3.2.1$$

where, the pressure gradient is assumed to be hydrostatic in the tank:

$$\frac{dP_t}{dz} = \rho_t(z)\, g$$

where,

P : Pressure.
z : Vertical coordinate distance.

ρ : Density.
g : Acceleration of gravity.
F : Friction force per unit length of manifold.
A : Cross- sectional area of manifold.
$\dot{m}$: Mass flow rate through manifold.

From Equation 3.2.1, it is clear that the pressure gradient in the manifold may be changed by varying either the cross-sectional area of the manifold (A) or the frictional characteristics of the manifold (F).

Hollands and Lightstone (1989) reviewed low-flow, stratified-tank solar water heating systems, to improve the solar collector efficiency. The authors stated that in a stratified tank the interface between the hot and cold fluids would have zero thickness and deviations from this ideal are clearly visible; however, in practice, destratification factors include inlet jet mixing, and plume entrainment, and heat conduction and side losses can cause significant deviations from the ideal stratification.

The study concluded that the inlet jet plays a significant role in mixing the storage tank. The momentum of the water entering the tank produced a mixing region that was usually localized to a small horizontal region near the inlet port L^* (the height of the mixing region). Extending this region will characterize the mixing in the storage tank. When the height of this region (L*) was nondimensionalized by dividing it by the height of the tank (L), L* appears to be a function of the Richardson number Ri. The study indicated that L^*/L was less than 0.05 if $Ri > 0.5$, but for smaller values of Ri, L^*/L rose sharply. Those values of Ri, were dependent on inlet port configuration. Experiments of Loehrke, et al. (1979) showed that good stratification was not achieved at a Richardson number as high as 4.7, since the incoming flow was turbulent.

A study by Al-Najem and El-Refaee (1997) concluded that the turbulent mixing (or eddy conductivity) factor caused by hydrodynamic disturbances at the inlet and outlet ports of storage tank played an important role in the performance of thermal stratification storage tanks. The authors also investigated the tank inflow situations that included two configurations: the upper inflow and the lower inflow. The authors found that the inlet hot water from the solar collector that enters the tank from the top would easily build

stratification, but colder inflow at the top of tank would completely mix the temperature field inside the tank.

Zurigat, et al. (1991) performed an analytical and an experimental investigation on the influence of inlet geometry on mixing in a stratified thermal energy storage. The authors found that the inlet geometry had a significant influence on the thermal stratification in a storage tank for Richardson numbers below 3.6 while the inlet geometry effect was negligible for Richardson numbers above 10.

Andersen and Furbo (1999) measured mixing or destratification during hot water discharge in solar tanks with different inlet designs. Based on measurements and on detailed simulation models, the influence of mixing on the yearly thermal performance of solar storage tanks was calculated. It was found that the decrease in the yearly thermal performance utilization of solar energy was up to 23% due to mixing during hot water draw offs.

Knudsen (2002) continued the theoretical work of Andersen and Furbo (1999) with an expanded analysis of the influence of mixing on solar storage tanks. Numerical simulations with detailed simulation models were carried out to investigate the influence on the thermal performance of different mixing degrees, hot water consumptions and consumption patterns. The investigations were conducted on different marketed solar tanks. The authors concluded that the thermal performance of the storage tanks would decrease up to 20% when the mixing during hot water draw offs was increased up 40% of the total tank volume.

Zachár, et al. (2003) also studied two different inflow situations, the upper inlet flow with a flat plate located opposite to the inlet and, the lower inflow configuration with similar arrangement, shown in Figure 8. Zachár concluded that the diameter of the plate and the distance between the plate and the top of the tank had a significant effect on the stratification within the tank when cold water entered at the top of the tank.

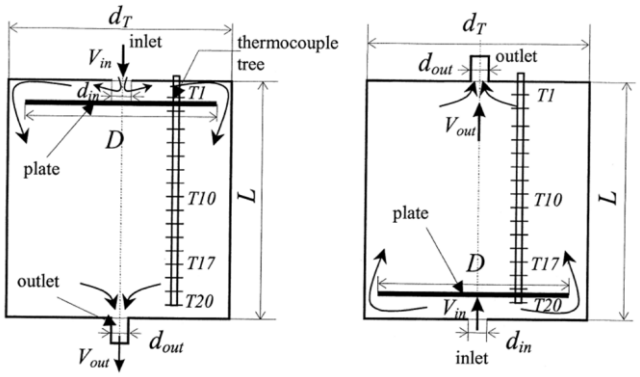

Figure 8 Diagram of a tank shows the upper inlet flow and, the lower inflow configurations.

Zachár, et al. (2003)

3.3 PLUME ENTRAINMENT

Plume entrainment often occurs in low flow systems when the availability of solar energy has decreased. As a result water entering the tank at the top is cooler than the water contained at the top of the tank producing a downward flowing plume (the cooler water sinking to its correct height in the tank). The resultant falling plume of cool water causes mixing and destroys stratification in the storage tank. In a review of low-flow in stratified solar storage tanks, Hollands and Lightstone (1989) reported on methods and inlet designs to eliminate plume entrainment. One suggested method was to connect a light flexible hose to the tank inlet. The outlet of the hose should float to the correct depth due to the buoyancy forces without entraining fluid as the plume does. However problems could arise if air bubbles attach to the hose. A second suggestion was to connect a vertical perforated manifold to the inlet port to force the water to travel through the manifold to the correct level according to its temperature. Finally, the third suggestion was to control the mass flow rate through the collector so the temperature of the fluid leaving the collector was constant, eliminating the possibility of plume entrainment. This strategy however, showed a reduction in collector performance.

Csordas, et al. (1992) performed numerical simulations to evaluate and compare two strategies by which plume entrainment was minimized by controlling the collector flow rate. One strategy called SCOT (Specified Collector Outlet Temperature) maintained a

constant collector outlet temperature, and the other FCTR (Fixed Collector Temperature Rise) strategy maintained a constant temperature rise from inlet to outlet of the collector. These strategies were evaluated by computer simulation previously, but only against a system model assuming a highly idealized, perfectly stratified tank. This study evaluated the strategies using a computer simulation model incorporating a more realistic tank model, one accounting for plume entrainment effects. It was found that the plume entrainment model reduced the performance of the system for all flow rate strategies. Furthermore, the variable flow rate with the FCTR strategy consistently out-performed the constant flow rate strategy. However, it was concluded that the extra hardware required for the variable flow rate strategy was unaffordable at that time.

Shah and Furbo (2003) concluded that by using a lower flow rate, the cold water travels to the bottom of the tank without creating any severe mixing, however, when the flow rate was increased by a factor of 10, the plume was almost half way up in the tank with the simple pipe but by using the hemispherical baffle plate the plume could break down, and with the flat baffle plate, the flow rose steadily in the tank in the annulus between the tank wall and the flat baffle plate.

3.4 HEAT CONVECTION AND CONDUCTION AND ENVELOPE LOSSES

Mixing due to natural convection takes place when the fluid entering the storage tank is colder or hotter than the nearby fluid; deference in fluid density give rise to natural convection currents which mix the fluid in the tank. The level of natural convection is a function of the temperature of the fluid entering the tank and the temperature distribution within the tank and the design and location of the inlet. Heat conduction within the tank wall also gives rise to the natural convection currents. Fluid close to the wall is cooled or heated to the mean tank temperature faster than the bulk of the fluid in the tank. The resulting horizontal temperature difference drives natural convection circulation.

Shyu and Hsieh (1987) studied unsteady natural convection in stratified tanks. The authors used a numerical simulation technique to determine the most appropriate configuration of tank wall material to reduce destratification by the tank wall conduction.

Three designs of tank walls were investigated: a wall without insulation on it, insulation placed over the exterior of the wall, and insulation placed over the interior.

The tank was initially stratified and the wall temperature was uniform at the high temperature level of the tank. It was concluded that insulating the interior surface of the tank not only reduced the heat transfer to the ambient air but also resulted in a substantial reduction in destratification, while the externally insulated tank reported the highest destratification.

Miller (1977) studied the effect of conduction through the wall on the stratified fluid in a cylinder. It was found that the degradation of the thermocline was ten times faster in aluminum tanks than in glass tanks. This showed that if the fluid was stored in a container made from a material of a thermal conductivity much greater than that of the fluid, convection currents were generated at the fluid/wall interface inside the container, causing degradation of the thermocline at a faster rate. This was confirmed by the study of Sherman, et al. (1979) in which tests were conducted on a fiberglass tank with no liner and with copper, aluminum, steel and stainless steel liners. Those tests showed that vertical conduction down the tank walls could reduce thermal stratification to a significant extent. However, computational results by Shyu and Hsieh (1987) showed that the tank configuration which best maintained the stratification was where the tank was insulated on the inside with conductive supporting walls outside. Interestingly, it was found that a tank with no insulation maintained stratification better than a tank with insulation outside of the conductive supporting walls. It was found that a tank with no insulation had a high heat leak to the room so that axial conduction in the wall did not play an important role in the heat transfer processes in the tank.

Knudsen, et al. (2005) investigated the flow structure and heat transfer in both the mantle and in the inner tank, as shown in Figure 9, for both hot and warm inlet temperatures to the mantle and for both initially stratified and initially mixed inner tanks. The authors concluded that a vertical mantle heat exchanger was able to help stratification in the inner tank even when the mantle inlet temperature was lower than the tank temperature at the input.

Figure 9 Glass mantle and inner tank.

Knudsen, et al. (2005)

3.5 METHODS TO CHARACTERIZE STRATIFICATION

This section reviews methods that had been proposed to characterize thermal stratification in storage tanks.

Rosen and Hooper (1992) concluded that if only the first law of thermodynamics is used, it is not possible to distinguish a stratified tank from a mixed one. However, a second law analysis allow different temperature distributions to be quantified in terms of the exergy content, ε, which is function of the temperature of the liquid (T) and the dead state temperature (T_o) (reference environmental temperature). Rosen and Hooper's analysis relied on knowing only the temperature, T, as a function of height and the dead state temperature, to calculate the exergy content.

Rosen, et al. (1999) calculated the exergy of the storage tank by Equation 3.5.1 which has been chosen for further analysis in this work and will be discussed in Section 5.3

$$\varepsilon_{Tank} = m \sum_{i=12}^{i=1} (H_i - H_o) - T_o(S_i - S_o) \qquad 3.5.1$$

where:

ε : Availability of energy in the tank, MJ.

i : Layer number.

H_i : Enthalpy of the layer, kJ/kg.

H_o : Enthalpy evaluated at environmental temperature, kJ/kg.

T_o : The environmental temperature (air temperature), K.

S_i : Entropy of the layer, kJ/kg ·K.

S_o : Entropy evaluated at environmental temperature, kJ/kg ·K.

Rosengarten, et al. (1999) used the second law to characterize thermally stratified hot water storage, with application to solar water heaters. A method of comparing different levels of stratification in liquid thermal storage devices was related the temperature distribution to a stratification effectiveness parameter. Rosengarten mentioned that Hermansson (1993) concluded that the reference environment temperature depends on the application, but did not specify what it should be. In some cases, the temperature used was the tank bottom temperature and in others the return water temperature. However, arbitrary choices of the dead state temperature, without a physical justification, could confuse and lead to misleading comparisons because exergy is highly dependent on this temperature. Rosengarten used the water inlet temperature as the dead state temperature in his non dimensional exergy term to calculate the stratification efficiency (η_{st}) as shown in Equation 3.5.2.

$$\eta_{st} = \frac{\xi}{mc(T_{del} - T_{mean})} = 1 - \frac{T_0}{H(T_{del} - T_{mean})} \int_0^H ln\left[\frac{T_{del}}{T(y)}\right] dy \qquad 3.5.2$$

where,

η : Stratification efficiency

ξ : Exergy of stored liquid, J.

m : Mass, kg.

c : Specific heat, J/kg · K.

T_{del} : Temperature at which water is delivered, K.

T_{mean} : Mass weighted mean tank water temperature, K.

T_o : Dead state temperature, K.

H : Tank height, m.

Haller, et al. (2009) pointed out in a review of methods to determine stratification efficiency that with systems that were not used to produce work, the choice of the dead state temperature (T_o) was arbitrary. Different authors have brought forward arguments for different choices of T_o.

Shah and Furbo (2003) evaluated the stratification by calculating the entropy efficiency, (Equation 3.5.3) which is the entropy difference between the fully stratified tank and a fully discharged tank divided by the entropy difference of the actual tank and a fully discharged tank. The fully discharged tank was assumed to be at the cold water inlet temperature, which was also the dead state temperature.

$$\eta_{S,Sh} = \frac{S_0 - S_{str0}}{S_0 - S_{exp}} \qquad 3.5.3$$

Panthalookaran, et al. (2007), pointed out that in the basic approach of the Rosen method to evaluate the difference or the ratio between the exergy (or available energy) contents of a stratified and a fully-mixed tank, the exergy of the stratified tank was evaluated using an equivalent temperature whose definition depends on the energy levels in the real system.

Panthalookaran, et al. (2007) evaluated the thermal performance of a storage tank by calculating the internal entropy generation ratio that was defined as the difference in the entropy change of the actual tank to the entropy change of a perfectly stratified tank, divided by the difference of entropy change of a fully mixed tank and a perfectly stratified (Equation 3.5.4).

$$R_{EG} = \frac{\Delta S_{real} - \Delta S_{stratified}}{\Delta S_{mixed} - \Delta S_{stratified}} \qquad 3.5.4$$

where,

$$\Delta S_{mixed} \geq \Delta S_{real} \geq \Delta S_{stratified}$$

Davidson, et al. (1994), Andersen, et al. (2007) used another method to evaluate the degree of mixing in a tank by a dimensionless number called the MIX-number. It is the difference in the moment of energy between a perfectly stratified tank and the actual tank, divided by the difference in the moment of energy between a perfectly stratified tank and a fully mixed tank (Equation 3.5.5).

$$MIX = \frac{(M_{str} - M_{actual})}{(M_{str} - M_{mix})} \quad 3.5.5$$

where,

M_{str} and M_{mix} : The largest and the smallest values of the moment of energy, respectively, J m.

The moment of energy of a storage tank (M) is an integration of the sensible energy content (E) along its vertical axis, weighted with the height of its location along the vertical axis (y). In practice a summation over i storage segments along the vertical axis is used to calculate M, i.e., by Equation 3.5.6, Haller, et al. (2009):

$$M = \sum_{i=1}^{N} y_i \, . \, E_i \quad 3.5.6$$

y : vertical distance, m.

E : energy, J.

3.6 SUMMARY OF THE LITERATURE REVIEW

Based on the review of previous research projects conducted on thermal stratification in storage tanks, inlet jet mixing, plume entrainment, heat convection, conduction, and envelope losses, the following conclusions can be made:

1. The stratified storage tank improves the solar heating system performance compared to a fully mixed tank temperature.
2. Thermal stratification within the storage tank decreases with increasing water or glycol flow rates.
3. Thermal stratification improves with:
    - increasing tank aspect ratio (*L/D*).
    - increasing the temperature difference (ΔT) between top and bottom of the tank.
    - increasing tank inlet and outlet diameters.
    - placing tank inlet and outlet ports near the tank wall.
    - directing tank inlet flow to the tank wall.
4. Tank inlet design has an impact on stratification. Placing the tank inlet at the bottom of the tank helps stratification.
5. Thermal stratification increases by using a manifold, which introduces the water heated by the heat exchanger to the tank at a level where the temperature of the water in the tank matches the temperature of the heated water.
6. When using an in-tank distribution manifold for hot water delivery, the pressure gradient in the manifold changes by varying either the cross-sectional area of the manifold (*A*) or the frictional characteristics of the manifold (*F*). In such cases, in order to improve the process of hot water delivery from the manifold to the right position, the pressure gradients of the two fluids must be matched.
7. Using a perforated manifold sometimes works more as a ‘‘mixing device’’ than as a stratifying device, because cold tank water may be drawn into the manifold through the lowest opening. Then, mixed fluid enters the tank through the top opening. However, a manifold with flaps working as “non-return valves” may reduce the unwanted flows into the lowest opening.
8. Using a flexible manifold connected to the heat exchanger and controlled by buoyancy forces provides more stratification than a rigid manifold, because of the flexibility of matching the pressure gradients inside and outside the manifold. However, a potential problem is the attachment of air bubbles to the manifold.

9. Thermal stratification is increased by placing a baffle with a gap in the tank center. This is better than a baffle with a gap near the tank wall.
10. Thermal stratification can occur in multi-tank arrangements (both series and parallel arrangements). In addition, parallel storage configurations present better stratification relative to the series case. However, in light of the difficulty of achieving a balanced flow distribution in the parallel flow configuration, system designers may choose to utilize the series configuration. This arrangement has the advantage of allowing the use of low cost conventional hot water storage tanks.
11. It was found from simulation studies that stratification tall tanks (3:1 aspect ratios of *L/D*), was improved when the inlet port is located close to the top.
12. Factors including inlet jet mixing, plume entrainment, heat wall conduction, and heat side losses can cause destratification.
13. If the temperature of the fluid leaving the collector is constant, the possibility of plume entrainment may be eliminated by controlling the flow rate. However it will reduce the collector thermal performance.
14. Conduction though vertical tank walls reduces thermal stratification inside the tank.
15. Convection currents are generated in the fluid if the thermal conductivity of the tank wall is greater than that of the fluid.
16. A tank without insulation stratifies better than a tank with insulation outside the conductive walls, because a tank without insulation has a heat leak to the surrounding so that axial conduction in the wall does not play an important role in the heat transfer processes in the tank.
17. Placing special insulation inside the tank walls enhances stratification; however, insulation placed outside increases the destratification due to the wall thermal conductivity.
18. The reduction of the thermocline is faster in a tank with higher wall thermal conductivity than one with less thermal conductivity; for example, it is ten times higher in an aluminum tank than in a glass tank.

CHEAPER 4: METHODOLOGY PROPOSED TO MEET THE OBJECTIVE

To meet the objective defined in Chapter 2, an approach was chosen involving experiments that utilized an electrical heater and a solar collector as the heat source. The methodologies used for experimental studies of these two are presented below.

4.1 EXPERIMENTAL STUDY

4.1.1. EXPERIMENTAL SET-UP

Experiments were conducted at the Heat Transfer Laboratory in the Department of Mechanical Engineering of Dalhousie University. Two sets of tests were conducted using electrical heaters and solar collectors as the heat source. Electrical heaters were used to simulate the output from a 3-m^2 flat plate solar collector. Experiments were also conducted using a 3-m^2 flat plate solar collector to study the performance of an actual SDHW system. The solar collector was placed on the rooftop of the laboratory building. The SDHW system was installed and modified to work with the immersion heat exchanger/manifold. The immersion heat exchanger was designed and built to be suspended from the top of the tank, and was able to accommodate various manifold designs. A schematic of the experimental set-up is shown in Figure 10.

A computer data acquisition system was used to monitor and record the data required for the thermal performance analyses, as shown in Appendix E. Computer subroutines were written and applied to control two solenoid valves. The first valve was installed in the water supply line to drain the trapped warm water inside the piping within the building to ensure that cold water enters the storage tank. The second valve was to drain the hot water from the top of the tank. To simulate the actual hot water consumption on a daily basis, the hot water was drawn from the storage tank as needed. Data collection was carried out continuously.

A water diffuser (horizontal flat plate) was installed in the bottom of the storage tank to reduce the penetration of the cold water jet into the storage tank, thereby reducing the mixing between the cold water, coming from the water supply, and the warm water, which was already in the tank.

The system was equipped with an air vent to remove the air from the top of the tank. This air vent also acted as a safety valve to protect the system in case of overheating on hot sunny days.

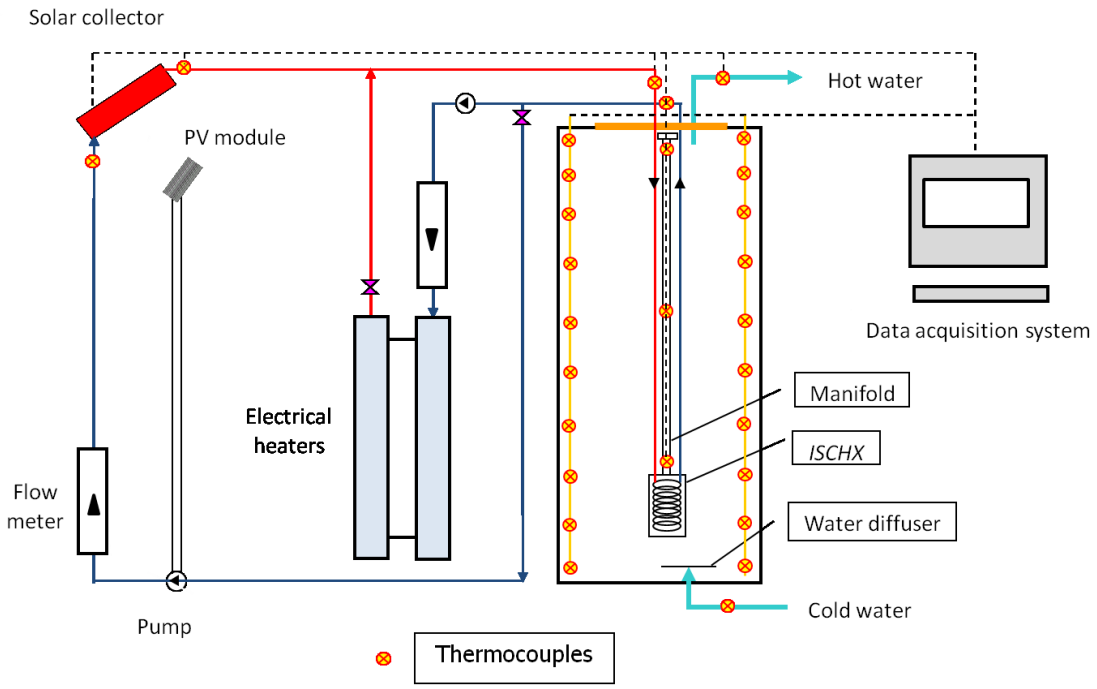

Figure 10 Schematic diagram of DSHW system.

Temperature, pressure and flow transducers were installed in strategic locations, and the data collected by the data acquisition system were recorded at three minute intervals on a dedicated computer on a continuous basis.

After installing the experimental set up, the system was tested against faulty computer control and leakage problems and all problems were satisfyingly addressed.

The experimental set-up consisted of the three major components of the SDHW system, which were the solar collector, the heat exchanger and the storage tank plus accessories. The components of the experimental set-up and the theory to calculate the errors of the measurements are presented in Appendix A and Appendix C, respectively.

4.1.2. EXPERIMENTAL PROCEDURE

4.1.2.1. EXPERIMENTS USING ELECTRICAL HEATERS

The experimental set-up was connected to two electrical heaters that simulate a 3-m^2 flat plate solar collector. These heaters were used to heat the glycol solution in day-to-day experimental tests.

4.1.2.2. EXPERIMENTS USING A SOLAR COLLECTOR

The experimental set-up was connected to a 3-m^2 flat plat solar collector to study the operation of an actual solar domestic hot water system. The solar collector was operated by controlling the hot and the cold paths of the glycol solution as shown in Figure 10.

4.1.2.3. STRATIFICATION MANIFOLD

Four manifolds were designed based on the literature review and experimentation. They were built and tested, then the thermal performance of each manifold was evaluated and compared in terms of tank stratification. The manifolds were installed and removed from the top of the tank through a small cover prepared for that purpose without removing the heat exchanger.

4.1.2.4 EXPERIMENTAL WORK

The following experiments were conducted:

1. System operated with the immersion shell-and- coil heat exchanger (ISCHX) with a longitudinally perforated manifold that extended from the top of the heat exchanger to the top of the tank to deliver the water heated by the heat exchanger to the tank in order to enhance the stratification as shown in Figure 10, then its thermal performance was studied in terms of the tank stratification, in order to determine the advantages and disadvantages of this design.
2. Enhancement of the longitudinally perforated manifold design with the objective of improving the process of delivering the heated water by the immersion heat exchanger to the storage tank at the level where the temperature of the water in the tank matches the temperature of the heated water, thereby enhancing stratification.

This was done by testing and comparing the performance of different types and sizes of perforated manifolds operated under the same heat load.

3. Each manifold design was tested under three simulated heat loads. Two represented a Nova Scotia sunny day and a cloudy day while the third load was a constant amount of heat added to the storage tank (20 MJ of electrical energy) by using the two electrical heaters. To achieve this mode of operation, isolation valves were closed to remove the solar collector from the glycol circuit as shown in Figure 10.
4. Tested the selected manifold design under actual conditions using a solar collector by controlling the isolation valves to operate the solar collector and isolate the electrical heaters as shown in Figure 10.

CHEAPER 5: SYSTEM ANALYSIS

The data acquisition system created a data file for the system parameters and storage tank temperatures for each test. These data were required for system performance analysis.

Each manifold design was tested under three simulated heat loads, two of which represented a sunny day and a cloudy day in Nova Scotia and were associated with the flow rate profiles as shown in Figures 11, 12. The third test represented a total heat load of 20 MJ added to the storage tank by two electrical heaters. This was achieved with two hours of electrical heating at a constant 2750 W and a glycol flow rate of 1.74 L/min.

Figures 11, 12 show the electric power and the associated glycol flow rate used to simulate the solar collector on sunny and cloudy days, versus the hour of the day. The simulation data for these tests were taken from previous experiments. These experiments were performed by the author on a sunny day (June 14, 2002) and cloudy day (June 15, 2002).

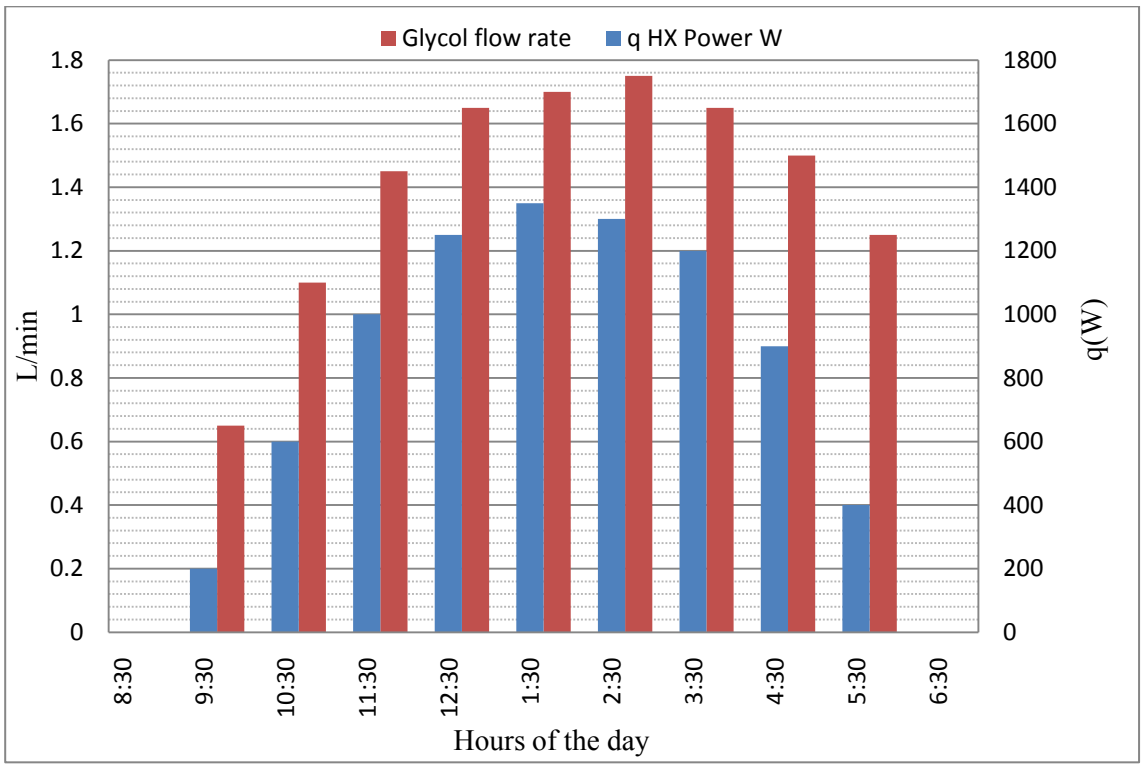

Figure 11 Electrical heat profile and glycol flow rate in simulating a clear sunny day.

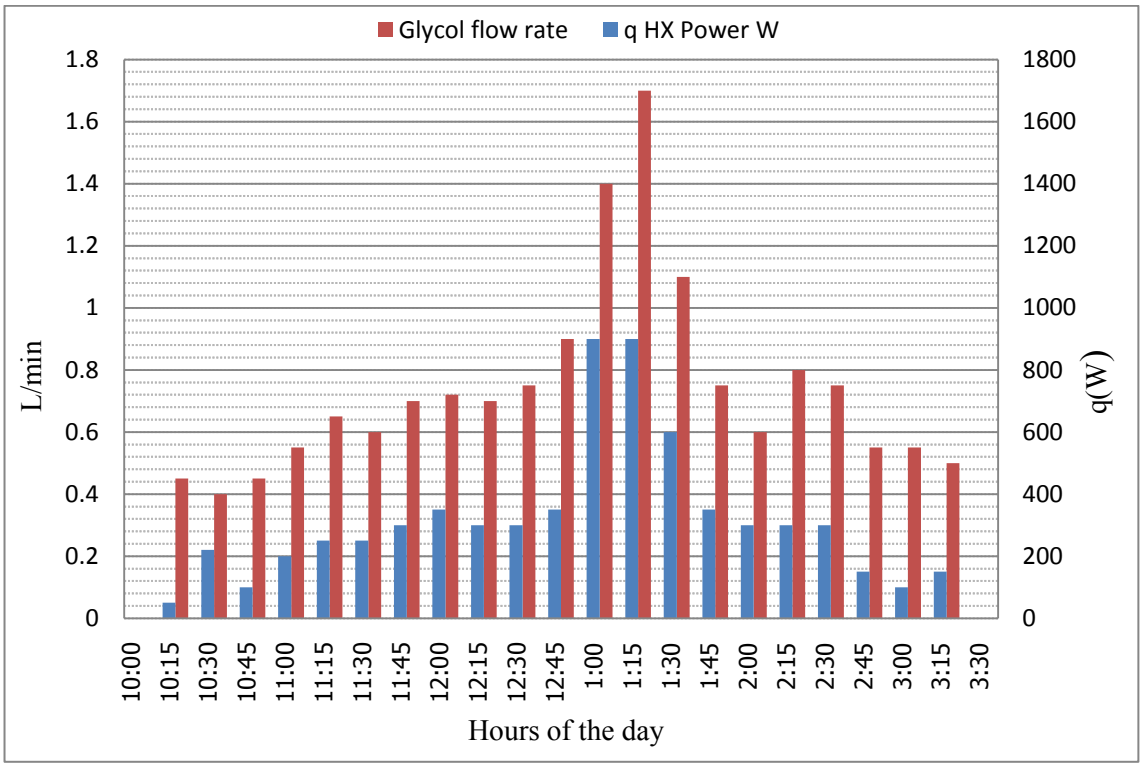

Figure 12 Electrical heat profile and glycol flow rate in simulating a cloudy day.

On those particular days, the variations in glycol flow rate were related to the weather conditions because the glycol pump was powered by a photovoltaic module. In this test, the glycol pump was driven by a DC motor powered by a DC power supply. The glycol flow rate is a function of DC motor voltage and current which, in reality, varied according to the solar radiation incident on the PV module. Although the sun rose before 8:30 AM on the sunny day for example, the pump did not start until 8:30 AM. This was related to the pump threshold current (the necessary current to start the pump). The flow rate in the afternoon was higher than in the morning because the glycol was hotter and less viscous after several hours of being heated. For example, as shown in Figure 11, the flow rate was 1.1 L/min at 600 W in the morning but 1.4 L/min at the same *HX* power in the afternoon. The peak glycol flow rate was 1.75 L/min, which occurred at 2:30 PM, while the peak electric power occurred at 1:30 PM (1300 W). In this case, the relatively high glycol flow rate for the ISCHX was due mainly to the lower flow resistance in the heat exchanger.

In order to test the manifold under a variety of conditions, each manifold was subjected to three simulated heat loads and three initial tank conditions (mixed tank, hot tank, and cold tank temperature) as explained in Chapter 6.

5.1 TEMPERATURE MEASUREMENT

Copper-constantan thermocouples (TT-T-24) were used to measure all temperatures. Forty-five thermocouples were installed in appropriate locations in the experimental set-up to measure the water, glycol, and air temperatures. Seven thermocouples, [chB(1) - chB(7)], were installed inside the manifold from the bottom to the top and in front of each opening to measure the heated water temperature as shown in Figure 13.

An additional twenty-two thermocouples were installed in two probes located in two corners of the tank to measure the temperature from the top to the bottom, ten of which were installed in a copper probe (Tbot, T2 - T9, Ttop), while the other twelve were installed in stainless steel probe (Tssx, Tssbot, Tss2 - Tss9, Tsstop, Tssy). The stainless steel probe was placed in a corner of the tank, as illustrated in Figure 14. The twelve thermocouples divided the tank into twelve layers. The Tssx and Tssy thermocouples were installed at the bottom and top edges of the tank, respectively, thus, these thermocouples covered only half layers compared to the other ten thermocouples.

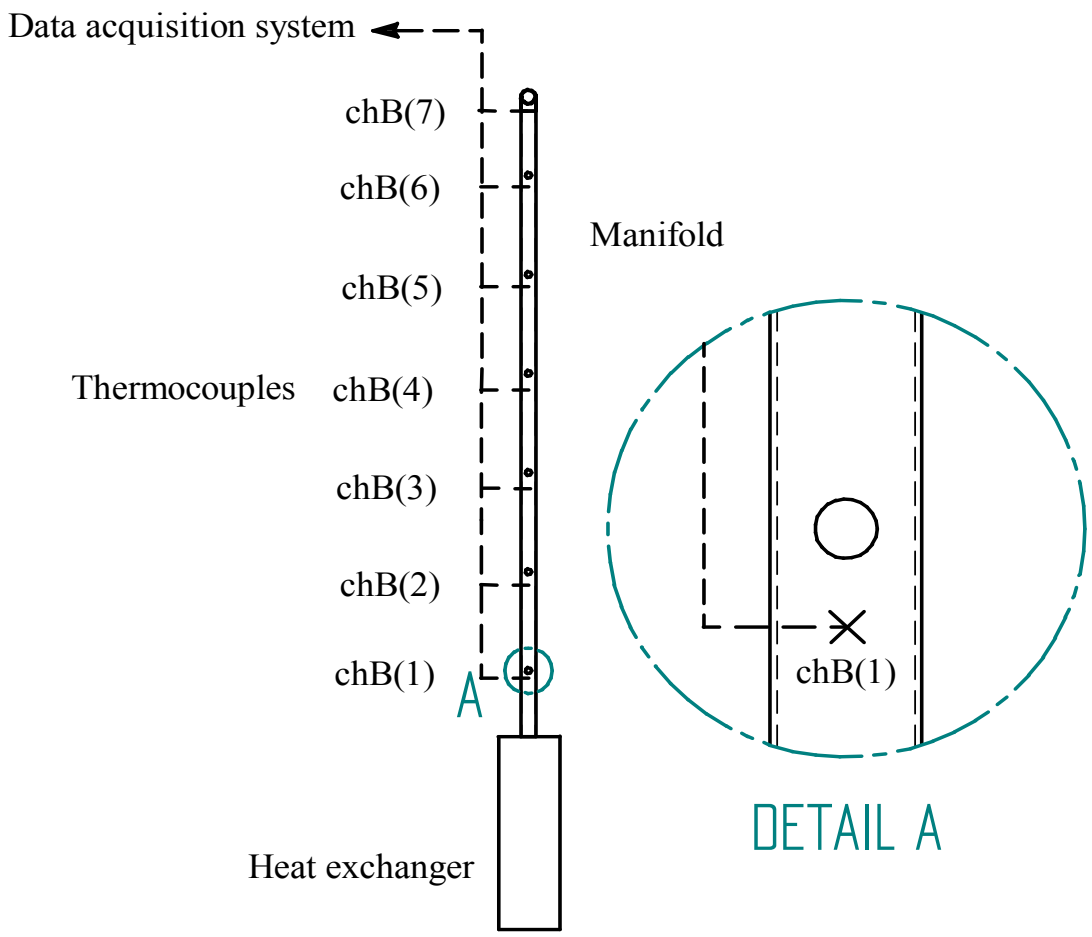

Figure 13 Diagram of typical manifold with the location of the thermocouples.

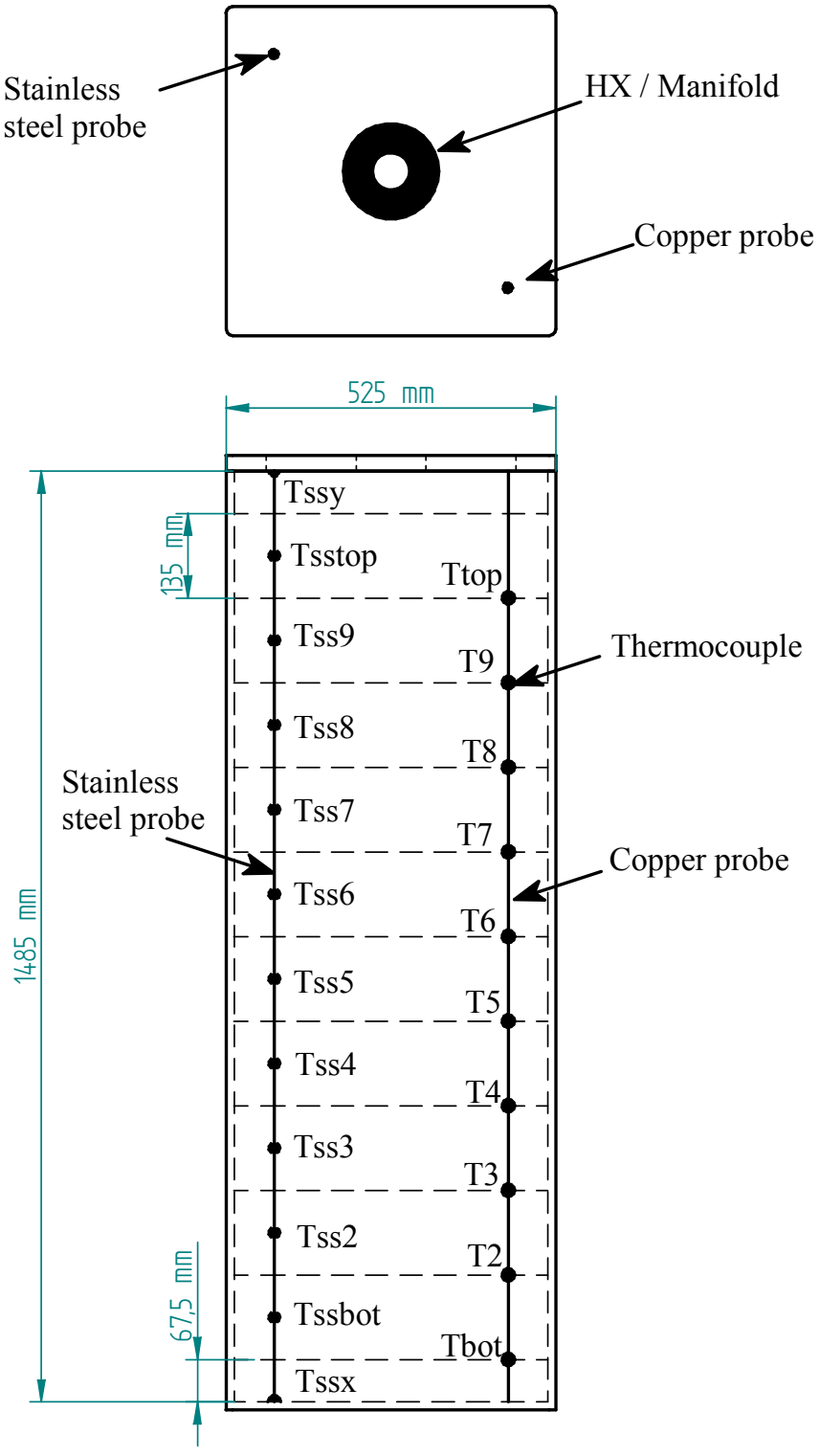

Figure 14 Locations of thermocouples for the two probes.

Figure 15 shows the temperature profiles as measured by the two probes. Figure 15 indicates that the temperature distributions inside the storage tank measured with the two probes were identical, therefore, the stainless steel probe data were used in the thermal performance analysis.

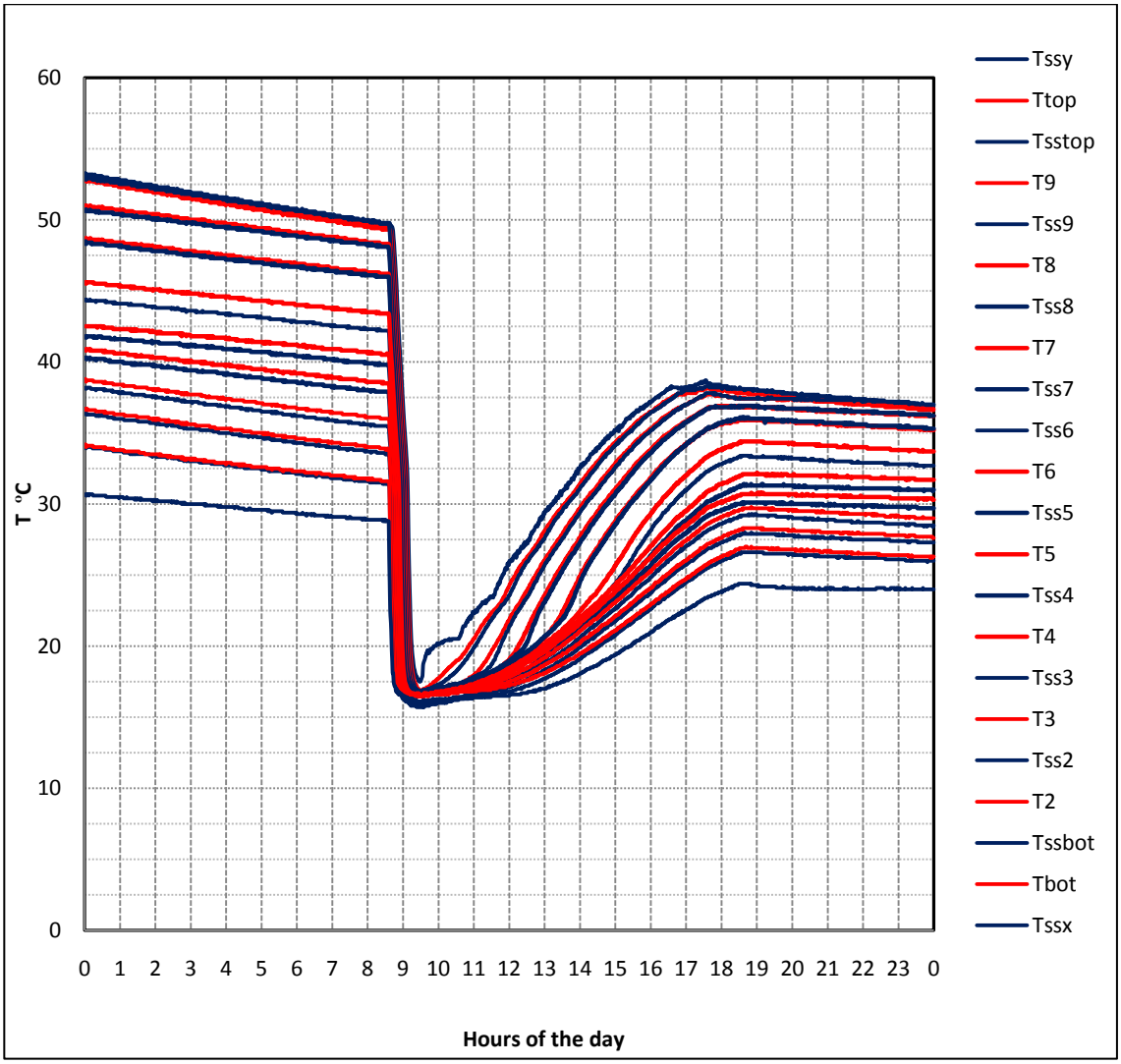

Figure 15 Temperature distribution inside the tank, as measured by the two probes.

5.2 BUOYANCY-INDUCED FLOWS

Water flow in the tank and the heat exchanger was controlled by natural circulation. This flow was the result of the density difference between the water inside and outside the heat exchanger and water at the bottom and top of the tank. This density difference created a pressure difference that resulted in natural circulation. The pressure difference were calculated using Equation 5.2.1. Controlling this flow without the complexity and expense of mechanical or electrical equipment reduced mixing and enhances stratification, thereby lowering the entropy inside the storage tank and increasing the availability of energy.

$$\Delta P = P_{tank} - P_{HX} = \sum_{i=1}^{n} h_i g \rho_{Tw} - \sum_{i=1}^{n} h_i g \rho_{HXw} \qquad 5.2.1$$

where,

ΔP : The differential pressure at the bottom, Pa.

P_{tank} : Pressure at the bottom of the tank, Pa.

P_{HX} : Pressure at the bottom of the heat exchanger, Pa.

i : Number of thermal layers in the tank.

h : Thickness of the thermal layer of the water in the tank, m.

g : Acceleration of gravity, m/s^2.

ρ_{Tw} & ρ_{HXw} : The density of the water inside the tank and inside the heat exchanger at level i, kg/m^3.

To illustrate this, consider the tank used in the experimental set-up with an immersion heat exchanger attached to a perforated manifold, as shown in Figure 16. Assume that the tank is stratified linearly, from 20ºC at the bottom of the tank to 66ºC at the top as shown in the Figure 16. The density varies from 998 kg/m^3 at the bottom to 980 kg/m^3 at the top of the tank. The 1.48 m column in the tank exerts a pressure of 13,771 Pa at the bottom of the tank. Assume that the water has been heated by the heat exchanger to a temperature of 50ºC. The average density of the water inside the heat exchanger is 988 kg/m^3. The pressure at the bottom of the heat exchanger and manifold column is

13,743Pa. The pressure exerted by the cold column creates a net pressure differential of 28 Pa. This pressure is available to circulate the heated water through the heat exchanger and perforated manifold and deliver it to the tank at 50ºC. At that layer, the temperatures match and the pressure difference equals zero.

A conventional hydraulic analysis of the ISCHX with a manifold is required to determine the flow rate that results from a pressure differential of 28 Pa. Not all of this pressure is available to deliver the heated water, as some pressure will be lost through the heat exchanger (the sharp entrance, shell, and sudden contraction of the heat exchanger) and the manifold pipe.

Values for pressure drops in the heat exchanger and the manifold can be calculated using Equations 5.2.2 to 5.2.6.

The pressure drop at the sharp entrance of the heat exchanger, which is 6 mm in diameter, can be calculated using Equation 5.2.2: Çengel and Cimbala (2006)

$$\Delta P = K_L \frac{1}{2} \rho V^2 \qquad 5.2.2$$

where, $K_L = 0.5$; the loss coefficient of the sharp entrance of the heat exchanger.

	(mm) from top	SS probe	T_{tank} (ºC)	ρ_{tank} (kg/m^3)	$T_{manifold}$ (ºC)	$\rho_{manifold}$ (kg/m^3)	P_{tank} (Pa)	$P_{manifold}$ (Pa)	ΔP (Pa)
	68	Tssy=	66	980	66	980	0	0	0
	135	Ttop=	64	981	64	981	650	650	0
	203		62	982	62	982	1300	1300	0
	270	T9=	59	983	59	983	1951	1951	0
	338		57	984	57	984	2603	2603	0
	405	T8=	55	985	55	985	3255	3255	0
	473		53	986	53	986	3908	3908	0
	540	T7=	51	987	51	987	4562	4562	0
	608		48	988	50	988	5217	5216	0
	675	T6=	46	989	50	988	5872	5870	1
	743		44	990	50	988	6527	6524	3
	810	T5=	42	991	50	988	7183	7178	5
	878		40	992	50	988	7840	7832	8
	945	T4=	38	993	50	988	8497	8486	11
	1013		35	993	50	988	9155	9140	15
	1080	T3=	33	994	50	988	9813	9794	19
	1148		31	995	45	990	10472	10449	22
	1215	T2=	29	995	40	992	11131	11106	25
	1283		27	996	35	993	11790	11764	27
	1350	Tbot=	24	997	30	995	12450	12423	28
	1418		22	997	25	996	13111	13082	28
	1485	Tssx=	20	998	20	998	13771	13743	28

Figure 16 Water temperature, pressure and density in the storage tank.

The pressure drop associated with flow across a tube bank (the coils of the heat exchanger as shown in Appendix A) was calculated using Equation 5.2.3: Incropera and DeWitt (2002)

$$\Delta P = N_L \chi \left(\frac{\rho V^2{}_{max}}{2} \right) f \qquad 5.2.3$$

where,

N_L=40 Number of the tubes crossing the flow.

χ =1.1 Correction factor.

$f = 5$ Friction factor.

The pressure drop at the sudden contraction was calculated using Equation 5.2.4: Çengel and Cimbala (2006).

$$\Delta P = K_L \frac{1}{2} \rho V^2 \qquad 5.2.4$$

where,

K_L = 0.405; The loss coefficient of the sudden contraction of the heat exchanger.

The pressure drop through the manifold was calculated using Equation 5.2.5: Çengel and Cimbala (2006)

$$\Delta P = h_L \, \rho \, g \qquad 5.2.5$$

where,

h_L: The head loss in the manifold was calculated using the *Darcy-Weisbach* Equation 5.2.6 for fully developed steady incompressible pipe flow:

$$h_L = f \frac{L}{D} \frac{V}{2g}^2 \qquad 5.2.6$$

Figure 17 show the pressure drops through the heat exchanger/manifold calculated using Equations 5.2.2 to 5.2.6 and using standard immersion heat exchanger dimensions

(Appendix A, Figures 62 and 63) and a manifold made of 19 mm ID pipe for different flow rates.

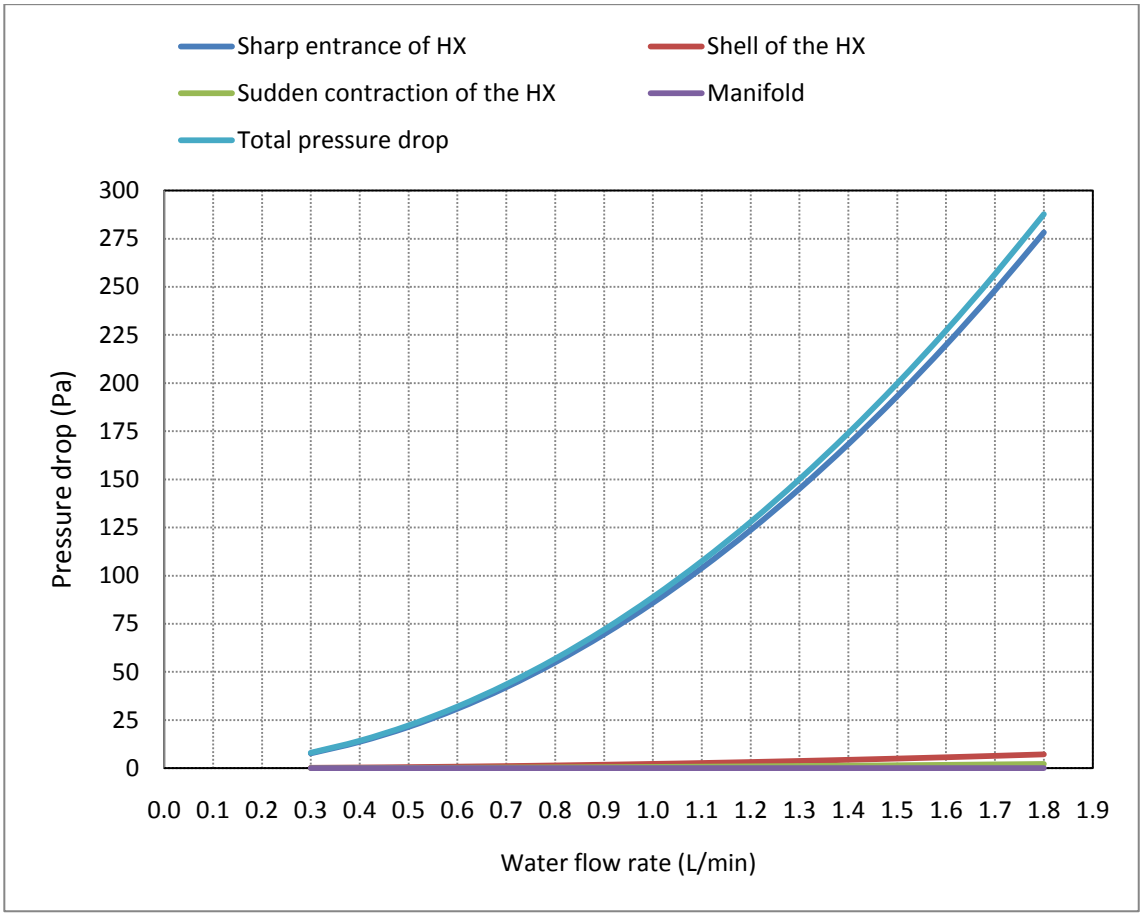

Figure 17 Pressure drop through the heat exchanger and manifold.

Figure 18 shows the water temperature at the heat exchanger outlet and the water flow rate through the heat exchanger for the test simulating a sunny day. A water temperature of 50ºC was associated with a flow rate of 0.5 L/min (0.008 kg/m^3) at 10:30 AM through the heat exchanger/manifold. From Figure 17, the pressure drop through the heat exchanger and the manifold at 0.5 L/m was 23 Pa, which left a 5 Pa (28 Pa - 23 Pa) pressure differential in the thermosiphon loop to drive the water through the manifold exit hole. This remaining pressure-differential-producing flow required a 0.01 m diameter hole to leave the manifold at the matching layer and calculated using Equation 5.2.7.

$$\Delta P = \frac{\rho V^2}{2} = \frac{\dot{m}_w{}^2}{2\rho\left(\pi\frac{D^2}{4}\right)^2} \qquad 5.2.7$$

where,

ΔP : The differential pressure

$\dot{m}_w$: The heated water flow rate through the manifold, kg/s.

ρ : The density of water at the outlet of the heat exchanger, kg/m^3.

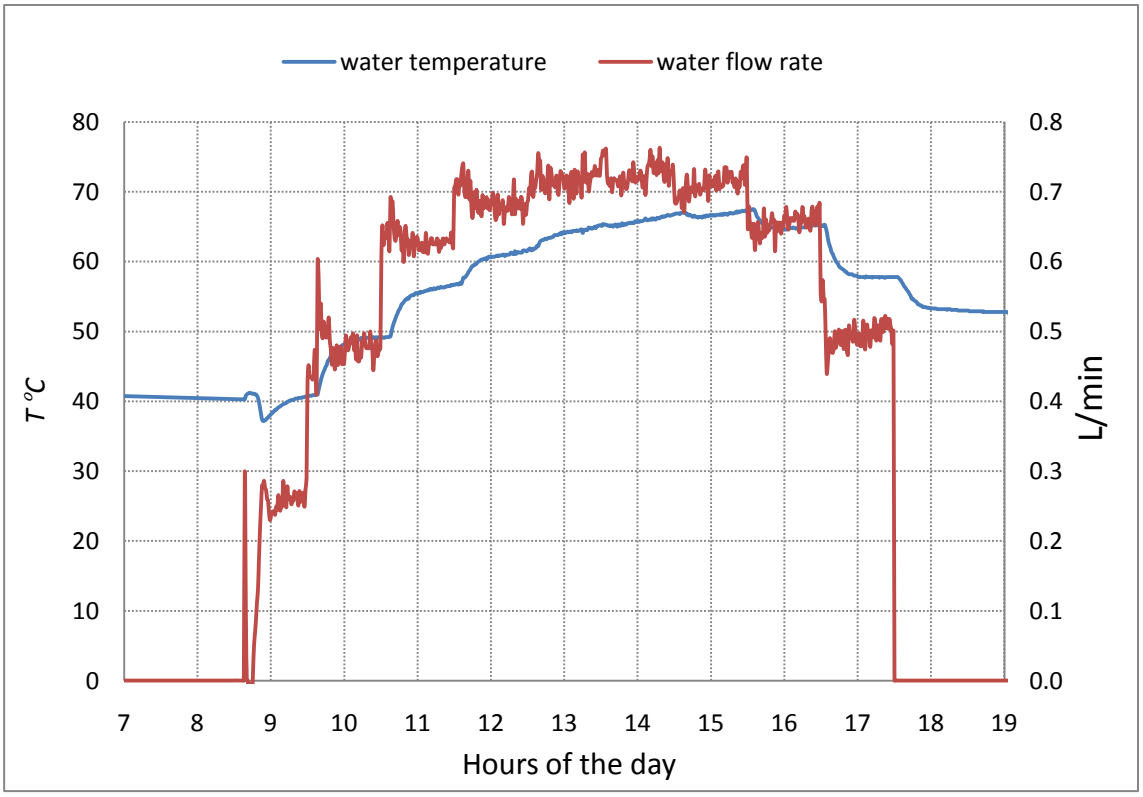

Figure 18 Water temperature at the heat exchanger outlet and water flow rate through the manifold.

With temperatures in the tank different than these shown in Figure 18 (38ºC to 66ºC), the buoyancy-induced forces were different, as the water flow rates until a hydraulic balance was achieved in the thermosiphon loop. This led to a higher or lower water outlet temperature, which will tend to increase or decrease the water flow rate.

Figure 19 shows the pressure difference between the column in the tank and the column in the heat exchanger versus the height of the storage tank starting from the top of

the tank, assuming that the water in the tank was linearly stratified from 20ºC to 66ºC and all hot water delivered to the top of the tank. The plot is for a system with 20 mm piping and water flow rate in a range of (0.3 - 2.5 L/min). Similar plots are expected for larger systems and larger diameter piping and stratifiers.

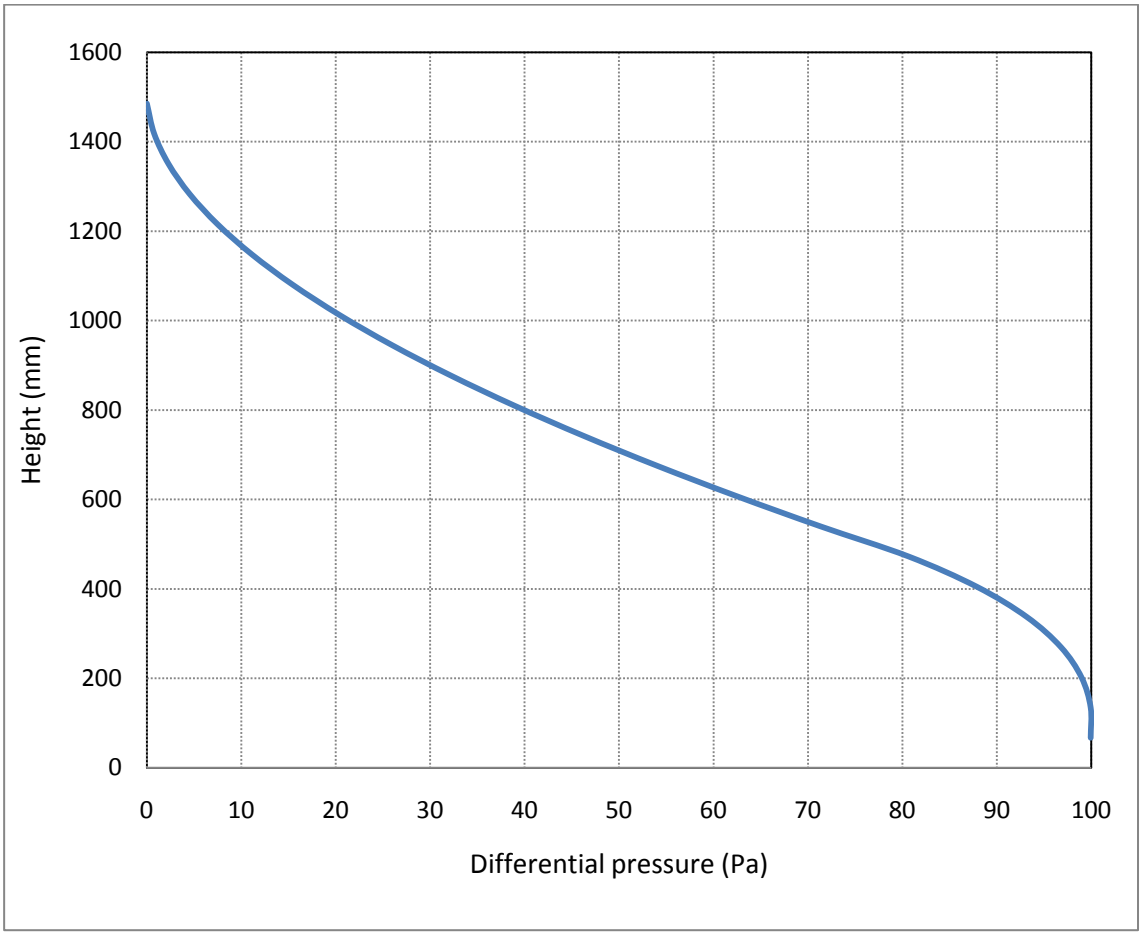

Figure 19 Differential pressure vs. tank height

In the case of a perforated manifold, this pressure difference drove the cold water from the tank into the lowest opening of the manifold as shown in Figure 20. The mixing of cold and hot water reduced the pressure differential between the tank and the manifold, due to the reduction of the temperature in the manifold. In addition, the higher flow rate in the manifold produced higher velocities, which increased the head losses in the manifold, again reducing the differential pressure difference between the tank and the

manifold. Equilibrium was established at a greatly reduced pressure differential, but significant degradation of the effectiveness of the manifold had taken place.

The implication of Figure 19 is that there should be a significant resistance to the flow of water from the tank into the manifold to reduce the flow of cold water from the lower portion of the tank into the manifold.

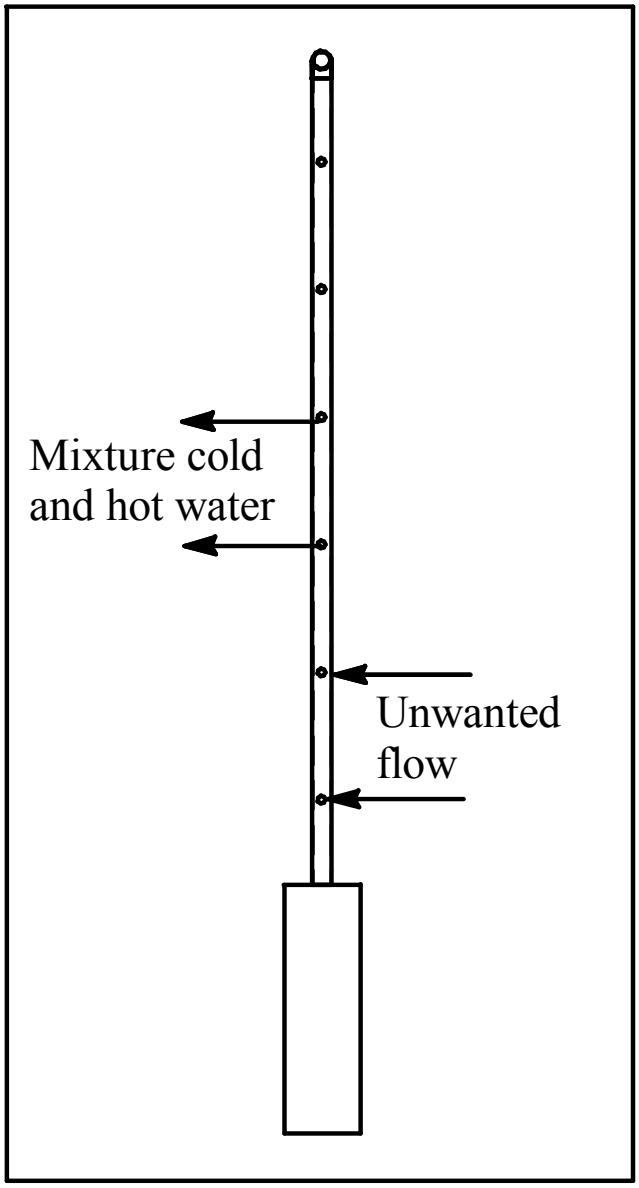

Figure 20 Diagram shows the unwanted flow from the tank to the manifold.

5.3 EVALUATION OF MANIFOLD PERFORMANCE

An availability analysis was used to quantify the level of stratification inside the storage tank and a merit factor was developed to evaluate the manifold thermal performance for each test. The availability changes were calculated based on the measured temperatures inside the tank. Five conditions were employed to evaluate the thermal performance of the various manifold designs that were designed and tested.

In the analysis, the variation of the tank availability during the tests for the actual tank (actual tank was the real tank while the fully mixed and the perfectly stratified tank were calculated tanks) and a perfectly stratified tank and fully mixed tank were calculated and plotted. The availability plots for the perfectly stratified and fully mixed tanks are based on calculated data, whereas the availability plots for the actual tank were based on measured data.

In the calculations for the perfectly stratified tank, the tank was divided into a top and bottom part. The temperature of the top part was equal to the temperature at the top of the actual tank at the end of the test, while the temperature of the bottom part was the dead state temperature. The mass of each part was based on the top and bottom temperatures, the energy stored in the actual tank and the energy added during the test. The fully mixed tank has the average temperature of the actual tank. The energy stored in the final actual (final actual tank was the actual tank at the end of the test), the perfectly stratified, and the mixed tanks were equal.

The evaluation of the performance of the various manifolds was based on a comparison of the availability and the entropy of the actual tank with the availability and the entropy of the perfectly stratified and fully mixed tanks. Availability and entropy ratios were calculated to compare the thermal performance of the manifolds. The most efficient manifold was the one resulting in a tank availability that was closest to the availability of a perfectly stratified tank. In other words, the most efficient manifold was the one resulting in higher availability and entropy ratios.

To evaluate the performance of a manifold using the above strategy, the thermal performance parameters of the system for the final actual, the mixed and the perfectly

stratified tank were calculated. These included the amount of heat stored in the tank and the heat lost from the tank. The availability of energy from the tank and the merit factor of the tank were then calculated based on entropy and enthalpy inside the tank.

The heat addition to the tank, Q_{added}, was calculated with respect to the energy contained in the tank at the beginning of the day, and was determined using Equation 5.3.1

$$Q_{added} = Q_{end} - Q_{start} \quad 5.3.1$$

where,

Q_{end} : heat stored at the end of the test, MJ.

Q_{start} : heat stored at the beginning of the test, MJ.

Both Q_{end} and Q_{start} are computed using Equation 5.3.2

$$Q = m_w C_{Pw} T_{Tank,ave} \quad 5.3.2$$

where,

m_w : Mass of the layer, kg.

C_{pw} : Water specific heat J/kg · K.

$T_{Tank\ ave}$: Tank average temperature at the start and the end of the test, ºC.

The tank was insulated from the surrounding after calculating the rate of heat loss from the tank by Equation 5.3.3

$$q_{lost} = h\,A\,(T_{tank,ave} - T_{air}) \quad 5.3.3$$

where:

A : Total tank area, m^2.

h : Overall heat transfer coefficient of the tank, $W/m^2 \cdot K$.

T_{air} : Temperature of the air around the tank, ºC.

The availability of the storage tank was the maximum work that can be obtained from the tank, as it comes into equilibrium with the dead state temperature. The availability of the energy in the storage tank (A_{Tank}) was calculated using Equation 5.3.4

$$A_{Tank} = \frac{m\left(\sum_{i=12}^{i=1}[(h_i - h_o) - T_o(s_i - s_o)]\right)}{1000} \quad 5.3.4$$

where:

A : Availability of energy in the tank, MJ.

m : Mass of the tank, kg.

i : Layer number.

h_i : Specific enthalpy of the layer, kJ/kg · K.

h_o : Dead state specific enthalpy, kJ/kg · K.

T_o : The dead state temperature[2], ºC.

s_i : Specific entropy of the layer, kJ/kg · K.

s_o : Dead state specific entropy, kJ/kg · K.

To calculate the availability of the perfectly stratified tank, the tank was divided into a top and bottom part. The top part had the actual tank top temperature, at the end of the test, and the bottom part had the dead state temperature. Since the bottom part of the perfectly stratified tank had the dead state temperature, the availability of the bottom part was zero. The mass of each part is calculated based on its temperature and the energy added during the test. The mass of the top part was calculated by Equation 5.3.5

$$m_{Top} = \frac{Q_{added}}{C_p\left(T_{Top} - T_0\right)} \quad 5.3.5$$

where:

[2] The dead state (reference) temperature (T_o) used for availability analysis is a critical parameter for proper assessment of the thermal performance of the system. This temperature should represent a state where the energy is no longer useful to the user of the system. For a SDHW system, the dead state temperature can be the cold water supply temperature or the temperature at the bottom of the tank or the minimum bottom temperature of the tank or the average tank temperature, since water is colder than the selected reference temperature has no useful energy for the user of system.

m_{Top} : The mass of the top part of the perfectly stratified tank, kg.

Q_{added} : The amount of energy added to the tank during the test, kJ.

C_p : Water specific heat kJ/kg · K.

To quantify the level of stratification in the storage tank (a reflection of the thermal performance of the manifold), a merit factor and availability and entropy ratios were calculated using Equations 5.3.7, 5.3.8.a, 5.3.8.b, 5.3.9. The availability ratios were used to compare the availability in the tank (at the end of the test) to the maximum availability. The maximum availability is the availability of a perfectly stratified tank.

$$F_{merit} = 1 - \frac{S_{Per} - S_{final\ actual}}{S_{per} - S_{mix}} \quad 5.3.7$$

$$A_{Ratio} = \frac{A_{final\ actual} - A_{ini}}{Q_{added}} \quad 5.3.8.a$$

$$A_{Ratio} = \frac{A_{final\ actual}}{A_{per}} \quad 5.3.8.b$$

$$S_{Ratio} = \frac{S_{per}}{S_{final\ actual}} \quad 5.3.9$$

S_{per} : Entropy of the perfectly stratified tank at the end of the test, kJ/K.

$S_{final\ actual}$: Entropy of the actual tank at the end of the test, kJ/K.

S_{mix} : Entropy of the fully mixed tank at the end of the test, kJ/K.

$A_{final\ actual}$: Availability of the actual tank at the end of the test, MJ.

$A_{initial}$: Availability of the initial tank at the end of the test, MJ.

A_{per} : Availability of the perfectly stratified tank at the end of the test, MJ.

Equations used to calculate the specific heat and the specific entropies and the specific enthalpies are in Appendix B.

The heat exchanger transfer rate ($\dot{q}$) was calculated by Equation 5.3.10

$$\dot{q}_{hx} = \dot{m}\, C_{pg} \left(T_{g,i} - T_{g,o}\right) \qquad 5.3.10$$

where,

$\dot{m}$: Glycol flow rate, kg/s.

C_{pg} : Glycol specific heat, kJ/kg · K.

$T_{g,i}$: Glycol inlet temperature to the heat exchanger, ºC.

$T_{g,o}$: Glycol outlet temperature from the heat exchanger, ºC.

5.4 MANIFOLD DESIGNS

The purpose of the manifold was to deliver the water heated by the heat exchanger to the correct level of the tank in order to enhance and maintain tank stratification. Four manifolds were designed, constructed and tested. The four manifolds were tested at three conditions which simulated (*i*) a fixed heat input to the tank (20 MJ of electrical energy over 2 hours), (*ii*) a sunny day and (*iii*) a cloudy day in Nova Scotia. Each test started with a mixed, cold, and a hot tank temperature. That led to nine tests for each manifold.

5.4.1 MANIFOLD #1

The first manifold was a basic design, consisting of a ¾ inch (19 mm ID and 22 mm OD) nominal diameter copper tube (type M) attached to the heat exchanger, with only horizontal water delivery ports at the top, to deliver the heated water to the top of the storage tank. Figure 21 shows the dimensions of the manifold.

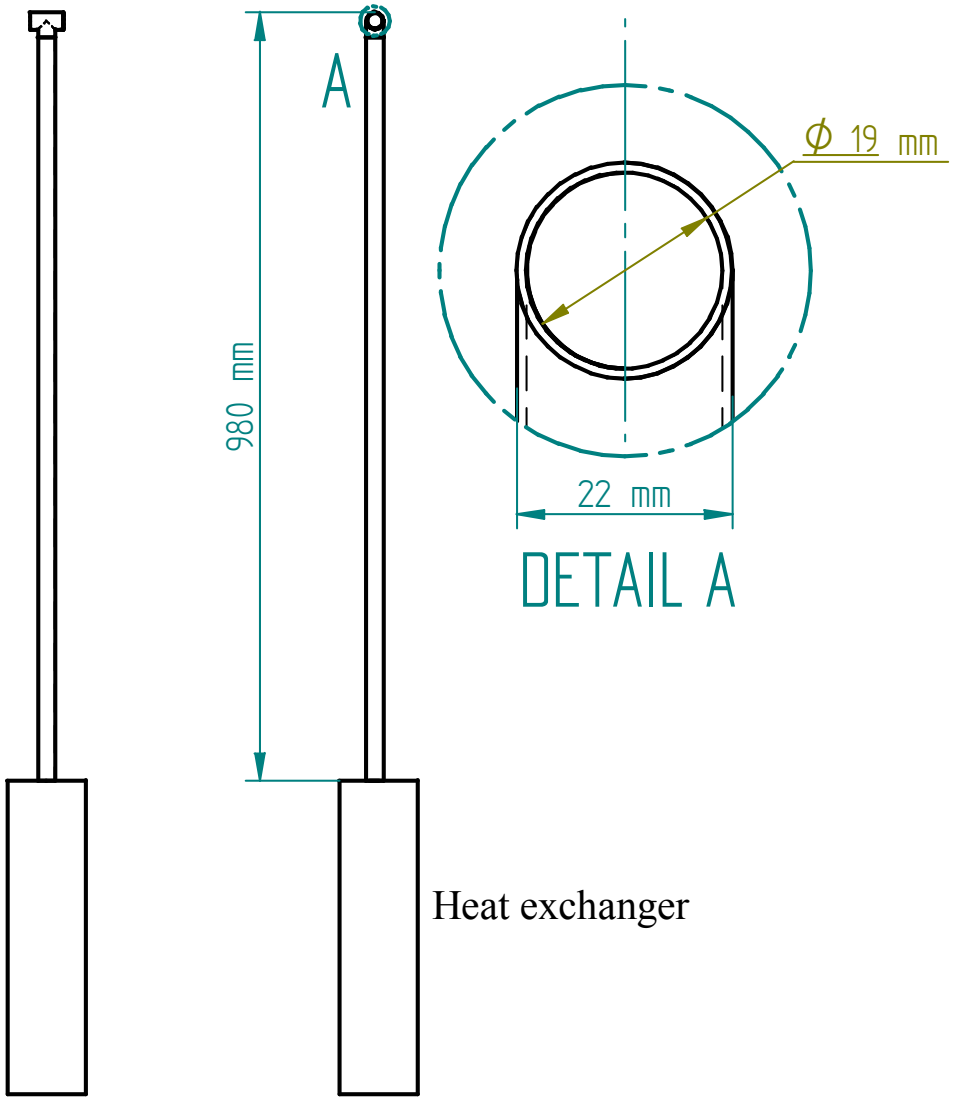

Figure 21 Dimensions of manifold #1.

5.4.2 MANIFOLD #2

Manifold #2 was a perforated manifold that consisted of a ¾ inch nominal diameter copper tube (type M) with seven ports, six at 9 mm in diameter and one (at the top) at 19 mm. This manifold was mounted on the immersion heat exchanger inside the tank. Figure 22 shows the dimensions of the perforated manifold.

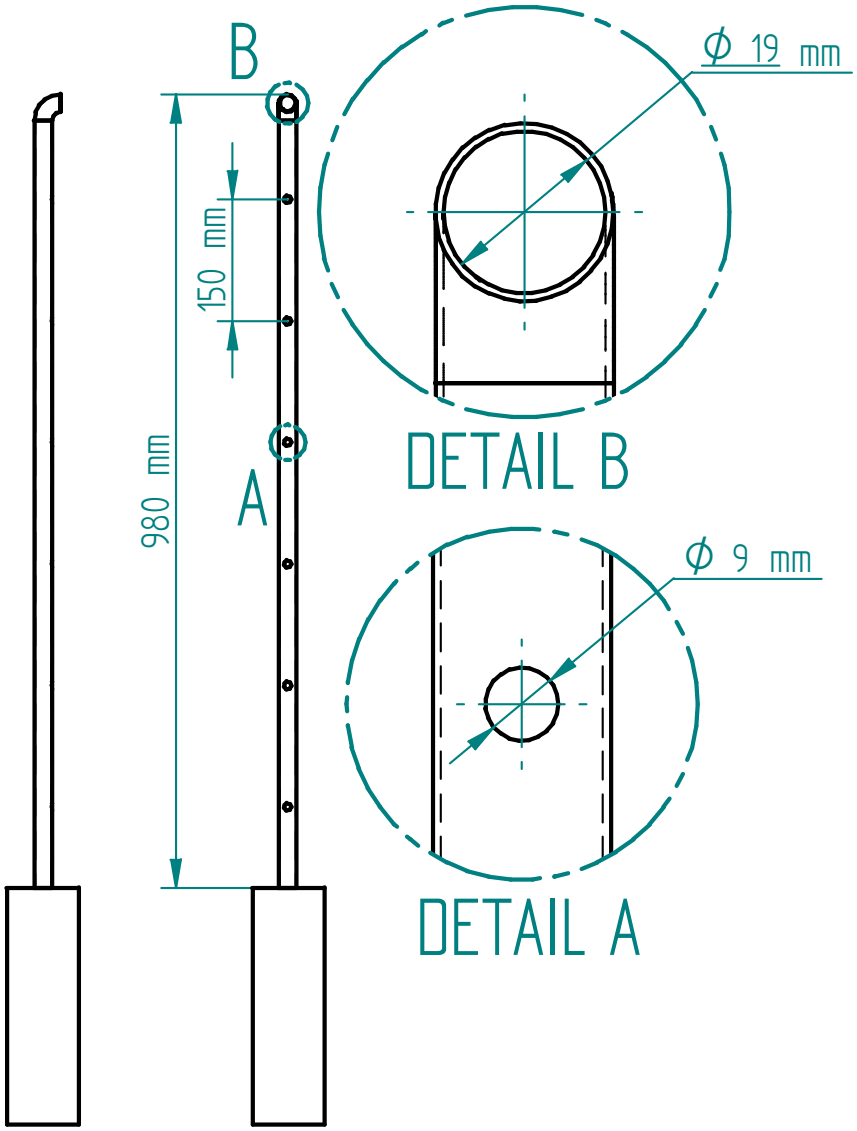

Figure 22 Dimensions of manifold #2.

5.4.3 MANIFOLD #3

Manifold #3, like manifold #2, was also a perforated manifold comprised of a ¾ inch diameter nominal copper tube (type M) with seven ports. In manifold #3, the diameters of the six small ports were 3 mm instead of 9 mm, as shown in Figure 23.

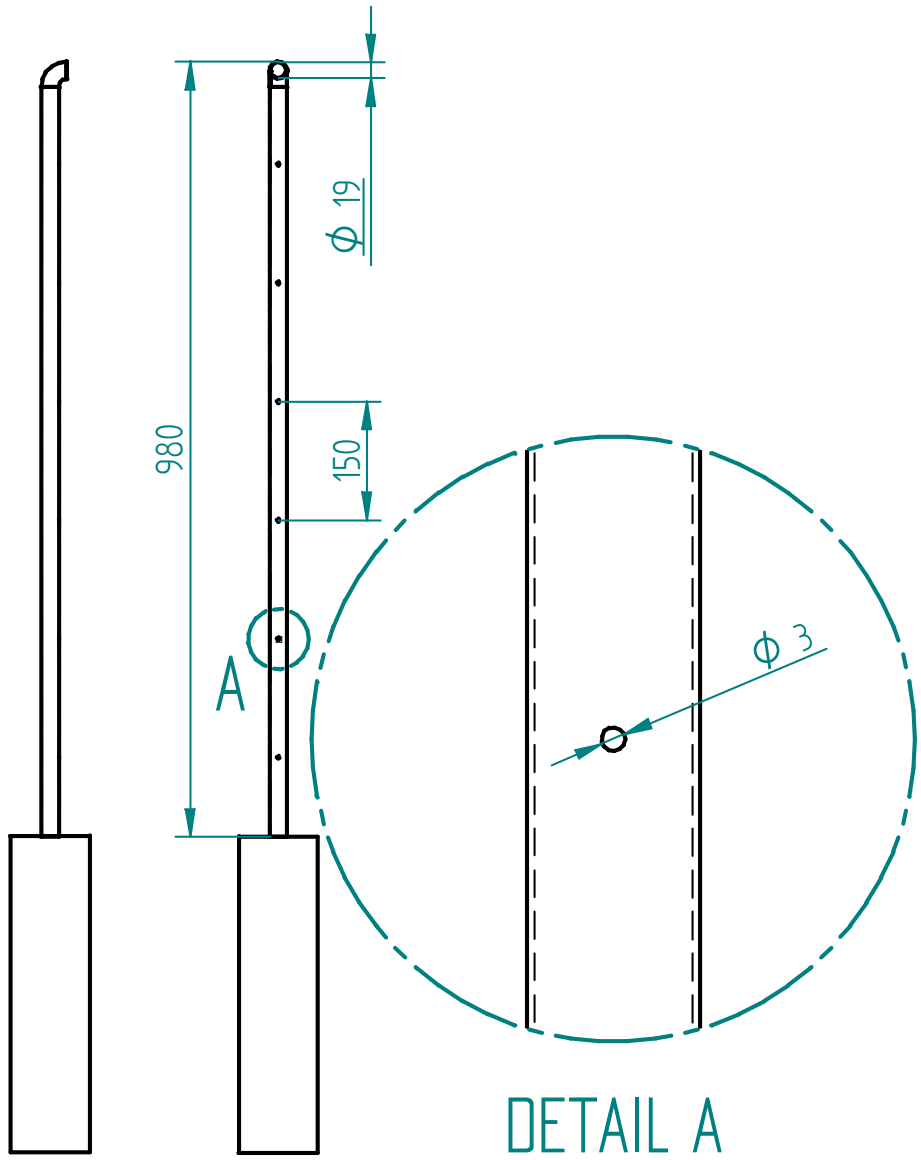

Figure 23 Dimensions of manifold #3.

5.4.4 MANIFOLD #4

Manifold #4 was designed to eliminate or reduce the undesired flow into the manifold through the lowest ports (due to the differential pressure at the bottom of the tank) and to perform satisfactorily in different heating conditions for the system (such occur on a cloudy or a sunny day, or starting with a hot, cold or mixed tank). Also, based on the discussion in Section 5.2, the differential pressure decreased gradually from the bottom to the top of the manifold. Therefore, it was expected that the manifold with different hole diameters, with the smallest diameter at the bottom of the manifold and then increasing gradually to the largest diameter at the top performed better. This design reduced unwanted flow from the tank through the lowest port and also reduced the hydraulic resistance at the top port of the manifold, allowing the heated water to exit the manifold at the level where the differential pressure between the two columns was zero.

The manifold pressure distribution included all dynamic pressure drops in the manifold/heat exchanger. Therefore, the fourth manifold was designed as a ¾ inch nominal diameter copper tube (type M) with seven ports. The port diameters on manifold #4 increase from 5 mm at the bottom of the manifold to 19 mm at the top, as shown in Figure 24.

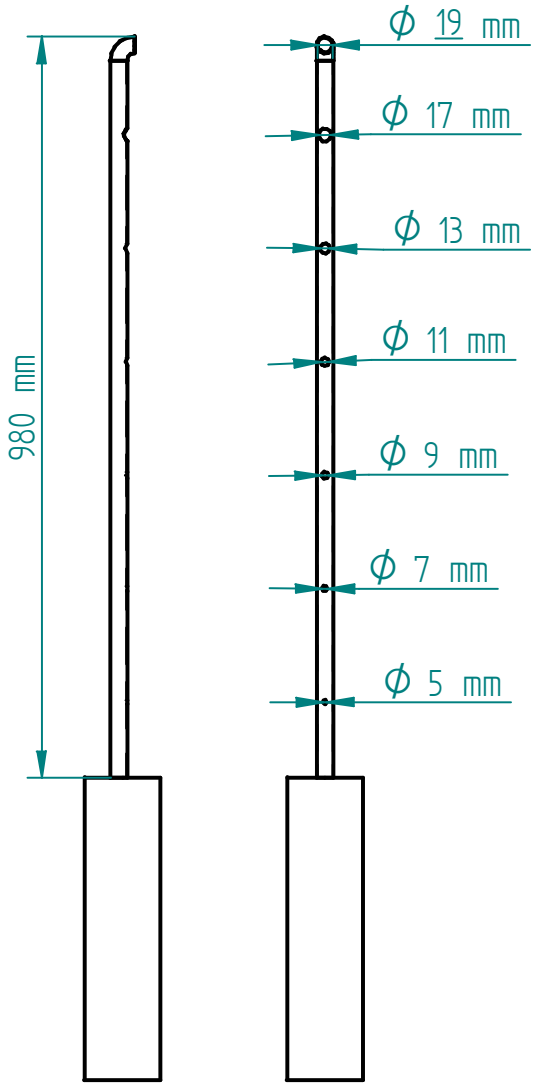

Figure 24 Dimensions of manifold #4.

CHEAPER 6: RESULTS AND DISCUSSIONS

In this section, the results of all experimental tests are presented and discussed. In addition, comprehensive comparisons between test results are discussed. Based on the findings of this work, design guidelines for SDHW system manifolds and immersion heat exchangers were developed.

Thirty-six tests were conducted on four manifolds, with 24 hours allotted for each test. The purpose of these tests was to subject each manifold to a variety of conditions in order to identify a heat exchanger/manifold design that enhances the thermal stratification in a SDHW system tank.

Experimental results are presented in graphical and tabular forms. For each test, temperature distributions inside the storage tank, as well as the availability and entropy of the actual tank, the fully mixed tank and the perfectly stratified tank are presented in Appendix D. As an example of the results, the graphs in this section are from the perforated manifold #2 tests. In this work the term "actual tank" referred to the storage tank used in the experiments while the terms "fully mixed tank" and "perfectly stratified tank" were used to describe fictitious temperature distributions in the storage tank. The "fully mixed tank" referred to tank that had a uniform temperature, which is the average temperature of the actual tank, and contains the same amount of energy as the actual tank. The "perfectly stratified tank" refers to an ideal tank that had same the amount of energy of the actual tank and it was ideally stratified. The availability ratios ($A_{final\ actual}/A_{perf}$) and entropy ratios ($S_{perf}/S_{final\ actual}$) were presented and used in Section 6.5 to compare the thermal performance of the different manifolds.

In order to test the manifolds under a variety of conditions, each manifold was subjected to three simulated heat loads representing a cloudy day, a sunny day, and a fixed heat input to the tank. Three initial tank conditions were applied:

- The cold tank condition referred to the initial tank condition obtained by draining the tank before the start of the test and filling it with the water from the cold water mains. As shown in Table 2, the cold water temperature was in the range of 10 – 21°C depending on the time of the year that the test was conducted. The difference

between the top and the bottom tank temperatures under the cold tank conditions was in the range of 1 – 2℃.

- The hot tank condition referred to the initial tank condition obtained by heating the tank in the previous day and the energy in the storage tank carried to the day of the test. The water temperature in the tank at the beginning of the tests was in the range of 18 – 51℃ as shown in Table 2.

- The mixed tank condition referred to the initial tank condition obtained by filling the tank with water in the previous day of the test. As result of heat loss and gains the temperature of the water after a full day approached room temperature. The water temperature in the tank at the beginning of the tests was in the range of 16 – 26℃ depending on the time of the year that the test was conducted. The difference between the top and the bottom tank temperature at the beginning of the each test was in the range of 1 – 2℃ as shown in Table 2.

6.1 RESULTS OF EXPERIMENTS CONDUCTED UNDER COLD TANK CONDITIONS

Figure 25 shows the temperature distributions inside the storage tank obtained under the cloudy day, sunny day, and a fixed heat input to the tank conditions for manifold #2. As shown in Figure 25, as soon as the heat addition started, the tank temperature started increasing.

In the test simulating a sunny day condition at 9:30 AM, the temperature throughout the tank was 16ºC at the beginning of the test as shown in Figure 25.b. When heat addition from the hot glycol started at 9:30 AM, the temperature at the top of the tank increased sharply, while the temperature at the bottom of the tank did not start to rise until 10:30 AM. At the beginning of the test, the differential pressure between the heated water inside the manifold and the cold water in the tank was relatively low. Therefore, a low water flow rate was produced inside the manifold, as shown in Figure 26. As a result, unwanted flow of cold water into the lower portion of the manifold was insignificant and

the heated water traveled directly to the top of the storage tank. This was not the case after 11:00 AM. Cold water was drawn into the manifold from the bottom of the tank, due to the higher differential pressure. The mixed water (hot water from the heat exchanger and cold water from the tank) in the manifold matched tank temperature at different levels causing several temperatures zones. After 11:00 AM, the temperatures at the lower zones began to increase gradually, and twelve distinct thermal zones could be distinguished from the bottom to the top of the tank, with a difference between them of about 1.5ºC. The temperature increased to 37ºC at 5:30 PM and at that time heat addition stopped.

Table 1 Temperature at top and bottom of the tanks at the start of the tests

Manifold #	Date	Test	Cold		Hot		Mixed	
			Tank T_{bot} °C	Tank T_{top} °C	Tank T_{bot} °C	Tank T_{top} °C	Tank T_{bot} °C	Tank T_{top} °C
Manifold #1	June 1,2,4, 2009	Cloudy day	12	14	20	46	19	20
	June 8,9,10, 2009	Sunny day	13	14	20	37	20	25
	May 19,20,21, 2009	Constant load	10	10	21	44	20	20
Manifold #2	July 9,13,15, 2009	Cloudy day	17	17	30	47	19	23
	July 6, 7,10, 2009	Sunny day	16	17	22	35	18	20
	June 17, 2009 July 1, 3, 2009	Constant load	14	15	18	46	20	23
Manifold #3	Aug 18, 25, 27, 2009	Cloudy day	21	21	37	51	22	24
	Aug 17, 19, 21, 2009	Sunny day	20	21	27	49	24	26
	Aug 13, 14, 15, 2009	Constant load	20	21	22	43	20	21
Manifold #4	Sep 10, 2009 Oct 8, 13, 2009	Cloudy day	16	17	30	50	16	17
	Oct 1, 5, 15, 2009	Sunny day	16	17	28	50	16	19
	Sep 11, 14, 24, 2009	Constant load	18	20	28	42	20	22

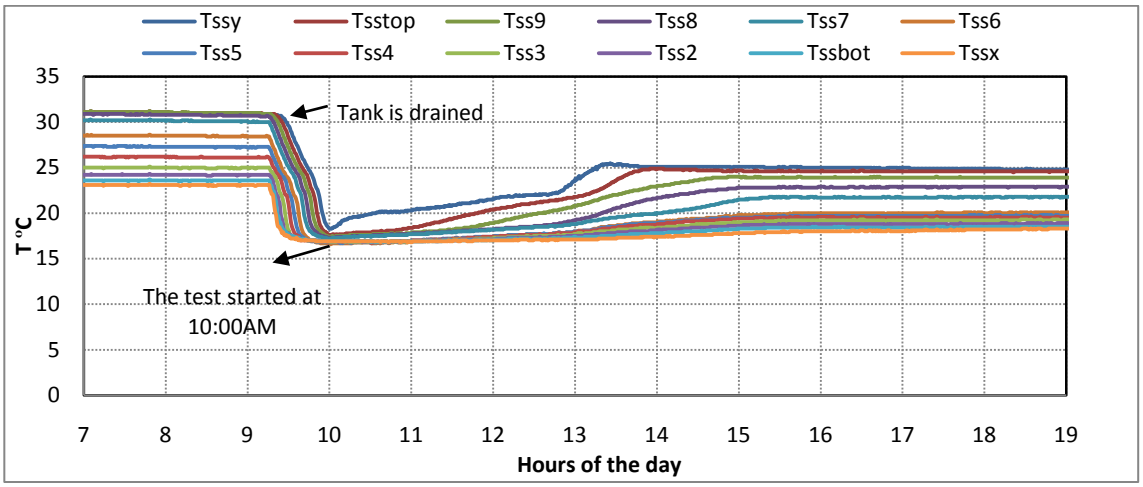

Figure 25. a. Cloudy day; cold tank condition.

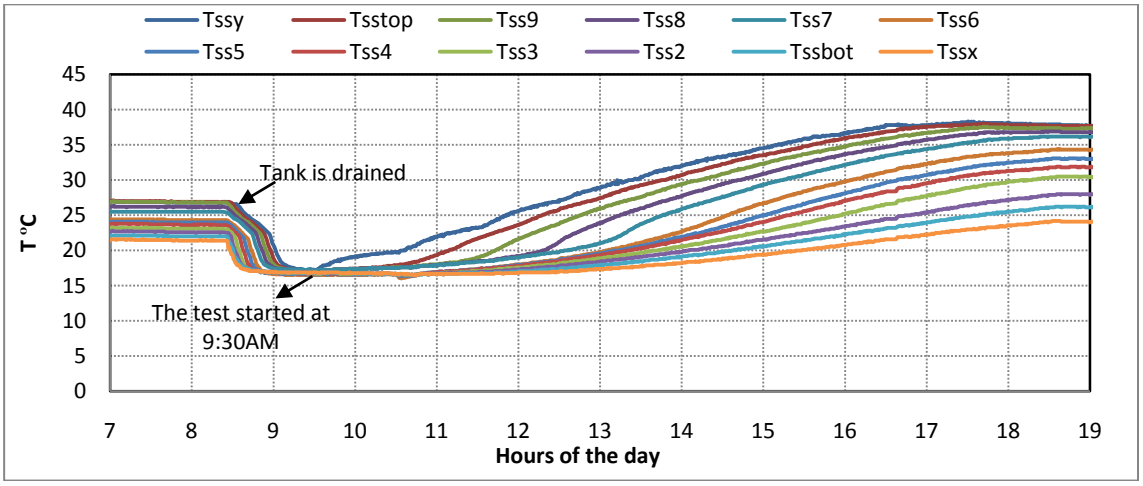

Figure 25. b. Sunny day; cold tank condition.

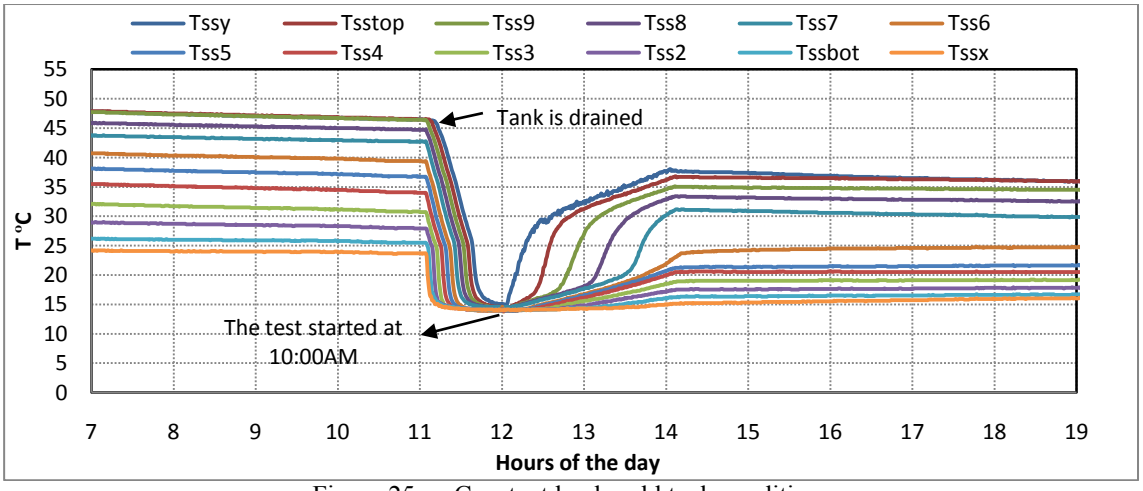

Figure 25. c. Constant load; cold tank condition.

Figure 25 Temperature distribution inside storage tanks of three tests (Manifold #2).

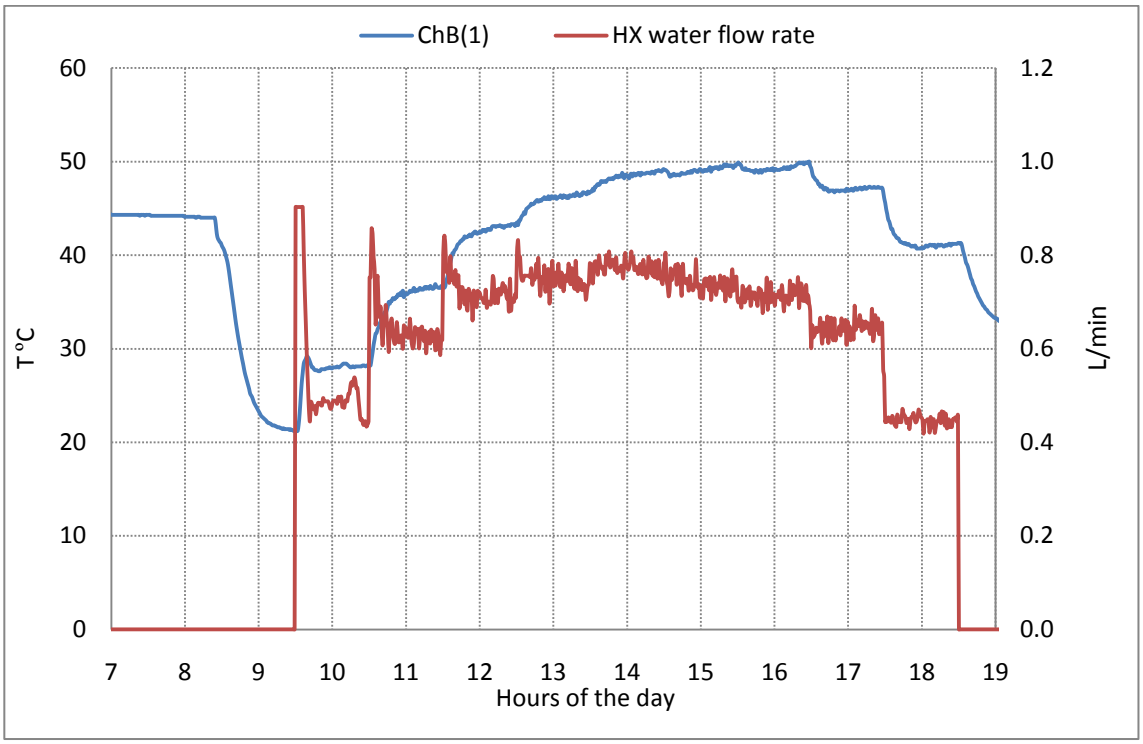

Figure 26 Water temperature at the heat exchanger outlet and water flow rate through the manifold for the test of sunny day; cold tank condition

6.2 RESULTS OF EXPERIMENTS CONDUCTED UNDER HOT TANK CONDITIONS

In tests that simulated the hot tank condition, the tank was heated the previous day and the energy in the storage tank was stored to the day of the test. This test was a simulation of a case when the previous day was a sunny day and the energy was stored for the following day (the day of the test), which might be a cloudy or sunny day.

Figure 27 shows the temperature distribution inside the storage tank during three tests simulating a cloudy day, sunny day, and fixed heat input, using Manifold #2.

On a cloudy day test, the water temperature inside the storage tank was higher than the glycol temperature most of the day. There was no differential temperatures controller, which would have stopped the solar pump from circulating the glycol through the solar collector. Therefore the storage tank was heating the glycol in some tests. Since this operation was contrary to the purpose of a solar collector the results for a cloudy day, with hot tank condition, were not used.

Figure 27 showed that on a sunny day, and constant heat load conditions, the temperature of the storage tanks increased at all levels of the storage tank, as soon as the tests started, which indicated that the perforated manifold was delivering the heated water to all levels at the appropriate temperature.

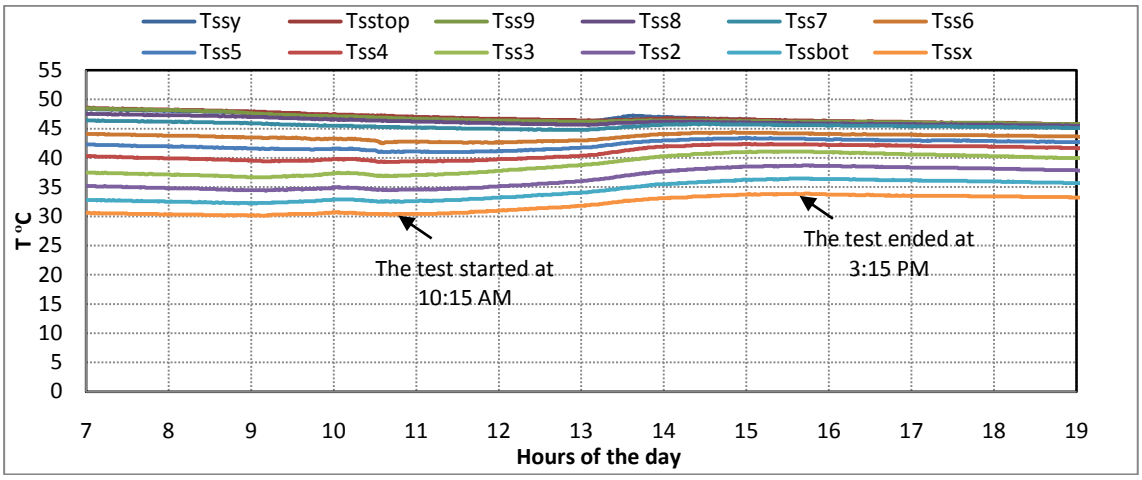

Figure 27. a. Cloudy day; hot tank condition.

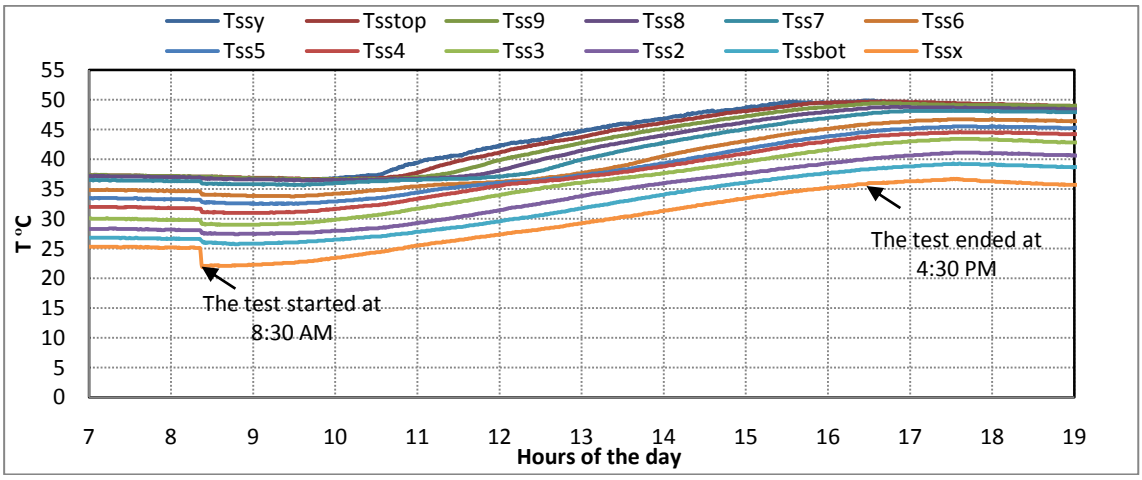

Figure 27. b. Sunny day; hot tank condition.

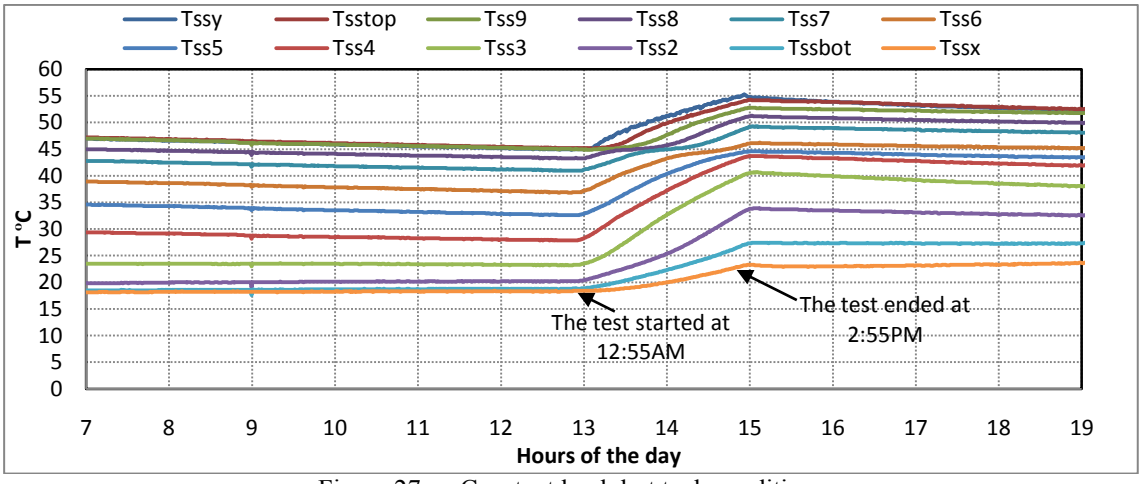

Figure 27. c. Constant load; hot tank condition.

Figure 27 Temperature distribution inside storage tanks of three tests (Manifold #2).

6.3 RESULTS OF EXPERIMENTS CONDUCTED UNDER MIXED TANK CONDITION

In mixed tank condition tests, the temperature of the water in the tank was close to the room temperature. This test was a simulation of a case when there was no energy stored and carried in the tank to the next day (the day of the test) which might be a cloudy or sunny day. Figure 28 shows the temperature distributions inside the storage tank obtained under the cloudy day, sunny day, and a fixed heat input conditions using manifold #2. As soon as the test started the temperature at the top of the tank increased, and the temperature of the bottom of the tank did not increase until the middle of the test.

In all tests the perforated manifold delivered the water heated by the heat exchanger to different levels inside the storage tank resulting in a stratified temperature distribution with clearly defined thermal zones from the bottom to the top of the tank. The temperature difference between the zones was varied from 1ºC to 3ºC.

Analyzing the thermal stratification zones presented in Figure 28 allowed quantifying the thermal performance of the perforated manifold.

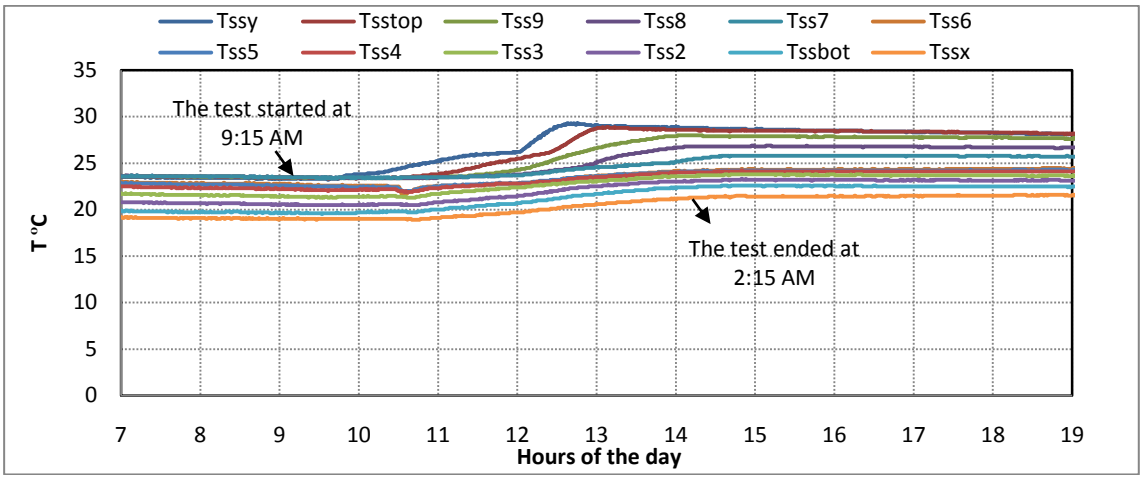

Figure 28. a. Cloudy day; mixed tank condition.

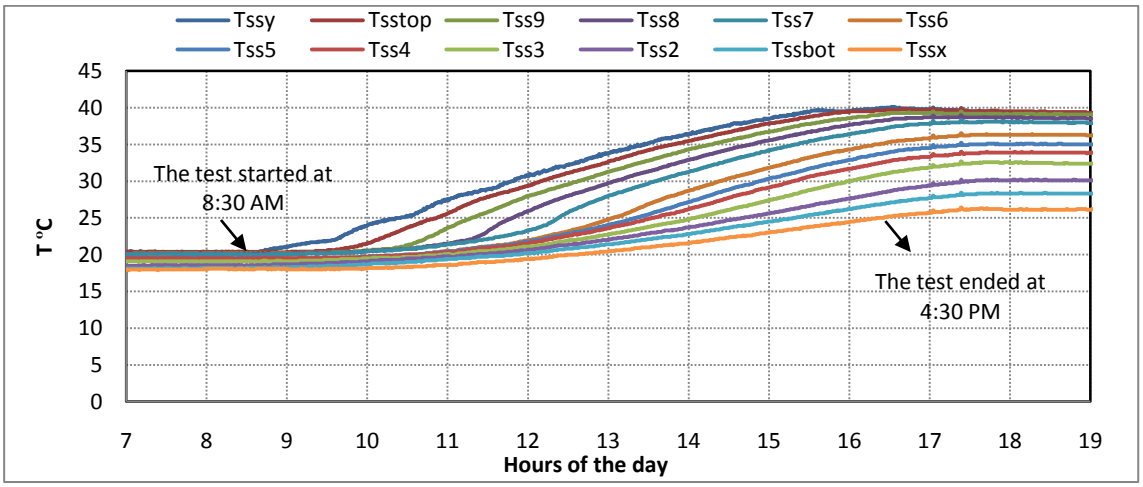

Figure 28. b. Sunny day; mixed tank condition.

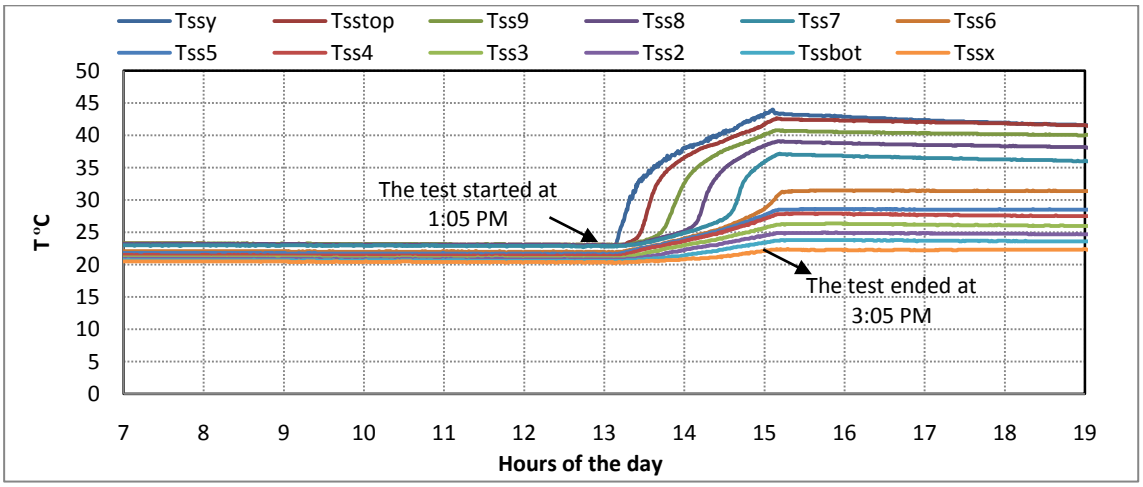

Figure 28. c. Constant load; mixed tank condition.

Figure 28 Temperature distribution inside storage tanks of three tests (Manifold #2).

6.4 AVAILABILITY IN THE STORAGE TANK

Availability was used to evaluate the level of stratification in this work. Availability was calculated for the perfectly stratified tank and fully mixed tank based on calculated data and for the actual tank based on measured data. The availability of the perfectly stratified tank, fully mixed tank and the actual tank for each test is shown in Figures 63 to 98 in Appendix D.

6.4.1 AVAILABILITY OF PERFECTLY STRATIFIED TANK

In the calculation of the availability of the perfectly stratified tank, the tank was divided into a top and bottom part. The mass of the water in the top part was calculated using Equation 5.3.5 and the energy added during the test was calculated using Equation 5.3.1. At the beginning of the tests, there was no energy added to the tank, therefore, the mass and the availability of the top part were zero. As a result, the mass of the water in the bottom part was equal to the total mass of the storage tank.

Since the entire tank is at the dead state temperature, the availability is equal to zero. Accordingly, at the beginning of all tests, the availability of the perfectly stratified tank was equal to zero.

At the end of the tests, the tank was divided to two parts. The mass of each part was determined based on its temperature, and the total energy added during the test as explained in Section 5.3. As a result, the availability plots of the perfectly stratified tank before the end of the tests were not useful for comparison purposes. The plots are included only to show the change of the availability over time.

6.4.2 AVAILABILITY OF FULLY MIXED TANK AND ACTUAL TANK

The availability of the fully mixed tank and the actual tank was calculated using Equation 5.3.4. If the test was a simulation of cold or mixed tank condition, the availability of the fully mixed tank and the actual tank at the beginning of the test was zero, because in both cases the tank temperature was equal to the dead state temperature (i.e. the average temperature of the initial tank). On the other hand, for tests that simulate the hot tank condition, the availability of the mixed tank is equal to zero for the same

reason, but the availability of the actual initial tank was not zero, because of the energy carried from the previous day.

For the above reasons, the comparison of the thermal performance of manifolds was based on the availability values calculated using the properties of the tanks at the end of the tests.

6.4.3 AVAILABILITY PLOTS

Figure 29 shows the availability for the perfectly stratified tank, actual tank, and fully mixed tank during a sunny day condition test with manifold #2. As soon as heat addition starts, availability started to increase until it reached a peak about an hour after the end of the tests. This time delay depended on the manifold effectiveness, where the most efficient manifold was the one which presents a shorter time delay after the peak of solar radiation. The drop in availability as seen in Figure 29 after the peak of the availability was attributed to heat losses and downward conduction and convection causing de-stratification of the tank as well as mixing at the top of the tank. Figures 29. a. and 29.c. show that at the beginning of test, the availability of the actual tank was zero, while in Figure 29. b. the availability of the actual tank was 0.053 MJ, due to the energy carried over from the previous day.

6.4.4 AVAILABILITY RATIO

A comparison of the thermal performance of the manifolds using the availability ratios ($A_{final\ \ actual}\ /A_{perf}$) was conducted. The availability ratio was calculated for each test. Because the availability ratio was very sensitive to the choice of the dead state temperature, and because the tests were done in different seasons (i.e., at different dead state temperatures), the average availability ratio was calculated for each manifold. The most effective manifold was the one with the highest average availability ratio.

The availability ratios were also affected by the initial tank condition. This indicated that the initial tank temperature distribution had an impact on manifold effectiveness. Figure 30 shows the availability ratios of manifold #2. Figure 30 shows that, the availability ratios for a fixed heat input with mixed tank, hot tank, and cold tank

conditions were 0.71, 0.87, and 0.72, respectively. Although the three tanks were subjected to same heat load, the availability ratios were different due to the effect of the initial tank condition on the effectiveness of the manifold.

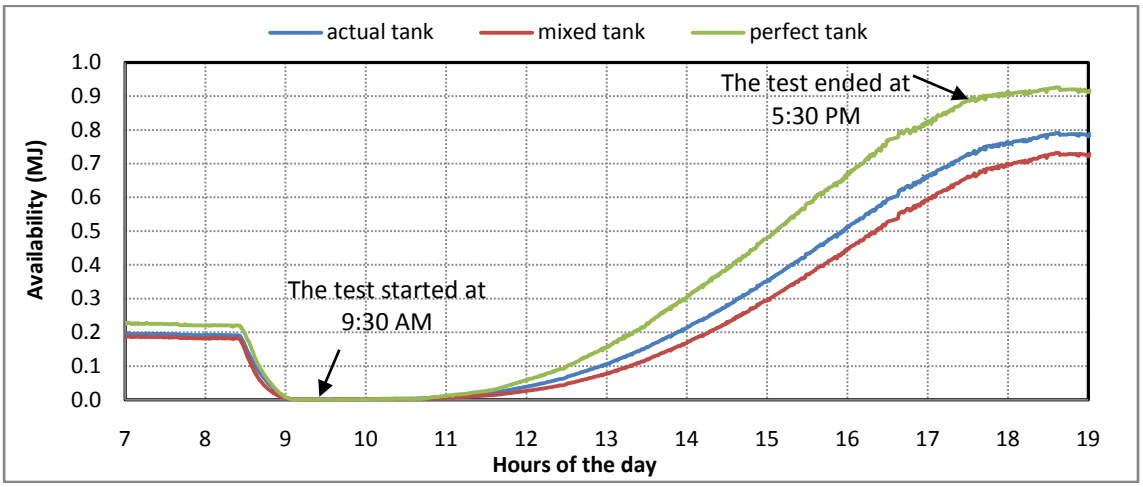

Figure 29. a. Sunny day; cold tank condition.

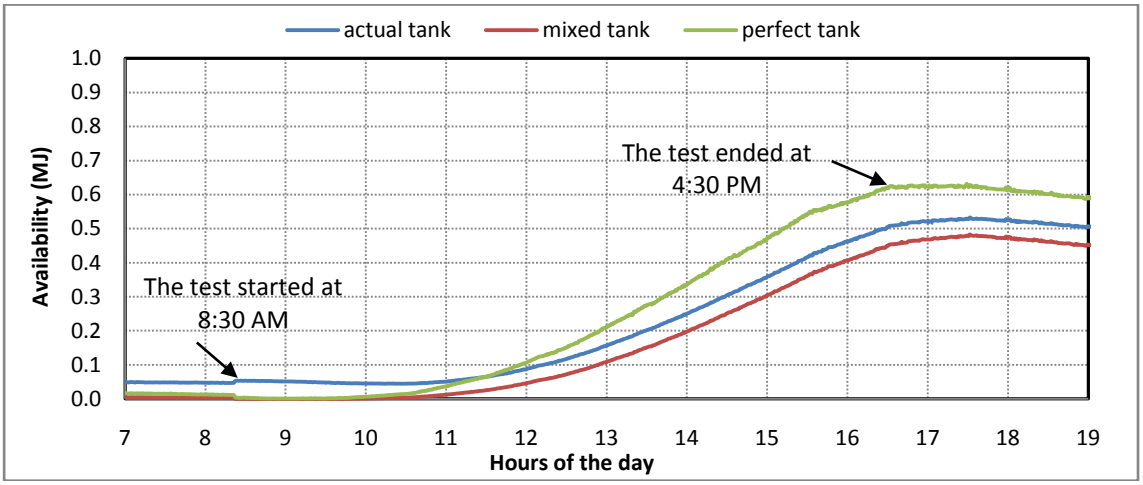

Figure 29. b. Sunny day; hot tank condition.

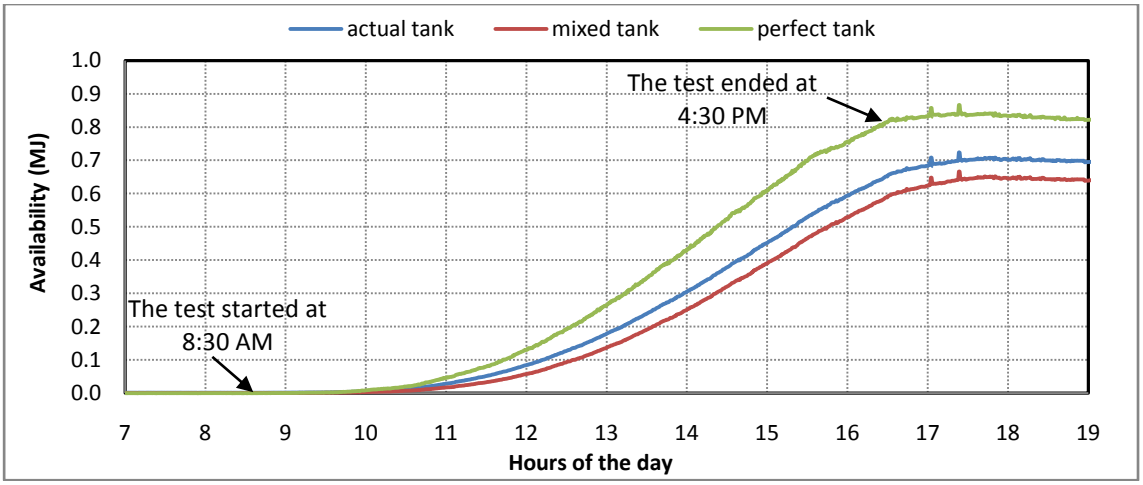

Figure 29. c. Sunny day; mixed tank condition.

Figure 29 Availability of energy from tanks during three tests simulating sunny day (Manifold #2).

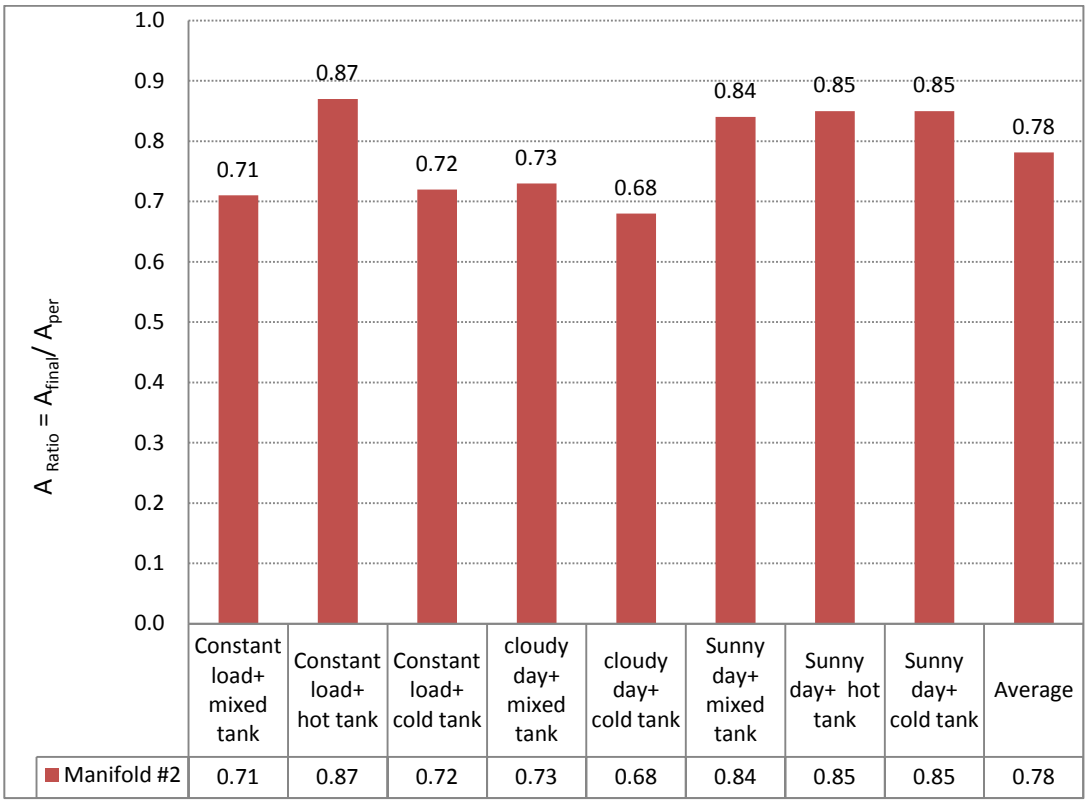

Figure 30 Availability ratios of manifold #2

6.5 ENTROPY IN THE STORAGE TANK

In the range of the storage tank temperature (15 – 70℃), the entropy of the water varied from 0.224 to 0.955 kJ/kg · K. As a result, the differences between the entropy of the perfectly stratified, entropy of the actual tank, and entropy of the fully mixed tank were very small and the plots of the entropies are almost identical to each other as seen in Figure 31. a, b, and c. Entropy was calculated using the entropy equation (Appendix B).

The entropy of the perfectly stratified tank, fully mixed tank and the actual tank for each test is shown in Figures 63 to 98 in Appendix D.

Figure 31 shows the entropy changes of the perfectly stratified tank, the actual tank, and the fully mixed tank during the tests that simulated sunny day conditions.

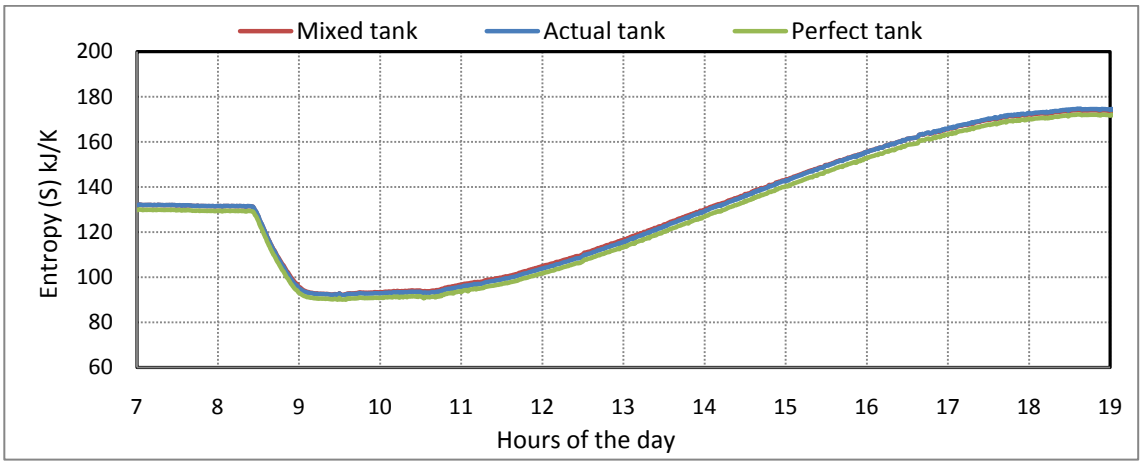

Figure 31. a. Sunny day; cold tank temperature.

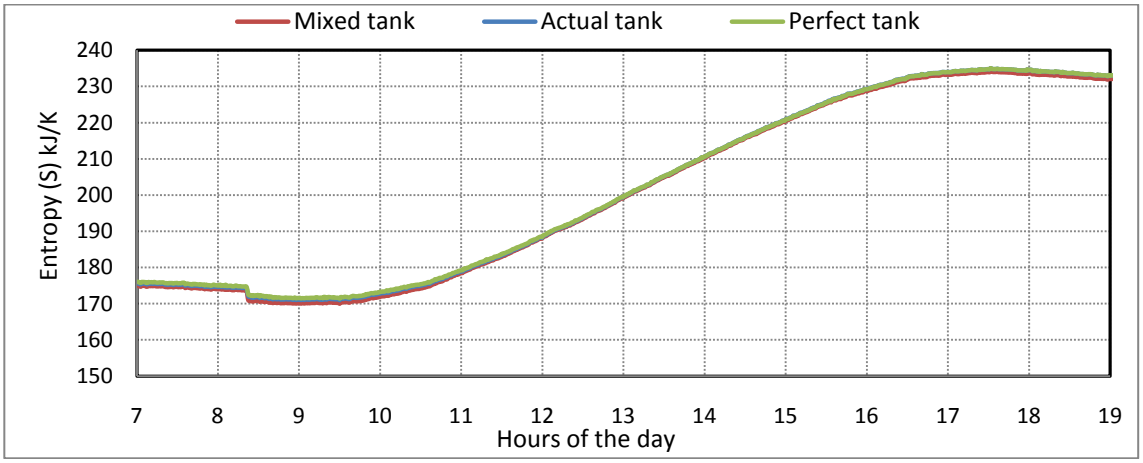

Figure 31. b. Sunny day; hot tank temperature.

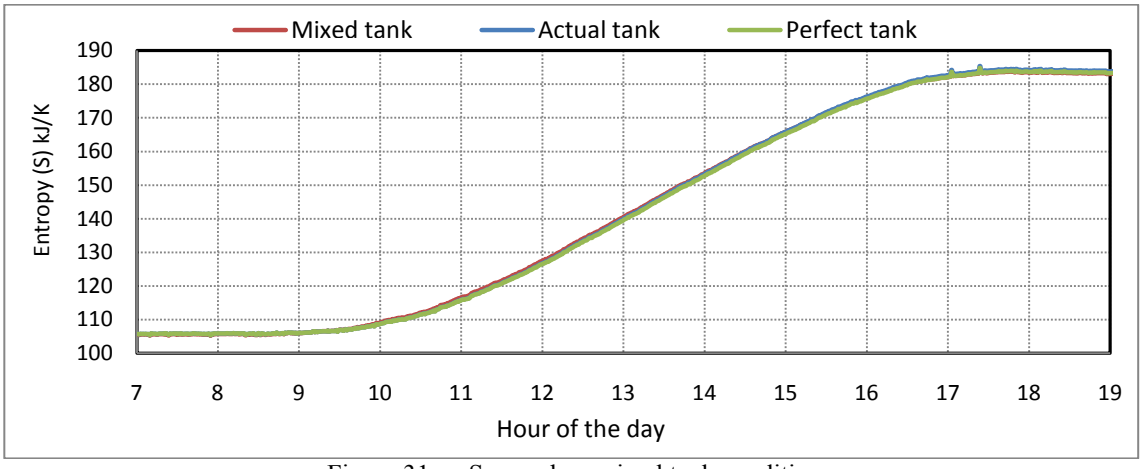

Figure 31. c. Sunny day; mixed tank condition.

Figure 31 The tank entropy during the tests simulating sunny day.

6.5.1 ENTROPY OF THE PERFECTLY STRATIFIED TANK

In the calculation of the entropy of the perfectly stratified tank, the tank was divided into a top and bottom part. The mass of the water in each part of the perfectly stratified tank was calculated as explained in Section 6.4.1.

At the beginning of the test, the entropy of the top part was zero because the water mass of the top part was zero, and the total entropy of the perfectly stratified tank was equal to the entropy of bottom part of the tank.

At the end of the test, the entropy of the top part was calculated using the top temperature of the final actual tank. On the other hand, the entropy of the bottom part of the tank was calculated using the dead state temperature. The total entropy of the tank was the entropy of top part plus the entropy of the bottom part.

6.5.2 ENTROPY OF THE FULLY MIXED TANK AND ACTUAL TANK

The entropy of the fully mixed tank was calculated using the average temperature of the actual tank, and the entropy of the actual tank was calculated using the temperature of the thermal layers as shown in Figures 25, 27, and 28.

6.5.3 ENTROPY RATIO

A comparison between the thermal performance of the manifolds in terms of entropy was conducted using the entropy ratios ($S_{per}/S_{final\ actual}$). The entropy ratio was calculated at the end of each test. Figure 32 shows the entropy ratios of manifold #2. Figure 32 shows that the entropy ratio was affected by the initial tank condition and the difference between the entropy ratios was very small because the entropy change in the range of the tank temperature was very small. For that reason, an average of the entropy ratios was calculated for each manifold. The most efficient manifold should be the one having a higher average entropy ratio. For example, the entropy ratio for a fixed heat input with mixed tank, hot tank, and cold tank condition was 0.996, 0.999, and 0.994, respectively. Although the three tanks were subjected to the same heat load, the entropy ratio was different for each test due to the effect of initial tank condition on the effectiveness of the manifold.

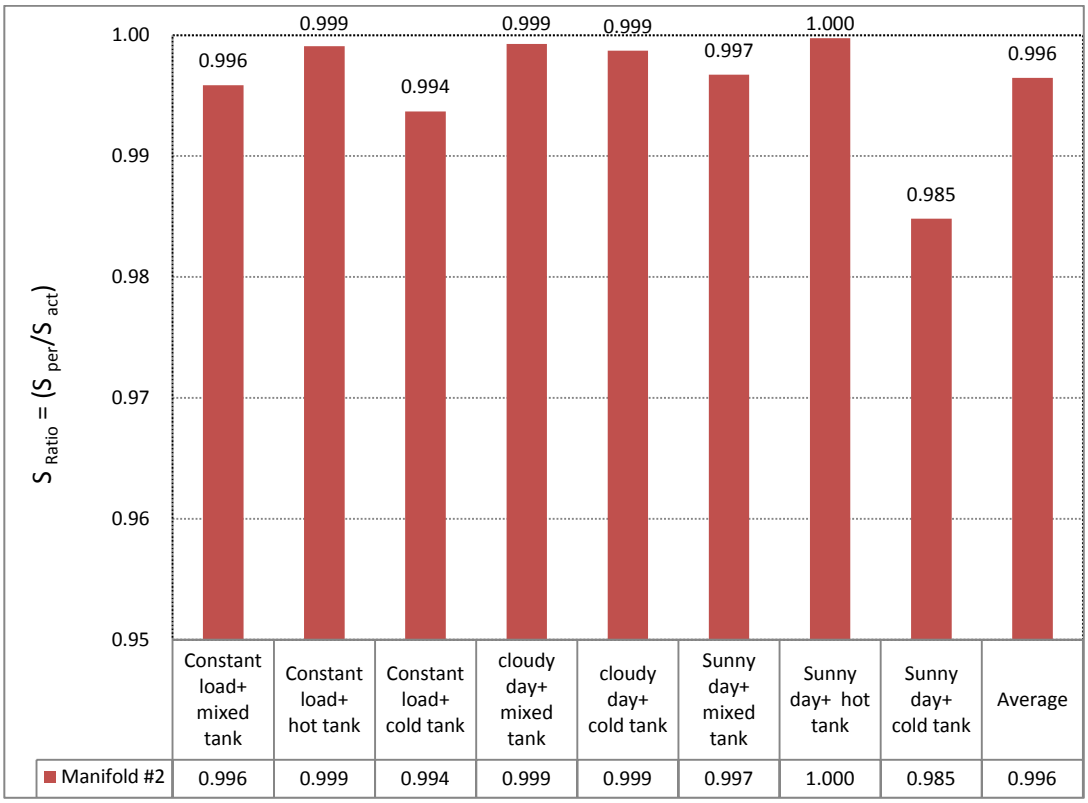

Figure 32 Entropy ratios of manifold #2

6.6 SELECTION OF DEAD STATE TEMPERATURE FOR AVAILABILITY ANALYSIS

Availability and entropy ratios as well as a merit factor were used to compare the thermal performance of the manifolds. Availability is highly dependent on the dead state temperature. As pointed out by Haller, et al. (2009), with systems that are not used to produce work, the choice of the dead state temperature (T_o) is arbitrary. However, arbitrary choices of the dead state temperature, without a physical justification, can confuse and lead to misleading comparisons. Different authors have argued for different choices of T_o. In some cases, the temperature used was the tank bottom temperature and in others the return water temperature Hermansson (1993)

In this work, thirty six tests were conducted. The preparation of each test took from one day to five days, hence the tests took five months. Both the ambient and the water temperatures varied substantially during the five month test period. As a result, the dead state temperature also varied. For example, cold water temperatures from the mains on

May 19, 2009 and August 21, 2009 were 10°C and 21°C, respectively, as shown in Table 1.

Due to the variation of temperature during the test period as well as the variation of the relative magnitudes of tank temperature, ambient temperature, cold water temperature and heated water temperature, the selection of the dead state temperature (T_o) is not a trivial task, with no obviously "right" or "wrong" T_o. Consequently, in the calculation of tank availability, several values of T_o were used in this work to identify the most suitable choice. The values of T_o used and the reasons are as follows.

i) T_o= bottom temperature of the initial tank ($T_{ssx,\ ini}$). This temperature was chosen because it was the lowest temperature of the tank.

ii) T_o = minimum bottom temperature of the tank during the test ($T_{ssx,\ min}$). This temperature was chosen because it was the lowest temperature recorded during the test.

iii) T_o = bottom temperature of the actual tank at the end of the test ($T_{ssx,\ final\ actual}$). This temperature was chosen because it was the lowest temperature in the tank when the comparison was conducted.

iv) T_o = average temperature of the initial tank ($T_{ini,\ aver}$). This temperature was chosen because it was a temperature that changed according to the conditions of the test.

6.7 SELECTION OF THE BOTTOM TEMPERATURE FOR THE PERFECTLY STRATIFIED TANK

The performance of the manifolds designed in this work was measured by comparing the availability and the entropy of the tank at the end of each test to the availability and entropy of a "perfectly stratified tank". As with the selection of the dead state temperature, there is more than one way to define a perfectly stratified tank. The "perfectly stratified tank" consists of two thermal zones. It is assumed that the temperature of the upper zone was uniform and equal to the maximum temperature reached at the end of a test, i.e. the top temperature of the final actual tank ($T_{ssy,\ final\ actual}$). However, there was more than one choice for the temperature of the bottom part. Two

approaches were used here, to select the temperature of the bottom part of the perfectly stratified tank:

i) In the first approach, it was assumed that as the water from the bottom of the tank was circulated through the heat exchanger, heated, and returned to the top of the tank. It occupied the top of the tank while the mass of the water at the top of the tank initially moved toward the bottom maintaining its initial stratification, as illustrated in Figure 33.

ii) In the second approach it was assumed that the bottom part of the perfectly stratified tank had the dead state temperature (T_o), as illustrated in Figure 34.

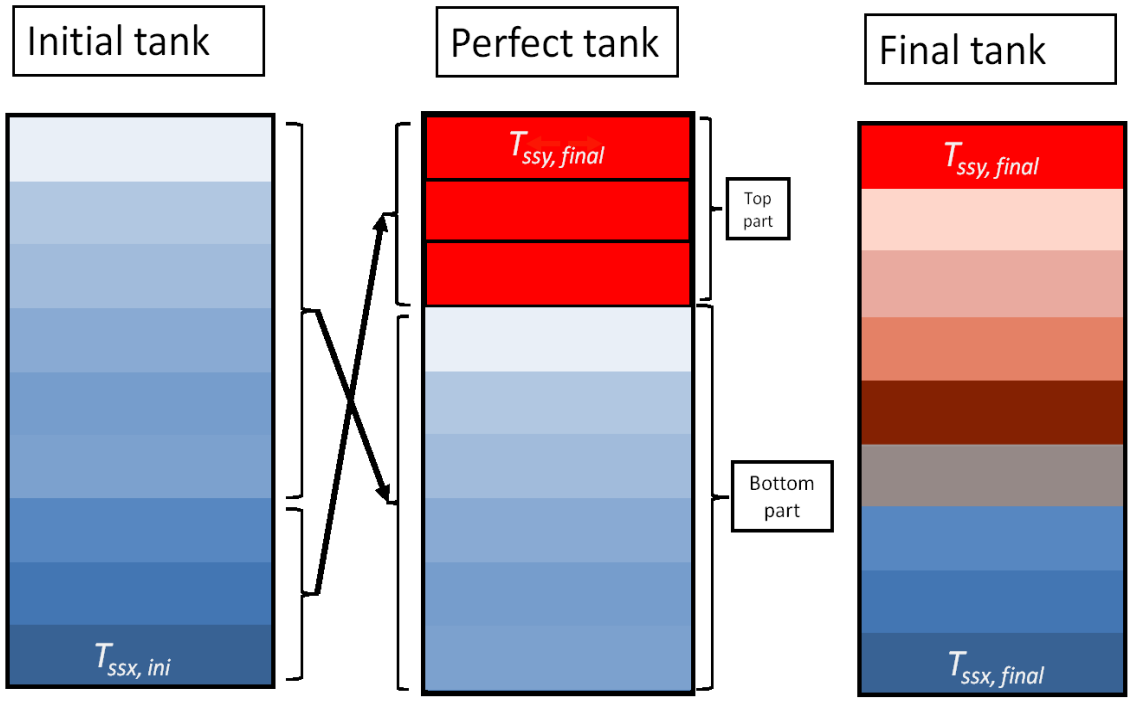

Figure 33 Diagram to illustrate the first approach.

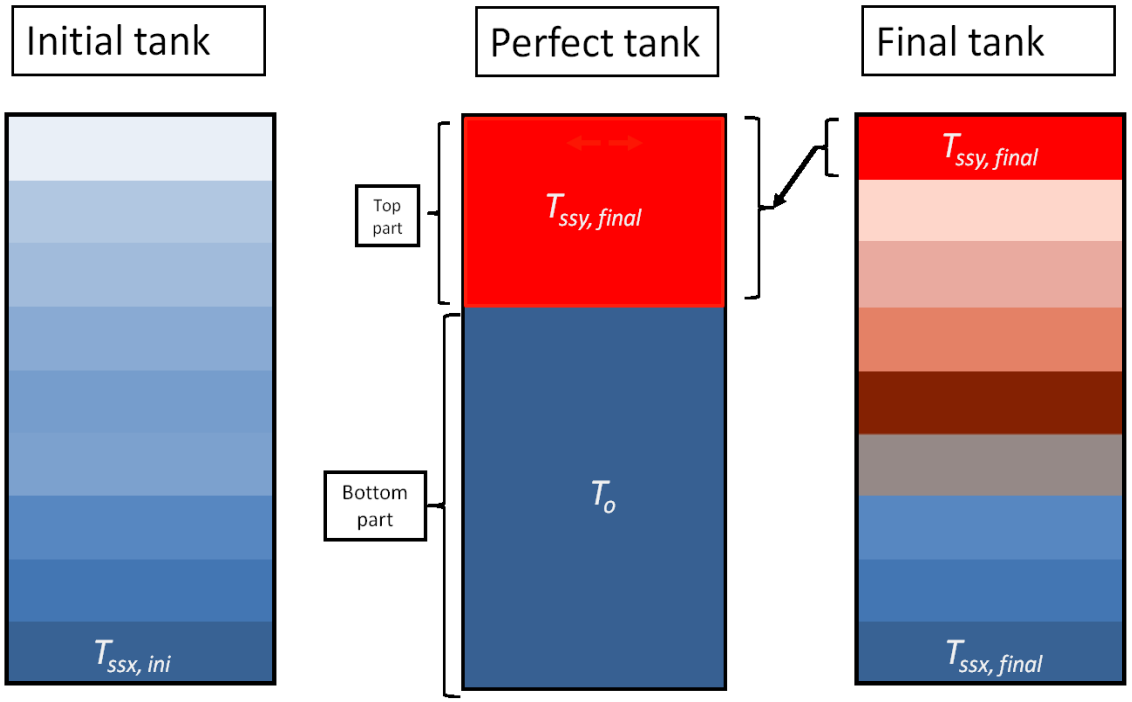

Figure 34 Diagram to illustrate the second approach.

6.8 EVALUATION OF MANIFOLD PERFORMANCE

To evaluate the performance of the manifolds designed and tested in this work, the availability and entropy at the end of each test were calculated based on the dead state temperatures and perfectly stratified tank definitions presented in Sections 6.6 and 6.7. The calculations were conducted using the following five conditions:

Condition #1[3]:

Perfectly stratified tank bottom temperature as per the first approach, and

$T_o = T_{ssx,\ ini}$ ($T_{bot\ layers,\ perfect} = T_{Top\ layers,\ ini}$)

Condition #2:

Perfectly stratified tank bottom temperature as per the second approach, and

$T_o = T_{ssx,\ ini}$ ($T_{bot\ part,\ perfect} = T_o$)

Condition #3:

Perfectly stratified tank bottom temperature as per the second approach, and

$T_o = T_{ssx,\ min}$ ($T_{bot\ part,\ perfect} = T_o$)

Condition #4:

Perfectly stratified tank bottom temperature as per the second approach, and

$T_o = T_{ssx,\ final\ actual}$ ($T_{bot\ part,\ perfect} = T_o$)

Condition #5:

Perfectly stratified tank bottom temperature as per the second approach, and

$T_o = T_{ini,\ aver}$ ($T_{bot\ part,\ perfect} = T_o$)

The procedure to calculate the availability, the entropy, and the merit factor using the first approach was:

1. The amount of energy added to the tank during the test was determined using Equation 5.3.1.
2. The mass of the top part of the perfectly stratified tank was calculated using Equation 5.3.5.

[3] As discussed in Sections 6.9.1, the results obtained using the first approach are inconsistent and unreliable. Therefore, no further analysis was done by changing the dead state temperature with the first approach.

3. The mass of each part of the perfectly stratified tank and its temperature were according to the first approach as illustrated in Figure 33.
4. The entropy of the top part was calculated using Entropy equation (Appendix B) and its temperature ($T_{ssy,\ final\ actual}$), while the entropy of the bottom part was calculated using the temperature of each layer separately.
5. The total entropy of the perfectly stratified tank was equal to the entropy of the top part plus the entropy of each layer of the bottom part of the perfectly stratified tank.
6. Tank availability for the final actual tank was calculated using Equation 5.3.4.
7. The merit factor and the availability ratio of the tank were calculated, at the end of each test, using Equations 5.3.7 and 5.3.8.a.
8. The availability ratios and the merit factors of the tanks for all tests were compared. The most effective manifold was the one presenting a higher average of availability ratio and average merit factor.

The procedure to calculate the availability, the entropy, and the merit factor using the second approach was:

1. The energy added to the tank during the test was determined using Equation 5.3.1.
2. The mass of the top part of the perfectly stratified tank was calculated using Equation 5.3.5, assuming the dead state temperature, as shown in Figure 34.
3. The availability of the top and the bottom parts were calculated based on the dead state temperature using Equation 5.3.4.
4. The entropy of the top and the bottom part of a perfectly stratified tank were calculated based on the top layer temperature of the final actual tank ($T_{ssy,\ final\ actual}$) and on the selected (T_o) using Entropy equation (Appendix B).
5. The total entropy of the perfectly stratified tank was equal to the entropy of the top part entropy plus the entropy of the bottom part entropy.

6. The merit factors, the availability ratios, and the entropy ratios, were calculated using Equations 5.3.7, 5.3.8.b, and 5.3.9, respectively.
7. Steps 1-6 are repeated for each test and the results are compared. The most effective manifold was the one presenting a higher average of availability ratio and average entropy ratio.

6.9 RESULTS

The availability ratios and merit factors for each manifold, based on the five set of assumptions, are presented and discussed in the following sections. In the figures presented, each color represents a manifold design and each group of columns represents tests conducted under similar conditions. Averages of the availability and merit factor ratios are plotted to show the most effective manifold. The most effective manifold is the one with in the highest average availability ratio and highest average merit factor.

6.9.1 RESULTS OBTAINED WITH CONDITION #1 ASSUMPTION

Figures 35 – 36 show the availability ratios and the merit factors calculated based on Condition #1. In each test a different manifold produced better results, therefore it is not possible to identify the most effective manifold from these comparisons. Furthermore the availability ratios and the merit factors produce substantially different results.

The availability ratios and the merit factor were affected by the initial tank conditions. For example, although the energy added to the tank during the “sunny day” tests was the same, the most effective manifold was different from one initial tank condition to another. In addition, the average of the availability ratios and the average of the merit factors showed inconsistent order in terms of the most effective manifold. This inconsistency between the average of the availability ratios and the average of the merit factors was due to the assumption that the bottom part of the perfectly stratified tank was the same as the top part of the initial tank and due to the dead state temperature that was used. Because of the inconsistent results, Condition #1 was considered unreliable to evaluate the thermal performance of the manifolds.

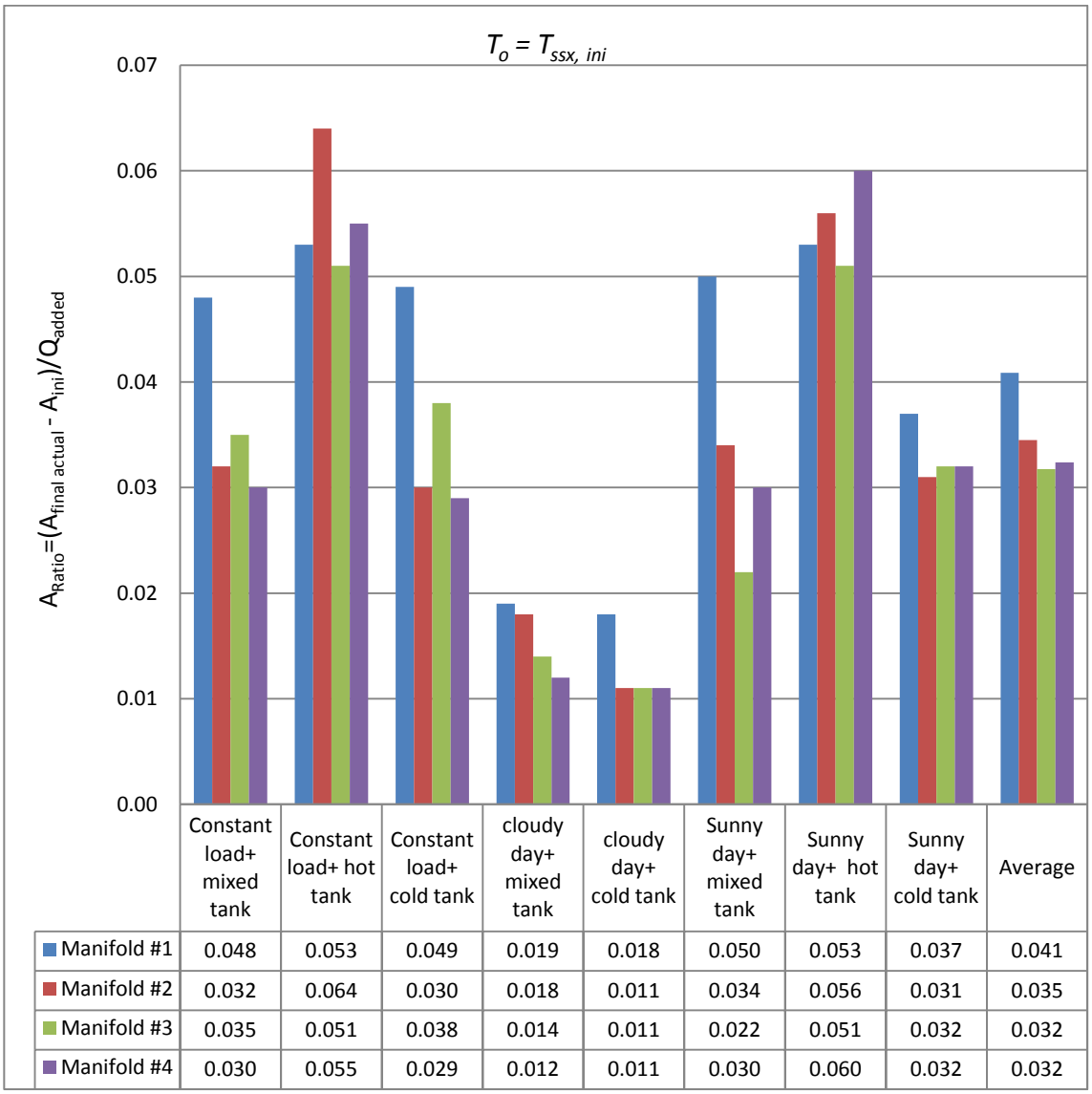

	Constant load+ mixed tank	Constant load+ hot tank	Constant load+ cold tank	cloudy day+ mixed tank	cloudy day+ cold tank	Sunny day+ mixed tank	Sunny day+ hot tank	Sunny day+ cold tank	Average
Manifold #1	0.048	0.053	0.049	0.019	0.018	0.050	0.053	0.037	0.041
Manifold #2	0.032	0.064	0.030	0.018	0.011	0.034	0.056	0.031	0.035
Manifold #3	0.035	0.051	0.038	0.014	0.011	0.022	0.051	0.032	0.032
Manifold #4	0.030	0.055	0.029	0.012	0.011	0.030	0.060	0.032	0.032

Figure 35 Availability ratios for the four manifolds analyzed by Condition #1.

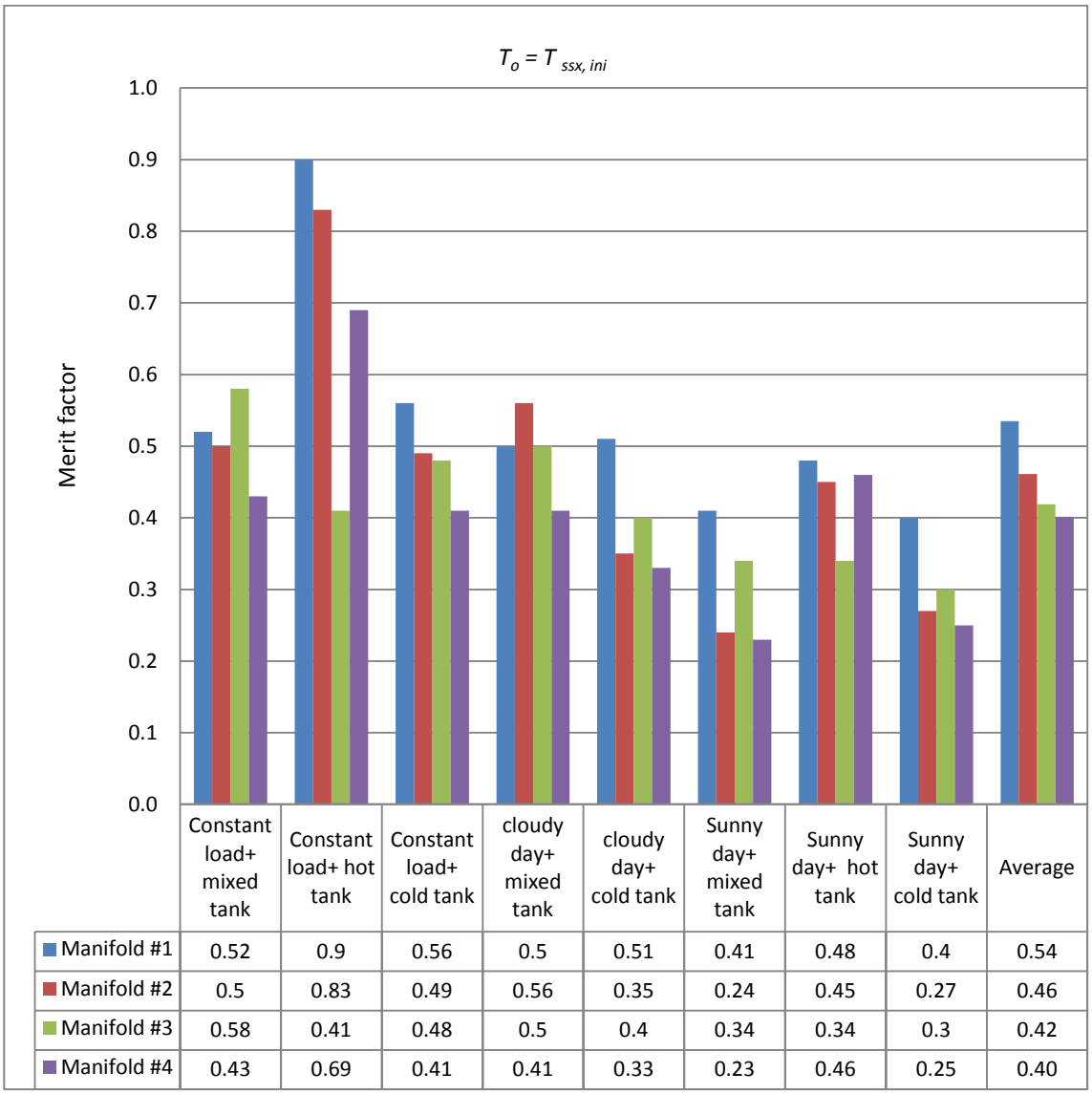

	Constant load+ mixed tank	Constant load+ hot tank	Constant load+ cold tank	cloudy day+ mixed tank	cloudy day+ cold tank	Sunny day+ mixed tank	Sunny day+ hot tank	Sunny day+ cold tank	Average
Manifold #1	0.52	0.9	0.56	0.5	0.51	0.41	0.48	0.4	0.54
Manifold #2	0.5	0.83	0.49	0.56	0.35	0.24	0.45	0.27	0.46
Manifold #3	0.58	0.41	0.48	0.5	0.4	0.34	0.34	0.3	0.42
Manifold #4	0.43	0.69	0.41	0.41	0.33	0.23	0.46	0.25	0.40

Figure 36 Merit factors of the four manifolds analyzed by Condition #1.

6.9.2 RESULTS OBTAINED WITH CONDITION #2 ASSUMPTIONS

Figures 37 – 38 show the availability ratios and the merit factors calculated using Condition #2. The figures indicate that Condition #2 produced substantially different conclusions in terms of the most effective manifold. This inconsistency between the average of the availability ratios and the average of the merit factors was due to the calculation of the entropy of the perfectly stratified tank, which was based on $T_{ssx,\ ini}$. The difference in the results between Condition #1 and Condition #2 is noticeable in the merit factors, not in the availability ratios. The availability did not change, because it depended on the dead state temperature ($T_{ssx,\ ini}$) which is the same in both conditions. Because of the inconsistent results, Condition #2 was considered unreliable to evaluate the thermal performance of manifolds.

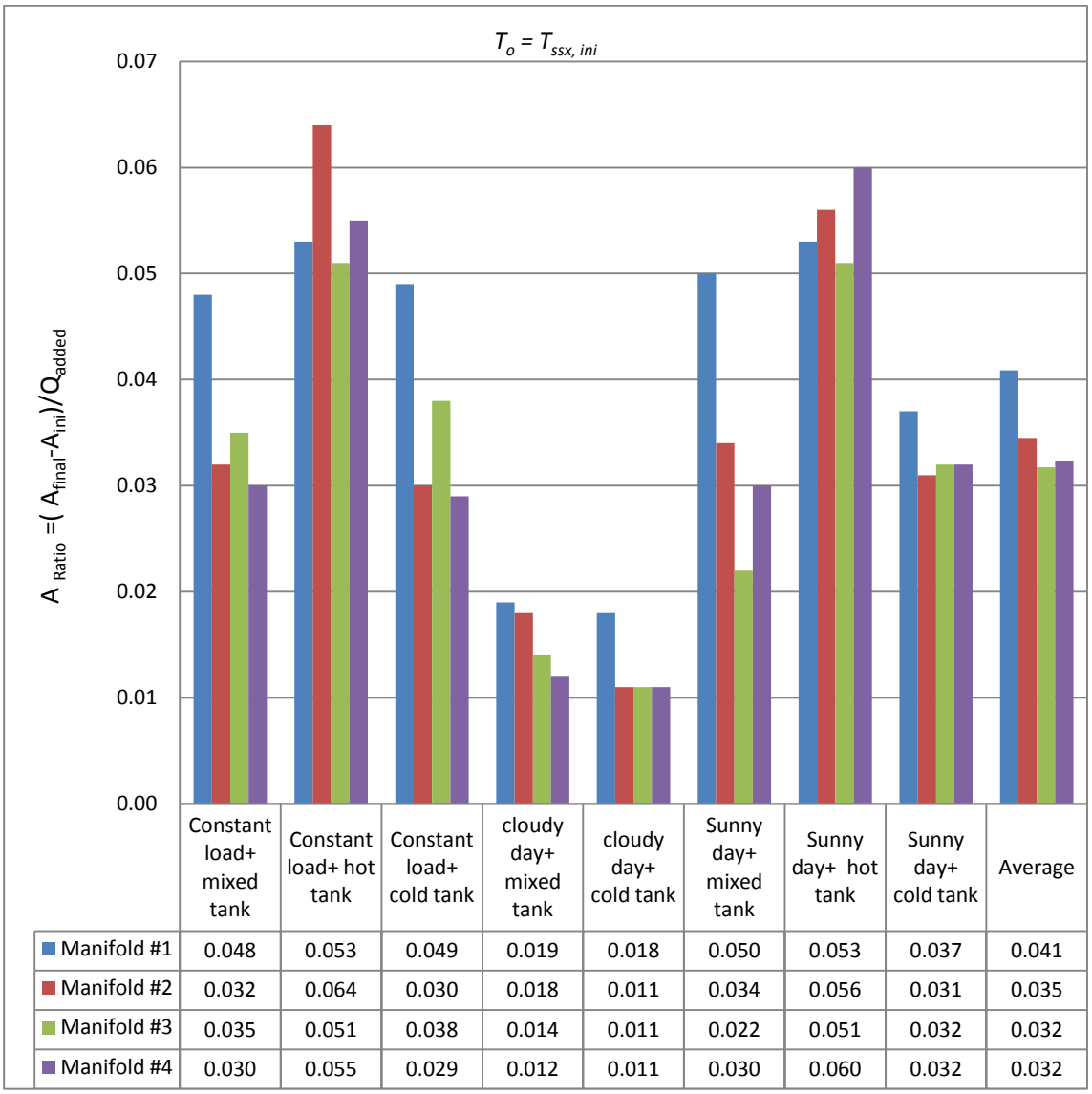

	Constant load+ mixed tank	Constant load+ hot tank	Constant load+ cold tank	cloudy day+ mixed tank	cloudy day+ cold tank	Sunny day+ mixed tank	Sunny day+ hot tank	Sunny day+ cold tank	Average
Manifold #1	0.048	0.053	0.049	0.019	0.018	0.050	0.053	0.037	0.041
Manifold #2	0.032	0.064	0.030	0.018	0.011	0.034	0.056	0.031	0.035
Manifold #3	0.035	0.051	0.038	0.014	0.011	0.022	0.051	0.032	0.032
Manifold #4	0.030	0.055	0.029	0.012	0.011	0.030	0.060	0.032	0.032

Figure 37 Availability ratios for the four manifolds analyzed by Condition #2.

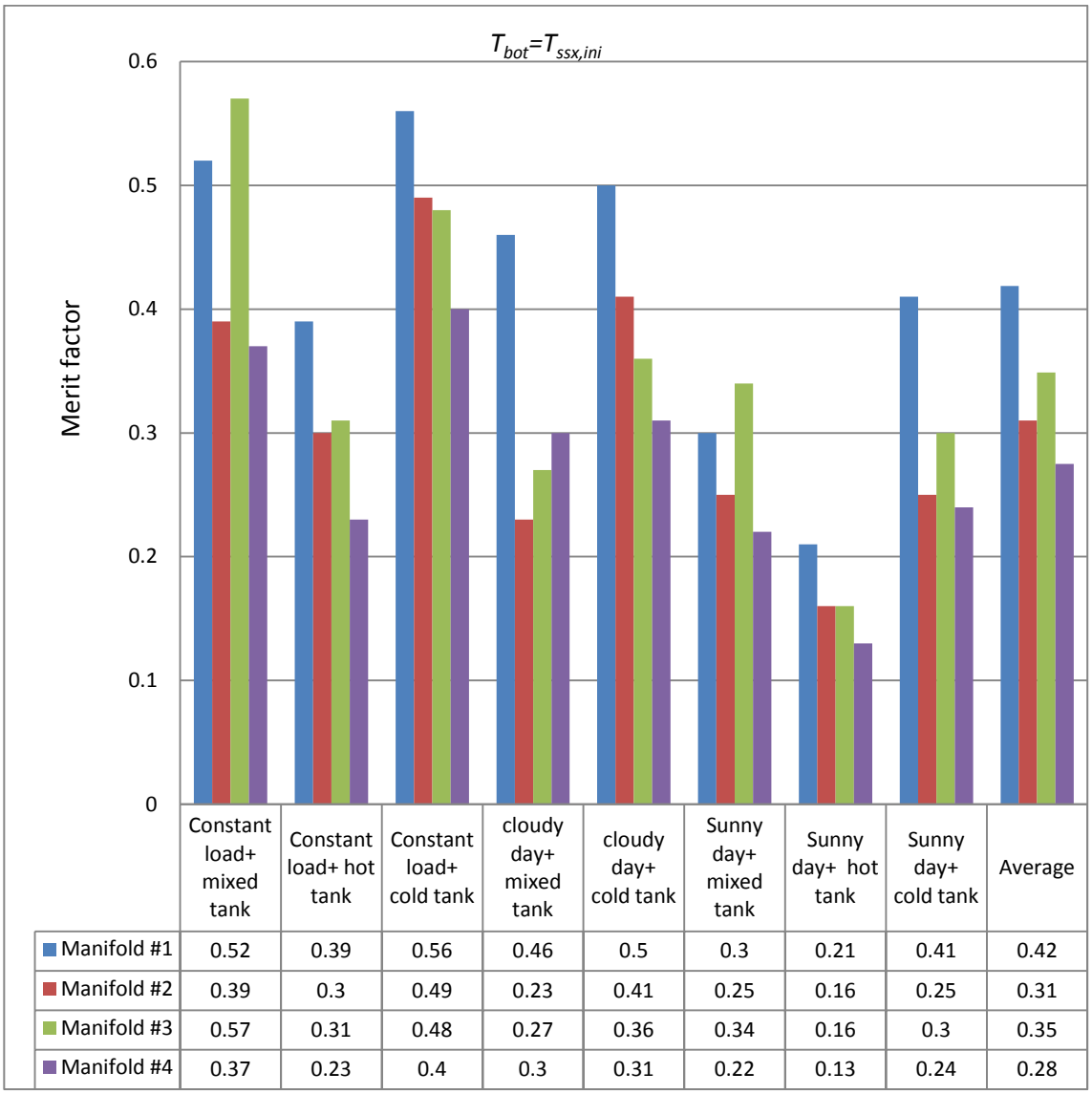

	Constant load+ mixed tank	Constant load+ hot tank	Constant load+ cold tank	cloudy day+ mixed tank	cloudy day+ cold tank	Sunny day+ mixed tank	Sunny day+ hot tank	Sunny day+ cold tank	Average
Manifold #1	0.52	0.39	0.56	0.46	0.5	0.3	0.21	0.41	0.42
Manifold #2	0.39	0.3	0.49	0.23	0.41	0.25	0.16	0.25	0.31
Manifold #3	0.57	0.31	0.48	0.27	0.36	0.34	0.16	0.3	0.35
Manifold #4	0.37	0.23	0.4	0.3	0.31	0.22	0.13	0.24	0.28

Figure 38 Merit factors of the four manifolds analyzed by Condition #2.

6.9.3 RESULTS OBTAINED WITH CONDITION #3 ASSUMPTIONS

Figures 39 – 40 show the availability ratios and the entropy ratios for Condition #3. The results indicated that the entropy ratios were more realistic than the availability ratios to compare the thermal performance of manifolds, because the availability ratios were greater than one in some cases.

Unrealistic values of the availability ratios were attributed to the selection of the dead state temperature ($T_{ssx,\ min}$), therefore Condition #3 was unreliable to evaluate the thermal performance of manifolds.

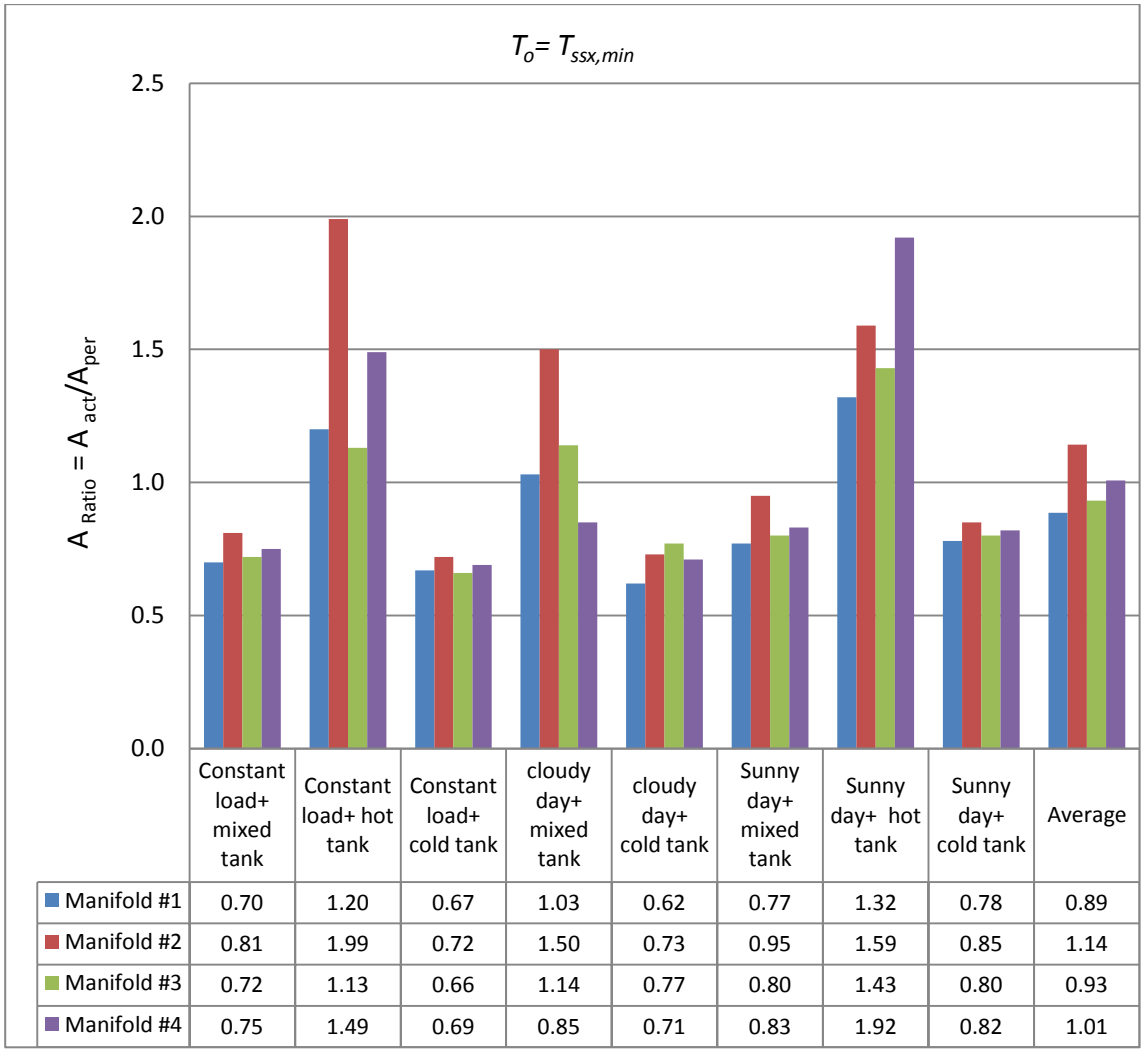

	Constant load+ mixed tank	Constant load+ hot tank	Constant load+ cold tank	cloudy day+ mixed tank	cloudy day+ cold tank	Sunny day+ mixed tank	Sunny day+ hot tank	Sunny day+ cold tank	Average
Manifold #1	0.70	1.20	0.67	1.03	0.62	0.77	1.32	0.78	0.89
Manifold #2	0.81	1.99	0.72	1.50	0.73	0.95	1.59	0.85	1.14
Manifold #3	0.72	1.13	0.66	1.14	0.77	0.80	1.43	0.80	0.93
Manifold #4	0.75	1.49	0.69	0.85	0.71	0.83	1.92	0.82	1.01

Figure 39 Availability ratios for the four manifolds analyzed by Condition #3.

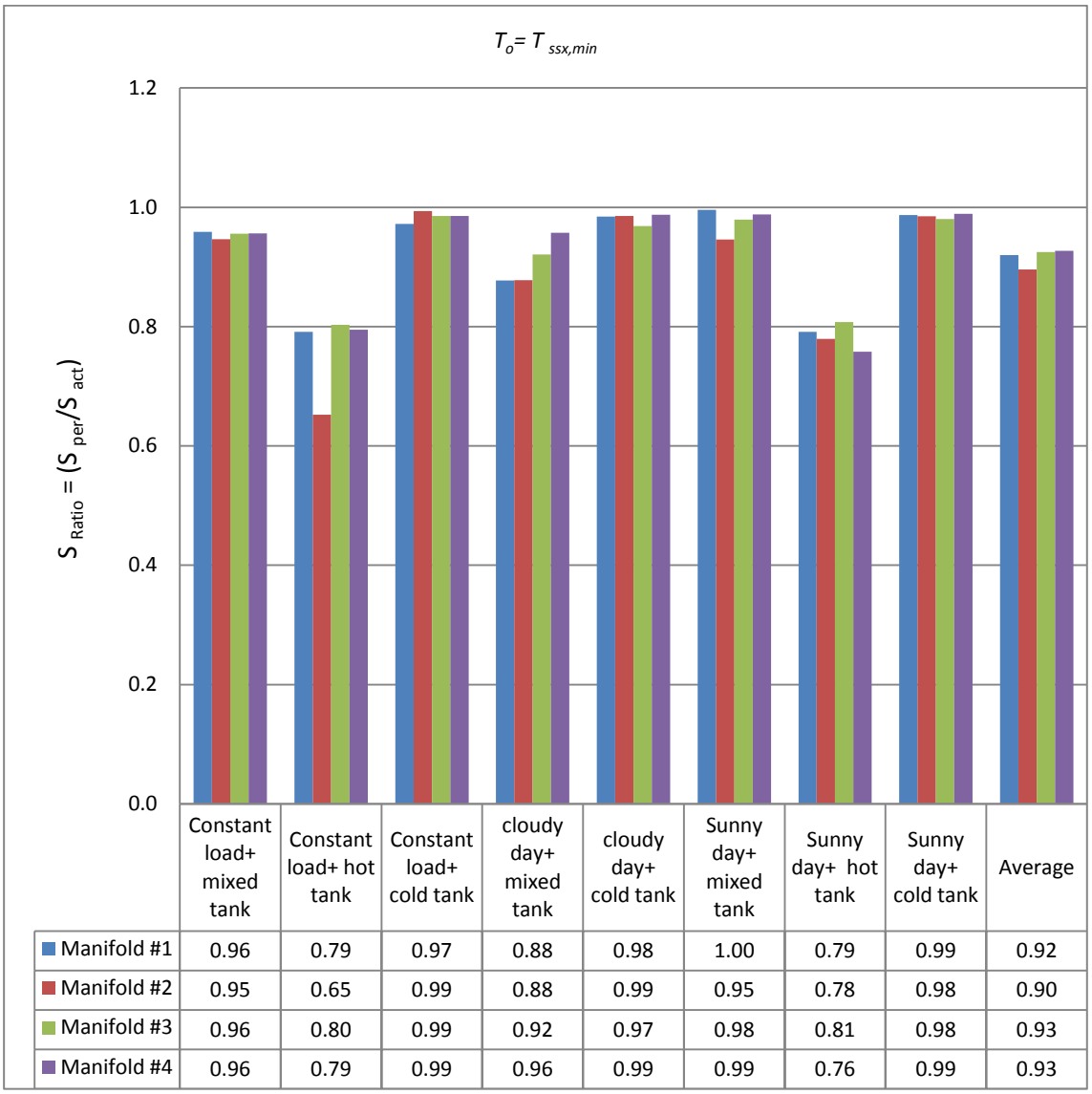

	Constant load+ mixed tank	Constant load+ hot tank	Constant load+ cold tank	cloudy day+ mixed tank	cloudy day+ cold tank	Sunny day+ mixed tank	Sunny day+ hot tank	Sunny day+ cold tank	Average
Manifold #1	0.96	0.79	0.97	0.88	0.98	1.00	0.79	0.99	0.92
Manifold #2	0.95	0.65	0.99	0.88	0.99	0.95	0.78	0.98	0.90
Manifold #3	0.96	0.80	0.99	0.92	0.97	0.98	0.81	0.98	0.93
Manifold #4	0.96	0.79	0.99	0.96	0.99	0.99	0.76	0.99	0.93

Figure 40 Entropy ratios for the four manifolds analyzed by Condition #3.

6.9.4 RESULTS OBTAINED WITH CONDITION #4 ASSUMPTIONS

Figures 41 – 42 show the availability ratios and entropy ratios calculated based on Condition #4. In this case the availability ratios were more realistic than the entropy ratios to compare the performance of manifolds, because the entropy ratios were greater than one in some cases. Unrealistic values of the entropy ratios were attributed to the selection of the dead state temperature ($T_{ssx,\ final\ actual}$). As a result, Condition #4 was unsuitable to compare the thermal performance of the manifolds. The reason was attributed to selecting the bottom temperature of the final actual tank ($T_{ssx,\ final\ actual}$) as dead state temperature.

The dead state temperature should represent a state where the energy is not useful to the user of the system (since the water is colder than the selected reference temperature, it has no useful energy).

In general, the perfectly stratified tank has higher availability and lower entropy than the actual tank and the most effective manifold should have higher average of availability ratios and higher average of entropy ratios than other manifolds.

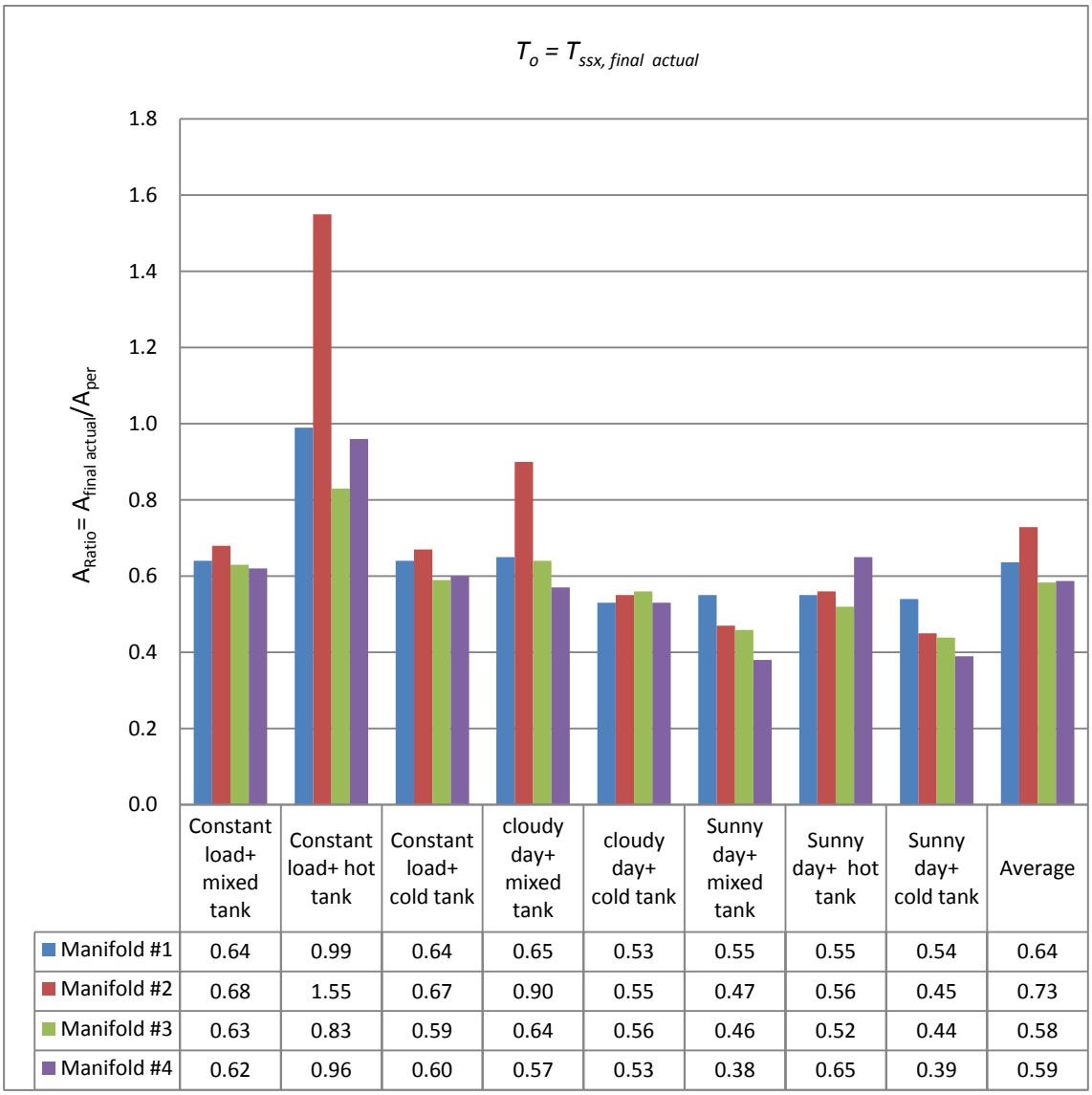

	Constant load+ mixed tank	Constant load+ hot tank	Constant load+ cold tank	cloudy day+ mixed tank	cloudy day+ cold tank	Sunny day+ mixed tank	Sunny day+ hot tank	Sunny day+ cold tank	Average
Manifold #1	0.64	0.99	0.64	0.65	0.53	0.55	0.55	0.54	0.64
Manifold #2	0.68	1.55	0.67	0.90	0.55	0.47	0.56	0.45	0.73
Manifold #3	0.63	0.83	0.59	0.64	0.56	0.46	0.52	0.44	0.58
Manifold #4	0.62	0.96	0.60	0.57	0.53	0.38	0.65	0.39	0.59

Figure 41 Availability ratios for the four manifolds analyzed by Condition #4.

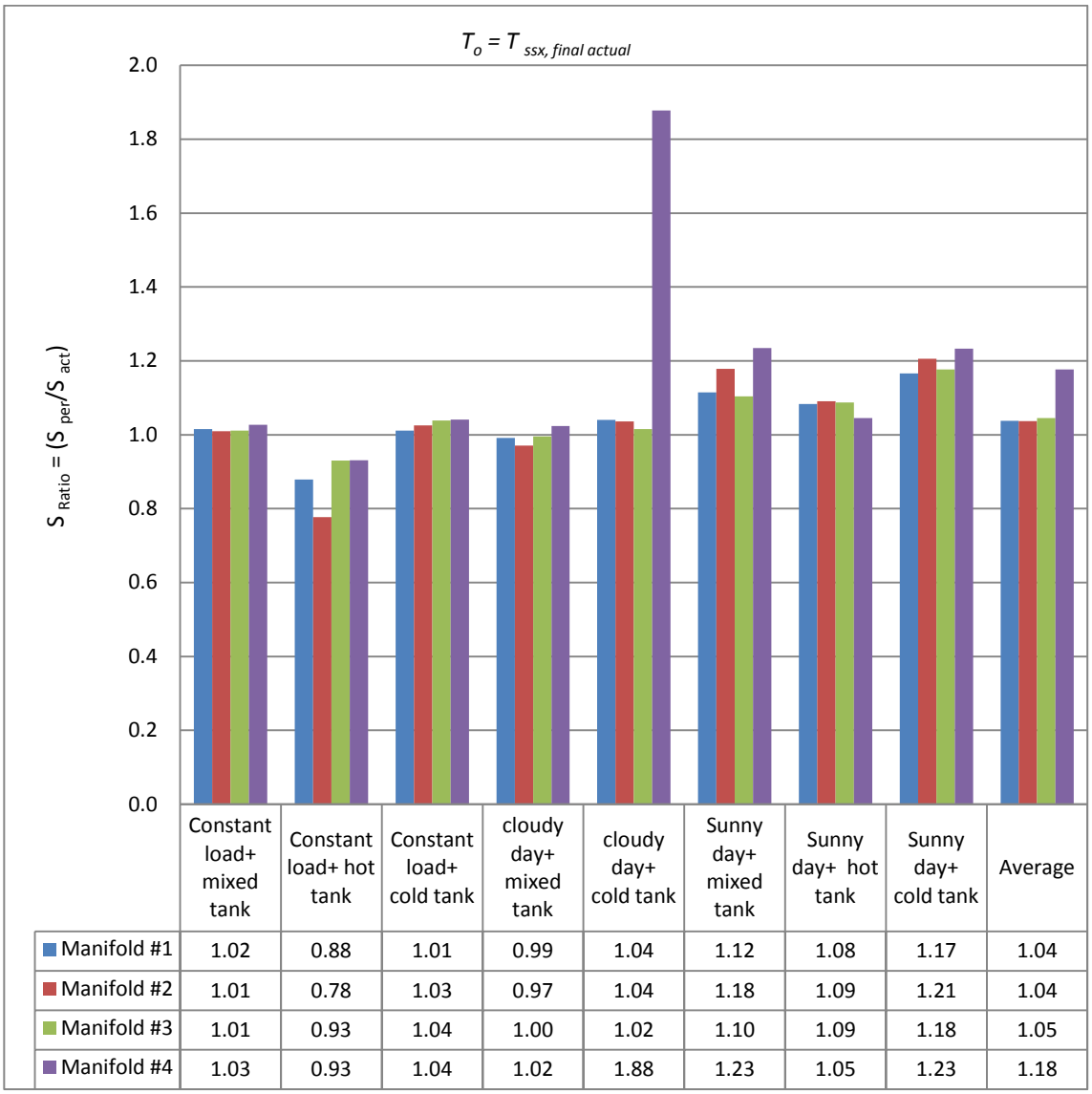

	Constant load+ mixed tank	Constant load+ hot tank	Constant load+ cold tank	cloudy day+ mixed tank	cloudy day+ cold tank	Sunny day+ mixed tank	Sunny day+ hot tank	Sunny day+ cold tank	Average
Manifold #1	1.02	0.88	1.01	0.99	1.04	1.12	1.08	1.17	1.04
Manifold #2	1.01	0.78	1.03	0.97	1.04	1.18	1.09	1.21	1.04
Manifold #3	1.01	0.93	1.04	1.00	1.02	1.10	1.09	1.18	1.05
Manifold #4	1.03	0.93	1.04	1.02	1.88	1.23	1.05	1.23	1.18

Figure 42 Entropy ratios for the four manifolds analyzed by Condition #4.

6.9.5 RESULTS OBTAINED WITH CONDITION #5 ASSUMPTIONS

Figures 43 – 44 show the availability ratios and the entropy ratios based on Condition #5. Condition #5 offered the most appropriate and consistent values of the average of the availability ratios and the average of the entropy ratios in terms of the most effective manifold.

Employing Condition #5 produced more realistic values of the availability ratios and entropy ratios than the previous Conditions, which means the perfectly stratified tank has higher availability and lower entropy than the actual tank.

In the previous Conditions, the order of the most effective manifold was inconsistent in terms of the highest average of the availability ratios and the highest average of the entropy ratios while with Condition #5 the results are consistent. The average of the availability ratios and the average of the entropy ratios indicate that the most effective manifold was manifold #2 and the reasons are analyzed in Section 7.2.

A graphical representation of Condition #5 for all the experimental work on the four manifolds is presented in Appendix D.

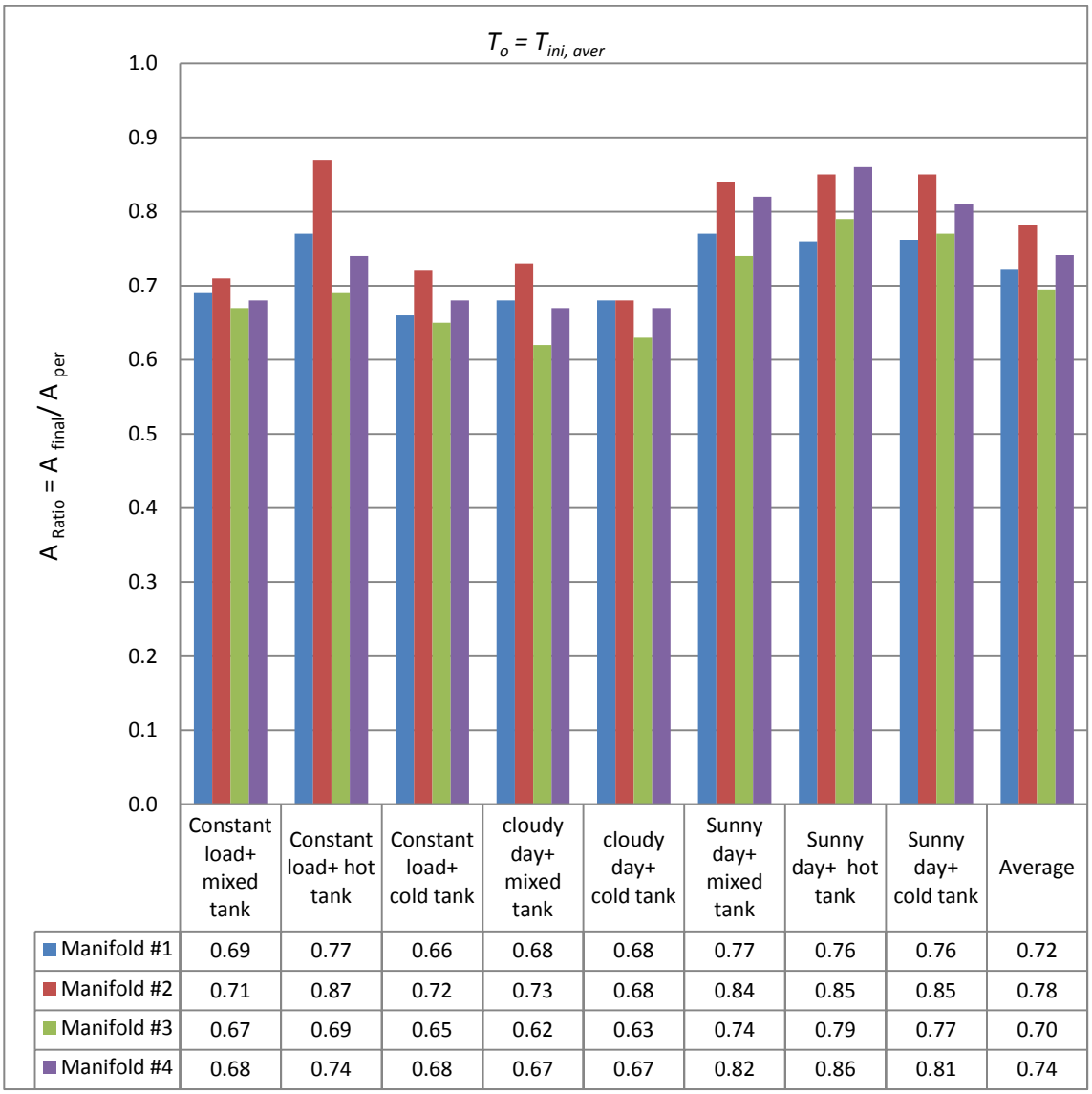

	Constant load+ mixed tank	Constant load+ hot tank	Constant load+ cold tank	cloudy day+ mixed tank	cloudy day+ cold tank	Sunny day+ mixed tank	Sunny day+ hot tank	Sunny day+ cold tank	Average
Manifold #1	0.69	0.77	0.66	0.68	0.68	0.77	0.76	0.76	0.72
Manifold #2	0.71	0.87	0.72	0.73	0.68	0.84	0.85	0.85	0.78
Manifold #3	0.67	0.69	0.65	0.62	0.63	0.74	0.79	0.77	0.70
Manifold #4	0.68	0.74	0.68	0.67	0.67	0.82	0.86	0.81	0.74

Figure 43 Availability ratios for the four manifolds analyzed by Condition #5.

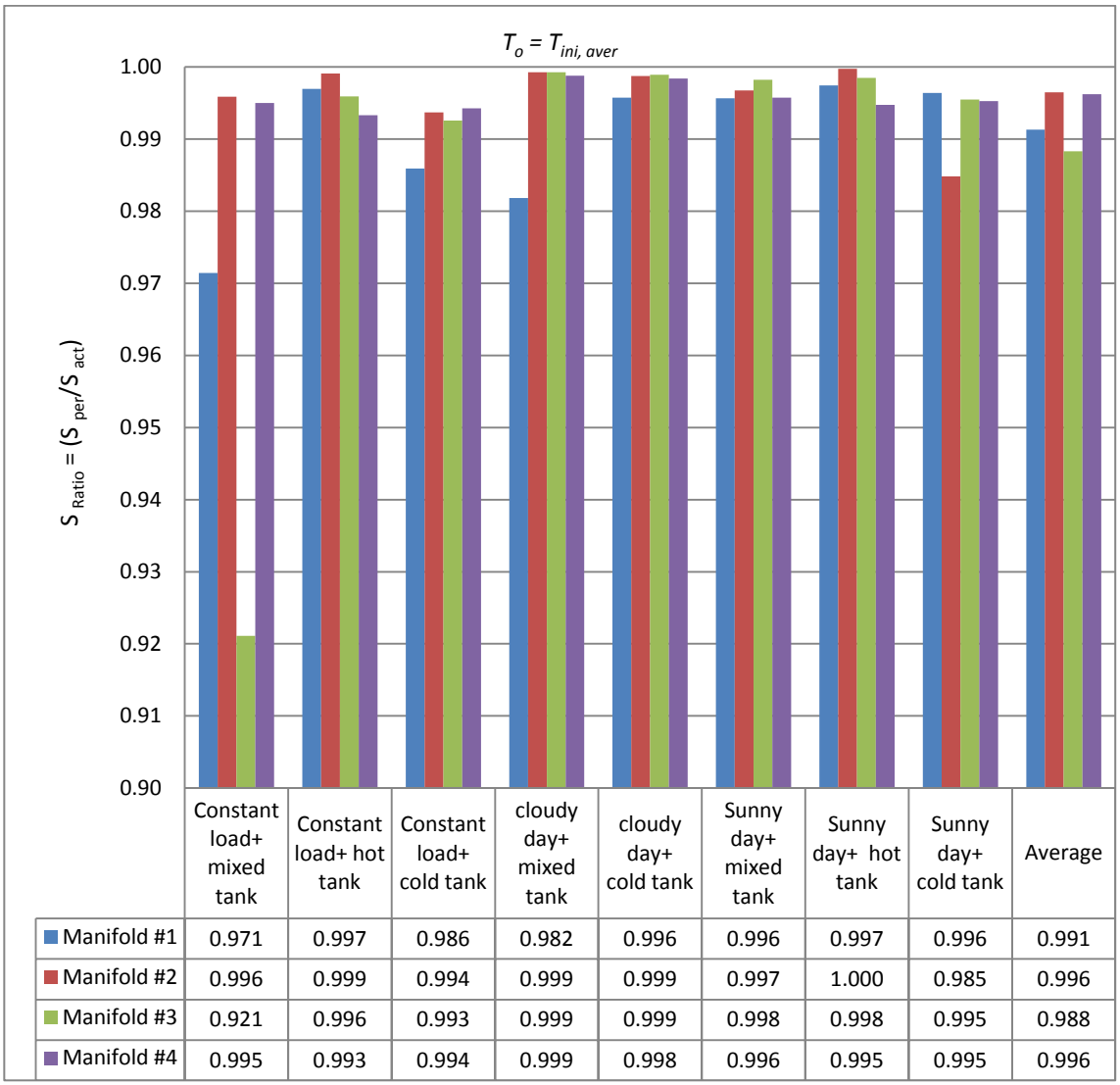

	Constant load+ mixed tank	Constant load+ hot tank	Constant load+ cold tank	cloudy day+ mixed tank	cloudy day+ cold tank	Sunny day+ mixed tank	Sunny day+ hot tank	Sunny day+ cold tank	Average
Manifold #1	0.971	0.997	0.986	0.982	0.996	0.996	0.997	0.996	0.991
Manifold #2	0.996	0.999	0.994	0.999	0.999	0.997	1.000	0.985	0.996
Manifold #3	0.921	0.996	0.993	0.999	0.999	0.998	0.998	0.995	0.988
Manifold #4	0.995	0.993	0.994	0.999	0.998	0.996	0.995	0.995	0.996

Figure 44 Entropy ratios for the four manifolds analyzed by Condition #5.

CHEAPER 7: DESIGNING A MANIFOLD FOR SDHW SYSTEM

7.1 HOT WATER INSIDE THE MANIFOLD

To design a manifold that will enhance thermal stratification in a SDHW system tank, it is necessary to understand the behavior of the hot water inside the manifold. Seven thermocouples, (chB(1) – chB (7)), were installed inside the manifold, from the bottom to the top and in front of each opening, to measure hot water temperature.

Also, in the perforated manifold, the pressure difference between the cold water in the tank and the hot water in the manifold forced the cold water into the lowest opening of the manifold. This reduced both the temperature of the hot water and the pressure differential between the tank and the manifold until equilibrium occurred.

Figures 45 – 47 show the temperatures measured in the perforated manifolds (#2, #3, and #4) and the heat input rates during the sunny day tests with cold tank condition. The tank temperature at the start of the test was 17°*C*, 21°*C*, and 17°*C*, respectively, for manifolds #2, #3, and #4. Although the heat addition was the same in each of these tests, the temperature distribution inside the manifolds was different from one manifold to another. The differences were due to differences in manifold design.

For example, as seen in Figures 45 – 47, the water temperature inside the manifolds (#2, #3, and #4) dropped at 2:00 PM from level chB(1) to level chB(2). The temperature dropped from 48°*C* to 37°*C,* 46°*C*, and 41°*C*, respectively. The drop was associated with the diameter of the hole at level chB(2). The diameters of the holes are 9mm, 3mm, and 5mm, in manifolds #2, #3, and #4, respectively. In another example, as shown in Figure 45 and Figure 47, the water temperature inside manifolds #2 and #4 went from 48°C to 33°*C* at 2:00 PM. The temperature drops occurred in two stages in manifold #2 (from 48°*C* to 37°*C* to 33°*C*) and in three stages in manifold #4 (from 48°*C* to 41°*C* to 37°*C* to 33°*C*), as the hole diameter gradually increased from the bottom to the top in manifold#4.

Figure 48 shows the water flow rate through manifold #2 and the temperature of the water inside the manifold at levels chB(1) and chB(2)) during the sunny day test with cold tank condition. The jumps that occurred every hour (10:30 AM, 11:30 AM, etc.) in the lower temperature of the manifold (at level chB(1)) were due to changes in heat input

rates during the test. Figure 48 shows that, as soon as the temperature at chB(1) increased, the flow rate inside the manifold decreased and the water temperature droped due to the cold water influx from the tank into the manifold through the lowest opening. The cold water from the tank reduced the temperature of the water rising from the heat exchanger.

For example, in Figure 45, the temperature in the manifold dropped from 46ºC to 34ºC and then to 28ºC at 1:00 PM, and from 50ºC to 40ºC and then to 37ºC at 4:00 PM. The 18ºC and 13ºC droped between chB(1) (the lowest thermocouple) and chB(3) (the third thermocouple from the bottom) indicated that water from the tank was drawn into the manifold through the two lowest openings. Most of the influx of cold water into the manifold was at levels (2) and (3), because above these levels there was little temperature change inside the manifold. This phenomenon depended on the diameter of the manifold holes.

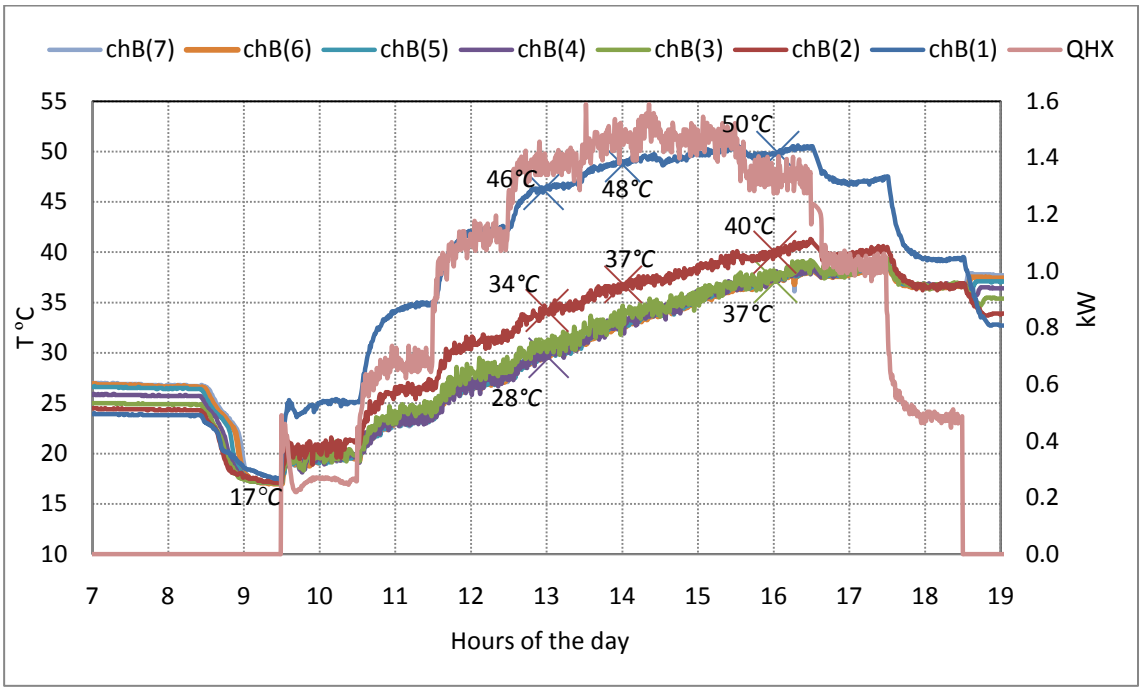

Figure 45 Temperatures inside manifold #2 and heat input rate of the heat exchanger.

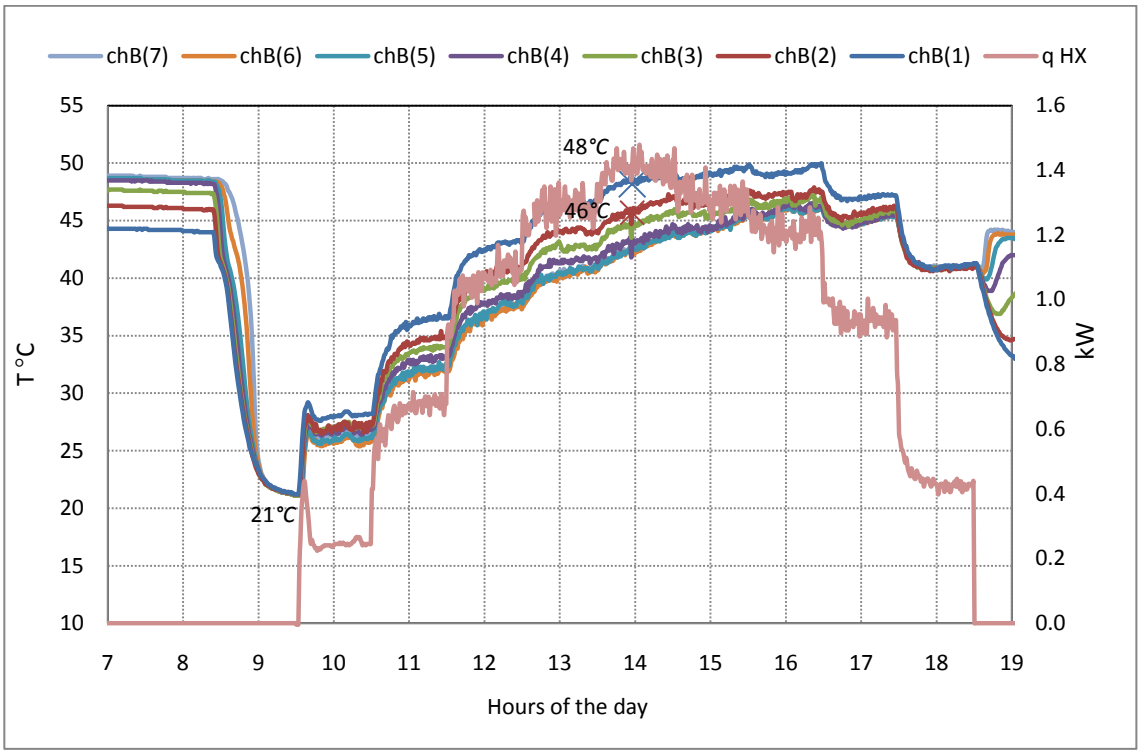

Figure 46 Temperatures inside manifold #3and heat input rate of the heat exchanger.

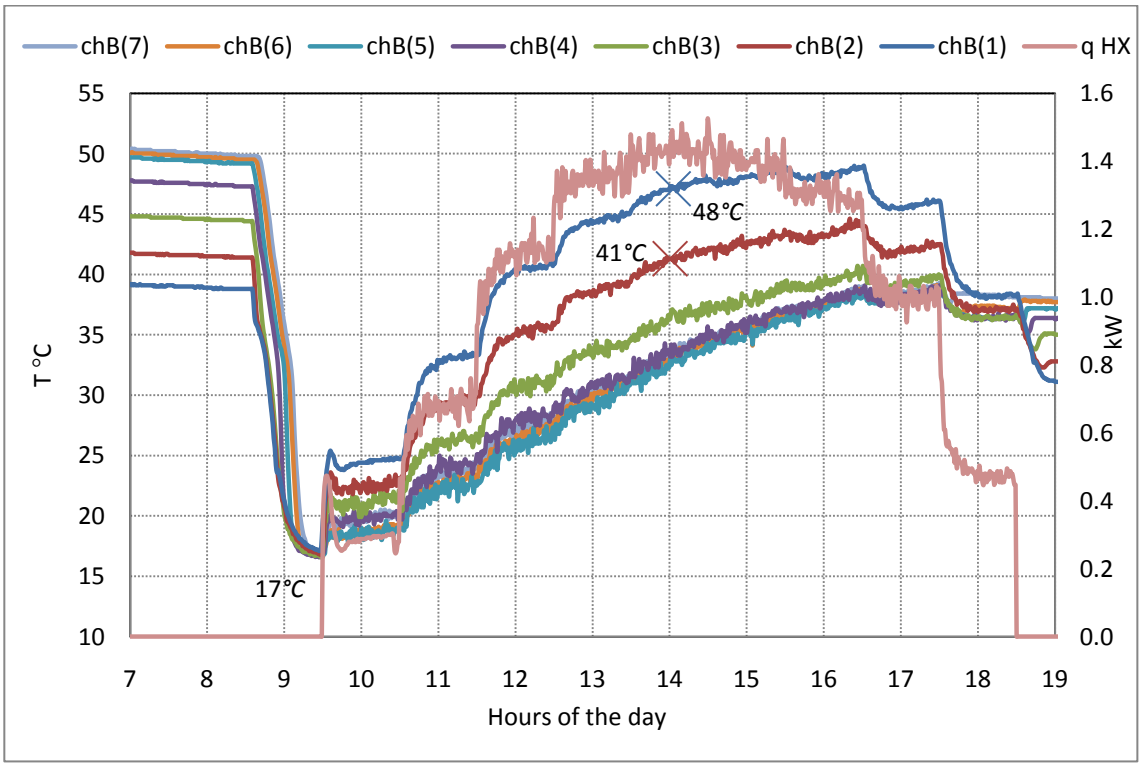

Figure 47 Temperatures inside manifold #4 and heat input rate of the heat exchanger.

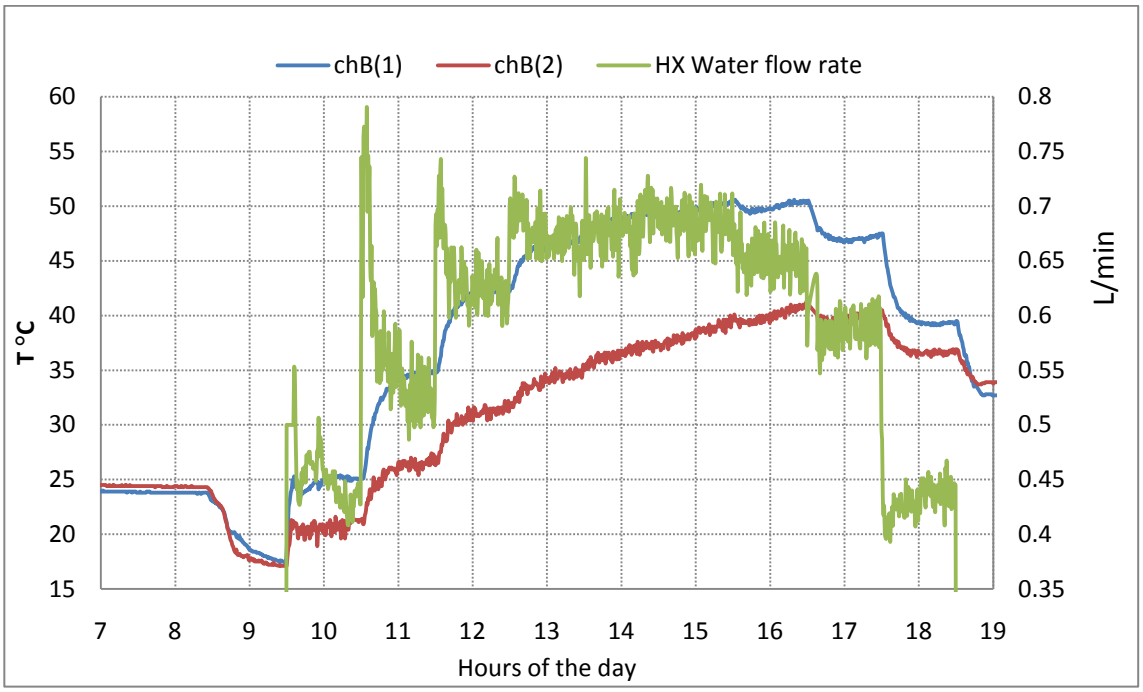

Figure 48 Water temperature inside the manifold at levels chB(1) and chB(2) and water flow rate through manifold #2 for the test of sunny day, cold tank condition

7.2 DESIGN GUIDELINES OF A MANIFOLD FOR SDHW SYSTEM

Thermal stratification within a tank is a function of the temperature of the water through the heat exchanger and the flow rate in the manifold. Based on the experimental results and the discussion in Section 5.2, an algorithm was developed to calculate the diameter of the holes required for the heated water to enter the tank at the matching temperature in order to improve stratification.

Using the water and glycol inlet and outlet temperatures from the heat exchanger and glycol flow rates during the tests, water flow rates through the manifolds were calculated. Top and bottom temperatures of the tanks and the temperature of the water outlet from the heat exchanger were also determined from the tests and plotted along with water flow rates through the manifolds, as shown in Figures 49 – 54.

Most of the time during the tests, the heated water temperature was higher than the tank temperature, and the heated water traveled to the top of the tank even if using a perforated manifold. For example, in Figure 50, the heated water was delivered to the top of the tank from 9:30 AM to 5:30 PM. On the other hand, if the heated water temperature was lower than the temperature at the top of the tank (e.g., in early morning or late afternoon), a perforated manifold enhanced stratification by delivering the water at the level where the temperature of the tank water matched the temperature of the heated water, thereby enhancing stratification. For example, in Figure 52, from the beginning of the test to 1:00 PM and from 2:00 PM to the end of the test, the perforated manifold was beneficial. In the latter case, in order to determine the diameter of the holes in the manifold, the water temperature at the top and the bottom of the tank as well as the heated water temperature and the corresponding water flow rate during the test had to be determined.

In the calculations of hole diameters, the tank was assumed to be uniformly stratified from the bottom to the top (according to the top and bottom temperatures) and the pressure differential between the manifold and the tank was determined according to the difference in densities. The pressure drops through the heat exchanger/manifold were calculated using Equations 5.2.2 – 5.2.6, and the diameter was calculated using Equation 5.2.7. In this calculation, if the water was heated by the heat exchanger at a temperature

higher than the tank top temperature, the diameter of the holes of the manifold was not important because the heated water traveled directly to the top of the tank, as shown in Figures 49 – 54. However, if the water heated by the heat exchanger was at a temperature lower than the tank's top temperature at the top of the tank, then the manifold hole diameter should be properly calculated. This was because the aim was to reduce the unwanted flow from the tank to the manifold and to allow the hot water to exit to the tank and enhance the stratification in the tank.

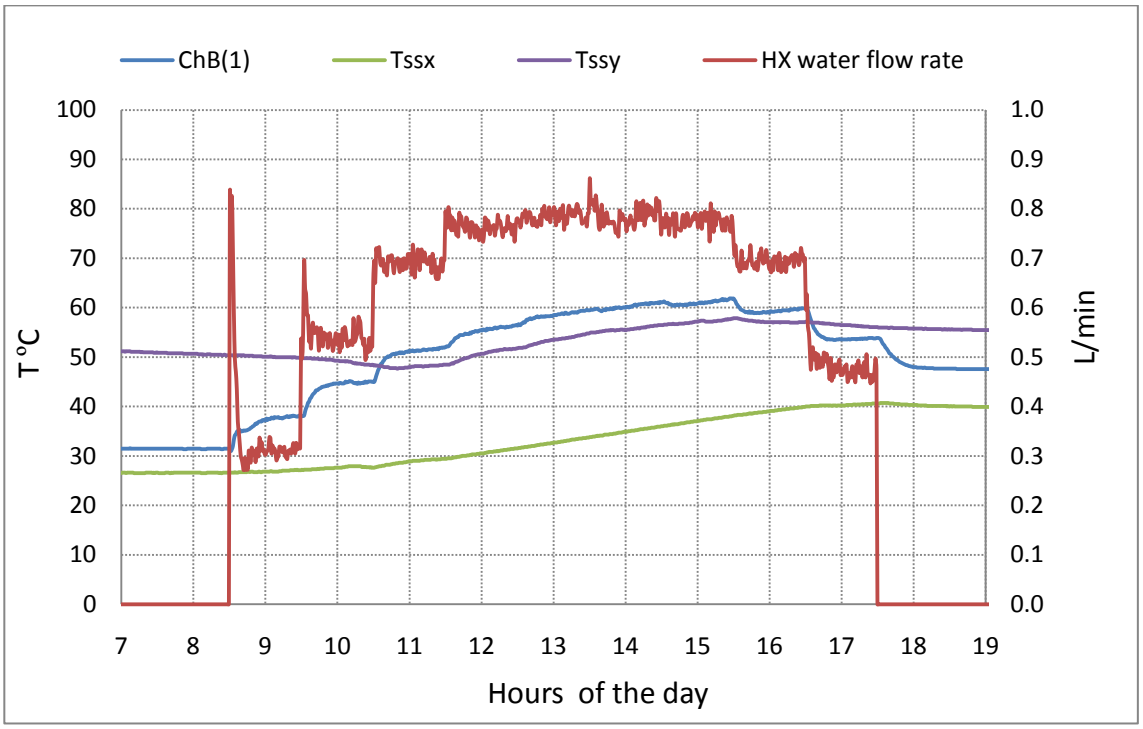

Figure 49 Water temperature at the heat exchanger outlet and water flow rate through the manifold during the test of manifold #3 (sunny day; hot tank condition).

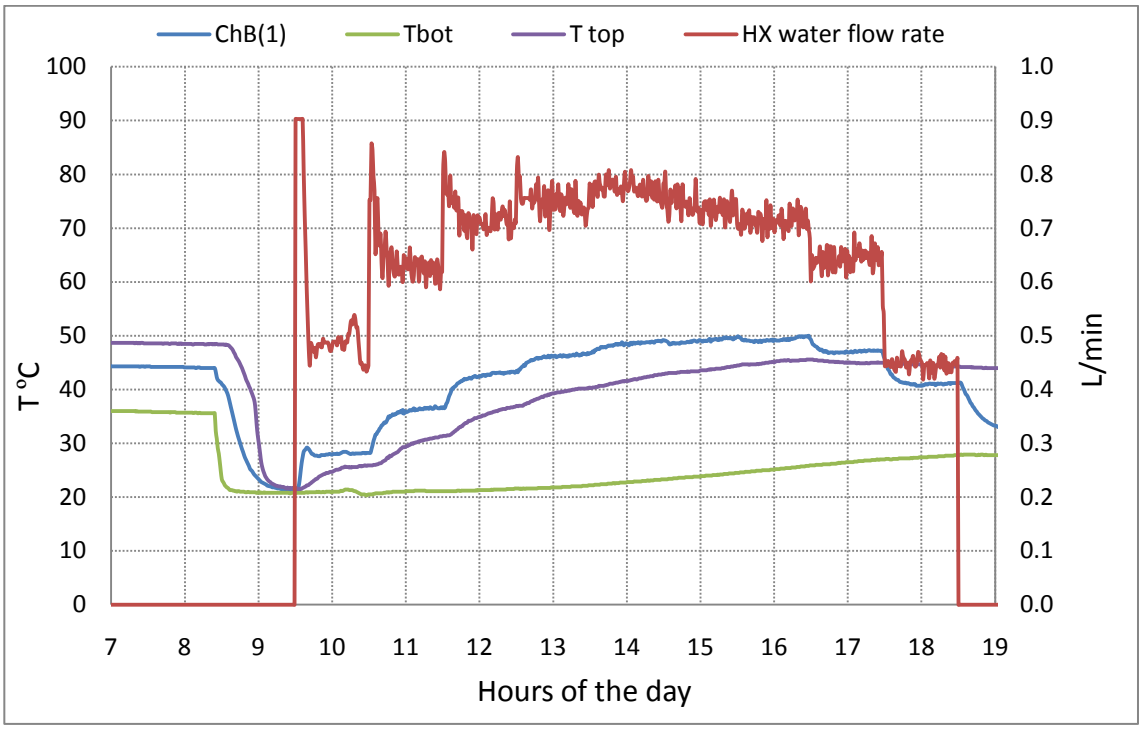

Figure 50 Water temperature at the heat exchanger outlet and water flow rate through the manifold during the test of manifold #3 (sunny day; cold tank condition).

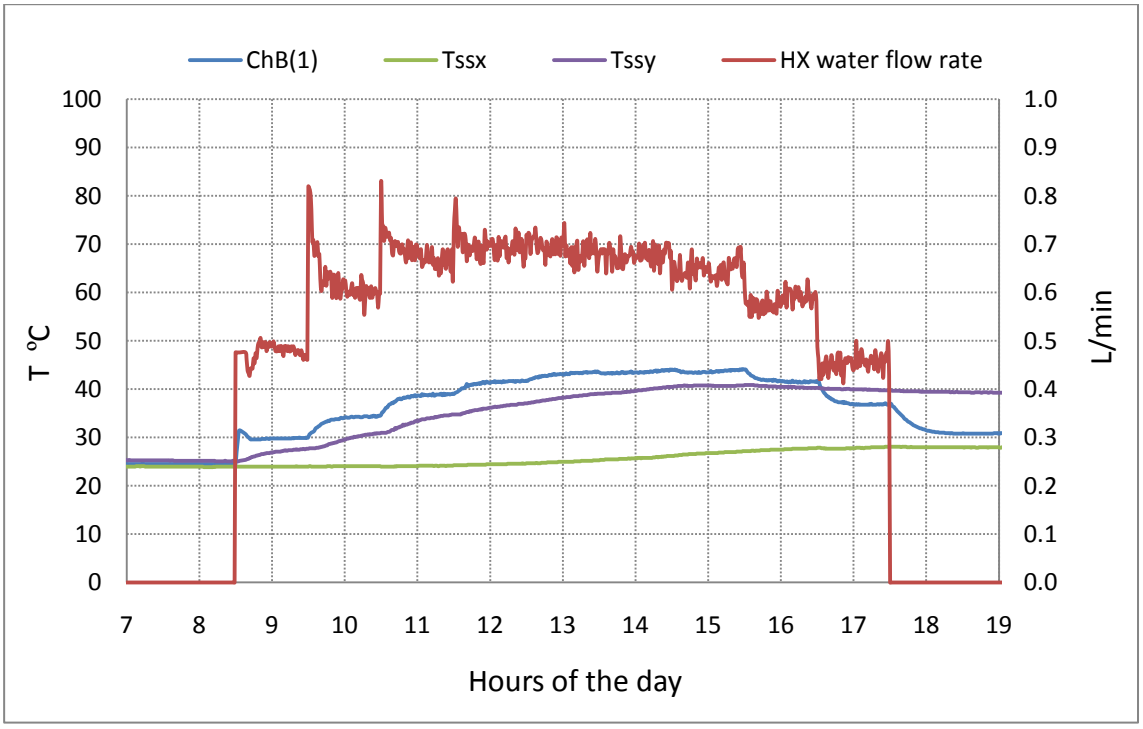

Figure 51 Water temperature at the heat exchanger outlet and water flow rate through the manifold during the test of manifold #3 (sunny day; mixed tank condition).

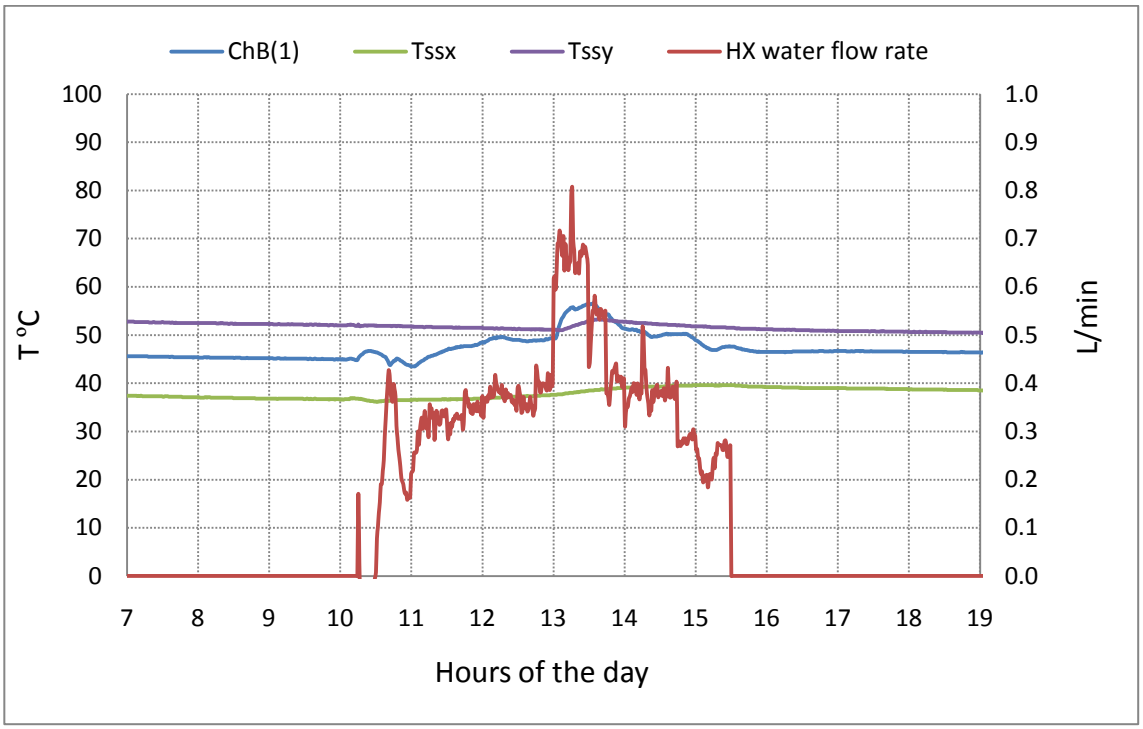

Figure 52 Water temperature at the heat exchanger outlet and water flow rate through the manifold during the test of manifold #3 (cloudy day; hot tank condition).

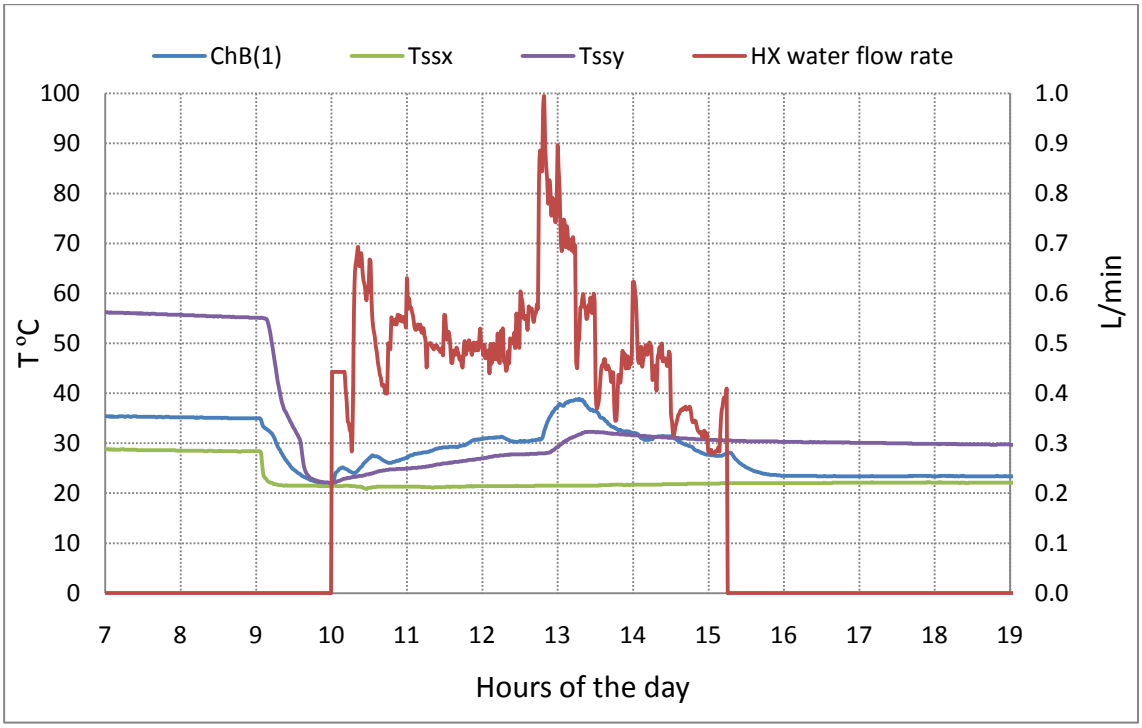

Figure 53 Water temperature at the heat exchanger outlet and water flow rate through the manifold during the test of manifold #3 (cloudy day; cold tank conditions).

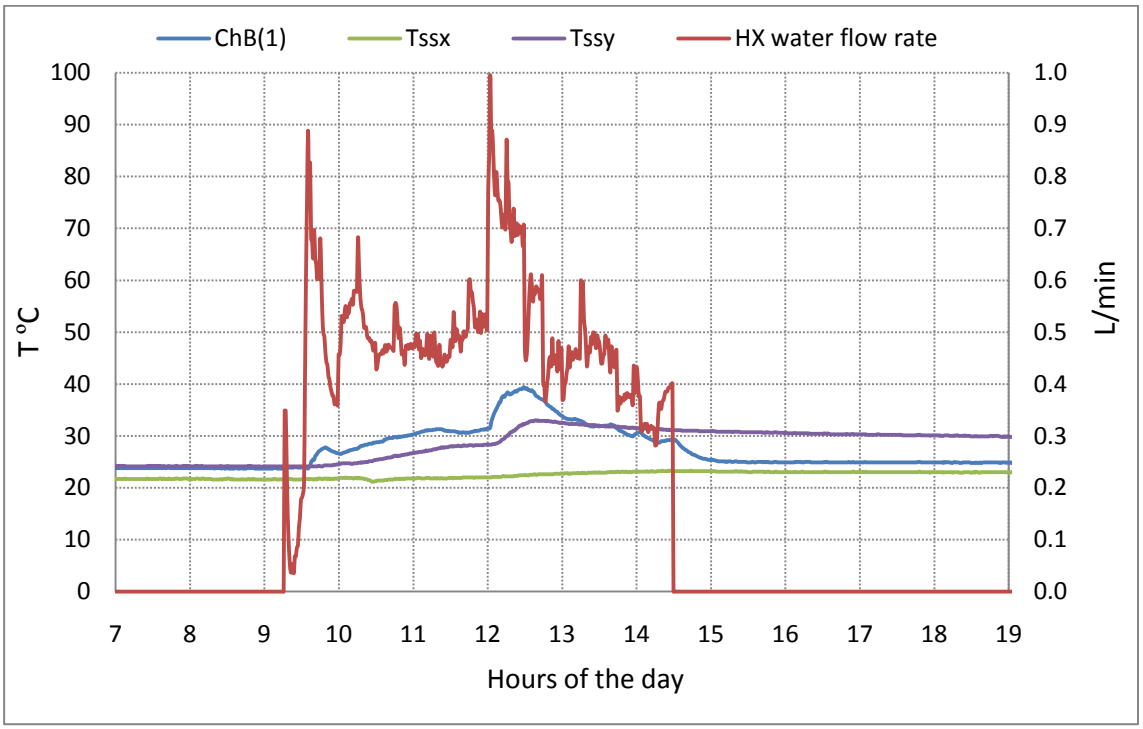

Figure 54 Water temperature at the heat exchanger outlet and water flow rate through the manifold during the test of manifold #3 (cloudy day; mixed tank conditions).

As shown in Table 2, the diameters of the holes were calculated for all tests based on the above parameters. For example, in the test that simulated a sunny day with hot tank condition, the temperature of the heated water at 5:00 PM was 55ºC and the corresponding density and flow rate of heated water through the manifold were 986 kg/m^3 and 0.45 L/min (0.0074 kg/s), respectively. The top and bottom tank temperatures were 58ºC and 40ºC, respectively. Assuming that the tank was stratified from the top to the bottom from 58ºC to 40ºC, respectively, the water in the tank and in the heat exchanger/manifold exerted a static pressure of 13,716 Pa and 13,741 Pa, respectively, at the bottom of the tank. The difference in pressure between the two columns was 25 Pa. From Figure 17, the water pressure drop through the heat exchanger and the manifold was 18 Pa. As a result, 7 Pa was available to drive the flow through the hole in the manifold. Applying Equation 7.2.1, the required diameter of the hole was calculated to be 9 mm.

$$\Delta P = \frac{\rho V^2}{2} = \frac{\dot{m}_w}{2\rho\left(\pi\frac{D^2}{4}\right)^2} \quad 7.2.1$$

where,

ΔP : The differential pressure, Pa.

$\dot{m}_w$: The heated water flow rate through the manifold, kg/s.

ρ : The density of water at the outlet of the heat exchanger, kg/m^3.

Table 2 Hole diameters required to enhance stratification.

	Sunny day and Hot tank condition	Sunny day and Cold tank condition	Sunny day and Mixed tank condition	Cloudy day and Hot tank condition	Cloudy day and Cold tank condition	Cloudy day and Mixed tank condition
Time	5:00 PM	6:00 PM	4:30 PM	12:00 PM	2:30 PM	2:30 PM
$m_{HX,\ w,\ out}$ *L/min*	0.45	0.45	0.4	0.35	0.35	0.35
$T_{HX,max,w,o}$ ºC	55	42	39	48	30	30
T_{ssy} ºC	58	45	40	51	30	31
T_{ssx} ºC	40	27	28	37	20	22
D_{max} *(mm)*	9	12	12	9	11	11

In another example of calculating the diameter of the hole, in a test that simulated sunny day, hot tank conditions, the temperature of the heated water at 10:30 AM was 45℃ and the corresponding density and flow rate of heated water through the manifold were 990 kg/m^3 and 0.5 L/min (0.0082 kg/s), respectively. The top and bottom tank temperatures were 48ºC and 27.5ºC, respectively, as shown in Figure 49. Assuming the tank was stratified from the top to the bottom from 48ºC to 27.5ºC, respectively, the water in the tank and in the heat exchanger/manifold exerted a static pressure of 13,801 Pa and 13,776 Pa, respectively, at the bottom of the tank. The difference in pressure between the two columns was 25 Pa. From Figure 17, the water pressure drop through the heat exchanger and the manifold was 22 Pa. As a result 3 Pa was available to drive the flow

through the hole in the manifold. Applying Equation 7.2.1, the required diameter of the hole was calculated to be 11 mm.

According to the tests results, Table 2 shows that the hole diameters required to enhance tank stratification vary from 9 mm to 12 mm. The average diameter in all tests is 10.6 mm. This result explains why manifold #2, containing 6 (9 mm) holes and a manifold outlet of 19 mm, was the most effective of the four manifolds.

Based on the above discussion, the design guidelines for manifolds for SDHW system with 20 mm piping and water flow rate in a range of (0.3 – 2.5 L/min) are as follows:

1. Estimate the top and the bottom temperatures in the tank to calculate the average density of the water in the tank. Assume that the tank is stratified linearly from top to bottom. Temperatures depend on the geographic location of the system.

2. Estimate the maximum temperature of the water at the outlet of the heat exchanger to calculate the density of the hot water inside the heat exchanger/manifold. The temperature of the hot water depends on the temperature distribution in the tank. The hot water temperature should match the water temperature in the tank at the level above the top of the heat exchanger to create the required pressure to circulate the hot water through the heat exchanger/manifold. An example to illustrate this is presented in Section 7.2.2.

3. Calculate the pressure difference between the hot water inside the heat exchanger/manifold and the cold water in the tank using Equation 5.2.1 associated with the estimated temperatures from steps 1 and 2.

4. Calculate the pressure drop through the heat exchanger /manifold using Equations 5.2.2 – 5.2.6 at different flow rates.

5. Calculate the minimum and the maximum required pressures to drive the natural flow through the heat exchanger/manifold by subtracting the pressure drop through the heat exchanger/manifold from the differential pressure (ΔP) at different flow rates.

6. From the above steps, choose a suitable hot water flow rate through the manifold ($\dot{m}_w$), as presented in the example in Section 7.3. The hot water flow rate can also be calculated using Equation 7.2.2.

$$\dot{m}_g C_{Pg}\left(T_{hgo} - T_{cgi}\right) = \dot{m}_w C_{Pw}(T_{hwo} - T_{cwi}) \qquad 7.2.2$$

where,

$\dot{m}_g$ & $\dot{m}_w$: Flow rate of the glycol and heated water by the *HX*, kg/s.

C_{Pg} & C_{Pw} : Glycol and the hot water's specific heat, kJ/kg · K.

T_{hgo} & T_{cgi} : The temperatures of the hot and cold glycol at the heat exchanger outlet and inlet, K.

T_{hwo} & T_{cwi} : The temperatures of the hot and cold water at the heat exchanger outlet and inlet, K.

7. Calculate the diameter (*D*) of the hole required for the available flow rate using Equation 7.2.1.

8. Estimate the length of the manifold. It extends approximately from the top of the heat exchanger nearly to the top of the tank.

9. Estimate the number of holes in the manifold. The number depends on tank dimensions and the required volume of the hot water in each layer.

7.3 AN EXAMPLE OF DESIGNING A MANIFOLD FOR SDHW SYSTEM

The diameter of the holes is not important if the water is heated by the heat exchanger at a temperature higher than the top temperature of the tank. This is because the heated water travels directly to the top of the tank at that time. As a result, the perforated manifold is effective in the early morning and late afternoon when the heated water is at temperatures lower than the temperature of the water at the top of the tank. Using the dimensions of the ISCHX and the storage tank, as shown in Figures 58, 59 and 60 in Appendix A, this example illustrates the steps in designing a manifold for the SDHW system.

In most situations, the maximum temperature that can be expected at the top of the tank and the minimum temperature that can be expected at the bottom of the tank are 60ºC and 10ºC, respectively. Assuming that the tank is stratified from the top to the bottom from 60ºC to 10ºC, respectively, the column of cold water in the tank exerts a static pressure of 13,809 Pa at the bottom of the tank.

To create enough pressure difference to circulate the hot water naturally through the heat exchanger/manifold, the water heated by the heat exchanger must be heated to a temperature higher than 34°*C*. This is because at 34°*C*, the corresponding density through the heat exchanger/manifold is 994 kg/m^3 and the column of hot water in the heat exchanger/manifold exerts a static pressure of 13,800 Pa at the bottom of the tank. The difference in pressure between the two columns is 9 Pa. Using Equations 5.2.2 – 5.2.6, the pressure drops through the heat exchanger/manifold are shown in Table 3. At a flow rate of 0.3 L/min, the water pressure drops through the heat exchanger/manifold is 8 Pa. As a result, 1 Pa is available to drive the flow through a hole in the manifold and that would be the minimum required pressure. Therefore, the water has to be heated to a temperature higher than 34°*C* to circulate the water through the manifold.

In this example, the temperature of the hot water is assumed to be at 40°C. The corresponding density through the heat exchanger/manifold is 992 kg/m^3. As result, the water in the heat exchanger/manifold exerts a static pressure of 13,790 Pa at the bottom of the tank. The difference of pressure between two columns is 20 Pa.

The hot water flow rate through the heat exchanger/manifold can be estimated using the pressure drop Table 3. Because the change in the density of the hot water at 34°C and 40°C is negligible, the pressure drop through the heat exchanger/manifold is the same, as shown in Table 3. As explained above, there will be no flow greater than 0.45 L/min because there is not enough pressure difference to drive the flow. Therefore, the hot water flow rate in the early morning or late afternoon is in the range of 0.3 – 0.45 L/min, and the associated pressure drop is in the range of 8 – 18 Pa. Subtracting the pressure drop from the pressure difference, the available pressure to drive the flow through the hole in the manifold is in the range of 12 Pa – 2 Pa. Applying Equation 7.2.1, the

required diameter of the hole is in the range of 13 mm to 6 mm, and the average of this range is 9.5 mm.

Table 3 Pressure drop through the heat exchanger/manifold at 34℃.

Hot water flow rate	Sharp entrance to the heat exchanger	Shell of the heat exchanger	Sudden contraction to the manifold $K_L = 0.405$	The manifold	Total pressure drop of the heat exchanger/manifold
	$h = K \times \frac{V^2}{2g}$	$NL = 40$ & $f = 5$ & $x = 1.1$	$h = K_L \times \frac{V^2}{2g}$	$h = f \times \frac{L}{d} \times \frac{V^2}{2g}$	
L/m	$P = h \times \rho \times g$	$\Delta P = NL\ (\chi)\left(\rho \frac{V^2_{max}}{2}\right) f$	$P = h \times \rho \times g$	$P = h \times \rho \times g$	Pa
0.3	8	0.2	0.06	0.0014	8
0.35	11	0.3	0.08	0.0016	11
0.4	14	0.4	0.11	0.0018	14
0.45	17	0.4	0.14	0.0021	18
0.5	22	0.6	0.17	0.0023	22
0.55	26	0.7	0.21	0.0025	27
0.6	31	0.8	0.25	0.0028	32
0.65	37	0.9	0.29	0.0030	38
0.7	42	1.0	0.34	0.0032	44

CHEAPER 8: CONCLUSIONS

An experimental study of four different manifolds and their respective thermal compatibility to a solar domestic hot water system was presented and discussed. The experimental work was carried out under the simulation of outdoor prevailing conditions in Halifax, Nova Scotia, Canada. Based on the experimental work presented and the discussion in Chapters 6, as well as the analysis of the results and corresponding discussion presented in Chapter 7, the following conclusions were drawn:

1. Stratification can be enhanced by using a perforated manifold under most operating conditions.
2. The pressure difference between the tank and the heat exchanger/manifold drives the hot natural circulation through the heat exchanger/manifold. The pressure difference is a function of the temperature of the cold and hot water.
3. A method to determine and design a perforated manifold that works with the standard Canadian SDHW system was established and evaluated experimentally.
4. Unwanted flow from the tank to the bottom of the manifold occurs due to differential pressure between the tank and the manifold.
5. Theoretically, gradually increasing the diameter of the holes in the manifold should reduce the unwanted flow of cold water from the tank to the manifold, but experimentally it was proven not to be the case.
6. An availability analysis approach was developed to evaluate the thermal performance of manifolds, which have been operated at different times of the year.
7. Availability is highly dependent on the dead state temperature. In a system which is not used to produce work, the dead state temperature is a critical parameter and depends on the surrounding conditions. In the case of an SDHW system, it can be the bottom temperature of the initial tank or the final actual tank or it can be the cold mains water temperature. The dead state temperature represents a state where the energy is no longer useful to the user of the system (since when the water is

colder than the dead state temperature has no useful energy). In this work, the reliable dead state temperature was the average temperature of the initial tank.

8. For SDHW systems that use an immersion heat exchanger/manifold, it is not recommended to use tanks that have their outlet at the top center, as the mixing of the hot and cold water occurs at the outlet of the manifold, which is located at the top center of the tank.

8.1. RECOMMENDATIONS FOR FURTHER WORK

Based on the findings of this work, the following is recommended:

1. Improvement of the performance of the manifold by using check valves that prevent the unwanted cold water flow from the tank into the manifold.
2. Development of a numerical model to study thermal stratification in the SDHW system tanks.
3. Validation of the manifold model with the experimental results.
4. Using the numerical model to extend the experimental study.
5. Conducting experiments to determine the number of holes according to the dimensions of the tank.
6. Testing and comparing the thermal performance of an external and immersion shell-and-coil heat exchanger with the manifold, in terms of *UA* and tank thermal stratification.

REFERENCES

Abernethy, R.B., Benedict, R.P., and Dowdell, R.B. 1985. ASME Measurement Uncertainty, Journal of Fluids Engineering, **107**: 161-164.

Al-Najem, N.M. and El-Refaee, M.M. 1997. A numerical study for the prediction of turbulent mixing factor in thermal storage tanks, Applied Thermal Engineering, **17**: 1173-1181.

Alsagheer, F. 2003. An experimental investigation of a new heat exchanger for solar domestic hot water system. Master of applied Science Thesis, Dalhousie University, Nova Scotia, Canada.

Altuntop, N., Arslan, M., Ozceyhan, V., and Kanoglu, M. 2005. Effect of obstacles on thermal stratification in hot water storage tanks, Applied Thermal Engineering, **25**: 2285-2298.

Andersen and Furbo. 1999. Thermal destratification in small standard solar tanks due to mixing during tapping. Proceedings of ISES solar world congress, **3**: 109 -111.

Andersen, E., Furbo, S., and Fan, J. 2007. Multilayer fabric stratification pipes for solar tanks, Solar Energy, **81**: 1219-1226.

Borgnakke and Sonntag. 2008. Fundamentals of thermodynamics, 7th edition. Wiley and Sons.

Çengel, Y.A. and Cimbala, J.M. 2006. Fluid mechanics : Fundamentals and applications. McGraw-Hill Higher Education, Boston.

Cruickshank, C.A. 2006. Simulation and testing of stratified multi-tank thermal storages for solar heating systems. Master of applied Science Thesis, Queen's University, Kingston, ON, Canada.

Csordas, G.F., Brunger, A.P., Hollands, K.G.T., and Lightstone, M.F. 1992. Plume entrainment effects in solar domestic hot water systems employing variable-flow-rate control strategies, Solar Energy, **49**: 497-505.

Davidson, J.H., Adams, D.A., and Miller, J.A. 1994. A coefficient to characterize mixing in solar water storage tanks, Journal of Solar Energy Engineering, **116**: 94.

Eames, P.C. and Norton, B. 1998. The effect of tank geometry on thermally stratified sensible heat storage subject to low Reynolds number flows, International Journal of Heat and Mass Transfer, **41**: 2131-2142.

Gari, H.N. and Loehrke, R.I. 1982. A controlled buoyant jet for enhancing stratification in a liquid storage tank. Journal of Fluids Engineering, **104**: 475-481.

Haller, M.Y., Cruickshank, C.A., Streicher, W., Harrison, S.J., Andersen, E., and Furbo, S. 2009. Methods to determine stratification efficiency of thermal energy storage processes – review and theoretical comparison, Solar Energy, **83**: 1847-1860.

Hermansson, R. 1993. Short term water heat storage. Ph.D. Thesis, Division of Energy Engineering, Lulea University of Technology, Lulea, Sweden.

Hollands, K.G. and Lightstone, M.F. 1989. A review of low-flow, stratified-tank solar water heating systems, Solar Energy, **43**: 97-105.

Incropera, F.P. and DeWitt, D.P. 2002. Introduction to heat transfer. Wiley, New York.

Jaluria, Y. and Gupta, S.K. 1982. Decay of thermal stratification in a water body for solar energy storage, Solar Energy, **28**: 137-143.

Knudsen, S. 2002. Consumers' influence on the thermal performance of small SDHW systems—Theoretical investigations, Solar Energy, **73**: 33-42.

Knudsen, S., Morrison, G.L., Behnia, M., and Furbo, S. 2005. Analysis of the flow structure and heat transfer in a vertical mantle heat exchanger, Solar Energy, **78**: 281-289.

Lavan, Z. and Thompson, J. 1977. Experimental study of thermally stratified hot water storage tanks, Solar Energy, **19**: 519-524.

Loehrke, R.I., Holzer, J.C., Gari, H.N., and Sharp, M.K. 1979. Stratification enhancement in liquid thermal storage tanks, Journal of Energy, **3**: 129-130.

MacLeod D. 1998. Evaluation of components in solar water heaters with photovoltaic powered pumps. Master of applied Science Thesis, Dalhousie University, Nova Scotia, Canada.

Miller, C.W. 1977. Effect of a conducting wall on a stratified fluid in a cylinder. *In* , Vol. AIAA paper No. 77-792, pp. 10 p.

Panthalookaran, V., Heidemann, W., and Müller-Steinhagen, H. 2007. A new method of characterization for stratified thermal energy stores, Solar Energy, **81**: 1043-1054.

Rosen, M. and Hooper, F. 1992. Modeling the temperature distribution in vertically stratified thermal energy storages to facilitate energy and exergy evaluation. Thermodynamics and the Design, Analysis and Improvement of Energy Systems, AES, **27**: 247-252.

Rosen, M., Pedinelli, N., and Dincer, I. 1999. Energy and exergy analysis of cold thermal storage systems. Department of Mechanical Engineering, Ryerson Polytechnic University, **23**: 1029.

Rosengarten, G., Morrison, G., and Behnia, M. 1999. A second law approach to characterising thermally stratified hot water storage with application to solar water heaters. Journal of Solar Energy Engineering, **121**: 185-227.

Shah, L.J. and Furbo, S. 2003. Entrance effects in solar storage tanks, Solar Energy, **75**: 337-348.

Shah, L.J., Andersen, E., and Furbo, S. 2005. Theoretical and experimental investigations of inlet stratifiers for solar storage tanks, Applied Thermal Engineering, **25**: 2086-2099.

Sherman, C., Wood, B.D., and and Mason, J. 1979. Effect of wall conduction on temperature relaxation in thermally stratified liquid thermal storage tanks. *In* , Vol. 1, pp. 591-595.

Shyu, R.J. and Hsieh, C.K. 1987. Unsteady natural convection in enclosures with stratified medium, Journal of Solar Energy Engineering, **109**: 127-133.

Sliwinski, B.J., Mech, A.R., and Shih, R.S. 1979. Stratification in thermal storage during charging, 6th International Heat Transfer Conference, Toronto, ON, : 149-154.

Wildin and Truman. 1985. Evaluation of stratified chilled water storage techniques. .

Zachár, A., Farkas, I., and Szlivka, F. 2003. Numerical analyses of the impact of plates for thermal stratification inside a storage tank with upper and lower inlet flows, Solar Energy, **74**: 287-302.

Zurigat, Y.H., Liche, P.R., and Ghajar, A.J. 1991. Influence of inlet geometry on mixing in thermocline thermal energy storage, International Journal of Heat and Mass Transfer, **34**: 115-125.

APPENDIX A

SOLAR COLLECTOR

To simulate an actual SDHW system test, the system used a liquid flat plate (*LFP*) collector as illustrated in Figure 55 manufactured by Thermo Dynamics Limited[4] with a gross area of 2.98 m^2, absorber area of 2.87 m^2, and single glazing of low iron tempered glass. The collector uses a Micro-Flo® absorber comprised of eight Sunstrip™ solar fins arranged in a serpentine fashion. The collector is installed on the roof of the C building on the Sexton Campus of Dalhousie University. The elevation difference between the solar collector and the heat exchanger / storage tank is about 12 m. The solar collector is tilted at an angle of 45° facing true south.

Figure 55 The solar collector.

[4] Thermo Dynamics Ltd. 101 Frazee Avenue, Dartmouth, Nova Scotia, Canada, B3B-1Z4,Tel: 902-468-1001, Fax: 902-468-1002

ELECTRICAL HEATERS

The maximum heating capacity of a 3 m^2 solar collector on a sunny Nova Scotia day is about 2 kW. Two 2.4 kW electrical heaters rated at 240 VAC (Figure 56) were used to heat the glycol solution and simulate the solar collector in daily experimental tests. The heaters are controlled with a POWER-STAT variable auto-transformer to provide the necessary power to heat the glycol solution. The electrical resistance of each heater is 24 ohms, and based on Ohm's law, at 210 V (Lab voltage) each heater provides 1840 watts. Therefore, two of these heaters were used. These electrical heaters are immersion heaters mounted in a thermally insulated heating chamber and designed to provide heat to a flowing medium.

Figure 56 The electrical heaters.

PUMP

The glycol circulation pump, shown in Figure 57, was manufactured by Procon[5] (model number 302A07OF12BC060 PSI). It has range of 0.2 – 4.4 L/min (0.05- 1.2 GPM) was used to circulate the collector coolant through the closed loop SDHW system.

Figure 57 The glycol circulation pump.

HEAT EXCHANGER

An immersion shell-and-coil heat exchanger (ISCHX), as illustrated in Figures 58 and 59, was used in this study. The heat exchanger is made of four vertical helical coils surrounded by a shell, and was manufactured by Thermo Dynamics Ltd. The heat exchanger has a threaded joint to allow installation of a longitudinally perforated manifold without removing the heat exchanger from the tank. A longitudinally perforated manifold that extends from the heat exchanger to the top of the tank was used to enhance thermal stratification. The purpose of the longitudinally perforated manifold was to deliver the water heated by the immersion heat exchanger to the tank at the level where the temperature of the water in the tank matched the temperature of the heated water, thereby enhancing stratification.

---

[5] PROCON 1313 E. Maple St., Suite 237, Bellingham, WA, US 98225, Tel: 360-685-4253, Fax: 360-685-4222.

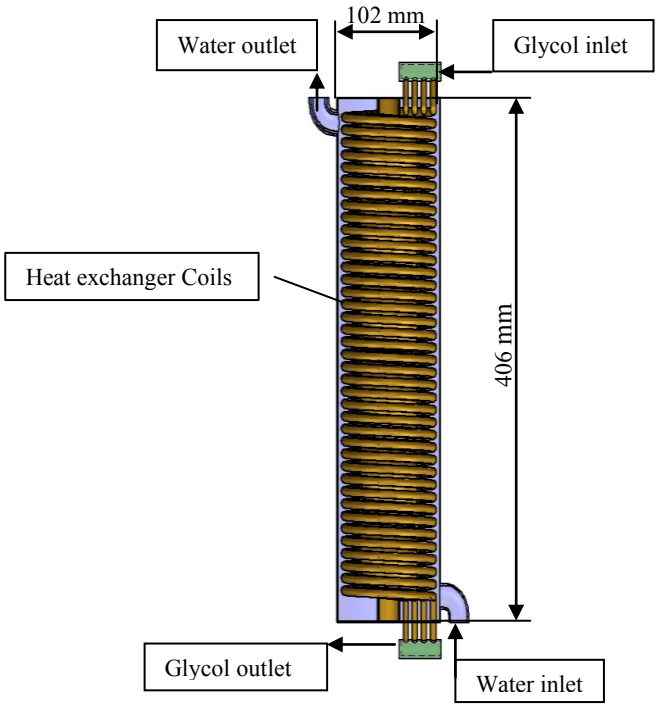

Figure 58 Schematic diagram of the heat exchanger.

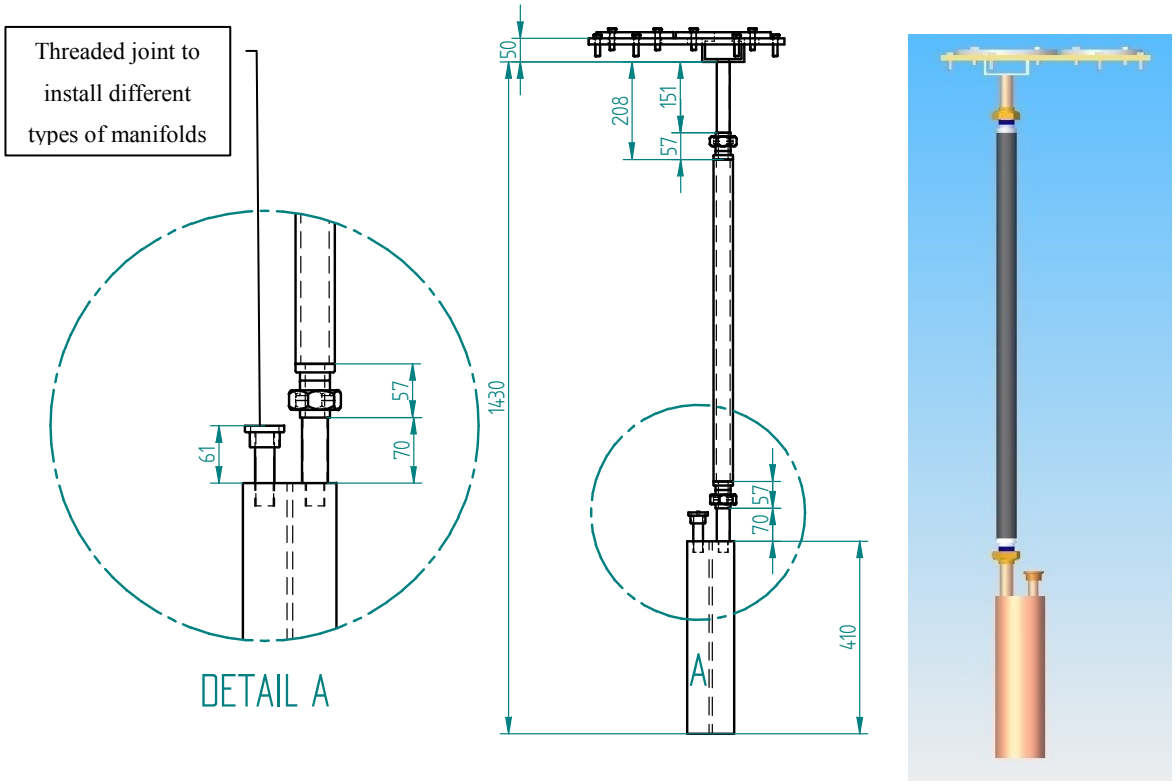

Figure 59 Diagram of the ISCHX showing the threaded joint to install the manifolds.

THERMAL STORAGE TANK

As shown in Figure 60, an acrylic tank of square cross-section with a volume of 370 liters was used in the experiments. The tank dimensions are 0.5 m x 0.5 m x 1.48 m high. The walls are made of 12.7 mm clear acrylic and reinforced with steel angle and threaded rod. A 15 cm x 15 cm acrylic diffuser plate is placed over the cold supply inlet to reduce mixing when charging the tank with cold water. The storage tank has an exit for the hot water at the top and an inlet to the cold water at the bottom. The tank is insulated by removable insulation.

Figure 60 The thermal storage tank.

PHOTOVOLTAIC MODULE

A photovoltaic module as shown in Figure 61 was used to provide the power required to the *DC* motor in case of using the solar collector set. The *PV* module is a Free Energy Europe *PV* [6], with a maximum power output of 12 W. The short-circuit current (I_{sc}) is 0.90 A. The open-circuit voltage V_{oc} is 22.0 V. The maximum voltage (V_{max}) and the maximum current (I_{max}) at maximum power (P_{max}) are 16 V, 0.75 A, respectively. The *PV* module was installed on the roof of the C building on the Sexton Campus of Dalhousie University. The *PV* module is placed at a slope of 45° facing south.

[6] 2, Rue Léon Droux, BP 66, 62302 Lens Cedex, France, Tel: +33 (0)3 21 79 3060 , Fax: +33 (0)3 21 43 6588

Figure 61 The photovoltaic module.

DC POWER SUPPLY

A DC power supply as shown in Figure 62 was used to provide the power required to the DC motor in case of using the electrical heaters set to replace the photovoltaic module in the SDHW system. The DC power supply installed with the DC motor to control the pump flow rate when using the electrical heaters. The DC power supply manufactured by Xantrex has a maximum voltage (V_{max}) and the maximum current (I_{max}) of 60 V, 5 A, respectively.

Figure 62 The DC power supply.

SOLAR IRRADIANCE MEASUREMENT

The intensity of the radiation in the plane of the collector and PV modules was measured by a spectral pyranometer Model CM6. This pyranometer uses a Moll thermopile, consisting of 14 elements of constantan-manganin, mounted under two optically ground hemispherical glass covers and has a *DC* voltage output signal, which is proportional to the level of irradiance. MacLeod D. (1998).

THERMOCOUPLES

Copper-Constantan thermocouples (TT-T-24) were used to measure all temperatures. Twenty-two thermocouples installed on two probes in the storage tank were used to measure the water temperature at ten levels along the depth of the tank. The temperature at the inlet and exit of the heat exchangers, the collector, and the storage tank as well as the temperatures indoor and outdoor were also measured by the same type of thermocouples.

PIPING

The connecting piping between the solar collector and the heat exchanger were made of 18.2 m long LIFE-LINE-C tubing. It consists of two 9.52 mm OD copper tubes (one supplying the collector with cold coolant, the other one returning the heated coolant to the heat exchanger) wrapped with non-hygroscopic glass fiber insulation and encased in a polyvinyl chloride (*PVC*) jacket. The LIFE-LINE-C heat loss coefficient is given by the manufacturer to be 0.144 W/m · K. For 17 m of tubing, the *UA* is then 2.4 W/K.
All of the other connection piping used was insulated copper.

DATA LOGGER

A Sciemetric Instruments[7] 8082A Electronic Measurement System (*EMS*) which has 80 electrically independent channels available for sensor connection was used for data collection. The 8082A can measure signals in the following ranges:

[7] **Sciemetric Instruments (World Headquarters),** 360 Terry Fox Drive, Ottawa, Ontario, Canada K2K 2P5,

- DC Voltage: - 4.096 to 4.096 volt
- DC Current: - 4.096 to 4.096 milli-ampere
- DC Resistance: 0 to 1.36 mega ohm
- AC Frequency: 0 to 20 kilohertz

The Sciemetric Instruments (*PC8*) pulse counter was used to count voltage pulses and convert them to analog DC voltage signals, which can be read by the *EMS*. The Sciemetric Instruments Model *RB01* single-board general-purpose controller for ON/OFF control was used to control the two solenoid valves.

A Sciemetric Instruments *PC8* Pulse Counter connected between the 8082A *EMS* and the flow meter was used to measure the glycol flow rate. The *PC8* Pulse Counters was used to count incoming pulses from the flow meter and to provide an analogue voltage for the data acquisition system.

APPENDIX B

The specific heat (C_p) calculated using Equation:

$$C_P = 4215 - (2.777)\,T + (7.046 \times 10^{-2})\,T^2 - (7.132 \times 10^{-4})\,T^3 + 2.898 \times 10^{-6})\,T^4$$

where,

T : water temperature, ºC. Borgnakke and Sonntag (2008)

The following equations were used to calculate specific entropies (s) and specific enthalpies (h), respectively and separately, for each layer according to its temperature.

They were also used to calculate the dead state specific entropy and specific enthalpy, (s_o) and (h_o), according to (T_o) where the subscript ($_o$) denotes the dead state *(reference)*. Borgnakke and Sonntag (2008)

$$s = (6 \times 10^{-8})\,T - (3 \times 10^{-5})\,T + (0.0154)\,T - 8 \times 10^{-5}$$

$$h = (6 \times 10^{-6})\,T - (0.0008)T + (4.2128)\,T + 0.0446$$

where,

s : Specific entropy, kJ/kg · K.

T : Water temperature, ºC.

h : Specific enthalpy, kJ/kg · K.

APPENDIX C

ERROR THEORY

Uncertainties of measured and derived quantities can be calculated using the method recommended by the American Society of Mechanical Engineers. Abernethy, et al. (1985).

It is a well-accepted principle in engineering that all measurements have an error (δ_k). The errors are the differences between the measurements and the true value. The error is usually expressed in two components, bias error (B) and precision error ($\in_k$).

BIAS ERROR

The bias error is the systematic error which is considered to remain constant during a given test. There is no statistical equation to define the bias limit (B). A bias error is assigned to each measured quantity that results from the instrumentation specifications. The total bias for each measured parameter 'P' at a recorded data interval 'i' can be calculated using Equation 1.

$$B_{pi} = \sqrt{B_1^2 + B_2^2 + \cdots B_K^2} \qquad 1$$

where, $B_1, B_2, \ldots, B_K$ are the bias values from 'k' components of error for measurement P.

PRECISION INDEX

The precision error can be determined by taking 'N' repeated measurements for the measured 'P' the characteristics of which can be approximated by the precision index (standard deviation of the data) and can be calculated using Equation 2.

$$S_P = \sqrt{\frac{\sum_{i=1}^{N}(x_i - \bar{x})^2}{N-1}} \qquad 2$$

where, N the number of recorded data intervals in set, x_i is measured data at each interval, i, and $\bar{x}$ is the mean value for the set.

The precision index of the average of a set of measurements is always less than that of an individual measurement according to Equation 3.

$$S_{\bar{x}} = \frac{S_P}{\sqrt{N}} \tag{3}$$

The total error of a measured quantity can be calculated by combining the bias and the precision errors using Equations 3 and 4.

$$U_{95\%} = \sqrt{B_{Pi}^2 + (tS_P)^2} \tag{4}$$

$$U_{95\%} = B_{Pi} + tS_P \tag{5}$$

where, $U_{95\%}$ and $U_{95\%}$ are the uncertainties for 95% and 99% two-sided confidence levels, respectively, and t is the Student's t value evaluated as a function of the degrees of freedom (ν) used in calculation $S_{\bar{x}}$ for large samples, (i.e., N > 30), t is set equal to 2, otherwise the Welch-Satterthwaite formula is used to provide ν ,according to Equation 6.

$$v = \frac{\left(\sum_{j=1}^{3}\sum_{i=1}^{k}\frac{S_{ij}^2}{N}\right)^2}{\sum_{j=1}^{3}\sum_{i=1}^{k}\frac{S_{ij}^4}{N_{vij}^2}} \tag{6}$$

where, S_{ij} represents the precision indices of the various error sources involved, and V_{ij} represents the degrees of freedom of these same error sources.

UNCERTAINTY OF DERIVED QUANTITIES

The uncertainty of derived quantity is propagated via the bias and precision indices of measured quantities calculated in both the total bias and the standard deviation. The final bias error of a calculated value, ν, is determined using sensitivity factors,θ, which propagate the error in measured parameters to the error in the final value. The sensitivity factors are defined as the partial derivatives as shown in Equation 7.

$$\theta_i = \frac{\partial v}{\partial Pi} \tag{7}$$

The bias in the calculated value is calculated using Equation 8.

$$B_v = \sqrt{\sum_{i=1}^{j} (\theta_i B_{Pi})^2} \tag{8}$$

where, the derived value, 'ν', is a function of 'j' measured parameters P_1, P_2,.., P_j, and $B_{p,i}$ is the bias of parameter 'P' at interval 'i', and calculated using Equation (1) for data index 'i'.

A similar equation applies for the precision index of the calculated value, S_v, using $S_{p,i}$ from Equation 2, and the total uncertainty is then calculated by Equation 3.

The manufacturing accuracies for the instruments which used in the experimental set-up are shown in Table 4.

Table 4 The manufacturing accuracy for the instruments which used in the experimental set-up

DEVICES	RANG		MANUFACTURING ERROR
T-type Thermocouples	Temperature	0 °C to 350 °C	±0.5%
Data acquisition system	**DC VOLTAGE**		
	Ranges	±8.192mV, ±40.96 mV,409.6 mV, ±4.096V	
	Resolution	2.0 µV on 8.192mV rang	
	Accuracy		0.1% + 2 digits
	RESISTANCE		
	Ranges	2000 Ω, 20 K Ω, 1.3 mΩ	
	Resolution	0.5 Ω on 2000 Ω scale	
	Accuracy		0.2% + digits
Power supply	Tracking accuracy		±(0.02% +5mV)
Flow meter	Industrial accuracy Calibrated accuracy	Full scale reading from 10% to 100% Full scale reading from 10% to 100%	±0.02 ±0.01

For example the error associated with the thermocouples measurements through the energy stored in the tank in a test of Manifold #2; Sunny day; Cold tank condition at (Appendix D Figure 75.a) at 2:00PM can be calculated as shown in Equation 9 and 10.

$$\mathrm{T_{avarage}} = \sum_{i=1}^{i=12} \frac{T_i}{12} = 25\,^{\circ}\mathrm{C} \qquad 9$$

$$Q_{stored} = m\,Cp\,\left(T_{avarage} - T_{cold}\right) = 37.93MJ \qquad 10$$

Because of 'm' and 'C_p' is a constant values and thermocouples error is ±0.5%, therefore the final Q_{stored} as shown in Equation 11.

$$Q_{stored} = 37.93 \pm 0.18\,MJ \qquad 11$$

APPENDIX D

The following graphs present the results of the fifth analysis condition (described in Section 6.9.5 and they are presented in the following order:

Figures 63 – 71 : show the results of the manifold #1.

Figures 72 – 80 : show the results of the manifold #2.

Figures 81 – 89 : show the results of the manifold #3.

Figures 90 – 98 : show the results of the manifold #4.

Each set of the results for the four manifolds are arranged in the same order as follows:

1. Temperature distribution in the solar storage tank during the test.
2. The availability of the actual tank, a perfectly stratified tank, and a fully mixed tank during the test.
3. The entropy of the actual tank, a perfectly stratified tank, and a fully mixed tank during the test.

Results from nine tests for each manifold are presented as follows:

1. Simulation of cloudy day; cold tank condition. At the start of the test, the tank was filled with cold water from the mains. The tank temperature was in the range of 10 – 21°C, as shown in Table 4.
2. Simulation of cloudy day; hot tank condition. At the start of the test, the tank temperature was in the range of 18 – 51°C, as shown in Table 4.
3. Simulation of cloudy day; mixed tank condition. At the start of the test, the tank temperature was in the range of 16 – 26°C, as shown in Table 4.

4. Simulation of sunny day; cold tank condition. At the start of the test, the tank was filled with cold water from the mains. The tank temperature was in the range of 10 – 21°*C*, as shown in Table 4.
5. Simulation of sunny day; hot tank condition. At the start of the test, the tank temperature was in the range of 18 – 51°C, as shown in Table 4.
6. Simulation of sunny day; mixed tank condition. At the start of the test, the tank temperature was in the range of 16 – 26°C, as shown in Table 4.

7. A fixed heat input; cold tank condition. At the start of the test, the tank was filled with cold water from the mains. The tank temperature was in the range of 10 – 21°C, as shown in Table 4.
8. A fixed heat input; hot tank condition. At the start of the test, the tank temperature was in the range of 18 – 51°C, as shown in Table 4.

9. A fixed heat input; mixed tank condition. At the start of the test, the tank temperature was in the range of 16 – 26°C, as shown in Table 4.

Table 5 Temperature at top and bottom of the tank at the start of the tests

Manifold #	Date	Test	Cold		Hot		Mixed	
			Tank T_{bot} ℃	Tank T_{top} ℃	Tank T_{bot} ℃	Tank T_{top} ℃	Tank T_{bot} ℃	Tank T_{top} ℃
Manifold #1	June 1,2,4, 2009	Cloudy day	12	14	20	46	19	20
	June 8,9,10, 2009	Sunny day	13	14	20	37	20	25
	May 19,20,21, 2009	Constant load	10	10	21	44	20	20
Manifold #2	July 9,13,15, 2009	Cloudy day	17	17	30	47	19	23
	July 6, 7,10, 2009	Sunny day	16	17	22	35	18	20
	June 17, 2009 July 1, 3, 2009	Constant load	14	15	18	46	20	23
Manifold #3	Aug 18, 25, 27, 2009	Cloudy day	21	21	37	51	22	24
	Aug 17, 19, 21, 2009	Sunny day	20	21	27	49	24	26
	Aug 13, 14, 15, 2009	Constant load	20	21	22	43	20	21
Manifold #4	Sep 10, 2009 Oct 8, 13, 2009	Cloudy day	16	17	30	50	16	17
	Oct 1, 5, 15, 2009	Sunny day	16	17	28	50	16	19
	Sep 11, 14, 24, 2009	Constant load	18	20	28	42	20	22

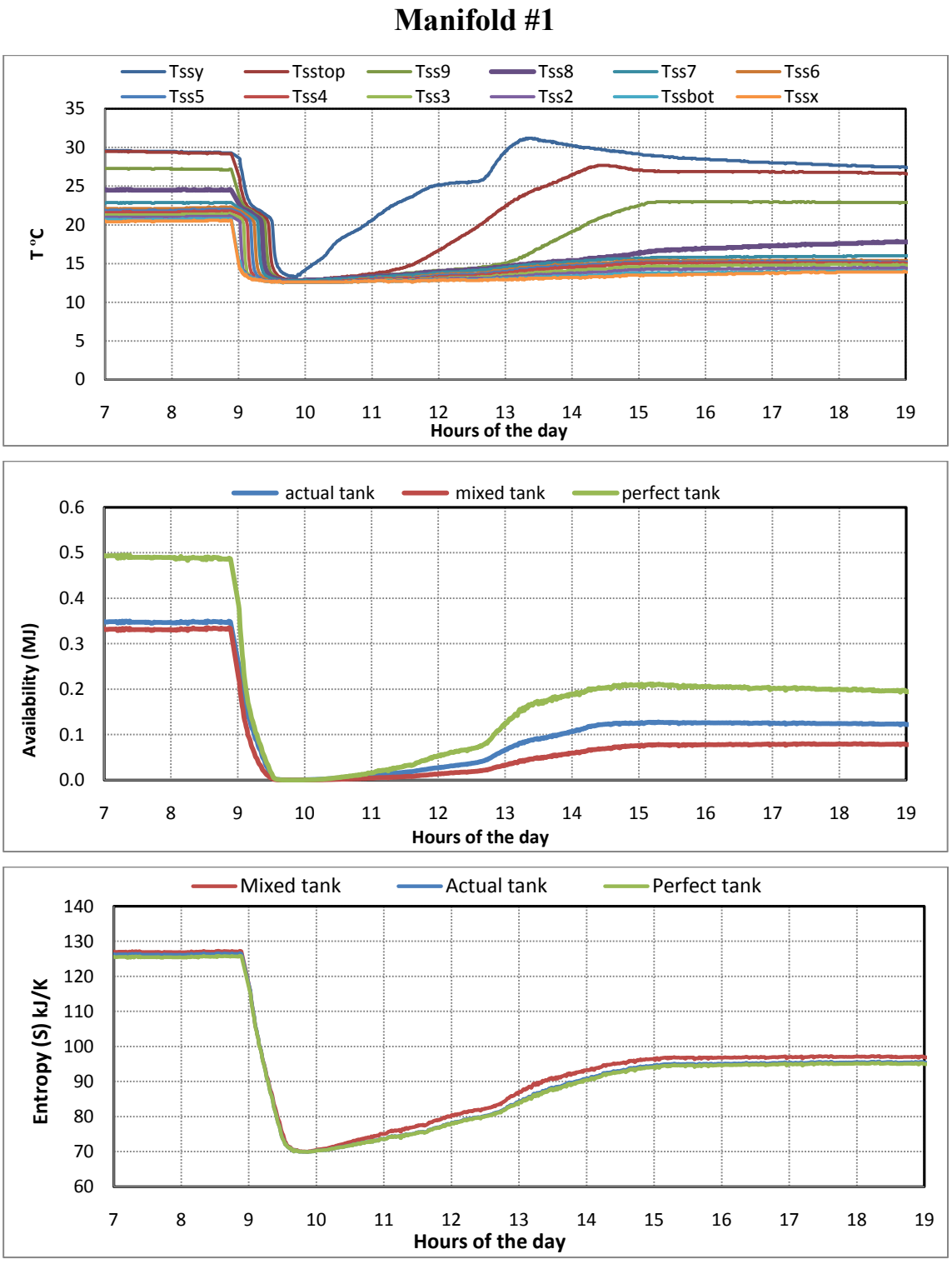

Figure 63 Manifold #1; Cloudy day; cold tank condition.

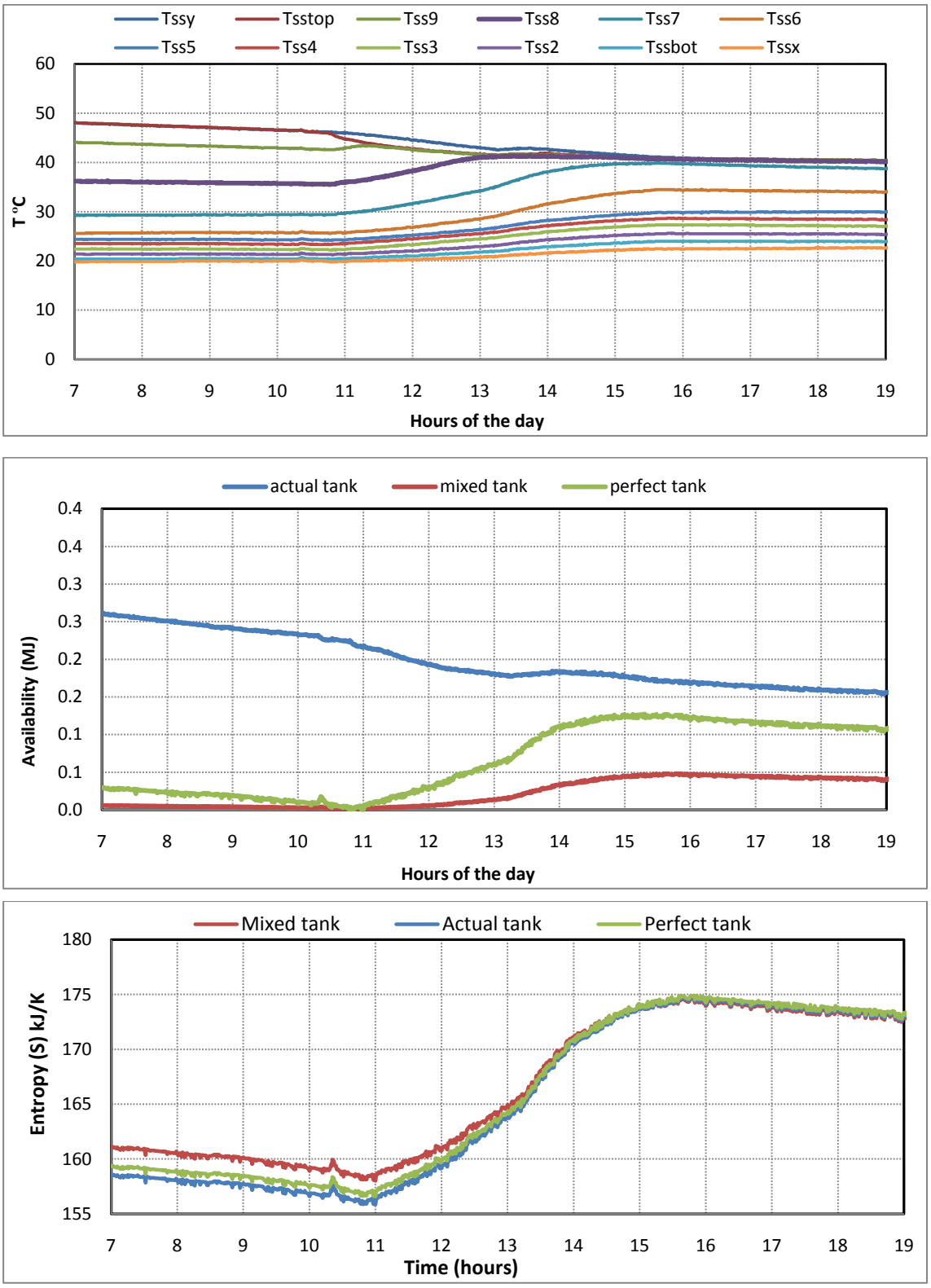

Figure 64 Manifold #1; Cloudy day; hot tank condition.

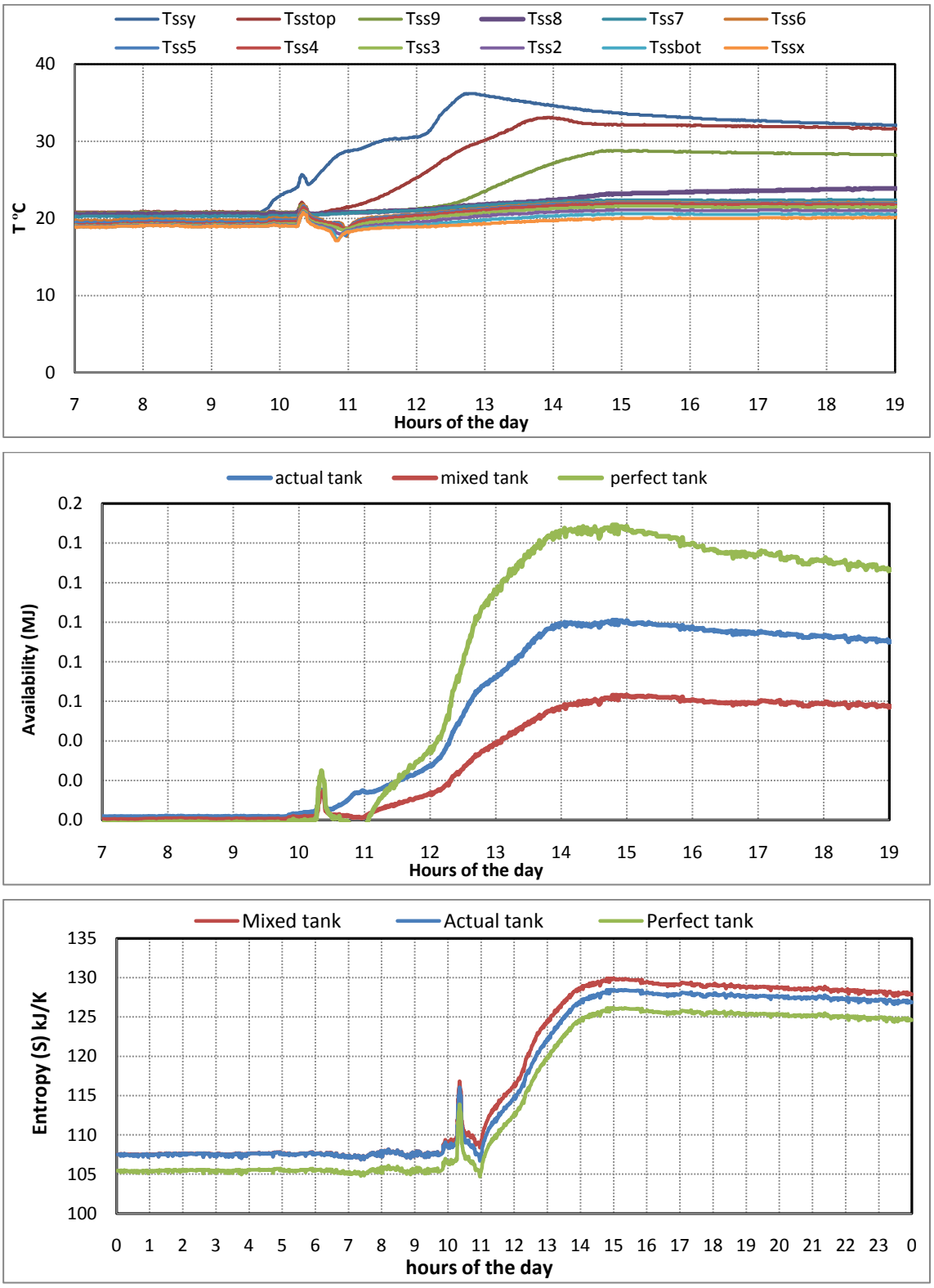

Figure 65 Manifold #1; Cloudy day; mixed tank condition.

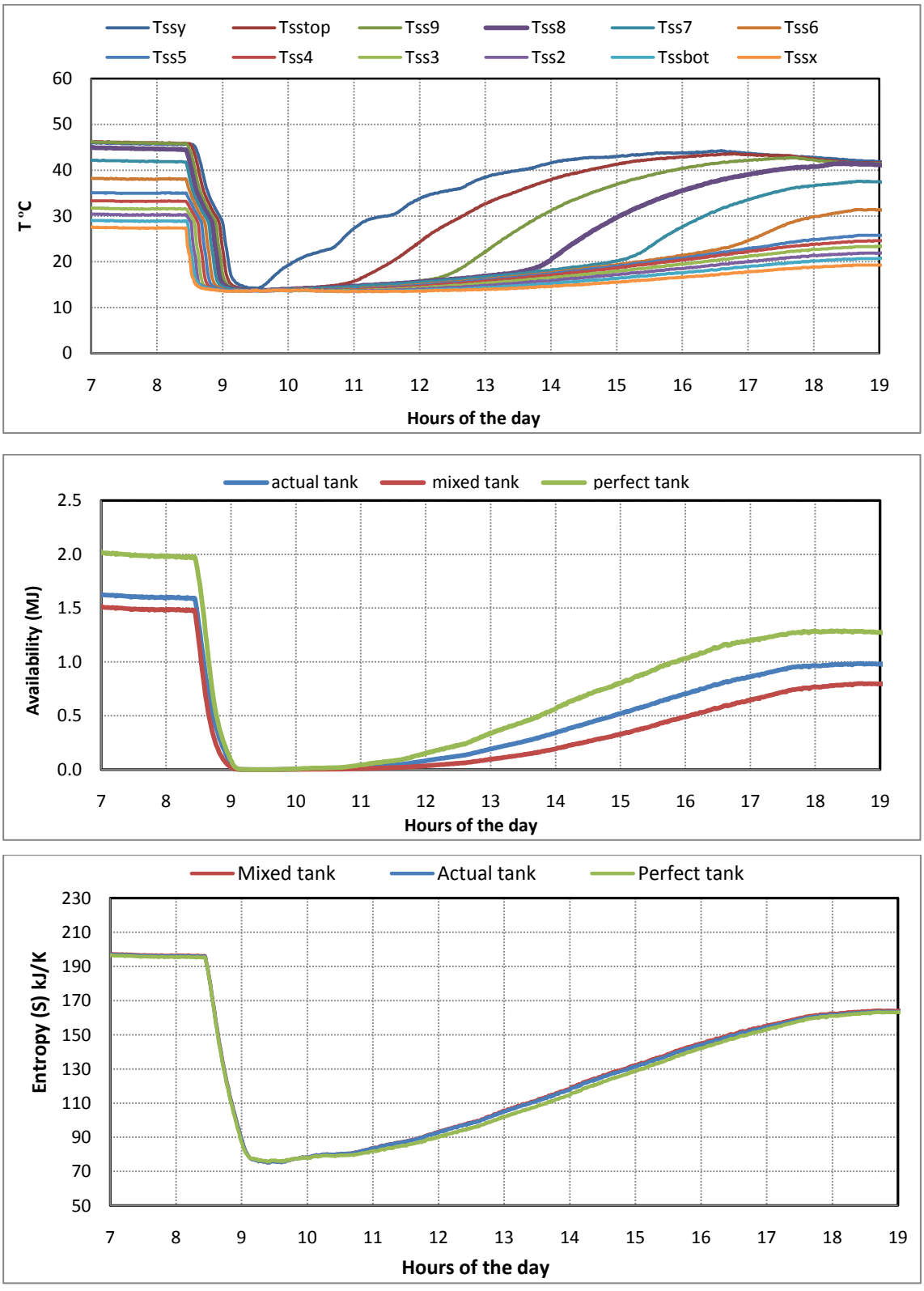

Figure 66 Manifold #1; Sunny day; cod tank condition.

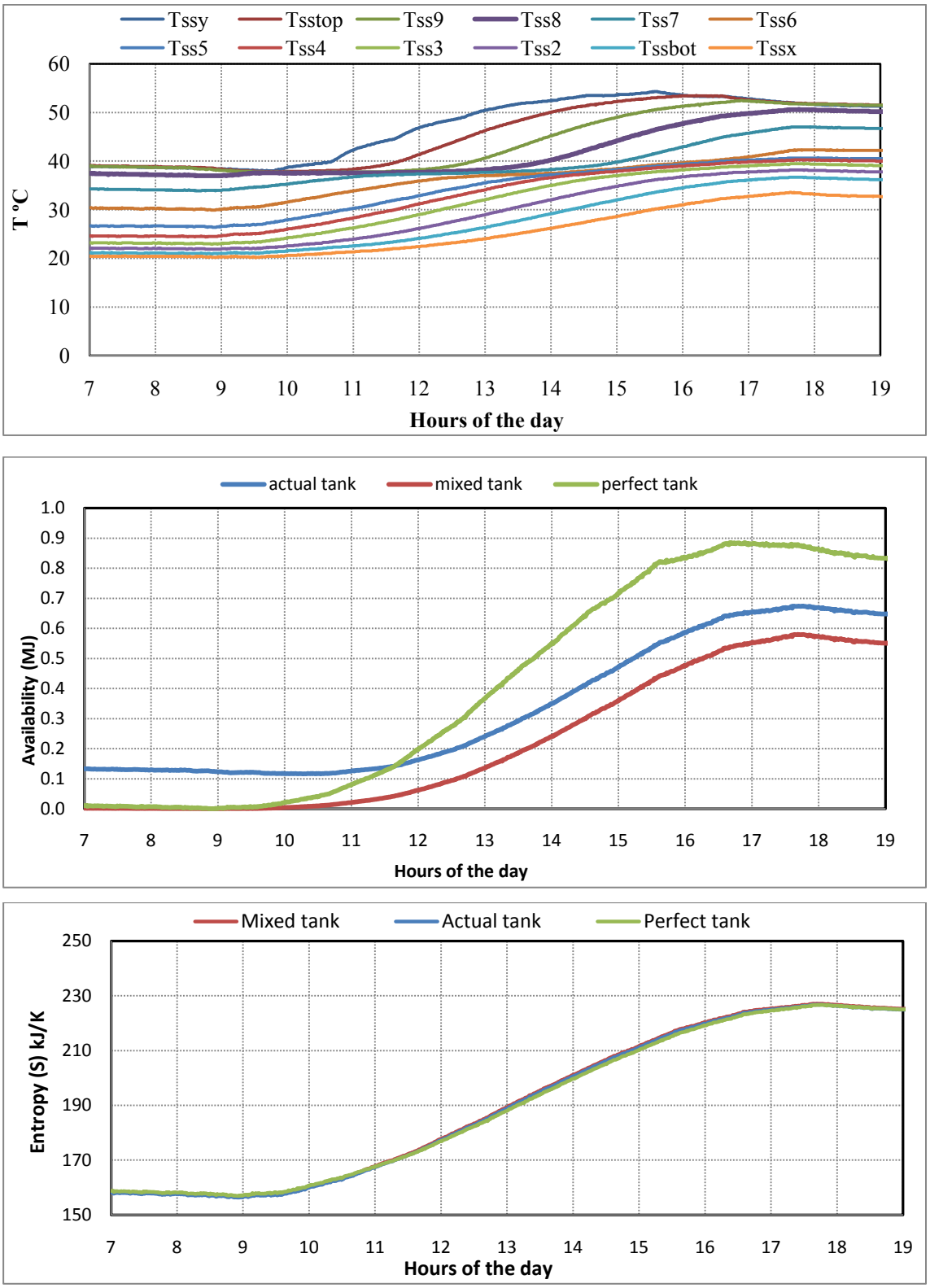

Figure 67 Manifold #1; Sunny day; hot tank condition.

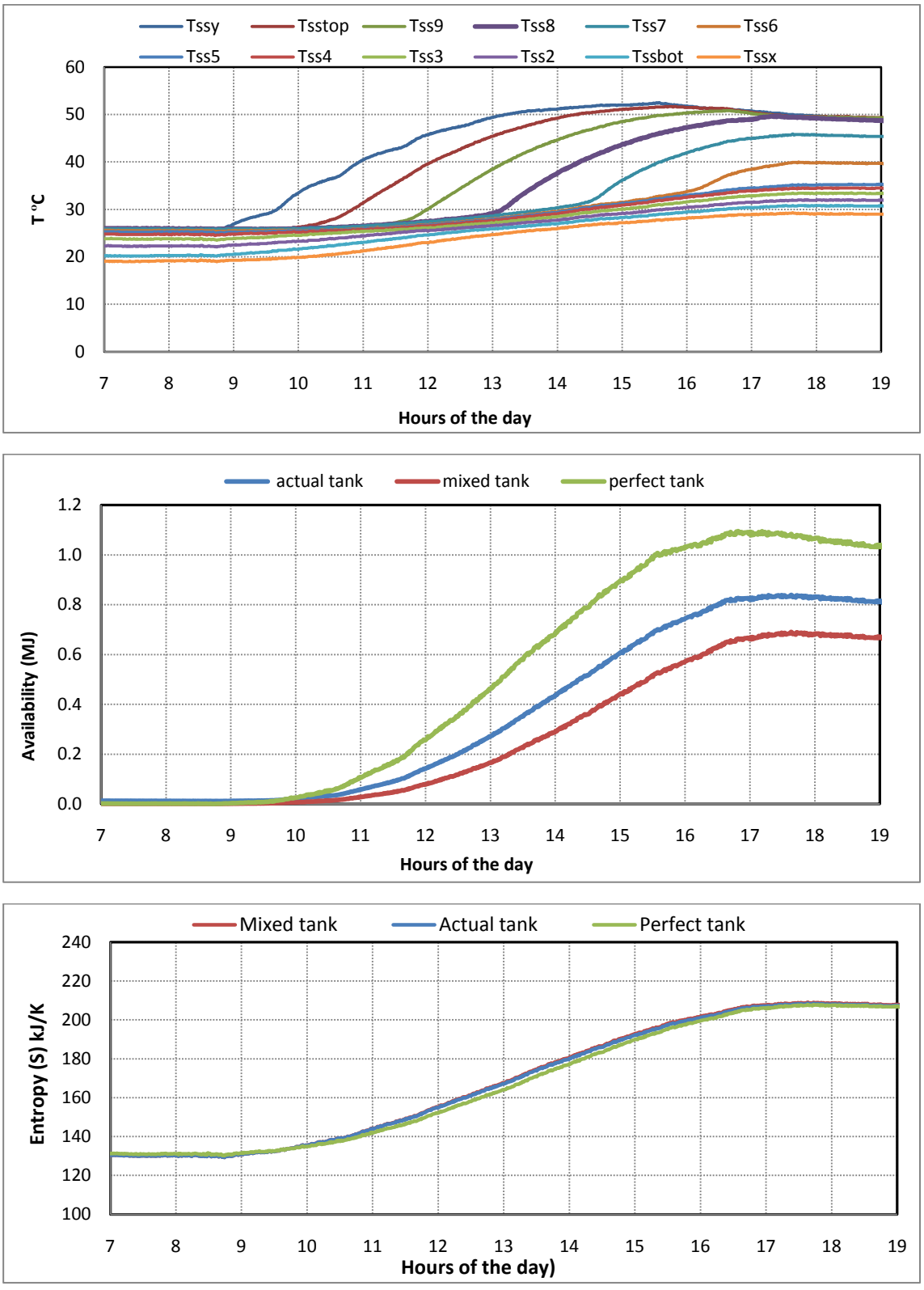

Figure 68 Manifold #1; Sunny day; mixed tank condition.

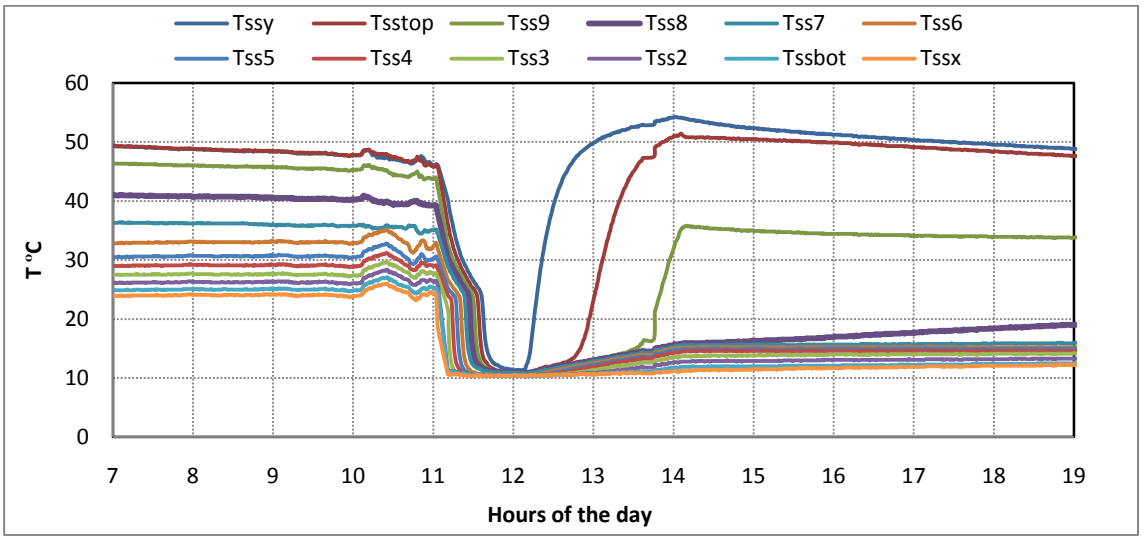

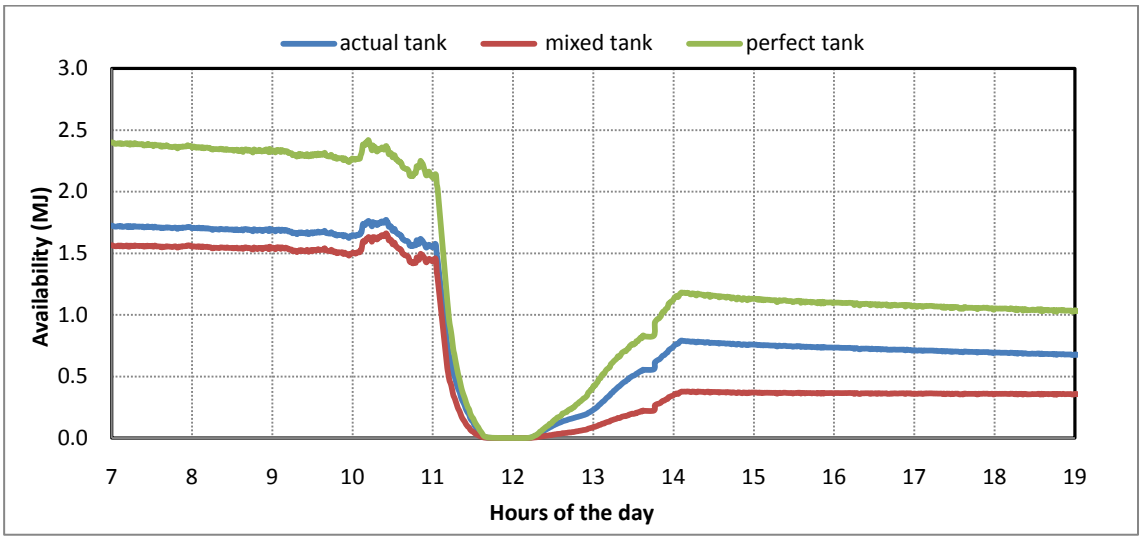

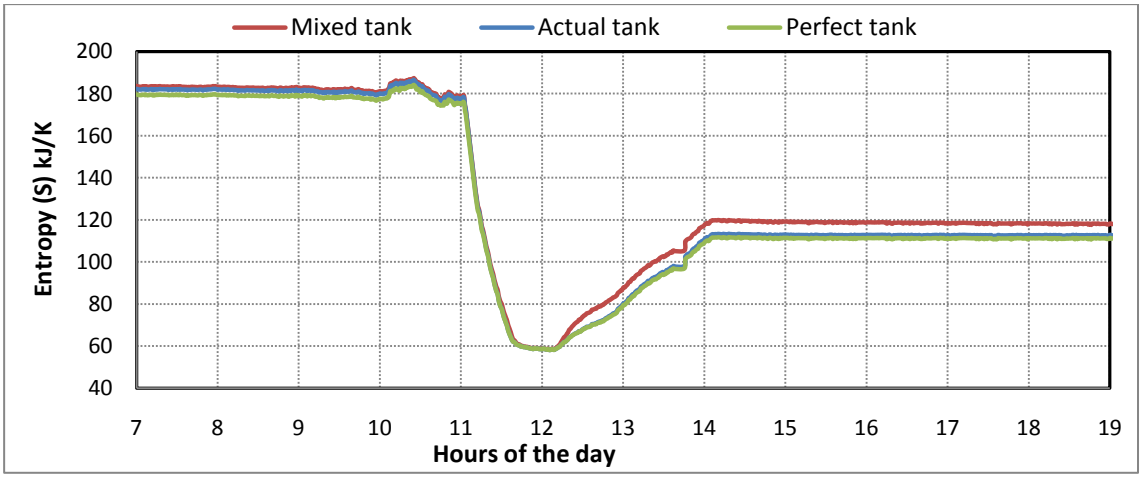

Figure 69 Manifold #1; Constant load, cold tank condition.

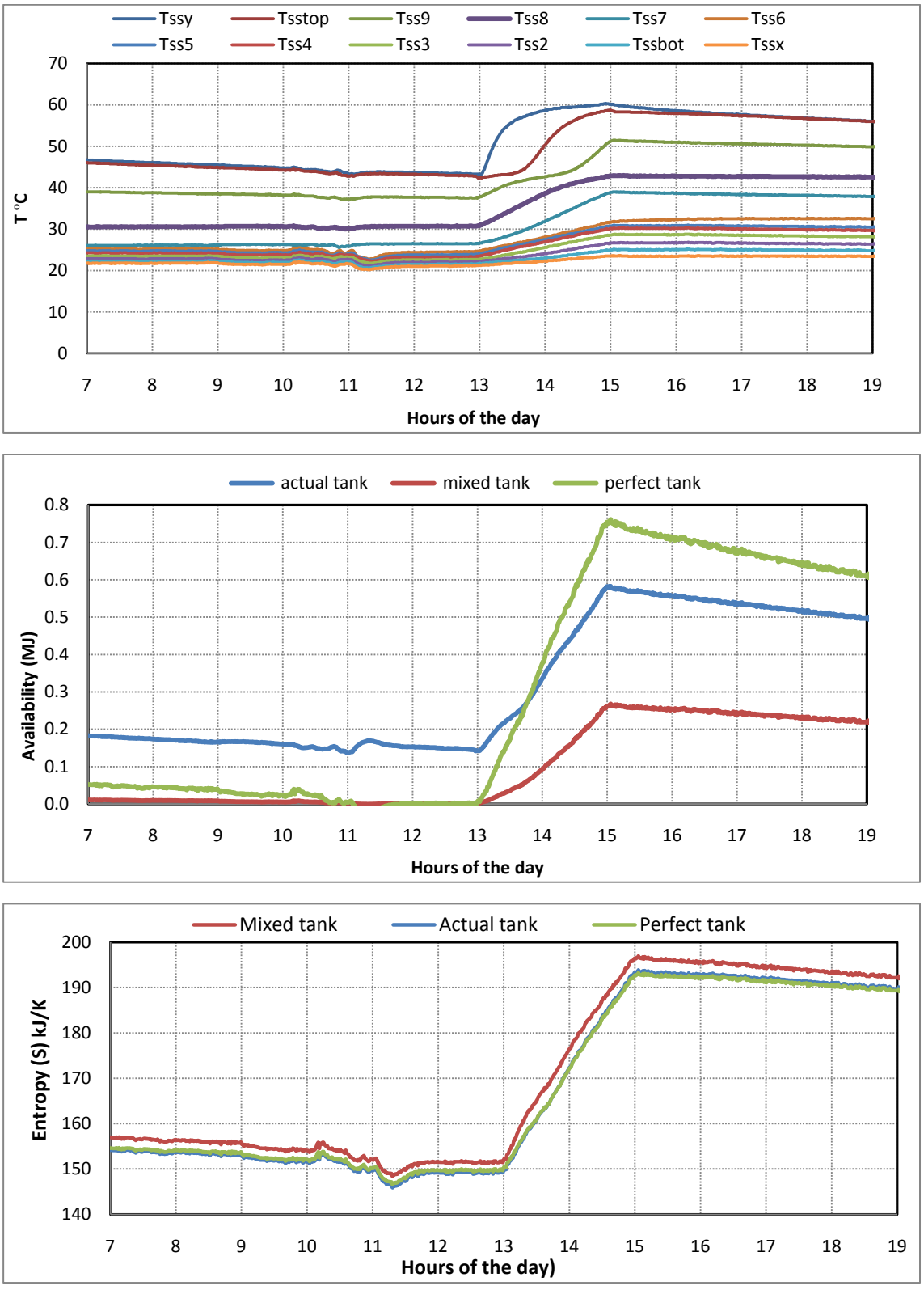

Figure 70 Manifold #1; Constant load; hot tank condition.

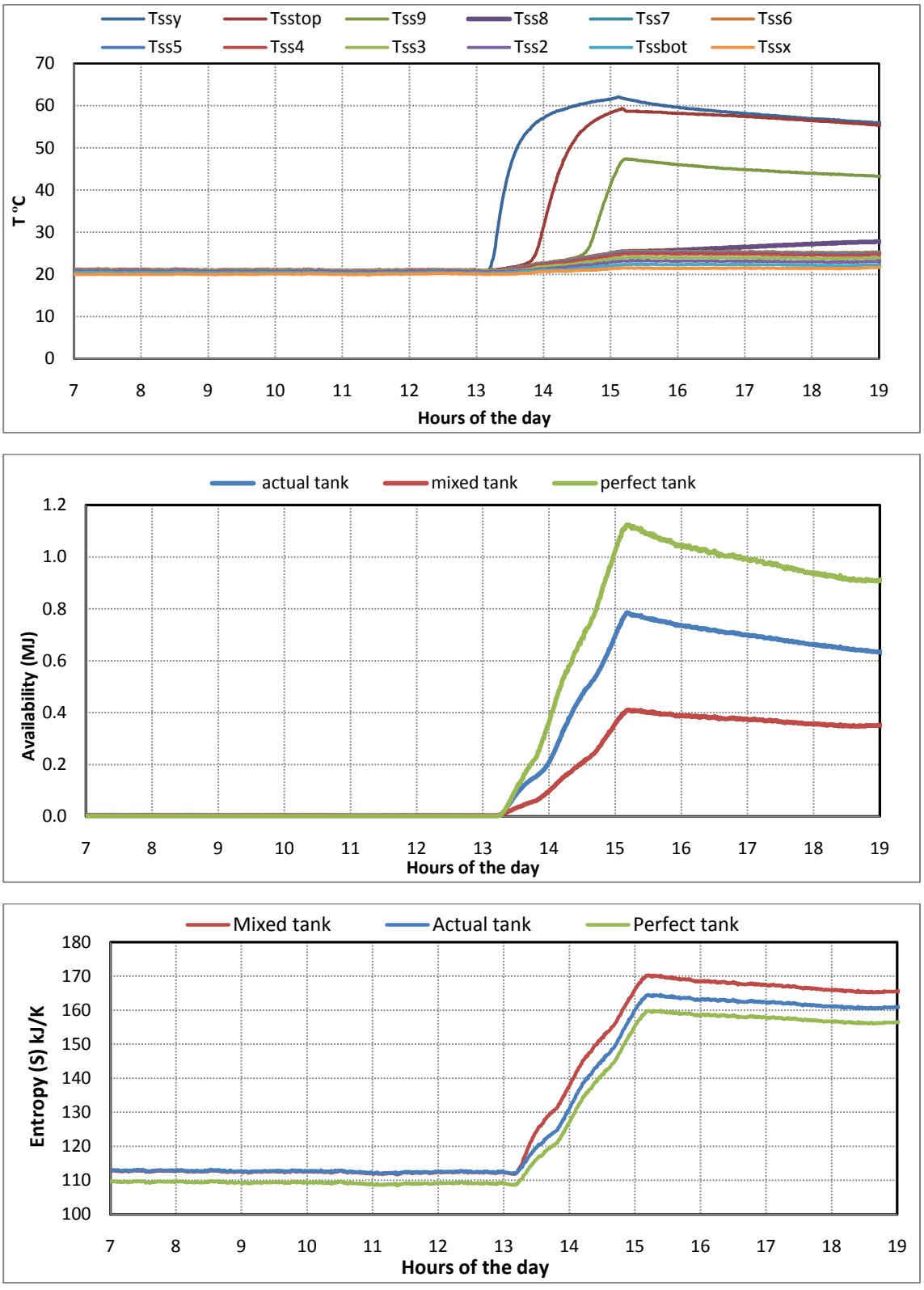

Figure 71 Manifold #1; Constant load; mixed tank condition.

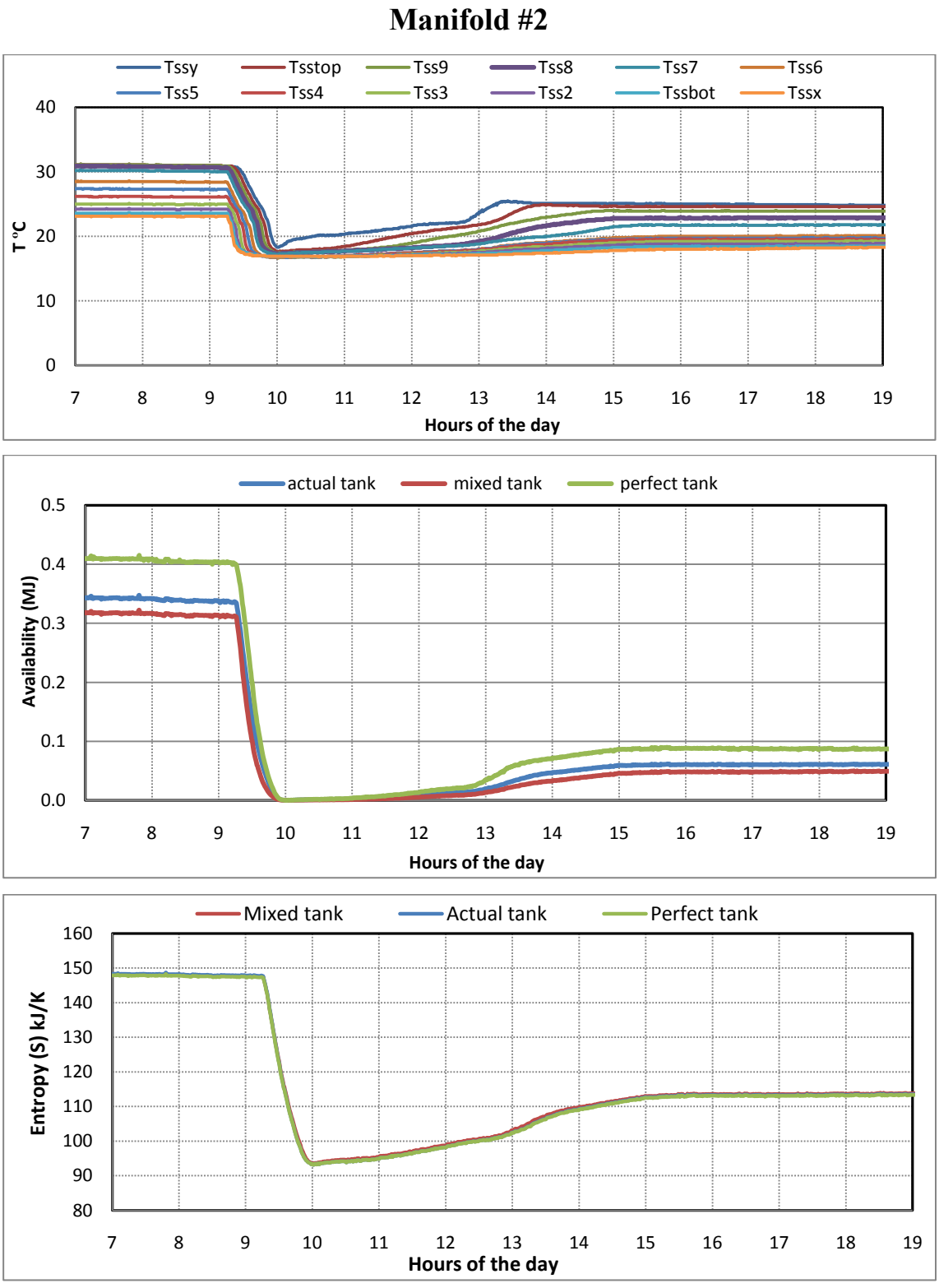

Figure 72 Manifold #2; Cloudy day; cold tank condition.

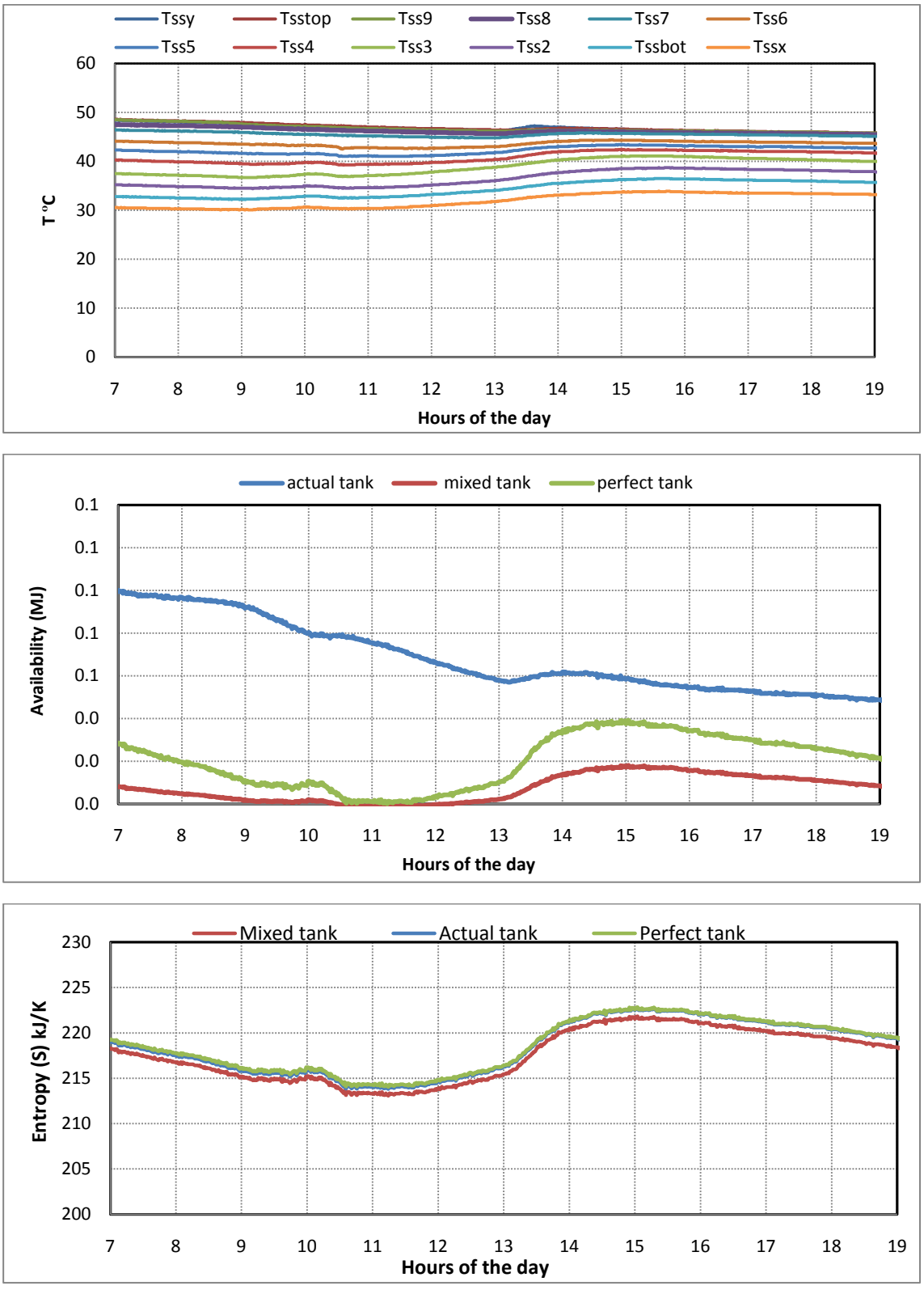

Figure 73 Manifold #2; Cloudy day; hot tank condition.

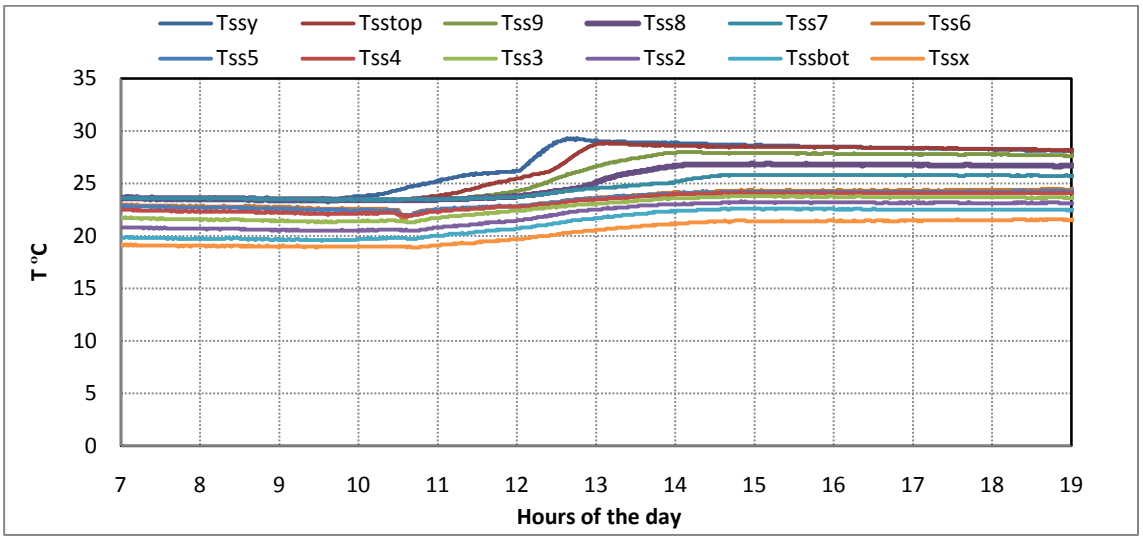

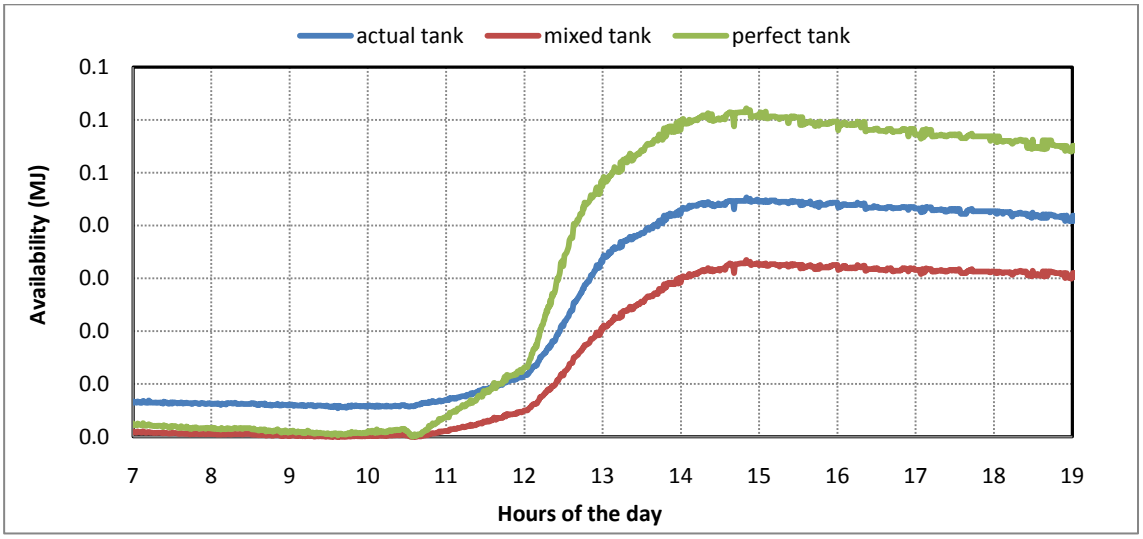

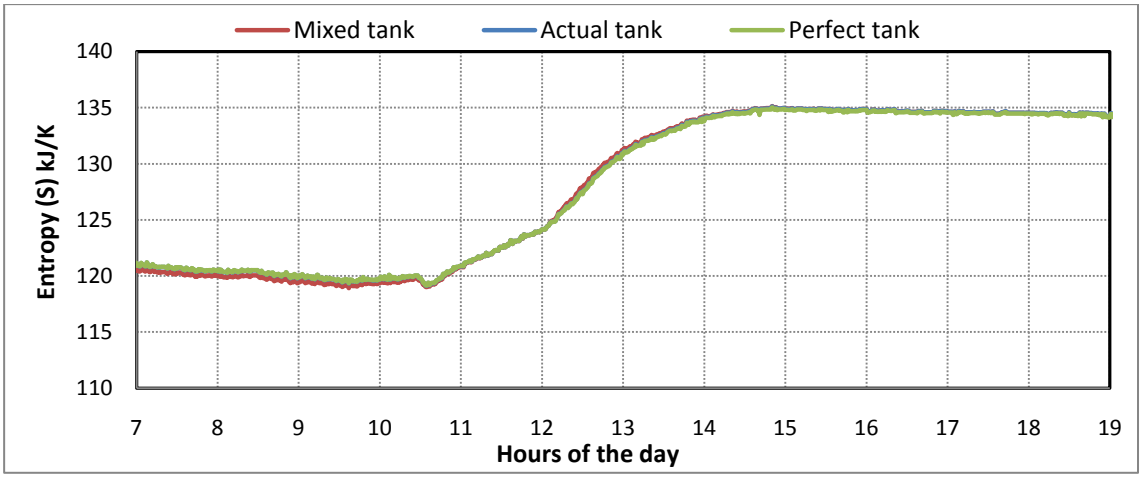

Figure 74 Manifold #2; Cloudy day; mixed tank condition.

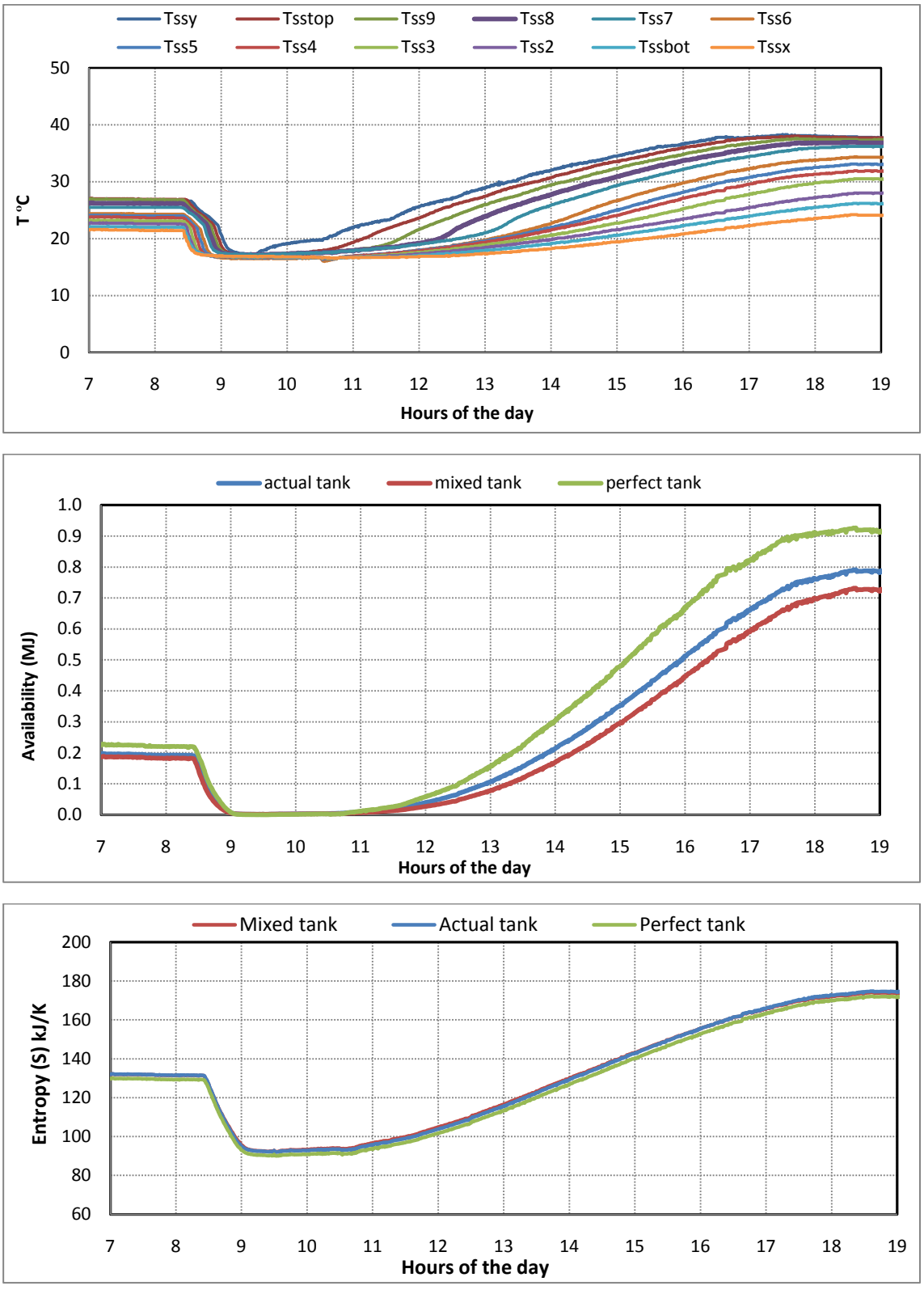

Figure 75 Manifold #2; Sunny day; cold tank condition.

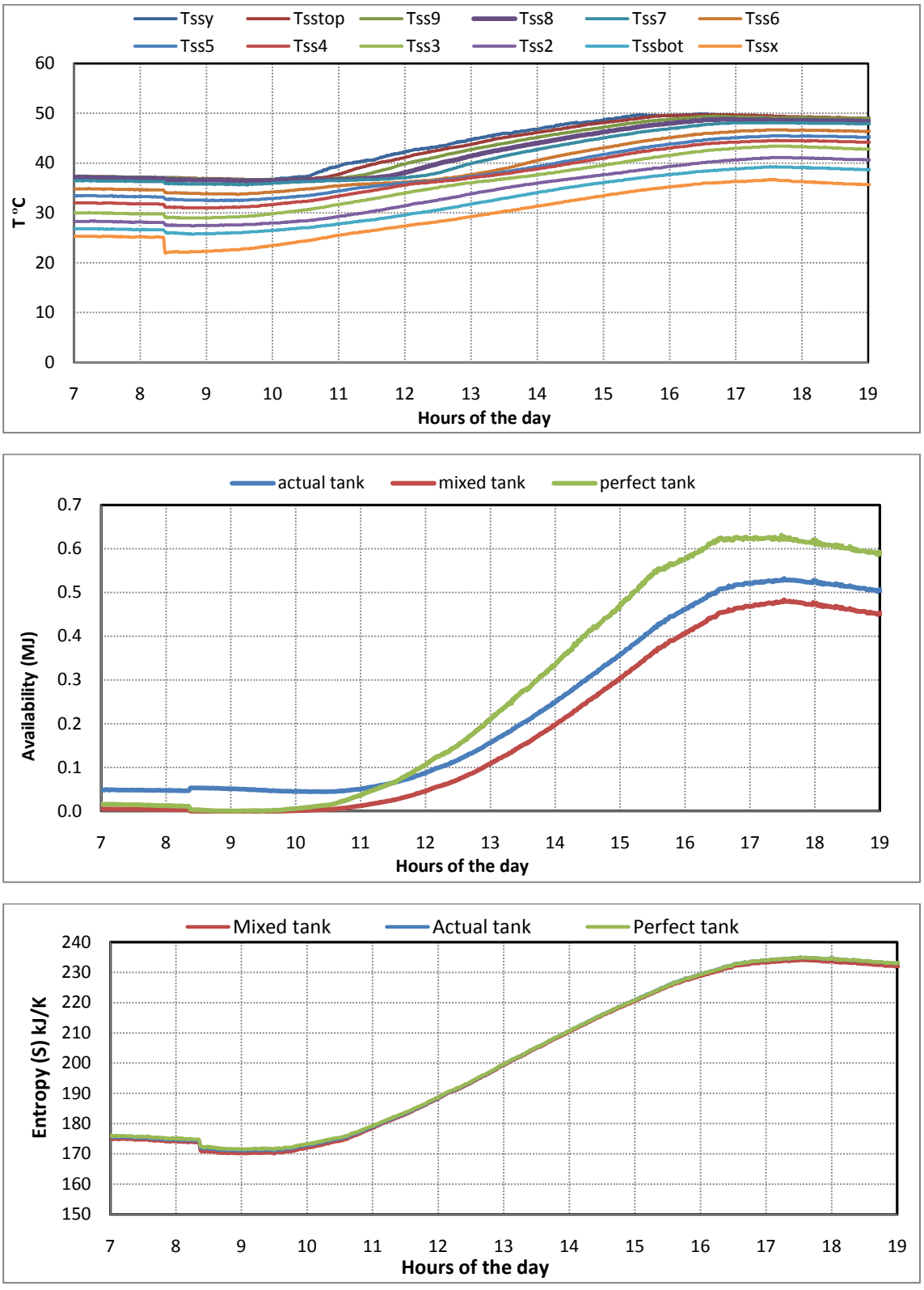

Figure 76 Manifold #2; Sunny day; hot tank condition.

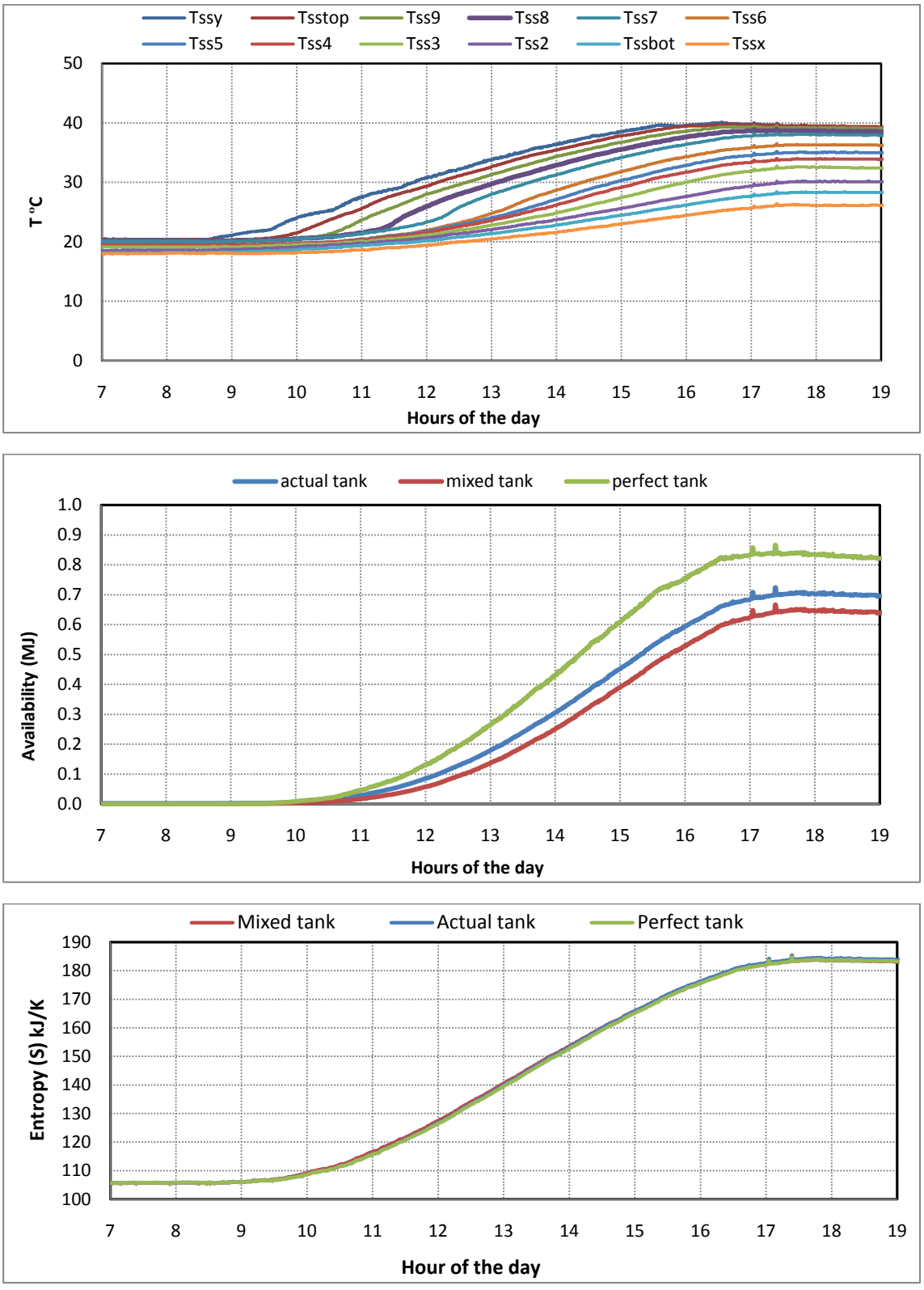

Figure 77 Manifold #2; Sunny day; mixed tank condition.

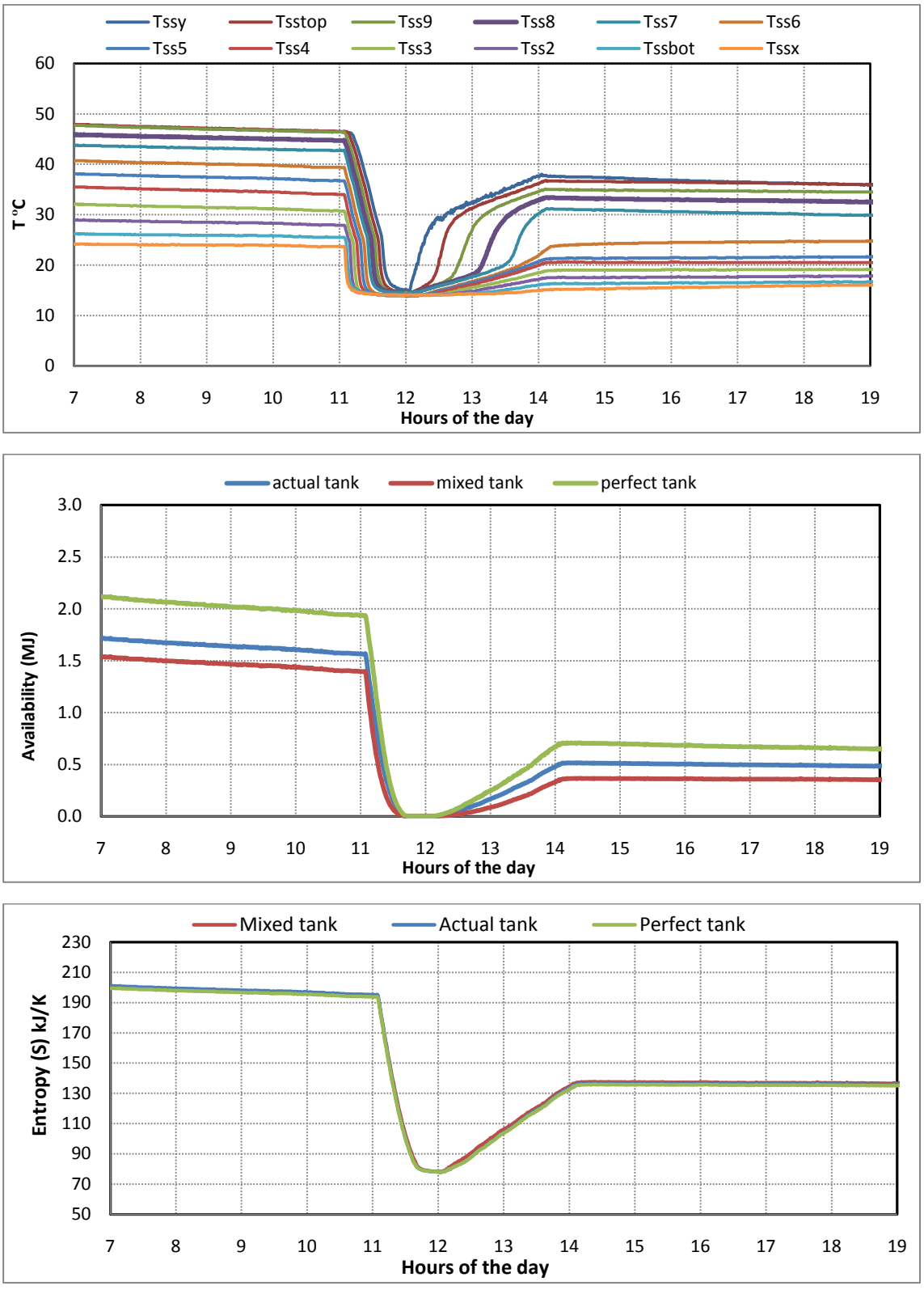

Figure 78 Manifold #2; Constant load; cold tank condition.

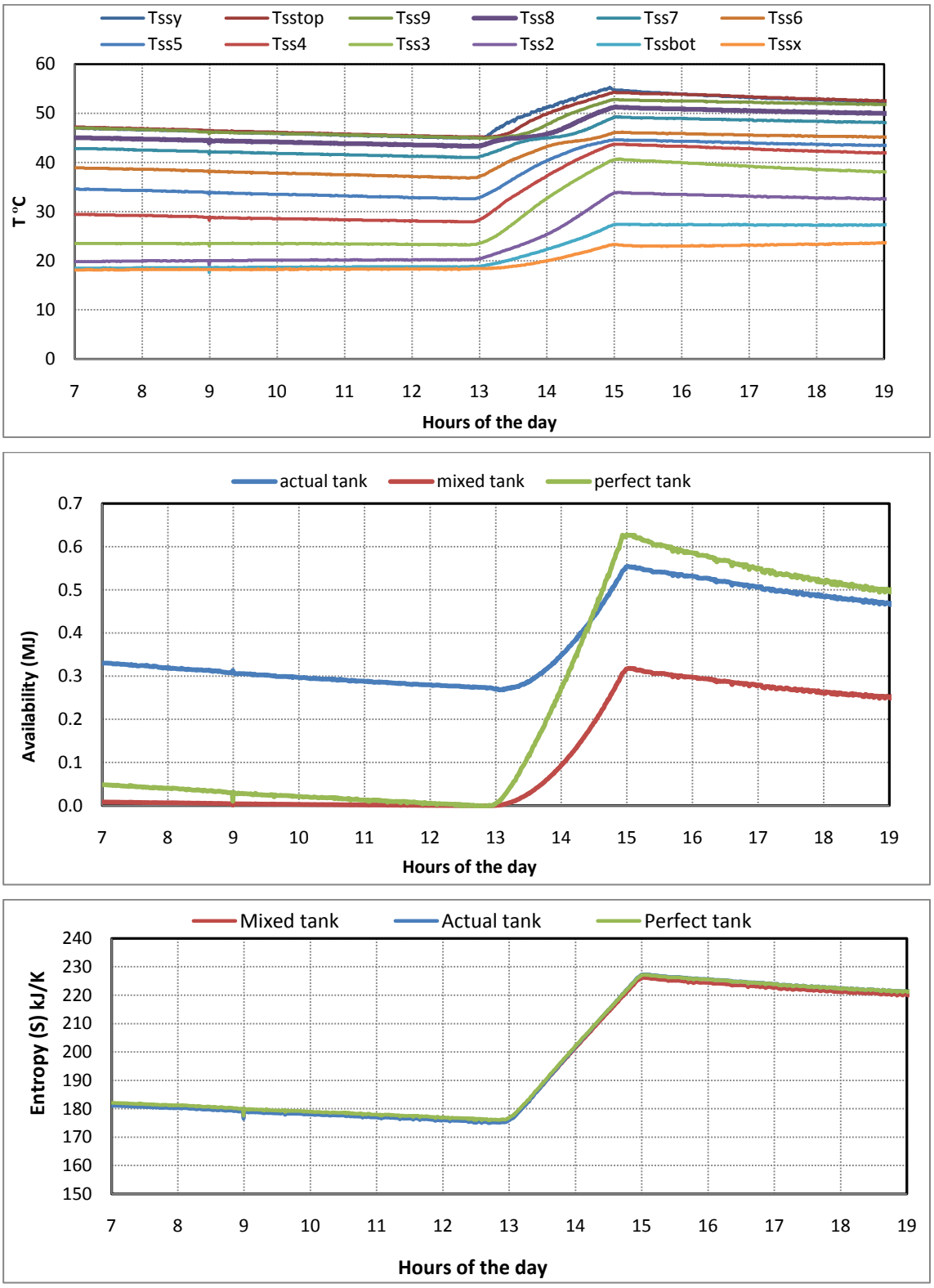

Figure 79 Manifold #2; Constant load; hot tank condition.

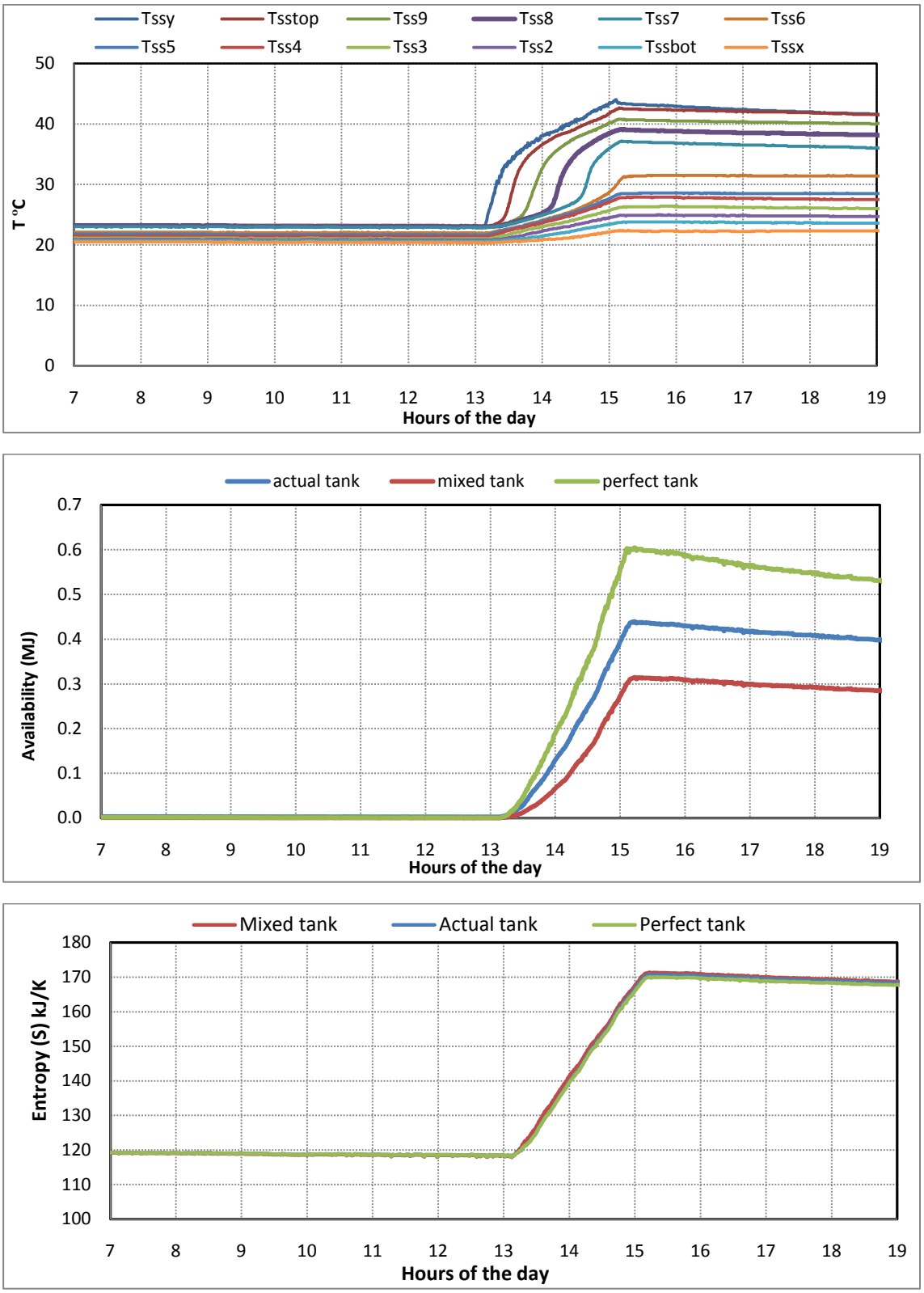

Figure 80 Manifold #2; Constant load; mixed tank condition.

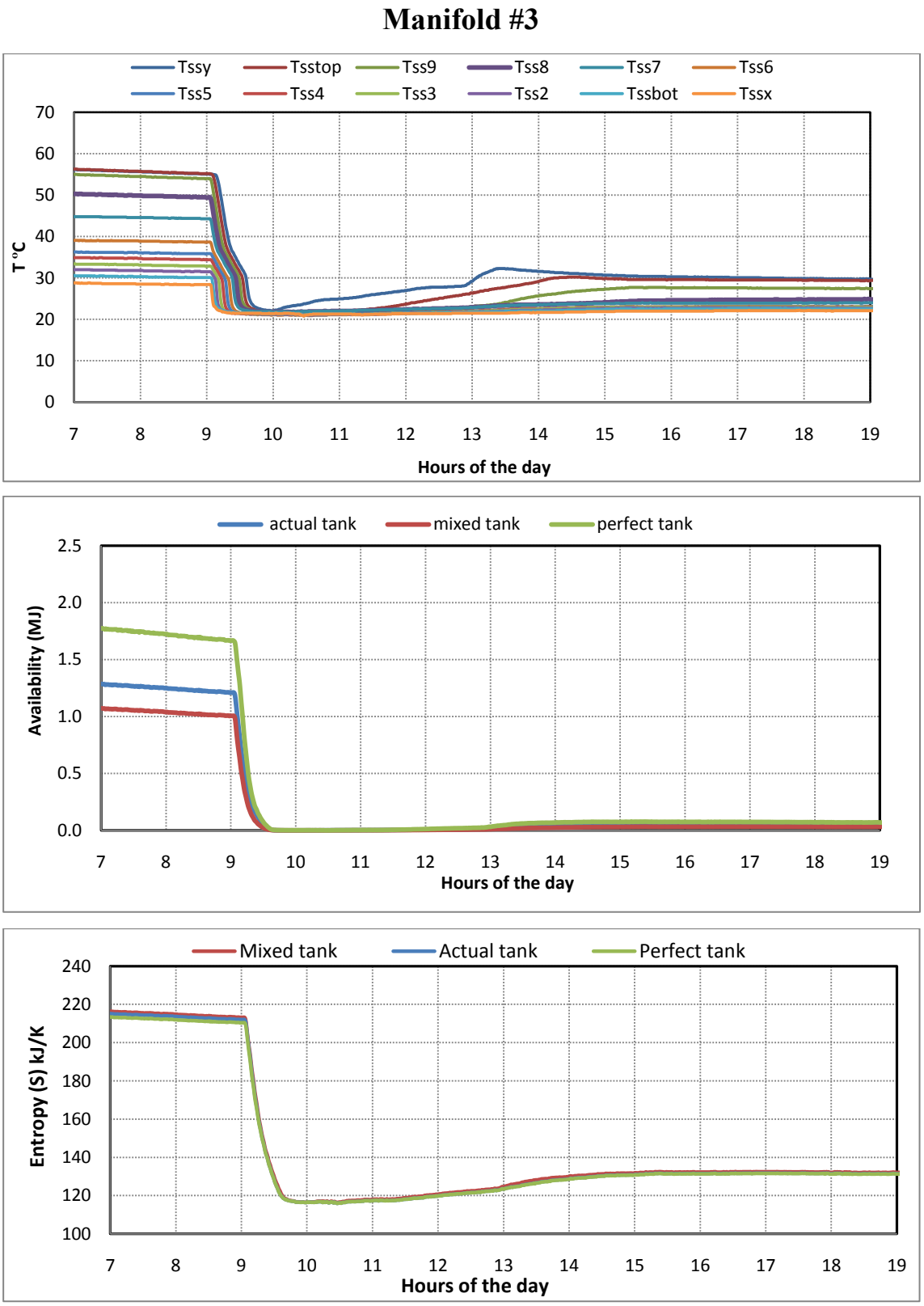

Figure 81 Manifold #3; Cloudy day; cold tank condition.

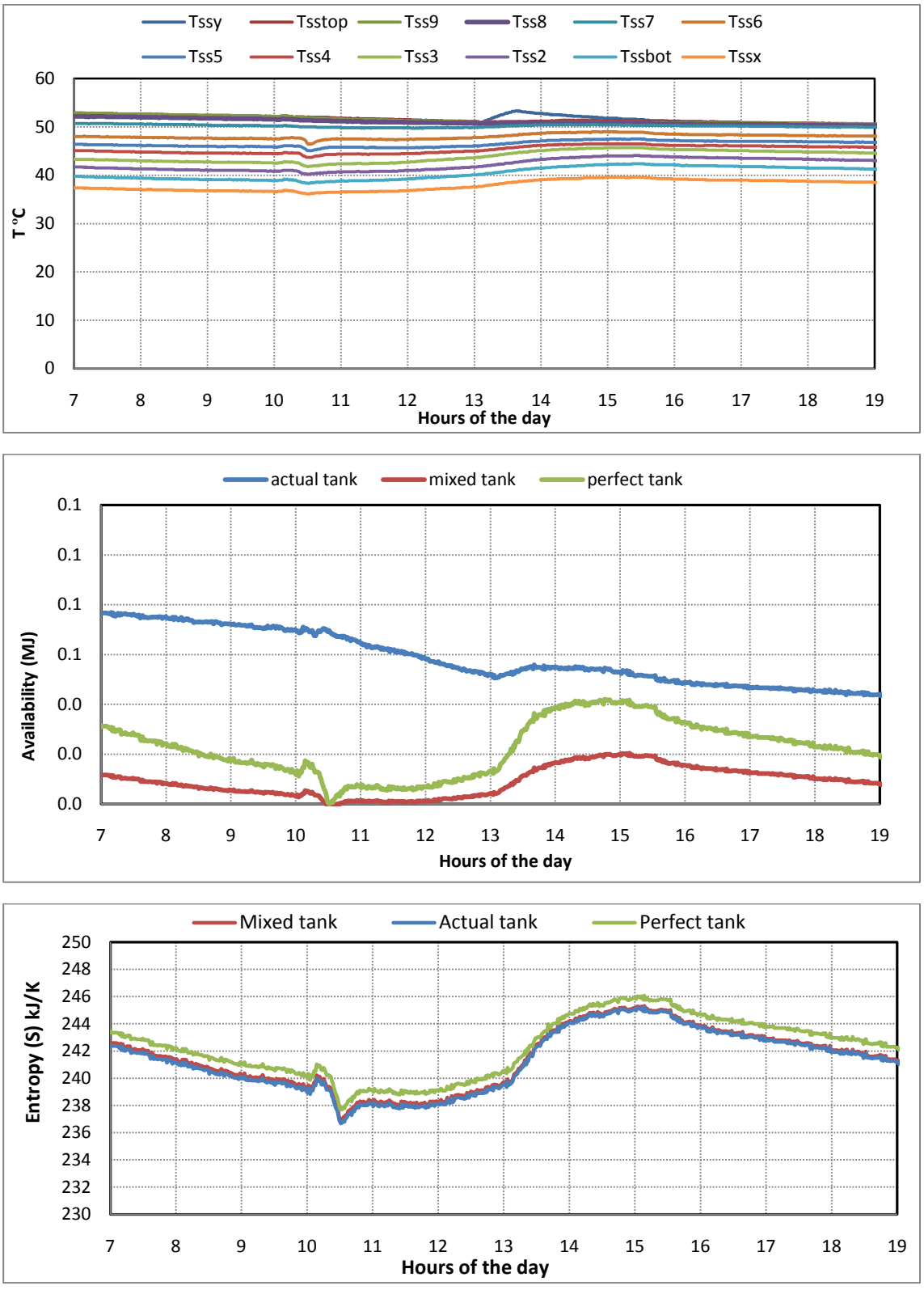

Figure 82 Manifold #3; Cloudy day; hot tank condition.

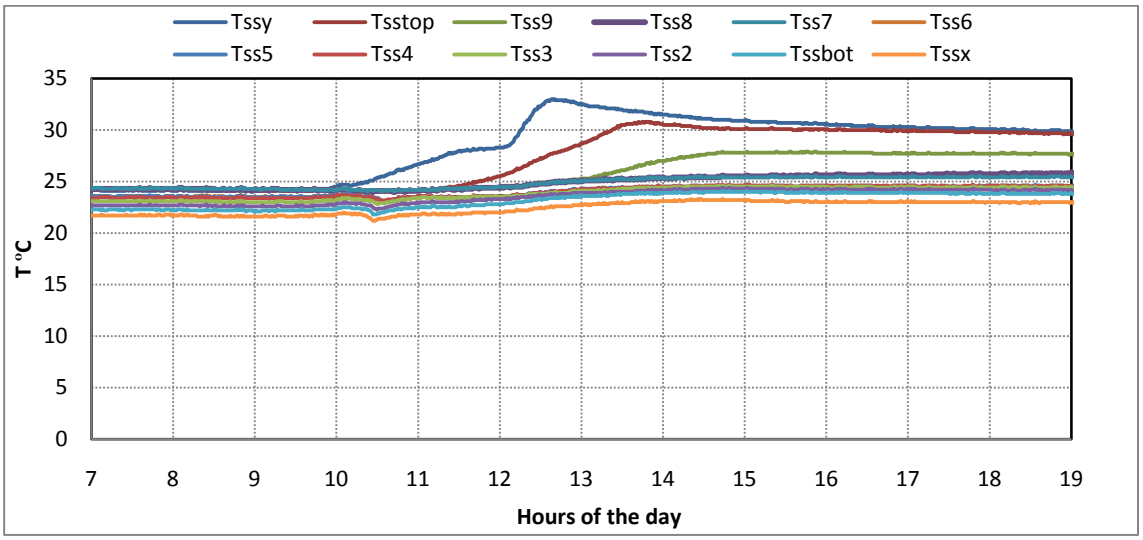

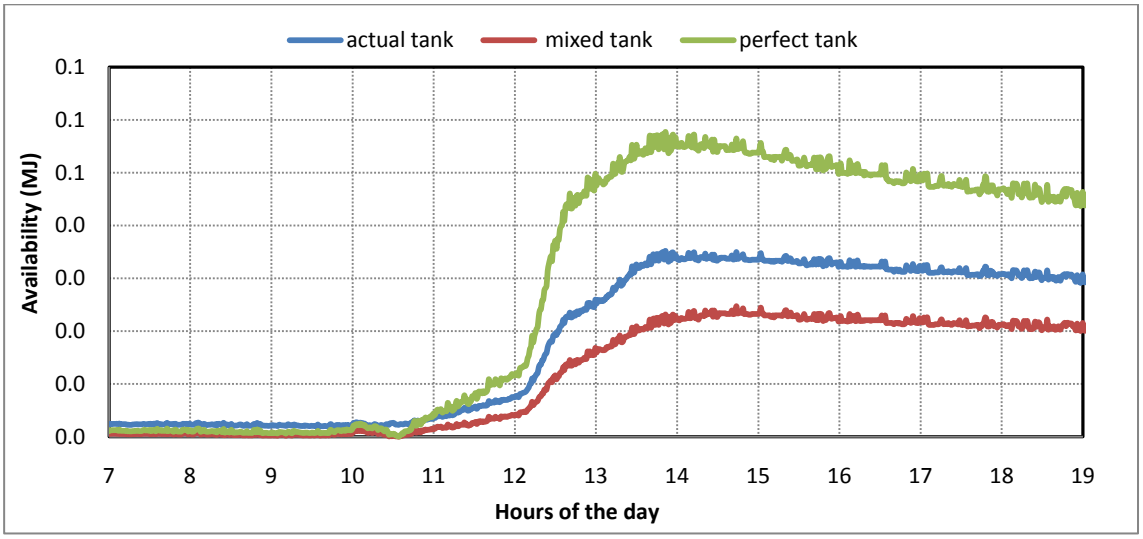

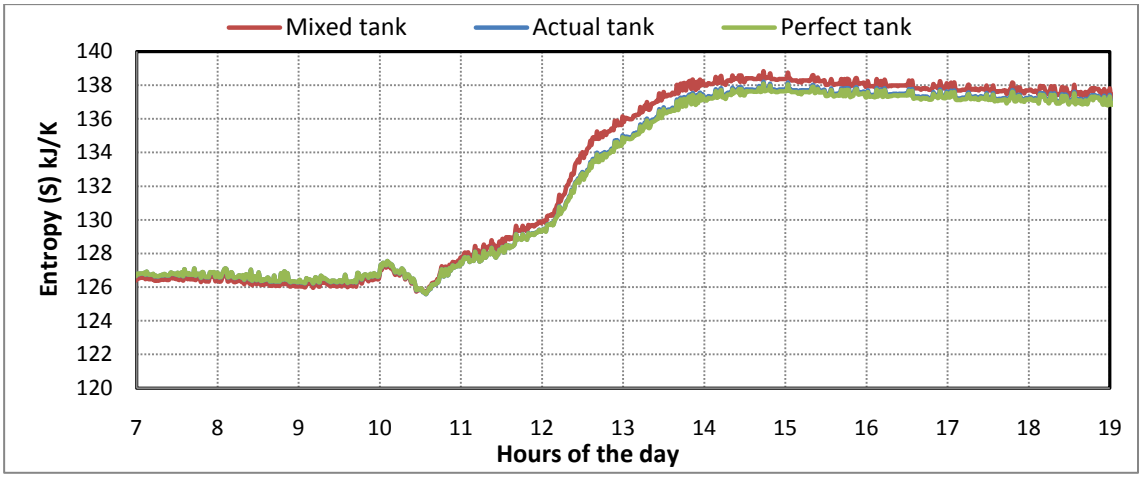

Figure 83 Manifold #3; Cloudy day; mixed tank condition.

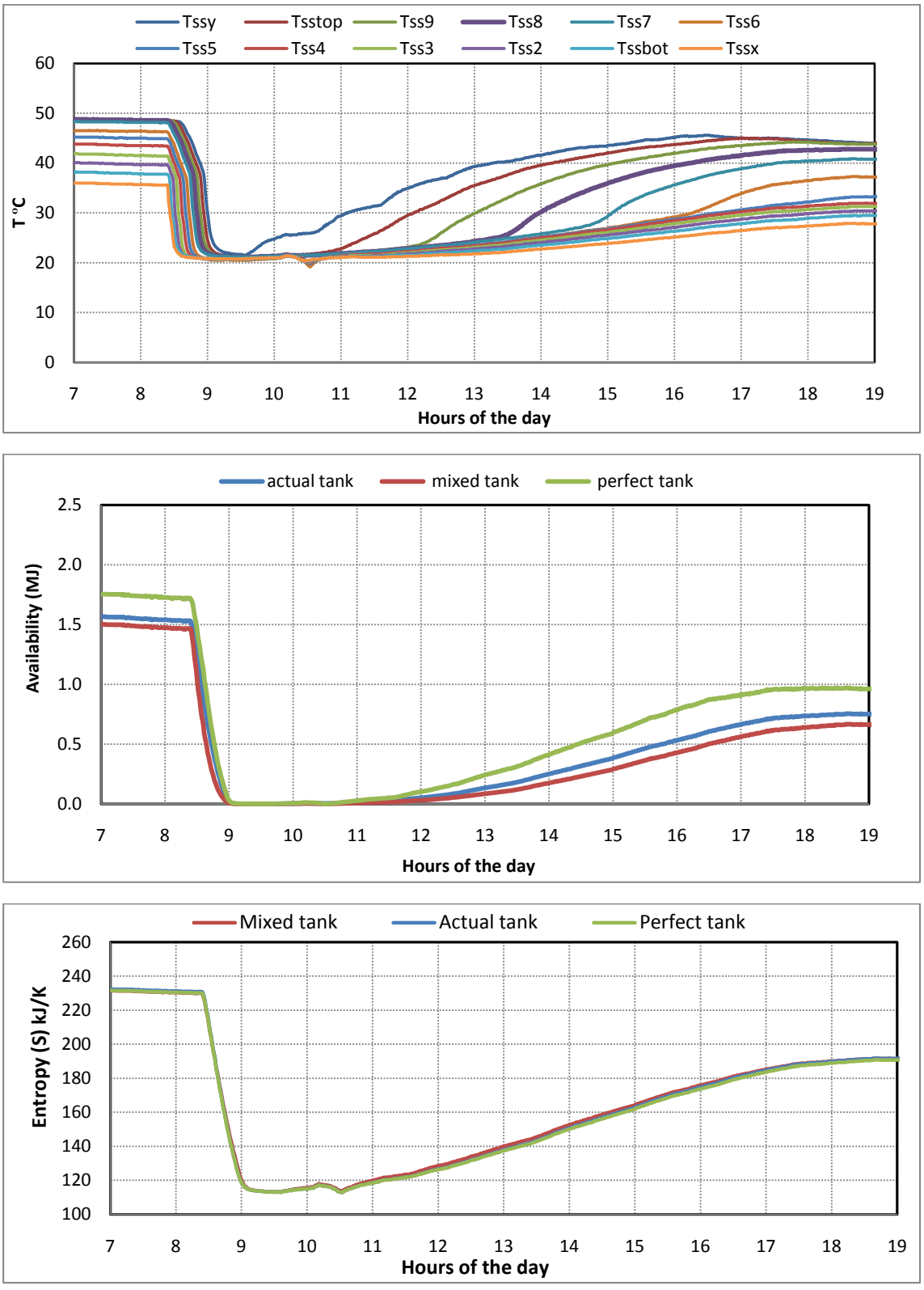

Figure 84 Manifold #3; Sunny day; cold tank condition.

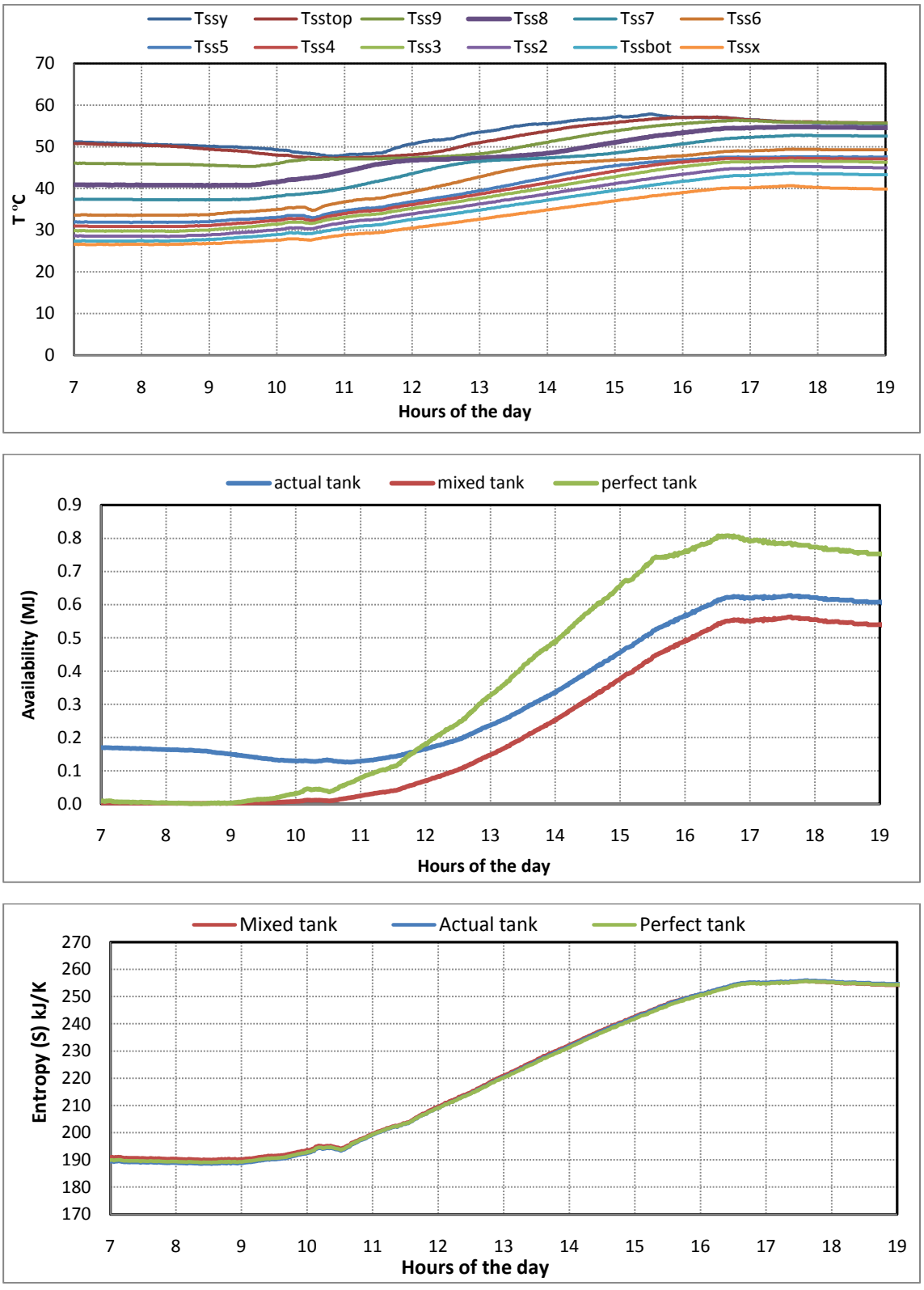

Figure 85 Manifold #3; Sunny day; hot tank condition.

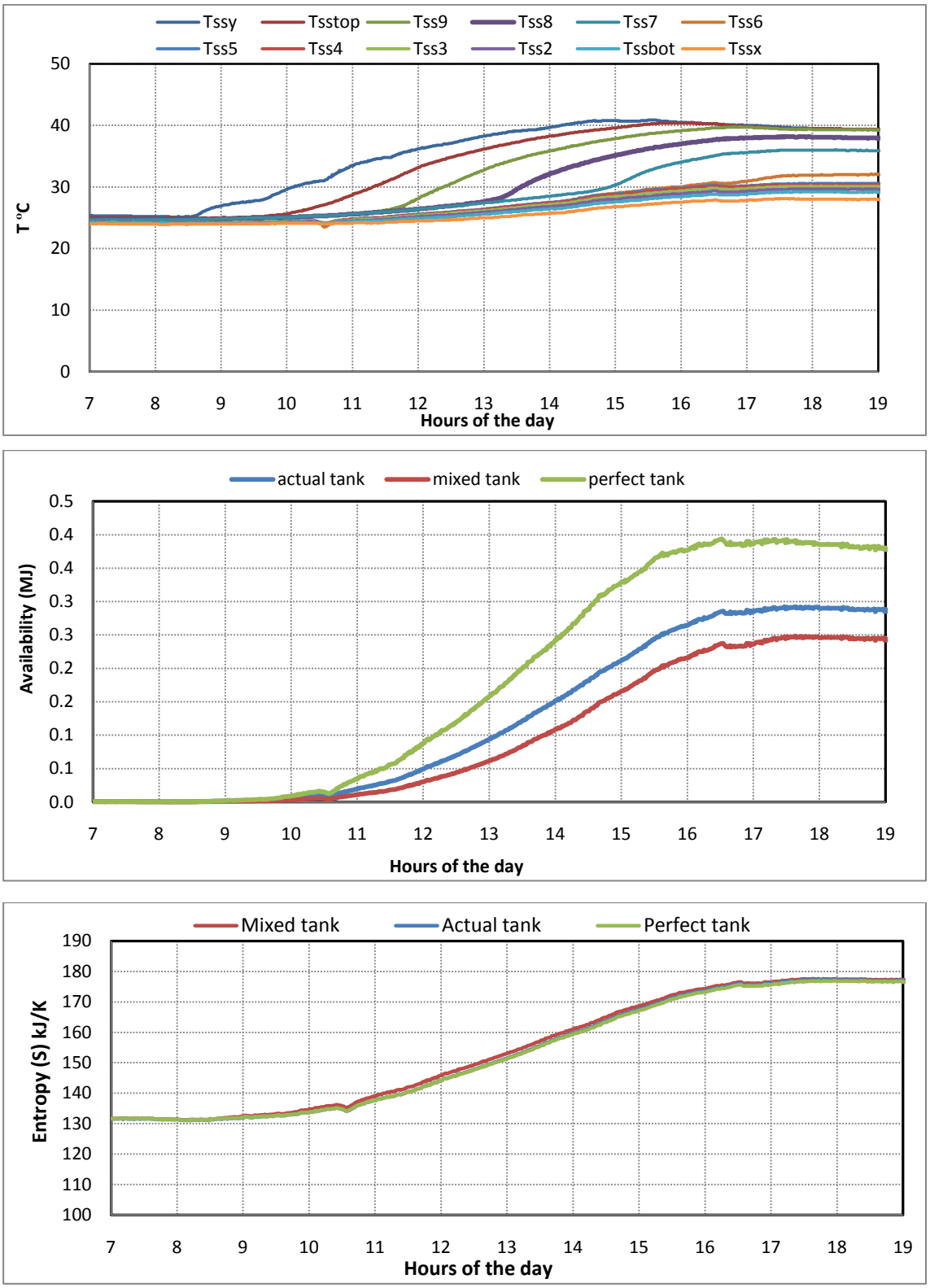

Figure 86 Manifold #3; Sunny day; mixed tank condition.

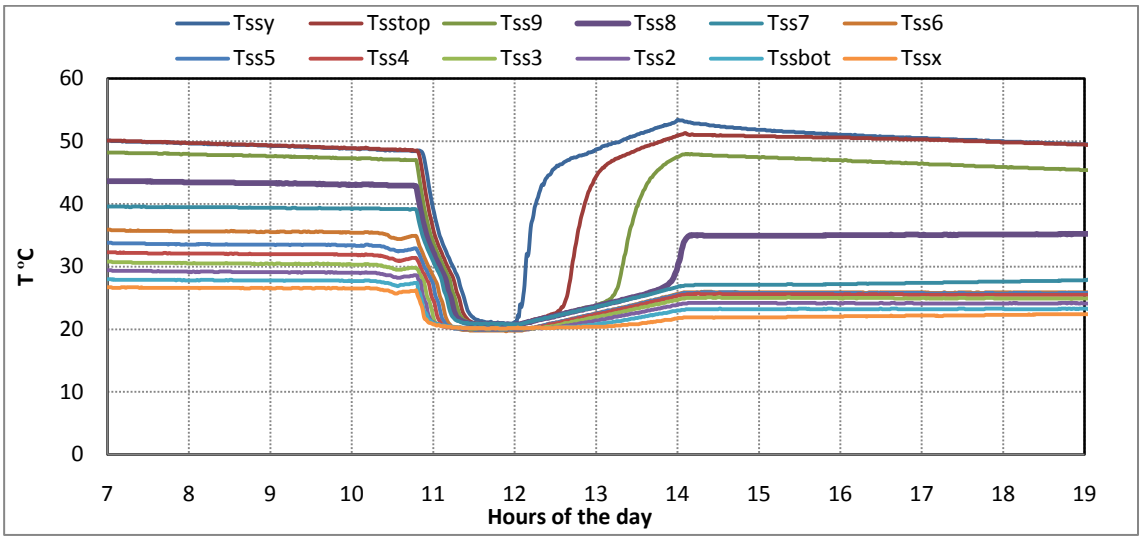

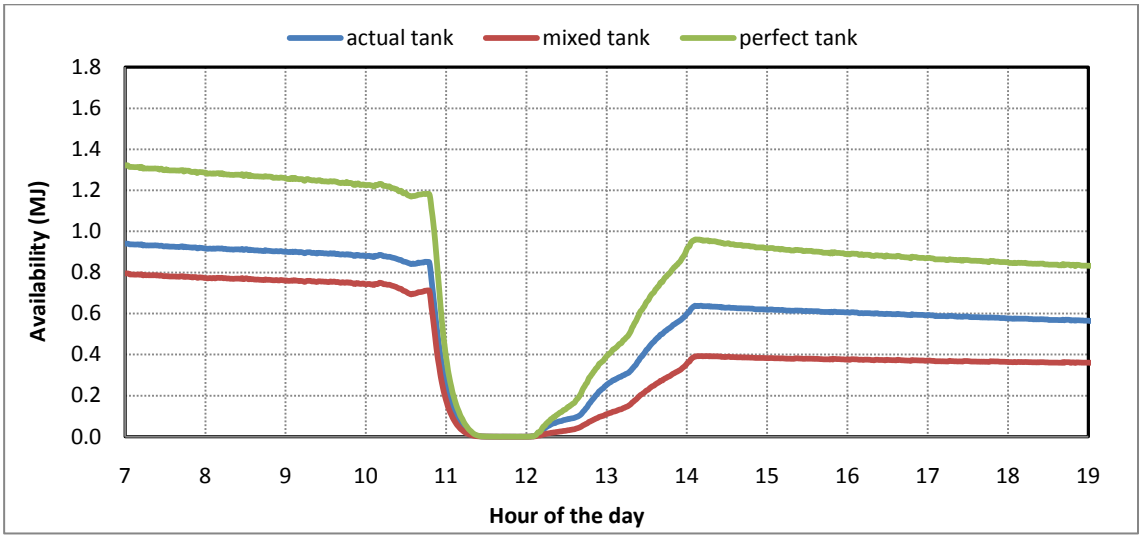

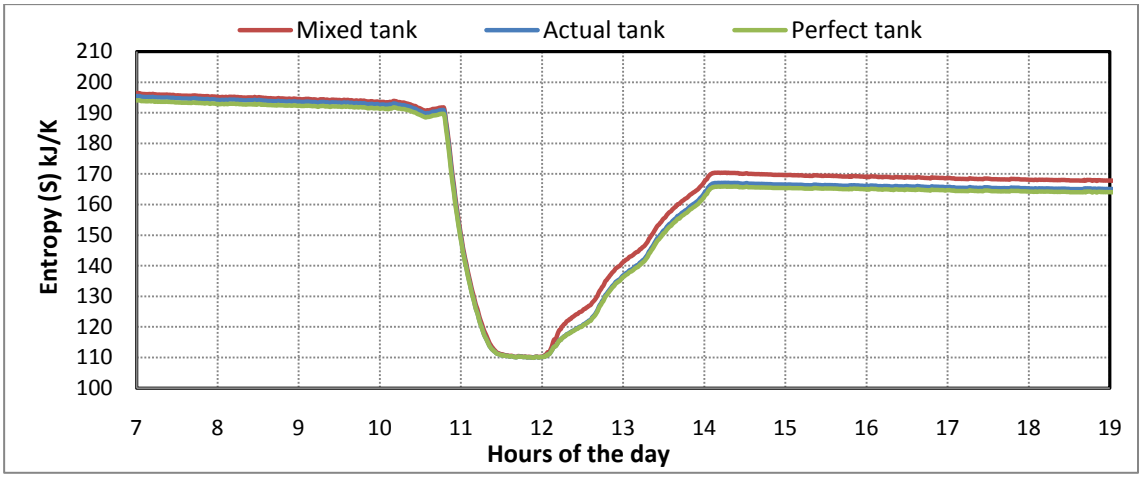

Figure 87 Manifold #3; Constant load; cold tank condition.

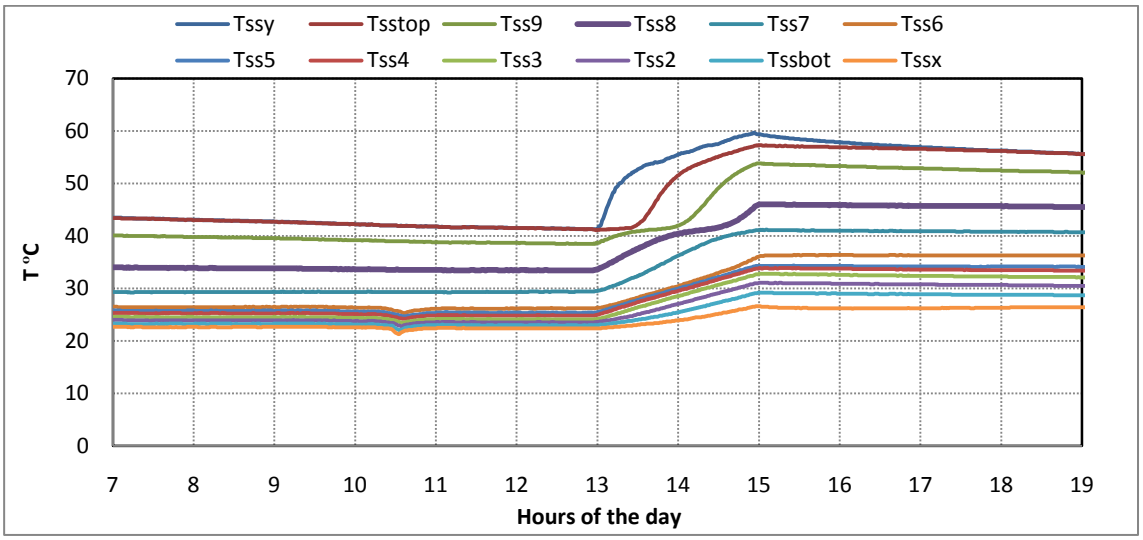

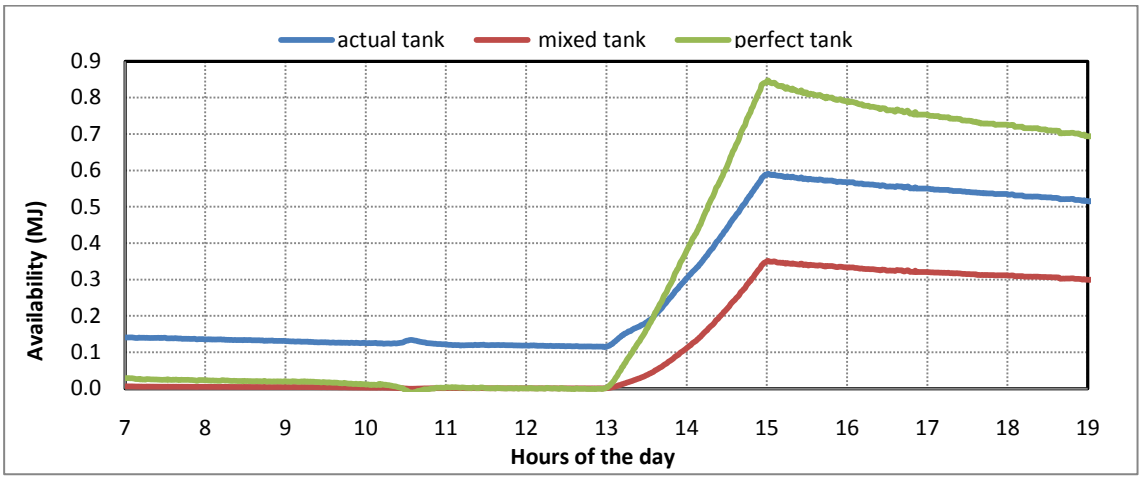

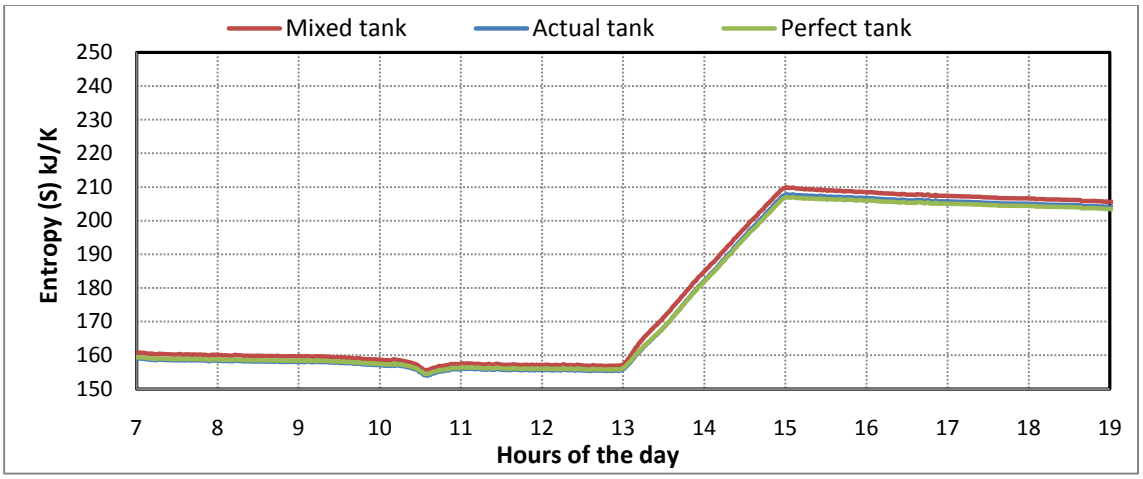

Figure 88 Manifold #3; Constant load; hot tank condition.

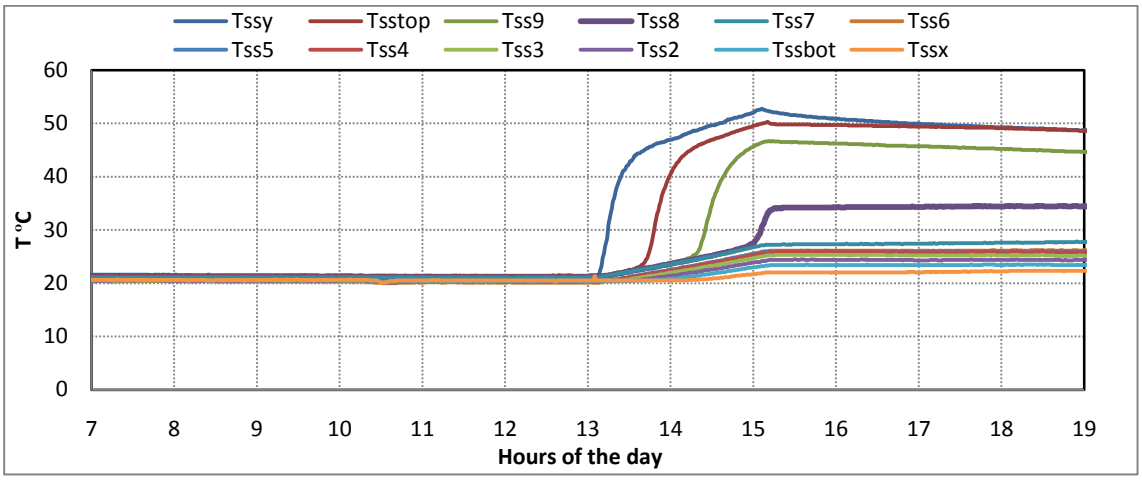

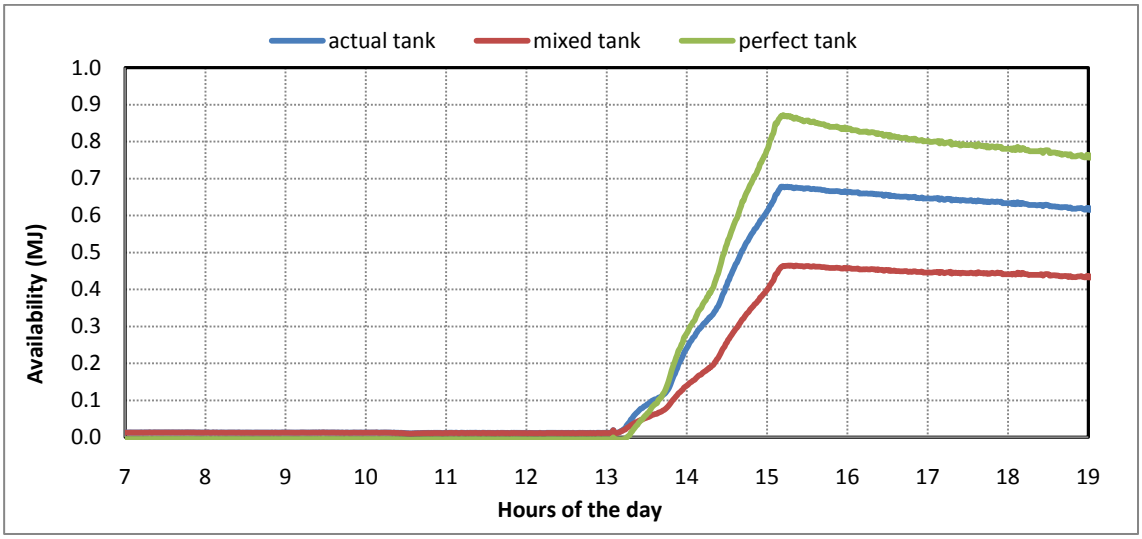

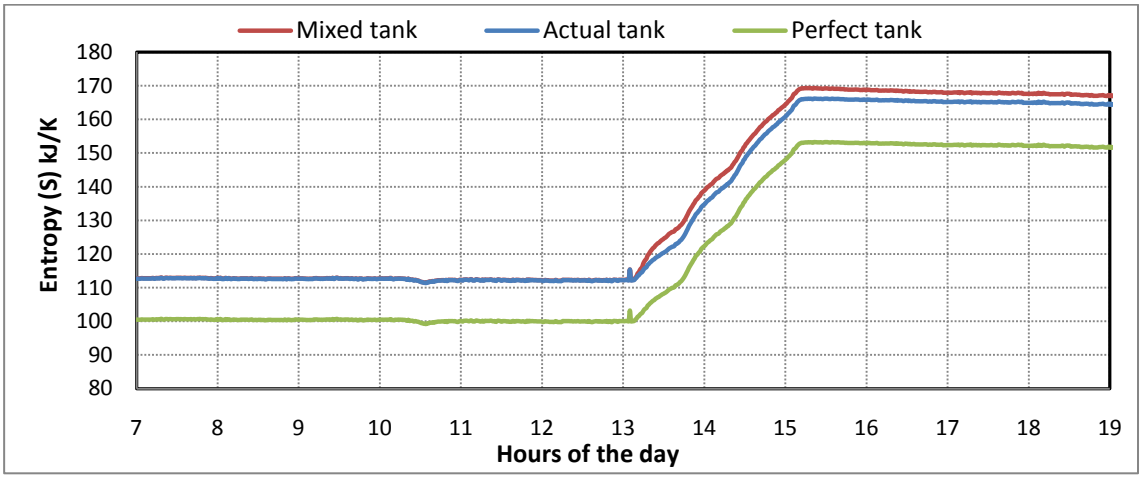

Figure 89 Manifold #3; Constant load; mixed tank condition.

Manifold #4

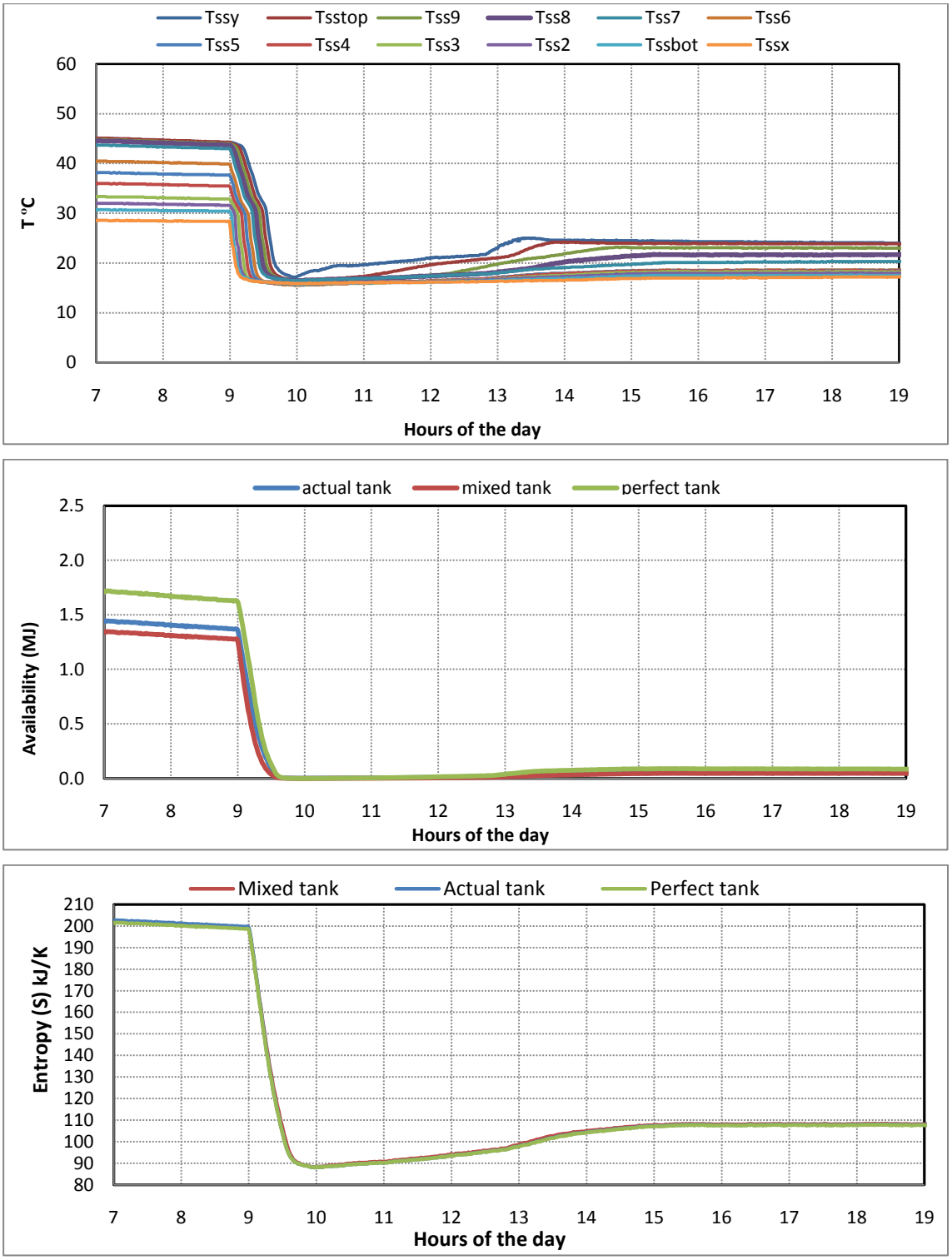

Figure 90 Manifold #4; Cloudy day; cold tank condition.

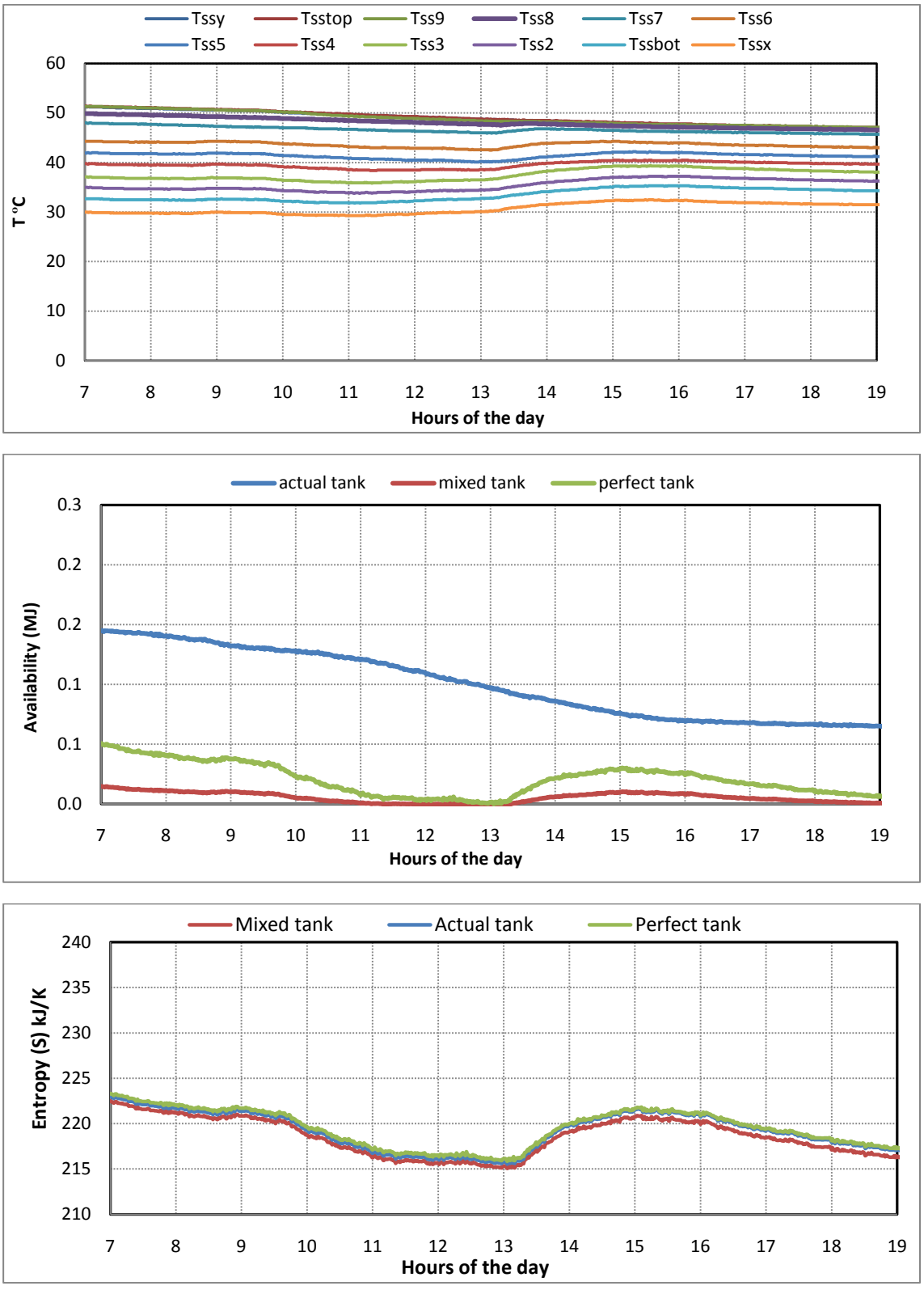

Figure 91 Manifold #4; Cloudy day; hot tank condition.

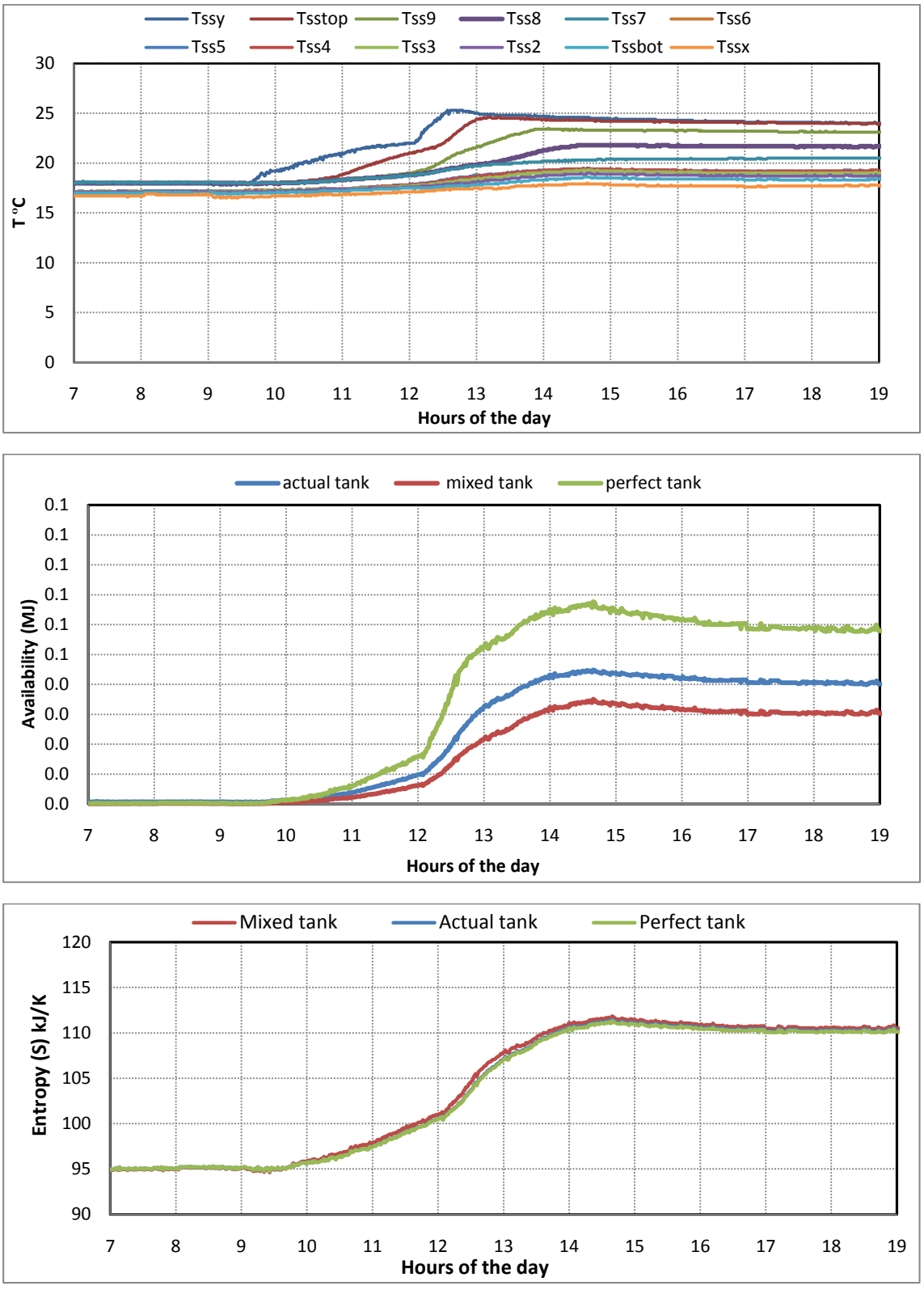

Figure 92 Manifold #4; Cloudy day; mixed tank condition.

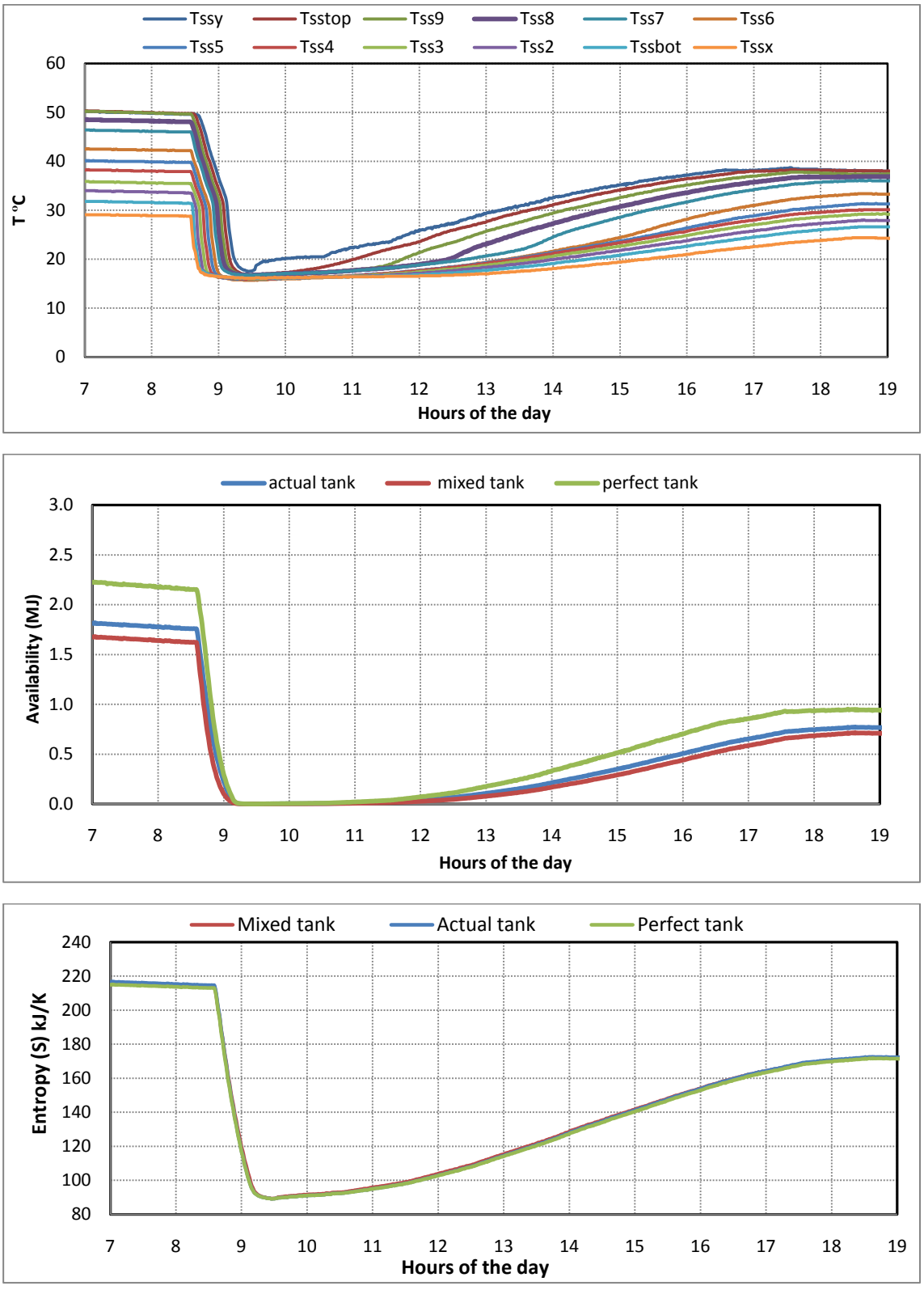

Figure 93 Manifold #4; Sunny day; cold tank condition.

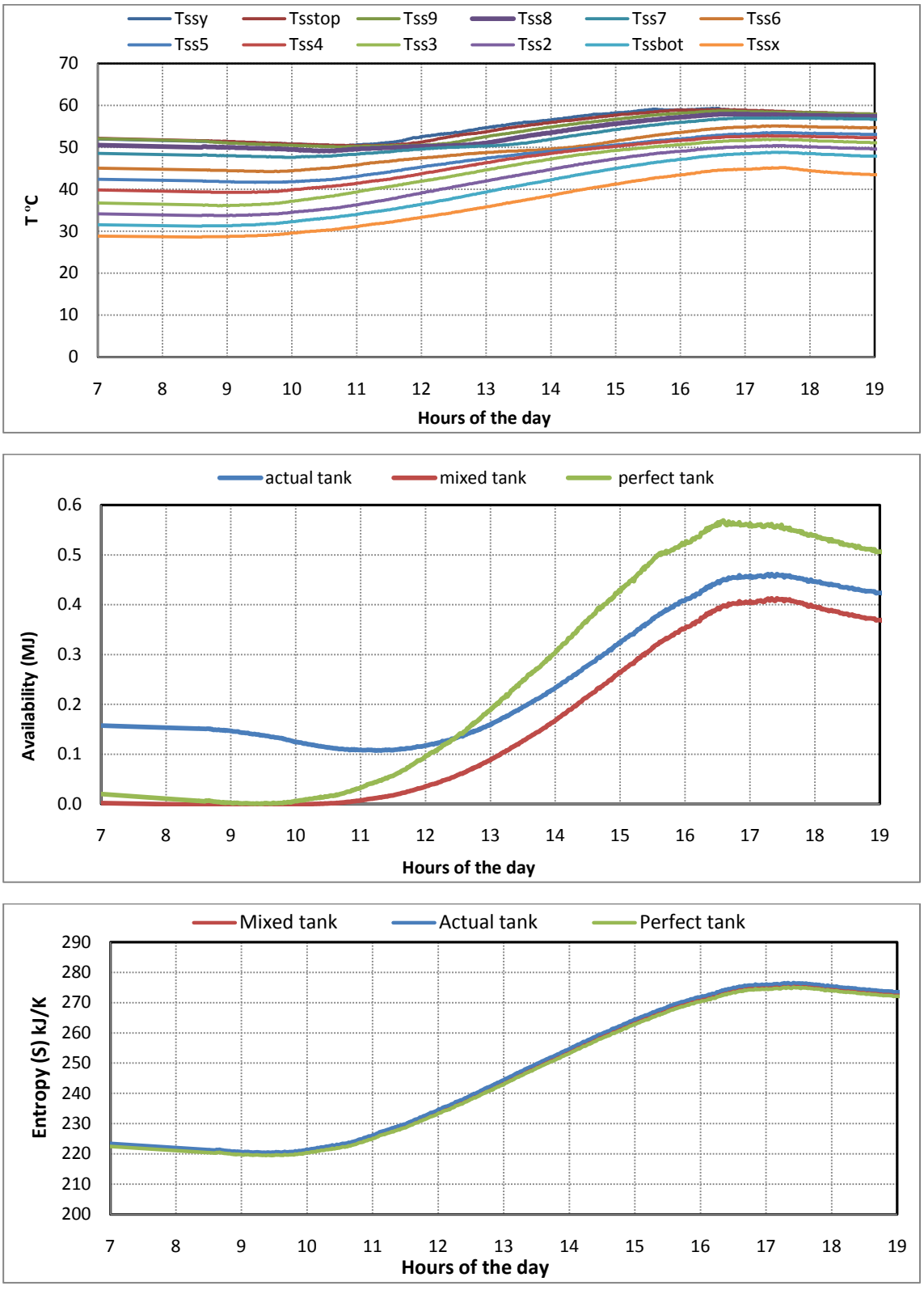

Figure 94 Manifold #4; Sunny day; hot tank condition.

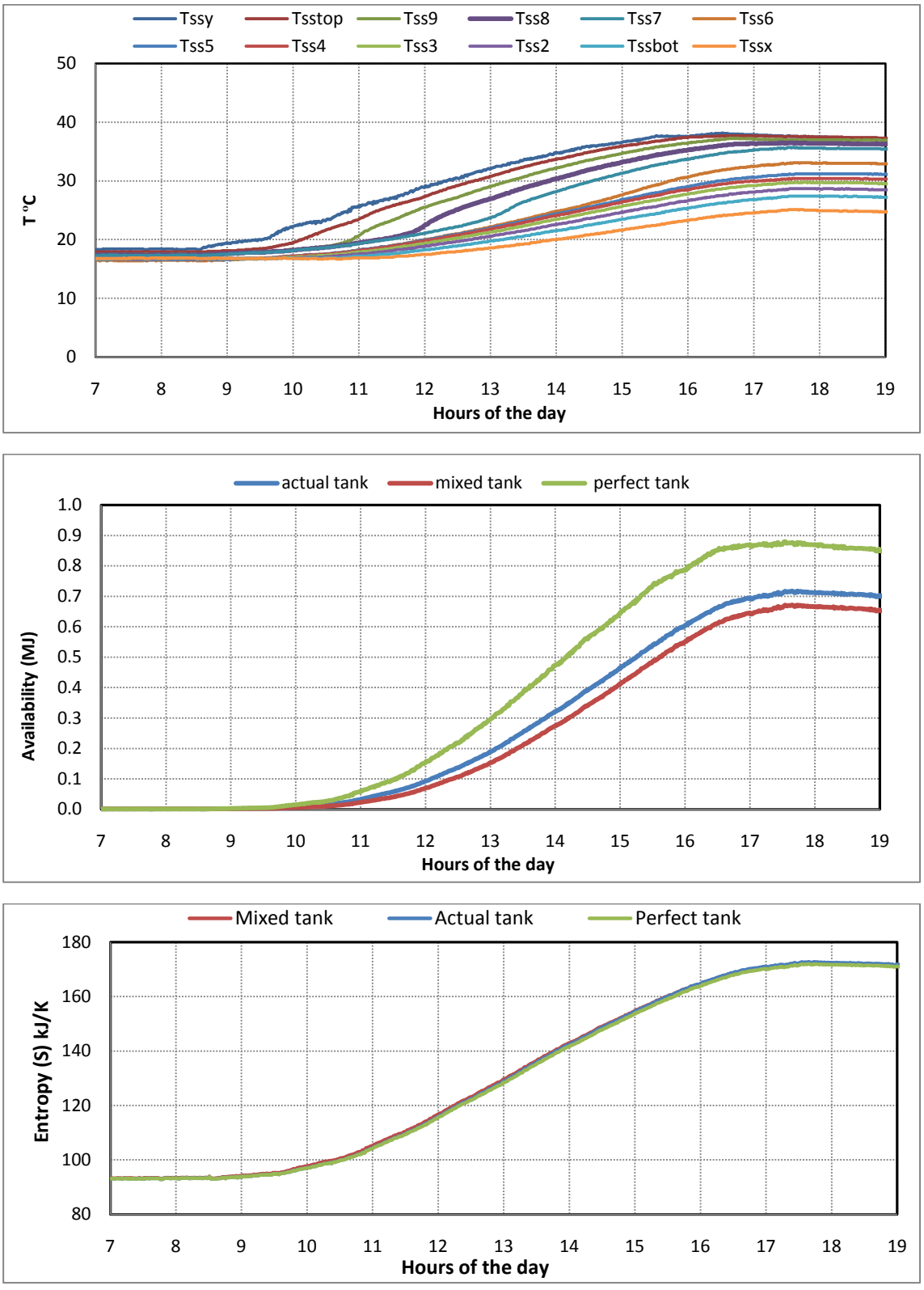

Figure 95 Manifold #4; Sunny day; mixed tank condition.

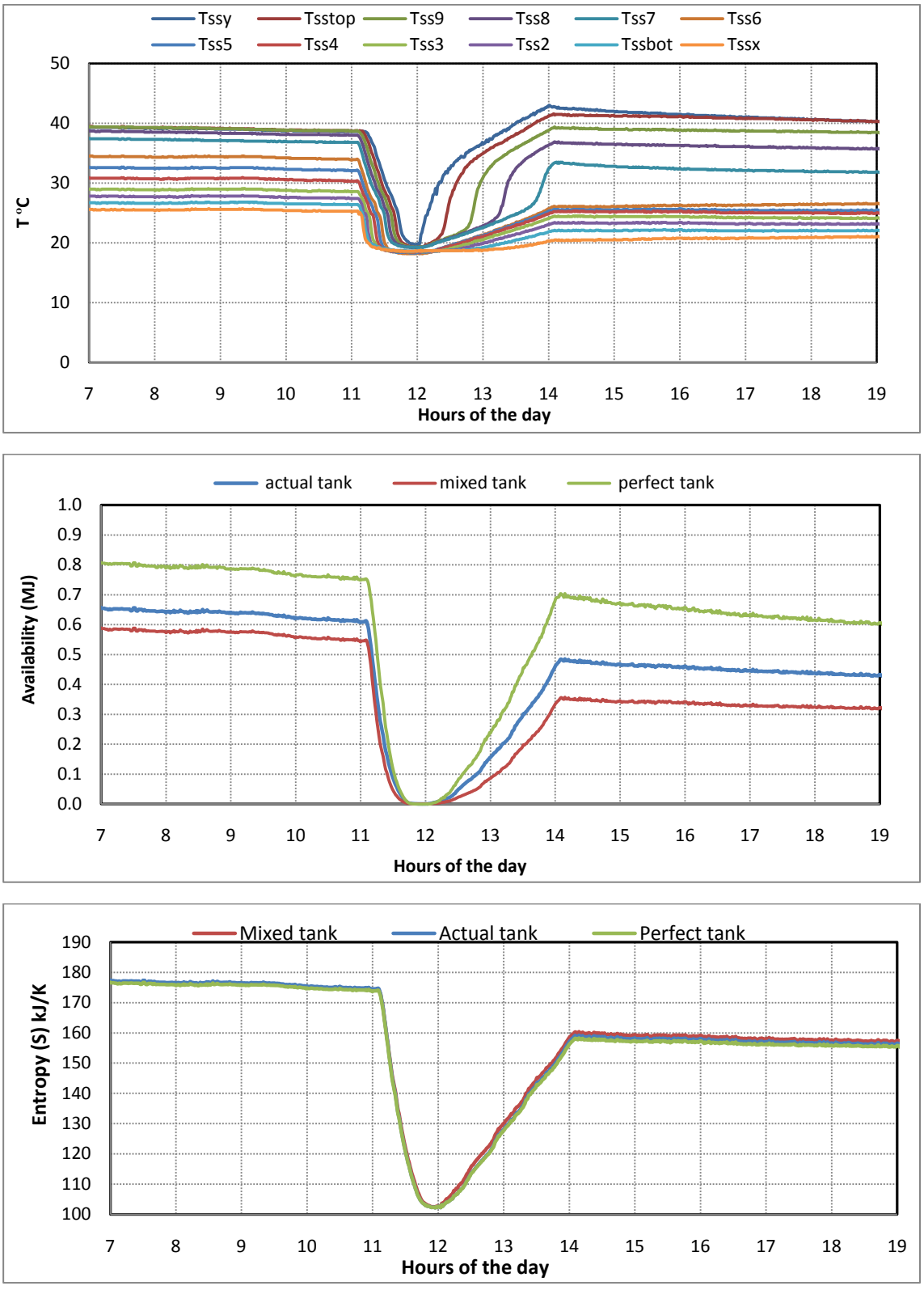

Figure 96 Manifold #4; Constant load; cold tank condition.

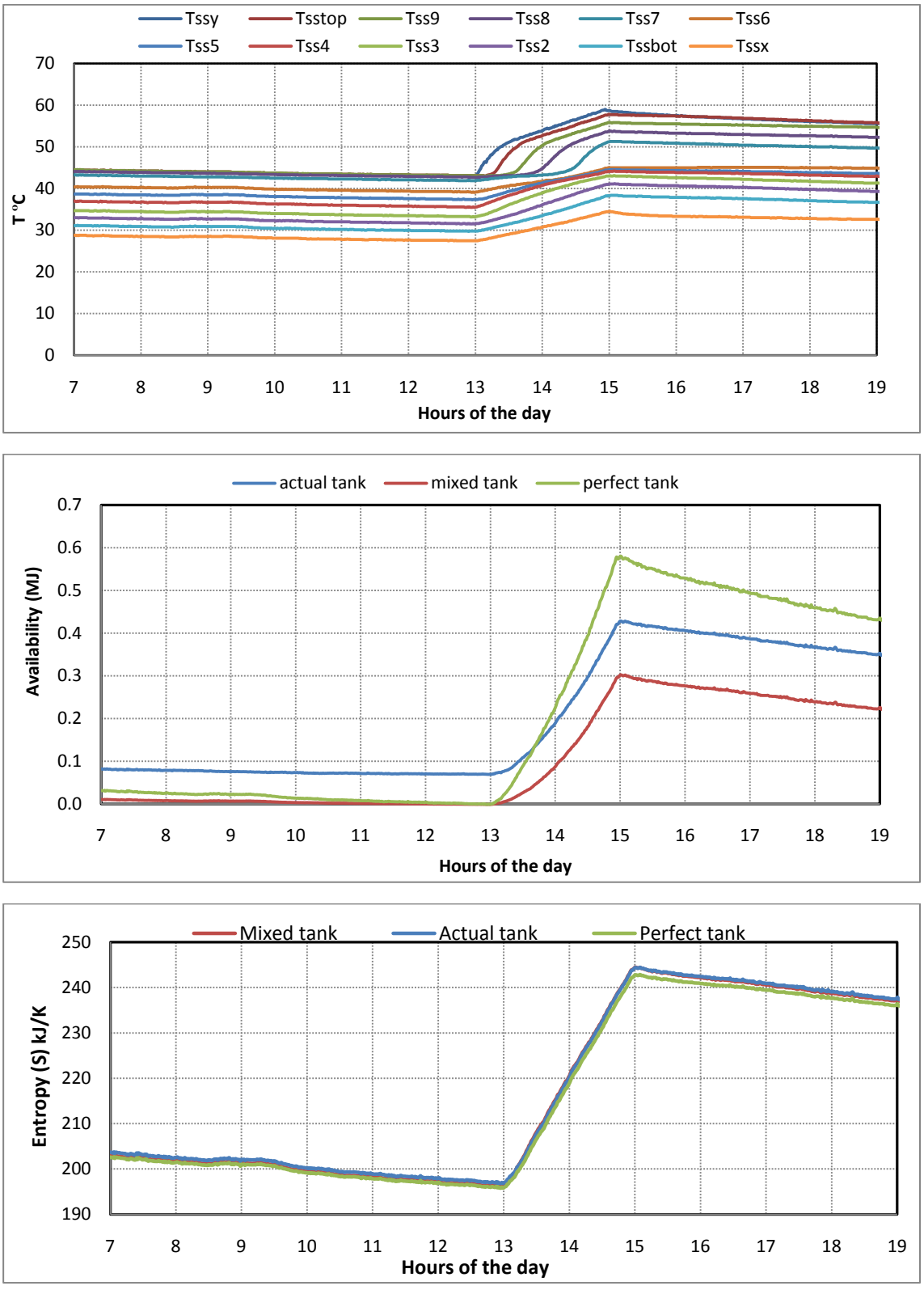

Figure 97 Manifold #4; Constant load; hot tank condition.

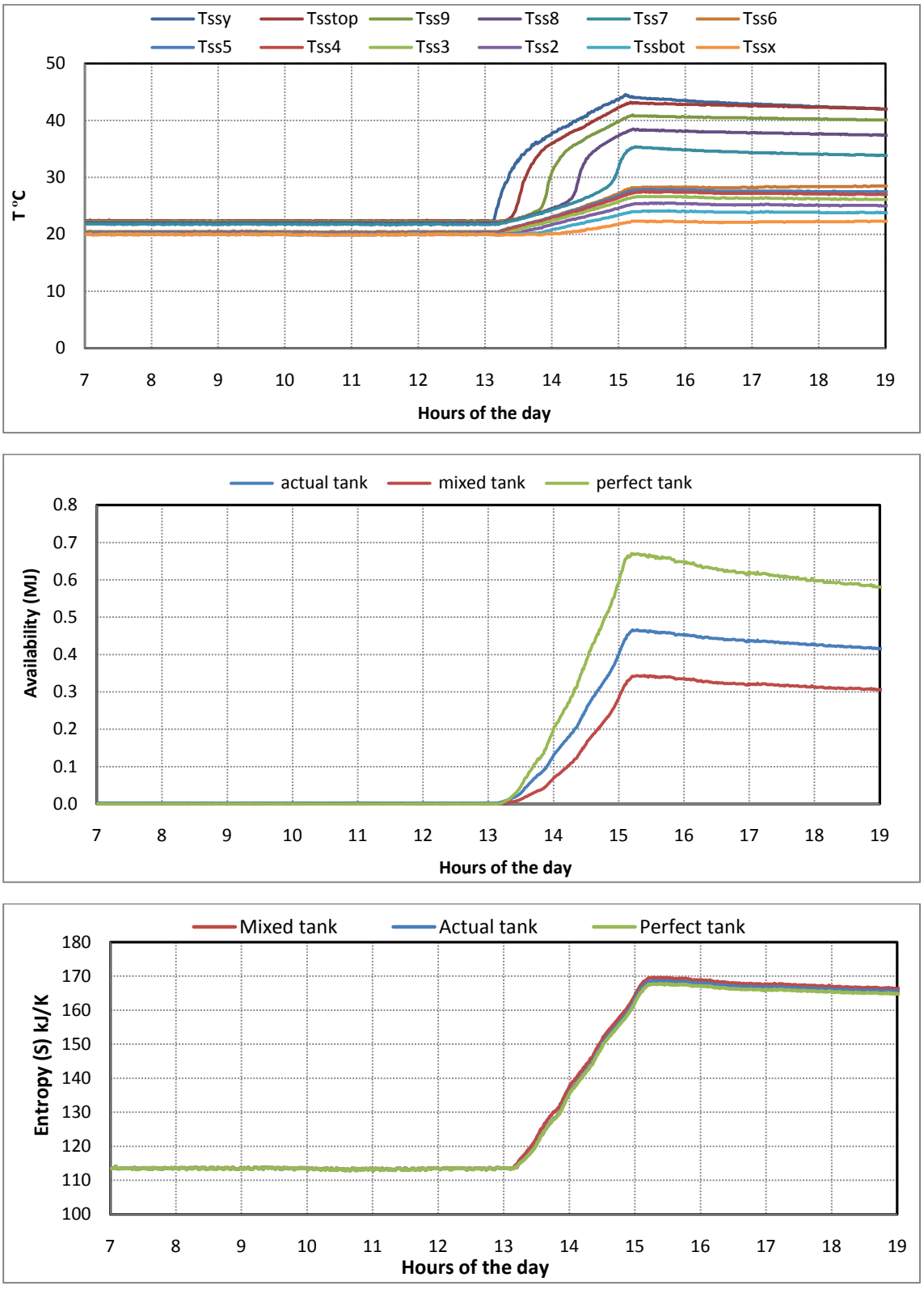

Figure 98 Manifold #4; Constant load; mixed tank condition.

APPENDIX E

THE COMPUTER PROGRAM THAT USED TO MONITOR AND RECORD THE DATA REQUIRED FOR THERMAL PERFORMANCE ANALYSIS

```
DECLARE SUB DATEMOD (DATEM$, DATEMS$, nday!, nweek!)
 CLEAR
CLS
REM DECLARE SUB DATEMOD (DATEM$, DATEMS$, nday!, nweek!)
REM  Printed on July 16th, 2009
DIM xlist$(66), lab$(66), TK2(10)
GOSUB LISTS
OPEN "COM1:9600,N,8,1" FOR RANDOM AS #1 LEN = 10000
PRINT                              #1,                              "SETCAL
1,9.998,98.92,480.3,989.89,1001.6,9985,682506,1000000"
PRINT #1, "SETAZ 0,1"
PRINT #1, "SETREF 1,1"
PRINT #1, "ECHO 0"
send$ = "INSTMOD 0,8082,0": PRINT send$: GOSUB PUTGETS
send$ = "MODULE 0": PRINT send$: GOSUB PUTGETS
PRINT send$
NWAIT = 250000

send$ = xlist$(1): PRINT send$: GOSUB PUTGETS
GOSUB PUTGETS: thermT = temp: PRINT USING "####.#"; thermT

CALL DATEMOD(DATEM$, DATEMS$, nday, nweek)
PRINT "nday ="; nday; "   nweek ="; nweek; "   "; DATEM$; "   "
REM GOSUB LISTS: GOSUB DEFAULTS

KEYIN:
PRINT : PRINT "Press a key:": PRINT
PRINT "A,a  M,m  E,e  L,l  T,t  P,p  S,s  D,d or V,v": BEEP
LOOP1: B$ = INKEY$: IF B$ = "" GOTO LOOP1
        IF B$ = "A" OR B$ = "a" GOTO AllTCP
        IF B$ = "M" OR B$ = "m" GOTO MONITOR
        IF B$ = "T" OR B$ = "t" GOTO tank
        IF B$ = "S" OR B$ = "s" GOTO SINGLE1

GOTO KEYIN:


PUTGETS:
FOR NNN = 1 TO NWAIT: NEXT NNN
PGC = 0
PGSA:
PRINT #1, send$: S$ = ""
GET1S:
```

```
FOR NNX = 1 TO NWAIT: NEXT NNX
IF LOC(1) = 0 THEN GOTO GET1S
a$ = INPUT$(1, #1): IF a$ = "," THEN a$ = CHR$(9)
IF LOC(1) > 0 THEN S$ = S$ + a$ ELSE GOTO GETPG5S
IF a$ <> CHR$(13) THEN GOTO GET1S
temp = VAL(S$)
GOSUB XERROR
GETPG5S:
S$ = "": IF LOC(1) > 0 GOTO GET1S
PGC = PGC + 1
IF PGC = 1 THEN GOTO PGSA
IF PGC = 5 THEN RETURN
IF PGC > 2 THEN PRINT PGC
IF temp < 10 THEN GOTO PGSA
RETURN

XERROR:
IF LEFT$(S$, 4) <> "9999" THEN RETURN
ERRORNUM$ = LEFT$(RIGHT$(S$, 5), 3)
REM BEEP: PRINT "#"; ERRORNUM$: XERR=1

RETURN

MONITOR:

PRINT : INPUT "INFORMATION CORRECT? (YES =1 or NO=0)", ninfo
IF ninfo = 0 THEN PRINT "Please correct the system information and
restart.": END
IF ninfo <> 1 THEN GOTO MONITOR
num = 5: mins = 1: NCHPS = 1
PRINT : INPUT "New file (1) or APPEND (0)", nfoa

aprn:
filename$ = "m " + DATEM$: filens$ = "m " + DATEMS$
PRINT "Opening files."
IF nfoa = 1 THEN OPEN filens$ FOR OUTPUT AS #2
IF nofa = 1 THEN PRINT #2, DATEM$
IF nfoa = 0 THEN OPEN filens$ FOR APPEND AS #2
opened = 1: tkread = 1: tktime = TIMER
filens$ = "m  " + DATEM$

PRINT
PRINT " Storage tank "
PRINT
IF nfoa = 0 THEN GOTO nfskip

     REM (Heading in Excel file)
PRINT #2, "Time "; CHR$(9); "Tbot"; CHR$(9); "T2"; CHR$(9); "T3";
CHR$(9); "T4";
PRINT #2, CHR$(9); "T5"; CHR$(9); "T6"; CHR$(9); "T7"; CHR$(9);
"T8"; CHR$(9); "T9";
```

```
PRINT #2, CHR$(9); "Ttop"; CHR$(9); "Tssx"; CHR$(9); "Tssbot";
CHR$(9); "Tss2";
PRINT #2, CHR$(9); "Tss3"; CHR$(9); "Tss4"; CHR$(9); "Tss5";
CHR$(9); "Tss6";
PRINT #2, CHR$(9); "Tss7"; CHR$(9); "Tss8"; CHR$(9); "Tss9";
CHR$(9); "Tsstop";
PRINT #2, CHR$(9); "Tssy"; CHR$(9); "chA(3)"; CHR$(9); "chA(2)";
CHR$(9); "chA(1)";
PRINT #2, CHR$(9); "chB(1)"; CHR$(9); "chB(2)"; CHR$(9); "chB(3)";
PRINT #2, CHR$(9); "chB(4)"; CHR$(9); "chB(5)"; CHR$(9); "chB(6)";
CHR$(9); "chB(7)";
PRINT #2, CHR$(9); "THXgin"; CHR$(9); "THXgout"; CHR$(9); "Tcw";
CHR$(9); "Tinside"

nfskip:
nfoa = 1: GOTO waiting

bmonitor1:

REM (Reading the thermocouples)
send$ = xlist$(2): GOSUB PUTGETS: Tbot = temp
send$ = xlist$(3): GOSUB PUTGETS: T2 = temp
send$ = xlist$(4): GOSUB PUTGETS: T3 = temp
send$ = xlist$(5): GOSUB PUTGETS: T4 = temp
send$ = xlist$(6): GOSUB PUTGETS: T5 = temp
send$ = xlist$(7): GOSUB PUTGETS: T6 = temp
send$ = xlist$(8): GOSUB PUTGETS: T7 = temp
send$ = xlist$(9): GOSUB PUTGETS: T8 = temp
send$ = xlist$(10): GOSUB PUTGETS: T9 = temp
send$ = xlist$(11): GOSUB PUTGETS: Ttop = temp
send$ = xlist$(13): GOSUB PUTGETS: THXgout = temp
send$ = xlist$(15): GOSUB PUTGETS: THXgin = temp

send$ = xlist$(18): GOSUB PUTGETS: Toutside = temp
send$ = xlist$(22): GOSUB PUTGETS: Tinside = temp

send$ = xlist$(25): GOSUB PUTGETS: Tssx = temp
send$ = xlist$(26): GOSUB PUTGETS: Tssbot = temp
send$ = xlist$(27): GOSUB PUTGETS: Tss2 = temp
send$ = xlist$(28): GOSUB PUTGETS: Tss3 = temp
send$ = xlist$(29): GOSUB PUTGETS: Tss4 = temp
send$ = xlist$(30): GOSUB PUTGETS: Tss5 = temp
send$ = xlist$(31): GOSUB PUTGETS: Tss6 = temp
send$ = xlist$(32): GOSUB PUTGETS: Tss7 = temp
send$ = xlist$(33): GOSUB PUTGETS: Tss8 = temp
send$ = xlist$(34): GOSUB PUTGETS: Tss9 = temp
send$ = xlist$(35): GOSUB PUTGETS: Tsstop = temp
send$ = xlist$(36): GOSUB PUTGETS: Tssy = temp
send$ = xlist$(14): GOSUB PUTGETS: chA(3) = temp
send$ = xlist$(23): GOSUB PUTGETS: chA(2) = temp
send$ = xlist$(24): GOSUB PUTGETS: chA(1) = temp
send$ = xlist$(38): GOSUB PUTGETS: chB(1) = temp
```

```
send$ = xlist$(39): GOSUB PUTGETS: chB(2) = temp
send$ = xlist$(40): GOSUB PUTGETS: chB(3) = temp
send$ = xlist$(41): GOSUB PUTGETS: chB(4) = temp
send$ = xlist$(42): GOSUB PUTGETS: chB(5) = temp
send$ = xlist$(44): GOSUB PUTGETS: chB(6) = temp
send$ = xlist$(45): GOSUB PUTGETS: chB(7) = temp
send$ = xlist$(46): GOSUB PUTGETS: Tcw = temp


REM (Storing in Excel file)

PRINT #2, TIME$;
PRINT #2, CHR$(9); :  PRINT #2, USING "#####.#"; Tbot;
PRINT #2, CHR$(9); :  PRINT #2, USING "#####.#"; T2;
PRINT #2, CHR$(9); :  PRINT #2, USING "#####.#"; T3;
PRINT #2, CHR$(9); :  PRINT #2, USING "#####.#"; T4;
PRINT #2, CHR$(9); :  PRINT #2, USING "#####.#"; T5;
PRINT #2, CHR$(9); :  PRINT #2, USING "#####.#"; T6;
PRINT #2, CHR$(9); :  PRINT #2, USING "#####.#"; T7;
PRINT #2, CHR$(9); :  PRINT #2, USING "#####.#"; T8;
PRINT #2, CHR$(9); :  PRINT #2, USING "#####.#"; T9;
PRINT #2, CHR$(9); :  PRINT #2, USING "#####.#"; Ttop;
PRINT #2, CHR$(9); :  PRINT #2, USING "#####.#"; Tssx;
PRINT #2, CHR$(9); :  PRINT #2, USING "#####.#"; Tssbot;
PRINT #2, CHR$(9); :  PRINT #2, USING "#####.#"; Tss2;
PRINT #2, CHR$(9); :  PRINT #2, USING "#####.#"; Tss3;
PRINT #2, CHR$(9); :  PRINT #2, USING "#####.#"; Tss4;
PRINT #2, CHR$(9); :  PRINT #2, USING "#####.#"; Tss5;
PRINT #2, CHR$(9); :  PRINT #2, USING "#####.#"; Tss6;
PRINT #2, CHR$(9); :  PRINT #2, USING "#####.#"; Tss7;
PRINT #2, CHR$(9); :  PRINT #2, USING "#####.#"; Tss8;
PRINT #2, CHR$(9); :  PRINT #2, USING "#####.#"; Tss9;
PRINT #2, CHR$(9); :  PRINT #2, USING "#####.#"; Tsstop;
PRINT #2, CHR$(9); :  PRINT #2, USING "#####.#"; Tssy;
PRINT #2, CHR$(9); :  PRINT #2, USING "#####.#"; chA(3);
PRINT #2, CHR$(9); :  PRINT #2, USING "#####.#"; chA(2);
PRINT #2, CHR$(9); :  PRINT #2, USING "#####.#"; chA(1);
PRINT #2, CHR$(9); :  PRINT #2, USING "#####.#"; chB(1);
PRINT #2, CHR$(9); :  PRINT #2, USING "#####.#"; chB(2);
PRINT #2, CHR$(9); :  PRINT #2, USING "#####.#"; chB(3);
PRINT #2, CHR$(9); :  PRINT #2, USING "#####.#"; chB(4);
PRINT #2, CHR$(9); :  PRINT #2, USING "#####.#"; chB(5);
PRINT #2, CHR$(9); :  PRINT #2, USING "#####.#"; chB(6);
PRINT #2, CHR$(9); :  PRINT #2, USING "#####.#"; chB(7);
PRINT #2, CHR$(9); :  PRINT #2, USING "#####.#"; THXgin;
PRINT #2, CHR$(9); :  PRINT #2, USING "#####.#"; THXgout;
PRINT #2, CHR$(9); :  PRINT #2, USING "#####.#"; Tcw;
PRINT #2, CHR$(9); :  PRINT #2, USING "#####.#"; Tinside


REM (Display in the screen)
PRINT
```

```
PRINT "Tssy "; CHR$(9); : PRINT USING "###.#"; Tssy
PRINT "Ttop "; CHR$(9); : PRINT USING "###.#"; Ttop;
PRINT "     Tsstop "; CHR$(9); : PRINT USING "###.#"; Tsstop
PRINT "T9 "; CHR$(9); : PRINT USING "###.#"; T9;
PRINT "     Tss9     "; CHR$(9); : PRINT USING "###.#"; Tss9
PRINT "T8 "; CHR$(9); : PRINT USING "###.#"; T8;
PRINT "     Tss8    "; CHR$(9); : PRINT USING "###.#"; Tss8
PRINT "T7 "; CHR$(9); : PRINT USING "###.#"; T7;
PRINT "     Tss7    "; CHR$(9); : PRINT USING "###.#"; Tss7
PRINT "T6 "; CHR$(9); : PRINT USING "###.#"; T6;
PRINT "     Tss6    "; CHR$(9); : PRINT USING "###.#"; Tss6
PRINT "T5 "; CHR$(9); : PRINT USING "###.#"; T5;
PRINT "     Tss5    "; CHR$(9); : PRINT USING "###.#"; Tss5
PRINT "T4 "; CHR$(9); : PRINT USING "###.#"; T4;
PRINT "     Tss4    "; CHR$(9); : PRINT USING "###.#"; Tss4
PRINT "T3 "; CHR$(9); : PRINT USING "###.#"; T3;
PRINT "     Tss3    "; CHR$(9); : PRINT USING "###.#"; Tss3
PRINT "T2 "; CHR$(9); : PRINT USING "###.#"; T2;
PRINT "     Tss2    "; CHR$(9); : PRINT USING "###.#"; Tss2
PRINT "Tbot "; CHR$(9); : PRINT USING "###.#"; Tbot;
PRINT "     Tssbot "; CHR$(9); : PRINT USING "###.#"; Tssbot
PRINT "Tcw  "; CHR$(9); : PRINT USING "###.#"; Tcw;
PRINT "     Tssx    "; CHR$(9); : PRINT USING "###.#"; Tssx
PRINT "THXgin"; CHR$(9); : PRINT USING "###.#"; THXgin;
PRINT "     THXgout"; CHR$(9); : PRINT USING "###.#"; THXgout
PRINT "Tinside"; CHR$(9); : PRINT USING "###.#"; Tinside;
PRINT "     Toutside   "; CHR$(9); : PRINT USING "###.#"; Toutside
PRINT
PRINT "chB(7)   "; CHR$(9); : PRINT USING "###.#"; chB(7)
PRINT "chB(6)   "; CHR$(9); : PRINT USING "###.#"; chB(6)
PRINT "chB(5)   "; CHR$(9); : PRINT USING "###.#"; chB(5)
PRINT "chB(4)   "; CHR$(9); : PRINT USING "###.#"; chB(4)
PRINT "chB(3)   "; CHR$(9); : PRINT USING "###.#"; chB(3)
PRINT "chB(2)   "; CHR$(9); : PRINT USING "###.#"; chB(2)
PRINT "chB(1)   "; CHR$(9); : PRINT USING "###.#"; chB(1)

REM PRINT "chA(3) " ; CHR$ (9) ; : PRINT USING "###.#";chA(3);
REM PRINT "chA(2) " ; CHR$ (9) ; : PRINT USING "###.#";chA(2);
REM PRINT "chA(1) " ; CHR$ (9) ; : PRINT USING "###.#";chA(1);


PRINT
waiting:
n = 1: secsnow = TIMER
IF secsnow < secsbef THEN GOTO closing
secsbef = secsnow: GOTO bmonitor1

closing:
secsbef = 0: PRINT "Closing files now."
CLOSE #2
CALL DATEMOD(DATEM$, DATEMS$, nday, nweek)
```

```
GOTO aprn

SINGLE1:
send$ = xlist$(1): GOSUB PUTGETS
GOSUB PUTGETS: thermT = temp: PRINT USING "####.#"; thermT
PRINT "thermistor reference temp. 1"
PRINT "2 (Tbot), 3(T2), 4(T3), 5(T4), 6(T5), 7(T6), 8(T7), 9 (T8),
10(T9), 11(Ttop),12(tank outlet)"
PRINT "13 THXgout; 15 THXgin"
PRINT "14 A(3)"
PRINT "17 cold water temp; 18 outside air; 22 inside air"
PRINT "20 collector inlet; 21 outlet; 22 inside air T"
PRINT "23 chA(2), 24 chA(1)"
PRINT "25 bot cover (Tssx), 26 (Tssbot), 27(Tss2), 28(Tss3),
29(Tss4), 30(Tss5), 31(Tss6)"
PRINT "32(Tss7), 33(Tss8), 34(Tss9), 35 (Tss,top), 36 top cover
(Tssy), 38 chB(T1)"
PRINT "39 chB(T2), 40 chB(T3), 41 chB(T4), 42 chB(T5), 44 chB(T6),
45 chB(T7), 46 Tcw"

SINGLE4:
PRINT
PRINT "Type in desired channel number (0 to stop); then
RETURN/ENTER"
INPUT "Type in N (or n) at anytime to change to a NEW channel", nch
IF nch = 0 THEN GOTO KEYIN
PRINT : PRINT "Channel:  "; nch; ":   "; lab$(nch)
more:
PRINT TIME$; "  ";
FOR i = 1 TO 10
send$ = xlist$(nch): GOSUB PUTGETS: sing = temp
PRINT USING "####.#"; sing;

SINGLE2:
    B$ = INKEY$
    IF B$ = "." THEN GOTO KEYIN
    IF B$ = "N" OR B$ = "n" THEN GOTO SINGLE4
    IF B$ <> "" THEN GOTO SINGLE2

NEXT i
PRINT
GOTO more

AllTCP:

EXA5:
PRINT : PRINT "   All Thermocouples ": PRINT
FOR i = 1 TO 63
    B$ = INKEY$
    IF B$ = "." THEN GOTO KEYIN
IF lab$(i) = "" THEN GOTO SKIP2
IF i = 19 THEN GOTO SKIP2
```

```
send$ = xlist$(i): GOSUB PUTGETS
PRINT USING "###   "; i; : PRINT "    "; lab$(i), : PRINT USING "
####.#"; temp; : PRINT "   ?C"
SKIP2:
NEXT i
PRINT

GOTO EXA5


tank:
    B$ = INKEY$
    IF B$ = "." THEN GOTO KEYIN

PRINT " Storage tank "
REM (Write (CLS) front tank: to go to the next group of reading

FOR i = 1 TO 10
send$ = xlist$(12 - i): GOSUB PUTGETS
PRINT USING "###"; 12 - i; : PRINT USING "######.#"; temp; : PRINT "
?C"
NEXT i

PRINT
GOTO tank


LISTS:
xlist$(0) = "DCV 0,2": lab$(0) = "zero voltage"
xlist$(1) = "THMST 1,2": lab$(1) = "thermistor temp."
xlist$(2) = "TCP 2,3,0": xlist$(3) = "TCP 3,3,0"
xlist$(4) = "TCP 4,3,0": xlist$(5) = "TCP 5,3,0": xlist$(6) = "TCP
6,3,0"
xlist$(7) = "TCP 7,3,0": xlist$(8) = "TCP 8,3,0": xlist$(9) = "TCP
9,3,0"
xlist$(10) = "TCP 10,3,0": xlist$(11) = "TCP 11,3,0"
xlist$(12) = "TCP 12,3,0": xlist$(13) = "TCP 13,3,0": xlist$(14) =
"TCP 14,3,0"
xlist$(15) = "TCP 15,3,0": xlist$(16) = "TCP 16,3,0": xlist$(17) =
"TCP 17,3,0"
xlist$(18) = "TCP 18,3,0": xlist$(19) = "TCP 19,3,0": xlist$(20) =
"TCP 20,3,0"
xlist$(21) = "TCP 21,3,0": xlist$(22) = "TCP 22,3,0": xlist$(23) =
"TCP 23,3,0"
xlist$(24) = "TCP 24,3,0": xlist$(25) = "TCP 25,3,0": xlist$(26) =
"TCP 26,3,0"
xlist$(27) = "TCP 27,3,0": xlist$(28) = "TCP 28,3,0": xlist$(29) =
"TCP 29,3,0"
xlist$(30) = "TCP 30,3,0": xlist$(31) = "TCP 31,3,0": xlist$(32) =
"TCP 32,3,0"
```

```
xlist$(33) = "TCP 33,3,0": xlist$(34) = "TCP 34,3,0": xlist$(35) =
"TCP 35,3,0"
xlist$(36) = "TCP 36,3,0": xlist$(38) = "TCP 38,3,0": xlist$(39) =
"TCP 39,3,0"
xlist$(40) = "TCP 40,3,0": xlist$(41) = "TCP 41,3,0": xlist$(42) =
"TCP 42,3,0"
xlist$(44) = "TCP 44,3,0": xlist$(45) = "TCP 45,3,0": xlist$(46) =
"TCP 46,3,0"


lab$(2) = "Tank T (bot)": lab$(3) = "Tank T (2)  "
lab$(4) = "Tank T (3)  ": lab$(5) = "Tank T (4)  "
lab$(6) = "Tank T (5)  ": lab$(7) = "Tank T (6)  "
lab$(8) = "Tank T (7)  ": lab$(9) = "Tank T (8)  "
lab$(10) = "Tank T (9)  ": lab$(11) = "Tank T (top)"
lab$(12) = "Tank out T  ": lab$(13) = "THXgout  "
lab$(15) = "THXgin  "
lab$(14) = "chA(3)": lab$(17) = "cold water in T"
lab$(18) = "outside air T": lab$(19) = "pump out T"
lab$(20) = "coll. in T   ": lab$(21) = "coll. out T"
lab$(22) = "T inside "
lab$(23) = "chA(2)": lab$(24) = "chA(1)"

lab$(25) = "bot cover T (Tssx)"
lab$(26) = "Tank Tss (bot)": lab$(27) = "Tank Tss (2)  "
lab$(28) = "Tank Tss (3)  ": lab$(29) = "Tank Tss (4)  "
lab$(30) = "Tank Tss (5)  ": lab$(31) = "Tank Tss (6)  "
lab$(32) = "Tank Tss (7)  ": lab$(33) = "Tank Tss (8)  "
lab$(34) = "Tank Tss (9)  ": lab$(35) = "Tank Tss (top)"
lab$(36) = "top cover T  (Tssy)"

lab$(38) = "chB(1)"
lab$(39) = "chB(2)   ": lab$(40) = "chB(3)  "
lab$(41) = "chB(4)   ": lab$(42) = "chB(5)  "
lab$(44) = "chB(6)   ": lab$(45) = "chB(7)  "
lab$(46) = "Tcw   "

xlist$(63) = "DCV 31,2": lab$(63) = "flux (W/m2)"
RETURN


END

REM PRINT #2,  CHR$(9); "Tssx";
REM PRINT #2,   CHR$(9); "T(top)"; CHR$(9); "T10"; CHR$(9); "T9";
CHR$(9); "T8";CHR$(9); "T7";
REM PRINT #2,  CHR$(9); "T6"; CHR$(9); "T5"; CHR$(9); "T4"; CHR$(9);
"T3";CHR$(9); "T(bot)";
REM PRINT
REM PRINT " Storage tank "
REM PRINT
```

```
REM msa:
REM PRINT #2, TIME$;
REM PRINT #2, CHR$(9);:  PRINT #2, USING "#####.#";Tssx
REM FOR i=1 TO 10
REM send$=xlist$(12-i): GOSUB PUTGETS
REM  PRINT  USING  "###";12-i;:  PRINT  USING  "######.#";temp;:PRINT  "
?C"
REM PRINT #2, CHR$(9);:  PRINT #2, USING "#####.#";temp;
REM NEXT i
REM PRINT #2, ""
REM PRINT "waiting   ";: FOR n=1 TO NWAIT: NEXT n
REM PRINT "waiting   ";: FOR n=1 TO NWAIT: NEXT n
REM PRINT "waiting   ";: FOR n=1 TO NWAIT: NEXT n
REM PRINT
REM GOTO msa
REM RETURN




REM + LEFT$(TIME$,2)+MID$(TIME$,4,2)
REM OPEN "O", #2, filens$
REM PRINT #2, "Tank temperatures on February 19, 2009."
REM PRINT #2, "Time";

SUB DATEMOD (DATEM$, DATEMS$, nday, nweek) STATIC

IF LEFT$(DATE$, 2) = "01" THEN MON$ = "Jan ": nday = 0
IF LEFT$(DATE$, 2) = "02" THEN MON$ = "Feb ": nday = 31
IF LEFT$(DATE$, 2) = "03" THEN MON$ = "Mar ": nday = 60
IF LEFT$(DATE$, 2) = "04" THEN MON$ = "Apr ": nday = 91
IF LEFT$(DATE$, 2) = "05" THEN MON$ = "May ": nday = 121
IF LEFT$(DATE$, 2) = "06" THEN MON$ = "Jun ": nday = 152
IF LEFT$(DATE$, 2) = "07" THEN MON$ = "Jul ": nday = 182
IF LEFT$(DATE$, 2) = "08" THEN MON$ = "Aug ": nday = 213
IF LEFT$(DATE$, 2) = "09" THEN MON$ = "Sep ": nday = 244
IF LEFT$(DATE$, 2) = "10" THEN MON$ = "Oct ": nday = 274
IF LEFT$(DATE$, 2) = "11" THEN MON$ = "Nov ": nday = 305
IF LEFT$(DATE$, 2) = "12" THEN MON$ = "Dec ": nday = 335


nday = nday + VAL(MID$(DATE$, 4, 2))
nweek = FIX(nday / 7)
derr = 1 + nday - nweek * 7
REM    at the start of a new year the number below must be advanced.
derr = derr + 5
IF derr > 7 THEN derr = derr - 7
IF derr = 5 THEN day$ = "Monday, "
```

```
IF derr = 6 THEN day$ = "Tuesday, "
IF derr = 7 THEN day$ = "Wednesday, "
IF derr = 1 THEN day$ = "Thursday, "
IF derr = 2 THEN day$ = "Friday, "
IF derr = 3 THEN day$ = "Saturday, "
IF derr = 4 THEN day$ = "Sunday, "
DATEM$ = day$ + MON$ + MID$(DATE$, 4, 2) + ", " + RIGHT$(DATE$, 4)
DATEMS$ = DATE$
REM MON$ + MID$(DATE$, 4, 2) + "," + RIGHT$(DATE$, 2) + " " +
LEFT$(day$, 3)

END SUB
```